National Technical University of Athens

School of Chemical Engineering

Thermodynamics and Transport Phenomena Laboratory

Thermodynamic modeling and simulation of CO₂ and H₂S removal processes from natural gas and flue gases

Ph.D. Thesis of

Anthoula S. Plakia

Supervisor: Epaminondas Voutsas, Professor

Athens, 2021

Thermodynamic modeling and simulation of CO_2 and H_2S removal processes from natural gas and flue gases

A dissertation

by

Anthoula S. Plakia

to

the School of Chemical Engineering

in partial fulfillment of the requirements for the degree of

Doctor of Philosophy

in

Chemical Engineering

Supervisor: Epaminondas Voutsas, Professor

Supervising Committee: Konstantinos Magoulas, Professor

                         Dimitrios Karonis, Professor

National Technical University of Athens

Athens, Greece

March 2021

The approval of this PhD dissertation by the School of Chemical Engineering of the National Technical University of Athens does not imply the acceptance of the author's opinions (Law 5343/32 Article 202 § 2).

Η έγκριση της διδακτορικής διατριβής από την Ανωτάτη Σχολή Χημικών Μηχανικών του Εθνικού Μετσόβιου Πολυτεχνείου δεν υποδηλώνει αποδοχή των απόψεων του συγγραφέα (Ν. 5343/32 Άρθρο 202 § 2).

Abstract

The subject of this thesis is thermodynamic modeling and simulation of acid gases removal processes from natural gas and flue gases.

Carbon dioxide (CO_2) is an acidic gaseous component, which exists naturally in atmosphere, due to the carbon cycle. However, human activities have increased its concentration, a fact that has as a result, significant environmental problems, such as the global warming. The combustion of fossil fuels is the main contributor of CO_2 emissions to atmosphere. Therefore, in this thesis, two origin sources of acid gases are examined: flue gases, emitted by fossil fuel combustion and natural gas, which is the cleanest fossil fuel. Thus, CO_2 should be removed from natural gas and flue gases and the removal processes are examined in this work. Hydrogen sulfide (H_2S) is also present in hydrocarbon resources, such as the natural gas, and it can cause serious problems to piping and other equipment, whereas it reduces its heating value. Therefore, it should also be removed from natural gas. The dominant process used in industry for the removal of acid gases is chemical absorption in aqueous alkanolamine solutions, even though last decades different and environmentally friendly solvents, such as the ionic liquids, have been proposed.

The correct description of phase and chemical equilibrium of acid gases-water-alkanolamines mixtures by a thermodynamic model is essential for the proper design and optimization of the process. Classic thermodynamic models, such as equations of state, are not capable of an accurate description of electrolyte mixtures. Therefore, the development of an appropriate thermodynamic framework, in order to describe such mixtures, is necessary.

To this purpose, the problem of phase and chemical equilibrium, related to acid gases-water-alkanolamines mixtures, is presented. More specifically, the electrolyte species dissociate in the liquid phase, where chemical reactions take place and ions are formed. Ions remain in liquid phase, whereas molecular species exist both in liquid and vapor phases. In order to solve this complex problem, in which phase and chemical equilibrium coexist, an approach, which describes this problem as analogous to bubble point calculation, is adopted. Therefore, the liquid phase composition is found by the solution of chemical equilibrium, whereas the pressure and vapor phase composition are found by solving the vapor-liquid equilibrium by a thermodynamic model.

The thermodynamic model selected is an EoS/G^E model, UMR-PRU, which combines Peng-Robinson EoS with UNIFAC via UMR mixing rules, because it provides a consistent description of the mixtures, due to the use of the same equations for both phases, and it is more suitable for electrolyte mixtures than classic equations of state. However, UMR-

PRU model needs modification in order to be extended to acid gases-water-alkanolamine mixtures. More specifically, Debye-Hückel term is incorporated, in order to account for the long-range electrostatic forces and the resulting model is called eUMR-PRU. Two alkanolamines have been examined in this thesis: Monoethanolamine (MEA) and Methyl-diethanolamine (MDEA). Thus, the eUMR-PRU is developed by fitting the binary interaction parameters to experimental vapor-liquid equilibrium data of acid gases, CO_2 and H_2S, in mixtures with H_2O, MEA and MDEA. The enormous number of intercorrelated parameters, needed to be estimated, implies the complexity of the problem. At this point, it should be also noted, that UMR-PRU model is extended to H_2S-gases (N_2, CH_4, C_2H_6) and H_2S-hydrocarbon mixtures as well, as there are no available parameters for these mixtures.

In the case of CO_2, the results of eUMR-PRU yield an average absolute relative deviation in partial pressure, greater than 30 % in all cases examined and the comparison with the results of electrolyte-NRTL, which is a commonly used model for such systems, implies that eUMR-PRU leads to similar or even better results and its extension to these mixtures has been successful. Furthermore, eUMR-PRU model can successfully describe the effect of methane on CO_2 solubility in aqueous alkanolamines, i.e. in CO_2-H_2O-MDEA mixtures, which is of great interest for the natural gas industry. For H_2S, the results of the model have been compared to the ones of electrolyte-NRTL and Kent-Eisenberg model, proving once more that the performance of eUMR-PRU is similar or in some cases even more accurate than the other models.

Recently, the need of "green", energy-effective and less volatile solvents has resulted to an increasing interest of the research community to ionic liquids and more specifically to acid gases solubility in ionic liquids, in order to use them as solvents in a physical absorption process for acid gas removal. Therefore, the accurate description of the vapor-liquid equilibrium of acid gases-ionic liquid mixtures by a thermodynamic model is an essential task, in order this model to be used in such a physical absorption process design.

Therefore, UMR-PRU model is further extended to CO_2-ionic liquid mixtures. The ionic liquids examined are twelve imidazolium-based with anions tetrafluoroborate, hexafluorophosphate and bis(trifluoromethylsulfonyl)imide in order to study the effect of anion and cation on CO_2 solubility. Firstly, the correct description of pure ionic liquids is necessary, as their critical properties cannot be measured and their extremely low vapor pressure should be correctly reproduced by a thermodynamic model in order to avoid any solvent loss in a process simulation. Therefore, the critical properties, Soave or Mathias-Copeman parameters of ionic liquids are fitted to density and vapor pressure data. After the definition of UNIFAC groups of ionic liquids used in this work, UMR-PRU binary interaction parameters have been fitted to experimental vapor-liquid equilibrium data of

CO_2-ionic liquid mixtures. The results are compared to the ones of Peng-Robinson coupled with van der Waals one fluid mixing rules and using k_{ij} and l_{ij} interaction parameters, expressed as correlations of temperature and carbon number of the cation. It is concluded, that UMR-PRU leads to more accurate results.

Process design is maybe the most important part of a chemical engineer's job. The application of the developed thermodynamic framework in process simulations is the next step needed. Therefore, eUMR-PRU model is incorporated in process simulators (ASPEN HYSYS V8.6 and UNISIM R451) through a CAPE-OPEN protocol and the implementation is found to be successful. At this point, it should be mentioned that the CO_2 removal from natural gas and not from flue gases has been examined. To this purpose, three different processes are simulated: CO_2 chemical absorption in a 30% w/w aqueous MEA solution, CO_2 physical absorption in methanol and CO_2 physical absorption in an ionic liquid. For the first process, acid gas thermodynamic package in HYSYS V8.6 is used, whereas for the next two, UMR-PRU and Peng-Robinson EoS are used. Sensitivity analysis has been performed in all cases, in order to define the important parameters of each process and their effect to the results. UMR-PRU is compared to the Peng-Robinson EoS simulation results and the three processes are compared to each other in order to find the most energy-effective process, which is concluded to be the one with ionic liquid as solvent. However, its use is not applicable due to its high viscosity and thus some suggestions of using mixtures of ionic liquid-methanol are made.

Σύνοψη

Το αντικείμενο της παρούσας διατριβής είναι η μοντελοποίηση και προσομοίωση διεργασιών απομάκρυνσης όξινων αερίων από φυσικό αέριο και απαέρια.

Το διοξείδιο του άνθρακα (CO_2) είναι ένα όξινο αέριο, το οποίο υπάρχει φυσικά στην ατμόσφαιρα, εξαιτίας του κύκλου ζωής του άνθρακα. Όμως, οι ανθρώπινες δραστηριότητες έχουν αυξήσει τη συγκέντρωση του, γεγονός το οποίο προκαλεί σημαντικά προβλήματα στο περιβάλλον, όπως η αύξηση της θερμοκρασίας του πλανήτη. Η καύση των ορυκτών καυσίμων είναι η κύρια πηγή εκπομπών CO_2. Για αυτό το λόγο στην παρούσα διατριβή εξετάζονται δύο πηγές προέλευσης όξινων αερίων: τα απαέρια διεργασιών καύσης ορυκτών καυσίμων και το φυσικό αέριο, το οποίο είναι το πιο «καθαρό» ορυκτό καύσιμο. Έτσι το CO_2 πρέπει να απομακρυνθεί από τα απαέρια και το φυσικό αέριο και οι διεργασίες απομάκρυνσης εξετάζονται σε αυτή τη διατριβή. Το υδρόθειο (H_2S) υπάρχει σε κοιτάσματα υδρογονανθράκων, όπως το φυσικό αέριο, και μπορεί να προκαλέσει προβλήματα στον εξοπλισμό, ενώ μειώνει και τη θερμογόνο δύναμη του καυσίμου. Για αυτό το λόγο πρέπει επίσης να απομακρυνθεί από το φυσικό αέριο. Η πιο συχνά χρησιμοποιούμενη διεργασία στη βιομηχανία για την απομάκρυνση των όξινων αερίων είναι η χημική απορρόφηση με διαλύτη υδατικό διάλυμα αλκανολαμίνης, αν και τις τελευταίες δεκαετίες και άλλοι διαλύτες, που είναι περισσότερο φιλικοί προς το περιβάλλον, όπως τα ιοντικά υγρά, έχουν προταθεί.

Η σωστή περιγραφή της φυσικής και χημικής ισορροπίας μιγμάτων όξινων αερίων-αλκανολαμίνης-νερού από ένα θερμοδυναμικό μοντέλο είναι απαραίτητη για το σωστό σχεδιασμό και τη βελτιστοποίηση της διεργασίας. Κλασσικά θερμοδυναμικά μοντέλα, όπως οι καταστατικές εξισώσεις, δεν είναι ικανά να περιγράψουν ηλεκτρολυτικά μίγματα. Για αυτό το λόγο, η ανάπτυξη ενός κατάλληλου θερμοδυναμικού προσομοιωτή, για την περιγραφή τέτοιων μιγμάτων, είναι απαραίτητη.

Για το σκοπό αυτό, ορίζεται το πρόβλημα της φυσικής και χημικής ισορροπίας που περιγράφει τα μίγματα όξινων αερίων-αλκανολαμίνης-νερού. Πιο συγκεκριμένα, οι ηλεκτρολύτες διαλύονται στην υγρή φάση, όπου χημικές αντιδράσεις λαμβάνουν χώρα, και σχηματίζονται ιόντα, τα οποία παραμένουν στην υγρή φάση, ενώ τα μόρια υπάρχουν και στη υγρή και στην ατμώδη φάση. Για την επίλυση αυτού του περίπλοκου προβλήματος, στο οποίο συνυπάρχει η ισορροπία φάσεων και η ισορροπία χημικών αντιδράσεων, ακολουθήθηκε μία προσέγγιση, η οποία περιγράφει το πρόβλημα ως ανάλογο ενός υπολογισμού πίεσης σημείου φυσαλίδας. Έτσι, η σύσταση υγρής φάσης προσδιορίζεται από την επίλυση της χημικής ισορροπίας, ενώ η πίεση και η σύσταση ατμώδους φάσης υπολογίζονται από ένα θερμοδυναμικό μοντέλο.

Το θερμοδυναμικό μοντέλο που επιλέχθηκε είναι ένα EoS/G^E μοντέλο, το UMR-PRU, το οποίο συνδυάζει την καταστατική εξίσωση Peng-Robinson με το μοντέλο συντελεστή ενεργότητας UNIFAC, επειδή περιγράφει με συνέπεια τα μίγματα, λόγω της χρήσης των ίδιων εξισώσεων και για τις δύο φάσεις. Επίσης είναι πιο κατάλληλο για ηλεκτρολυτικά μίγματα από ό,τι οι κλασσικές καταστατικές εξισώσεις. Παρόλα αυτά, για να χρησιμοποιηθεί το UMR-PRU σε μίγματα όξινων αερίων-αλκανολαμινών-νερού χρειάζεται μία τροποποίηση. Η εισαγωγή του όρου Debye- Hückel είναι απαραίτητη, ώστε να ληφθούν υπόψιν οι ηλεκτροστατικές αλληλεπιδράσεις μεγάλης απόστασης και το μοντέλο που προκύπτει ονομάζεται eUMR-PRU. Δύο αλκανολαμίνες μελετήθηκαν σε αυτή την εργασία: η μονοαιθανολαμινή (MEA) και η μεθυλ-διεθανολαμίνη (MDEA). Έτσι, το eUMR-PRU αναπτύσσεται μέσω προσαρμογής σε πειραματικά δεδομένα ισορροπίας φάσεων των όξινων αερίων CO_2 και H_2S σε μίγματα με H_2O, MEA και MDEA. Ο τεράστιος αριθμός παραμέτρων που αλληλοεπιδρούν, και οι οποίες πρέπει να υπολογιστούν, υποδηλώνει την πολυπλοκότητα του προβλήματος. Σε αυτό το σημείο θα πρέπει επίσης να αναφερθεί η επέκταση του UMR-PRU μοντέλου στα μίγματα υδρόθειου με αέρια (N_2, CH_4, C_2H_6) και υδρόθειου με υδρογονάνθρακες, μιας και δεν υπάρχουν διαθέσιμες παράμετροι για αυτά τα μίγματα.

Στην περίπτωση του CO_2, τα αποτελέσματα του eUMR-PRU έχουν ένα μέσο απόλυτο σχετικό σφάλμα στη μερική πίεση, μεγαλύτερο του 30 % σε όλες τις περιπτώσεις που εξετάστηκαν και η σύγκρισή τους με αυτά της electrolyte-NRTL υποδηλώνει πως το eUMR-PRU έχει παρόμοια ή ακόμα καλύτερα σε κάποιες περιπτώσεις αποτελέσματα και ότι η επέκτασή του σε αυτά τα μίγματα ήταν επιτυχής. Επίσης, η επίδραση του μεθανίου στη διαλυτότητα του διοξειδίου σε υδατικά διαλύματα αλκανολαμινών, είναι ιδιαίτερης σημασίας για τη βιομηχανία φυσικού αερίου και για αυτό το λόγο η επίδρασή του στην ισορροπία ατμού-υγρού του μίγματος CO_2-H_2O-MDEA μελετήθηκε. Για το H_2S, τα αποτελέσματα του μοντέλου συγκρίθηκαν με αυτά της e-NRTL και του Kent-Eisenberg και αποδείχτηκε για μία ακόμη φορά ότι η απόδοση του μοντέλου είναι παρόμοια ή σε κάποιες περιπτώσεις ακόμα πιο ακριβής από τα άλλα μοντέλα.

Πρόσφατα, η ανάγκη για πιο «πράσινους», ενεργειακά αποδοτικούς και λιγότερο πτητικούς διαλύτες έχει ως αποτέλεσμα το αυξημένο ενδιαφέρον της επιστημονικής κοινότητας για τα ιοντικά υγρά και πιο συγκεκριμένα για τη διαλυτότητα των όξινων αερίων σε αυτά, με σκοπό να χρησιμοποιηθούν ως διαλύτες σε διεργασία φυσικής απορρόφησης για την απομάκρυνση όξινων αερίων. Επομένως, η σωστή περιγραφή της ισορροπίας φάσεων των μιγμάτων όξινων αερίων-ιοντικών υγρών από ένα θερμοδυναμικό μοντέλο είναι απαραίτητη, ώστε να χρησιμοποιηθεί το μοντέλο αυτό στο σχεδιασμό μίας διεργασίας φυσικής απορρόφησης.

Για αυτό το λόγο, το μοντέλο UMR-PRU επεκτείνεται ακόμη σε μίγματα CO_2-ιοντικού υγρού. Τα ιοντικά υγρά που εξετάζονται είναι δώδεκα ιμιδαζολικά ιοντικά υγρά με ανιόντα τετραφθοροβορικό, εξαφθοροφωσφορικό και δις(τριφθορομεθυλο σουλφονυλο)-ιμίδιο. Αρχικά, η σωστή περιγραφή των καθαρών ιοντικών υγρών είναι απαραίτητη, επειδή οι κρίσιμες ιδιότητες και η εξαιρετικά χαμηλή τάση ατμών τους πρέπει να αναπαράγεται σωστά, ώστε να αποφευχθούν πιθανές απώλειες διαλύτη σε προσομοιώσεις διεργασιών. Για αυτό το λόγο, οι κρίσιμες ιδιότητες, και οι παράμετροι Soave ή Mathias-Copeman των ιοντικών υγρών υπολογίζονται μέσω προσαρμογής σε πειραματικά δεδομένα πυκνότητας και τάσης ατμών. Μετά τον ορισμό των ομάδων της UNIFAC για τα ιοντικά υγρά, υπολογίζονται οι δυαδικές παράμετροι αλληλεπίδρασης του UMR-PRU, μέσω προσαρμογής σε πειραματικά δεδομένα ισορροπίας ατμού-υγρού των μιγμάτων CO_2-ιοντικού υγρού. Τα αποτελέσματα, συγκρίνονται με αυτά της Peng-Robinson, για την οποία χρησιμοποιούνται τόσο k_{ij} όσο και l_{ij} δυαδικές παράμετροι αλληλεπίδρασης, οι οποίες εκφράζονται ως συσχέτιση με τη θερμοκρασία και τον αριθμό ατόμων άνθρακα. Συμπεραίνεται ότι τα αποτελέσματα του UMR-PRU είναι σε μεγαλύτερη συμφωνία με τα πειραματικά δεδομένα.

Ο σχεδιασμός διεργασιών είναι ίσως το σημαντικότερο μέρος της εργασίας ενός χημικού μηχανικού. Η εφαρμογή του θερμοδυναμικού πακέτου που αναπτύχθηκε σε προσομοιώσεις διεργασιών είναι το επόμενο βήμα που πρέπει να γίνει. Επομένως, το μοντέλο eUMR-PRU ενσωματώνεται σε εμπορικούς προσομοιωτές διεργασιών (ASPEN HYSYS V8.6 και UNISIM R451), μέσω ενός πρωτοκόλλου CAPE-OPEN και αποδεικνύεται ότι η ενσωμάτωση αυτή είναι επιτυχής. Στο σημείο αυτό θα πρέπει να σημειωθεί ότι εξετάστηκε η απομάκρυνση του CO_2 από φυσικό αέριο και όχι από απαέρια. Για το σκοπό αυτό, τρεις διαφορετικές διεργασίες προσομοιώνονται: η χημική απορρόφηση διοξειδίου του άνθρακα σε ένα υδατικό διάλυμα μονοαιθανολαμίνης 30% w/w, η φυσική απορρόφηση διοξειδίου του άνθρακα σε μεθανόλη και η φυσική απορρόφηση διοξειδίου του άνθρακα σε ένα ιοντικό υγρό. Για την πρώτη διεργασία χρησιμοποιείται το μοντέλο acid gas του HYSYS V8.6, ενώ για τις δύο επόμενες χρησιμοποιείται το UMR-PRU και η Peng-Robinson. Πραγματοποιούνται αναλύσεις ευαισθησίας και σε όλες τις διεργασίες, με σκοπό να προσδιοριστούν οι σημαντικές παράμετροι κάθε διεργασίας. Το UMR-PRU συγκρίνεται με τα αποτελέσματα της Peng-Robinson και οι τρεις διεργασίες συγκρίνονται με σκοπό να προσδιοριστεί η πιο ενεργειακά-αποτελεσματική διεργασία, η οποία, όπως συμπεραίνεται είναι αυτή με το ιοντικό υγρό. Ωστόσο, η χρήση του σε μία τέτοια διεργασία δεν είναι πρακτικά εφαρμόσιμη, λόγω του υψηλού ιξώδους, για αυτό γίνονται κάποιες προτάσεις για χρήση μιγμάτων μεθανόλης-ιοντικού υγρού.

Acknowledgements

The journey to the final destination of writing and defending my Ph.D thesis seemed endless and difficult. However, even if I did not notice, each day was just another step to the final scope.

This scope could not be fulfilled without the help of other people, colleagues and friends. First and foremost, I am grateful to my supervisor, Prof. Epaminondas Voutsas, for the opportunity to work on this topic and his advice and guidance throughout this time, because without it, it would not be possible to complete this work. I would also like to thank the rest supervising committee members, Prof. Kostis Magoulas and Prof. Dimitrios Karonis for their support and guidance.

Furthermore, I appreciate the help of my senior colleagues, Dr. Georgia Pappa and Dr. Christos Boukouvalas, who has given me advice about computational issues and more specifically the Cape-Open application. Special thanks to Dr. Vicky Louli, for her support and guidance during all these years and especially during the last year of my studies.

I would also like to thank Dr. Nefeli Novak for her advice, especially about the Cape-Open application, Dr. Eleni Boli and Dr. Myrto Dardavilla. Special thank is towards Dr. Eirini Petropoulou for the time she devoted to advising and supporting me, every time I needed. I am also grateful to my fellow PhD students, because each of them has helped me towards these years. Vassilis Koulocheris has shared his ideas with me about the ways to overcome problems, which I faced in research, whereas the younger ones, Akis Tassios, Ioulia Georgiopoulou and Nikos Prinos, have supported me, especially towards the tough last year of my studies. The funny moments, which I had with my fellow PhD students, have always been a pleasant break of the work, that I will not forget.

Moreover, I would like to thank the diploma students Konstantinos Bitos, Elina Kleisioti for their work and happy moments, we had together. Especially, I would like to thank my brother, Dimosthenis Plakias, who has also been a diploma student, for his work, advice and support towards these years.

Last but not least, I would like to thank the rest of my family: my mother who has always been listening and trying to understand my problems concerning my Ph.D. thesis, my father, who has always a funny way to make me think positively and especially Tasos, because of his encouragement, confidence in my abilities and patience. Finally, I would

like to thank all my friends and ex-coworkers Marina, Elpianna and Georgianna, and especially my friend Dimitra for her support and encouragement towards the years.

Anthi,

Athens, 2021

Χαλεπά τα καλά

Πλάτων

Table of Contents

List of Tables

List of Figures

List of Symbols-Abbreviations

AAD%   Average Absolute Deviation % $(\frac{1}{NP}\sum abs(exp-calc)*100)$

AARD%   Average Absolute Relative Deviation % $(\frac{1}{NP}\sum \frac{abs(exp-calc)}{exp}*100)$

α_{CO_2} CO_2 loading, moles CO_2/moles amine

α_{H_2S} H_2S loading, moles H_2S/moles amine

BPP   Bubble point pressure (bar)

BBT   Bubble point temperature (K)

c_1, c_2, c_3 Mathias-Copeman parameters for pure components

CCS   Carbon Capture and Storage

CN   Carbon number

D   dielectric constant

DIPPR   Design institute for Physical Properties

e-NRTL   electrolyte non-random two liquid activity coefficient model

EoS   Equation of State

EoS/G^E Equation of State coupled with activity coefficient models through advanced mixing rules

eUMR-PRU   electrolyte UMR-PRU

G   Gibbs free energy

GPA   Gas Processing Association

HC   Hydrocarbons

Hysys   Aspen Hysys

IP   Interaction parameters

KE   Kent-Eisenberg

LNG   Liquified natural gas

LPG   Liquefied petroleum gas

MC   Mathias-Copeman expression

MW	Molecular Weight
NG	Natural gas
NP	Number of data Points
NRTL	Non-random two liquid activity coefficient model
P	total pressure (bar)
PR	Peng-Robinson EoS
R	universal ideal gas constant
SRK	SRK
T	absolute temperature (K)
UMR-PRU	Universal mixing rules combined with PR and UNIFAC
VLE	Vapor-Liquid equilibrium
x	liquid phase mole fraction
y	vapor phase mole fraction

Greek Symbols

γ	activity coefficient
θ	surface area fraction
ϕ	volume fraction
ω	acentric factor

Subscripts

c	critical value
s	solvent mixture
in	initial
tot	total
exp	experimental
calc	calculated

Superscripts

E   excess property

R   residual term

C, SG   Staverman-Guggenheim contribution in combinatorial term

DH   Debye- Hückel term

1. Introduction

In this chapter, the scope and the research gaps, which this thesis fills, are discussed. Furthermore, the structure of this thesis is presented and the contents of each chapter are analyzed, in order the reader to get familiar with them.

Global warming is a worldwide problem and it has been recognized as a priority recently, as it is verified by the Paris Agreement, which is a convention between many countries to struggle for setting the boundaries to the temperature increase, below 2 degrees Celsius compared to the pre-industrial level. Human activities have resulted to global warming, due to the unrestrained increase of greenhouse gases, such as carbon dioxide, which is the main contributor, nitrous oxide and fluorinated gases. Transport and electricity are the two sectors that emit the largest amounts of carbon dioxide, whereas fossil fuel is the predominant energy source that they use. Natural gas is the cleanest one among fossil fuels and its use is increasing towards the years.

Acid rain is another worldwide problem, which is caused by sulfuric acids, and it has significant effect on materials, buildings, monuments and human health. The combustion of fossil fuels contributes to sulfur dioxide emissions to the atmosphere, whereas some industrial processes can result to hydrogen sulfide emissions to the atmosphere, which is rapidly oxidized to sulfur dioxide. Furthermore, hydrogen sulfide is toxic, corrosive for the equipment and can be lethal to human beings as well.

For all these reasons, combustion plants include specific processes for flue gases treatment, in order to remove carbon dioxide, whereas fuels are treated in order the sulfur emissions to be reduced as well. Natural gas is also treated, because acid gases reduce its heating value and they can be corrosive to the equipment. For a long period of time, researchers have been focused on the study of various technologies for acid gases removal and their optimization. The predominant one, is acid gas chemical absorption in aqueous alkanolamine solution, whereas there are many others, such as physical absorption, physical or chemical adsorption, hybrid processes etc. Chemical absorption is very effective, due to the chemical reactions taking place, even though its energy requirements in regeneration are high because of them.

Physical solvents have less energy requirements in regeneration than chemical absorption, but their operation is optimum at high pressures and low temperatures, a fact that increase the operating cost. For instance, refrigerated methanol has been proposed as a solvent for acid gas absorption and it is widely used in Rectisol process. Recently, ionic liquids have been proposed as appealing solvents, due to their unique properties, such as low vapor pressure, which renders them green solvents, no-corrosiveness, high thermal and chemical stability and low energy requirements in regeneration.

Process design and optimization is one of the main chemical engineering aspects, and it is of a great importance, in order to produce the required products with the most effective, environmentally friendly processes and with the lowest cost. For that purpose, accurate thermodynamic models are essential.

Acid gases solubility in aqueous alkanolamine solutions or in other solvents is described by many models in literature. Semi-empirical ones are easy to apply, but they lack an accurate thermodynamic framework. Activity coefficient models are rigorous, but they have limited prediction capability, whereas they need different equation for the prediction of liquid and vapor phases. Equations of state, in order to be used in non-ideal mixtures, are coupled with activity coefficient models and they have great prediction capability. In this case, the same equation can be applied for the description of the various phases, whereas equations of state (EoS) can predict not only the phase equilibrium but also various properties, such as densities, enthalpies, entropies, heat capacities, which play a vital role for the energy calculations in a process.

The scope of this thesis is the development of an EoS/G^E model able to describe accurately acid gases-water-alkanolamine and CO_2-ionic liquid mixtures, in order to be used for process simulation. For that purpose, UMR-PRU model, which has already been successfully applied to mixtures encountered in natural gas processing, such as hydrocarbons, nitrogen, water, alcohols and glycols, is extended to acid gases-water-alkanolamine mixtures. Two alkanolamines are studied: monoethanolamine and methyl-diethanolamine and fourteen ionic liquids, i.e. with anions BF_4^-, PF_6^-, Tf_2N^- and imidazolium-based cations in order to examine the effect of cation and anion on absorption efficiency. For UMR-PRU model extension to acid gases-water-alkanolamine mixtures, Debye-Hückel term has been added to account for long-range electrostatic forces. The simultaneous calculation of phase and chemical equilibrium, which is required for these mixtures, is the most challenging and stiff part of this thesis, due to algorithmic difficulties and the great number of intercorrelated parameters, needed to be estimated. UMR-PRU is successfully extended to these mixtures and it leads to results comparable to those of other widely used models presented in literature (electrolyte NRTL and Kent-Eisenberg). Furthermore, in order to extend UMR-PRU to CO_2-ionic liquid mixtures, it is necessary to have proper description of pure component properties, such as liquid density and vapor pressure. The correct prediction of both properties is an innovative step, because the scientific researchers focus only on the correct density description, although the prediction of extremely low vapor pressures for ionic liquids is vital, in order to correctly reproduce the physical absorption process with no solvent losses. The successful UMR-PRU model extension to the aforementioned mixtures comprises the next step towards the use of a single thermodynamic model for the description of the whole value chain of natural gas, whereas it is a first step towards the use of UMR-PRU in flue gases treatment.

After the extension of UMR-PRU model to these mixtures, it is incorporated in a process simulator (HYSYS V8.6 and UNISIM R451) through CAPE-OPEN protocol, in order to be

used for process simulation. Concerning the first category of mixtures studied, UMR-PRU is successfully incorporated in a process simulator, and it is tested in simple separators. Furthermore, the whole CO_2 absorption process is simulated by a thermodynamic package, proposed by the process simulator. Concerning the second category of mixtures studied, UMR-PRU has successfully been incorporated in UNISIM and it has been used for the simulation of CO_2 removal from natural gas by using an ionic liquid as solvent. The performance of the model in this process is compared to the one of Peng-Robinson EoS, whereas the solvent is compared to another physical solvent, i.e. methanol. CO_2 physical absorption using an ionic liquid has much lower energy requirements than the one with methanol, and it is proposed as an attractive alternative for these processes, if specific problems are overcome, especially the high viscosity of an ionic liquid. Therefore, an ionic liquid is mixed with methanol, in order to have an applicable, energy-effective and environmental-friendly solvent with high absorption capacity.

The structure of this thesis is as follows:

Firstly, the problem needed to be solved is presented. Therefore, acid gases, carbon dioxide and hydrogen sulfide origin and emissions are presented, whereas the origin and composition of natural gas and flue gases are analyzed as well (Chapter 2). The necessity of acid gas removal from flue gases and natural gas is well perceived in this chapter, whereas in the next one, the main processes that can be used for acid gas removal are reported, giving emphasis to the ones studied in this work and comparing the various solvents applicable to such processes (Chapter 3).

Following the problems caused by acid gases and the processes used, in order to overcome them, the problem from the thermodynamic perspective should be described. Therefore, in Chapter 4, the phase and chemical equilibrium problem is described and the algorithms used in literature and more specifically in this thesis are presented. After the problem presentation, the thermodynamic models applicable to such processes are discussed, and the extension of the UMR-PRU model in acid gases-water-alkanolamine mixtures is presented (Chapter 5).

Subsequently, the model development and its results are presented. In order to develop a proper thermodynamic model, the collection of the appropriate training and test datasets is necessary. Therefore, the evaluation of the database is presented and the results of eUMR-PRU model (UMR-PRU coupled with the Debye-Hückel term) for CO_2-H_2O-MEA, CO_2-H_2O-MDEA, CO_2-H_2O-MEA-MDEA and CH_4-CO_2-H_2O-MDEA are presented and compared to electrolyte NRTL (Chapter 6). Afterwards, the database and the results of eUMR-PRU model for H_2S-H_2O-MEA, H_2S-H_2O-MDEA, CO_2-H_2S-H_2O-MEA and CO_2-H_2S-H_2O-MDEA are presented and compared to those of a semi-empirical model (Kent-

Eisenberg) and an activity coefficient model (electrolyte-NRTL). Furthermore, mixtures containing H_2S and other gases or hydrocarbons also examined (Chapter 7).

In the next chapter (Chapter 8), the database and the results of UMR-PRU model in pure ionic liquids and in binary CO_2-ionic liquid mixtures are presented. Firstly, properties of pure ionic liquids are described (vapor pressure and liquid density). Secondly, the results of UMR-PRU in binary mixtures are compared to those of a modified Peng-Robinson equation of state. K_{ij} and l_{ij} interaction parameters are used as correlations of temperature and carbon number, in case of Peng-Robinson, whereas l_{ij} is also implemented in case of UMR-PRU.

After the presentation of the modeling results, it is necessary, UMR-PRU to be tested in a more applied task. For that reason, UMR-PRU is incorporated in a process simulator through CAPE-OPEN protocol in order to be used in process simulations. In case of eUMR-PRU, it is tested in flash tanks in H_2S-MEA-H_2O and H_2S-MDEA-H_2O mixtures and the solution of phase and chemical equilibrium by the process simulator is proved to be successful. UMR-PRU is used for the simulation of the whole CO_2 physical absorption process using ionic liquids and methanol and it is compared to Peng-Robinson EoS. Both ionic liquid and methanol are tested as solvents and a sensitivity analysis with focus on energy requirements is performed. The effect of the correct heat capacity calculations by the model regarding the energy requirements is also examined and it is proven that the calculation of both vapor-liquid equilibrium and thermodynamic properties, such as heat capacity, by a model (i.e. equation of state) is an incomparable advantage over other models. Furthermore, the process of CO_2 absorption in aqueous alkanolamine solution is also examined and a built-in simulator model is used. The results of all processes are compared to each other (Chapter 9).

Finally, the conclusions of this thesis are presented (Chapter 10) and possible future work, that can be performed in this subject is also proposed (Chapter 11).

2. Introduction to acid gases

This chapter provides a synopsis of the main problems caused by acid gases and specifically carbon dioxide (CO_2) and hydrogen sulfide (H_2S), which are examined in this thesis. Furthermore, flue gases emitted by industries are also analyzed, because they are the main contributors of CO_2 to the atmosphere, whereas natural gas is also examined, due to the concentration of acid gases in it and the necessity of their removal from it.

2.1. Introduction

Acid gas is any gaseous compound, which forms an acidic solution, when it is dissolved in water. Two of the main constituents of acid gases are carbon dioxide and hydrogen sulfide. Carbon dioxide exists naturally in atmosphere due to the carbon cycle and it is vital for animals and human beings. However, it is also emitted by human activities, such as transportation, electricity and industry. Among all industries, fossil fuel industries emit the largest amounts, about 33-40 % of the total[1]. Carbon dioxide, among other greenhouse gases, is responsible for global warming and for this reason it has been decided to be reduced worldwide.

Hydrogen sulfide exists naturally in atmosphere and it is formed from anaerobic decomposition of organic sulfur components by bacteria, but it is also emitted anthropogenically due to the combustion of fossil fuels and specific industrial processes, such as desulfurization. Hydrogen sulfide is highly toxic and dangerous for humans and animals, corrosive to the equipment, whereas it also has a negative environmental impact, due to acid rain and hence it should be removed.

Except for the removal of CO_2 from flue gases for environmental and health issues, acid gases should also be removed from fossil fuels, such as natural gas. Natural gas consists of hydrocarbons, mainly methane, but it also has quantities of hydrogen sulfide and carbon dioxide. These two substances reduce its heating value and may cause problems to the equipment.

In this chapter, the most significant problems, caused by both substances, are presented in detail and their emission sources are discussed, whereas an analysis of flue gases and natural gas is also given.

2.2. CO$_2$ emissions and global warming

Carbon is an essential component for life and it is able to move around between seawater, atmosphere, rocks, plants and animals during the carbon cycle. It moves from the atmosphere, where it exists as carbon dioxide, to the plants, through photosynthesis, and to the oceans, where it is absorbed by living material. Afterwards, it is moved from plants to animals, through food chain, whereas it moves from both plants and animals to soil, rocks etc., and finally from living things back to atmosphere through respiration. The described process is known as the carbon cycle[2].

Carbon concentration has been almost steady for many years, due to the carbon cycle. Nevertheless, the carbon cycle has been affected by human activities, especially after the Industrial Revolution. The main activity, which results to changes in carbon cycle is burning of fossil fuels. Without human intervention, the carbon existence in fossil fuels would not be a problem, because of its slow leakage into the atmosphere. However, burning fossil fuels results to rapid release of carbon into the atmosphere, some proportion of which, will remain there. In Figure 2.1, the main human activities, which resulted to CO$_2$ emissions in US in 2018, are depicted.
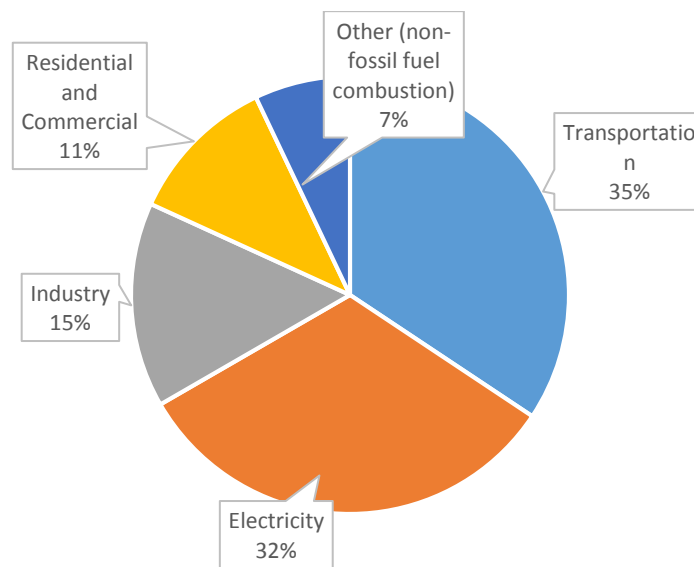
Figure 2.1: The proportion of human activities in CO$_2$ emissions in US in 2018[3].

The main activity which results to high CO$_2$ emissions, is transportation. Movements of goods and people by vehicles are included in this sector, which emit mainly carbon dioxide, as a result of combustion of fossil fuels, such as gasoline in internal combustion engines. Electricity is another sector, which emits large amounts of CO$_2$, whereas industry follows. The electricity sector involves production, transmission and distribution of electricity, while the industry sector includes the production of goods and materials. CO$_2$ emissions of this sector can be direct, i.e. emissions generated mainly by the combustion

of fossil fuels for energy production and by leaks in industrial processes, or indirect, which are generated by burning of fossil fuels in order to produce electricity, that is used to power industrial buildings and facilities[3].

Carbon dioxide is one of the main greenhouse gases and plays a vital role to the temperature of Earth. Greenhouse gases absorb emitted energy and they re-emitted it to many directions. One of these energy types is heat, which in some point is re-emitted to the surface of Earth and results to a higher temperature[4]. Global warming is a worldwide problem, which already affects people, and it is an emergency for countries to act, a fact that has been recently confirmed by the Paris Agreement.

The Paris Agreement is a convention between many nations worldwide to make a great effort to struggle climate change by keeping the temperature increase below 2 degrees Celsius above the level of pre-industrial era, whereas the ideal goal is to keep it below 1.5 degrees Celsius. Furthermore, this agreement aims to make the countries able to handle the impacts of climate change and for that purpose, financial, technological support and an improved building framework will be provided even to most vulnerable countries[5].

To this effort, greenhouse gases, which are mainly carbon dioxide, methane, nitrous oxide and fluorinated gases, must be reduced. In 2018, carbon dioxide constituted the 81% of the greenhouse gas emissions, whereas methane constituted the 10%.

2.3. H_2S emissions

Hydrogen sulfide is a colorless gas with unpleasant smell, which is present in atmosphere and it has a great impact on the climate. It is naturally formed from volcanoes, geothermal vents, ponds and coastal wetlands, where bacteria, during anaerobic decomposition of organic sulfur components, produce it. Except for natural sources, the presence of hydrogen sulfide in the atmosphere is also a consequence of production and industrial processes and mainly of the combustion of fossil fuels. It is worth mentioning, that human activities emit larger amount of sulfur gases than natural sources, mostly in the form of SO_2[6].

A process, which principally produces H_2S, is hydrodesulfurization of gas streams in oil refineries with hydrogen. This process is used in order to remove sulfur from feedstocks:

$$[S]_{content}+H_2 \rightarrow \text{Hydrocarbon product} + H_2S$$

Hydrodesulfurization is an established technology for sulfur removal from crude oil, gasoline, kerosene and diesel oil. This process takes place at high temperatures (290-455 °C), high pressures (150-3000 psi) and uses gas hydrogen and metal catalysts[7].

This process is necessary for the reduction of sulfur content of automobiles fuels as well, because sulfur components lead to emission of sulfur oxides to atmosphere, which has an unfavorable effect on environment, whereas sulfur compounds can also deactivate metal catalysts. For all these reasons, hydrodesulfurization is an essential process[8].

When H_2S is released to the atmosphere, it is rapidly oxidized by atmospheric oxidants to SO_2 and finally sulfate. Therefore, the amounts of H_2S in the atmosphere are small, even though they may be high near volcanoes or in regions with highly polluting industrial activity[6].

Hydrogen sulfide is toxic and corrosive. It irritates eyes, nose and throat at about 5 ppm. At 30 ppm human cannot smell it and this can be misinterpreted as a safe condition. However, above this concentration, it is quickly absorbed by blood and it has as a result poor oxygen uptake. At 1000 ppm it is fatal[8]. In Table 2.1 the main effects of H_2S on human health are presented.

Table 2.1: The effects of various concentrations of H_2S on human health[9]

H_2S concentration in ppm	Symptoms
0.00011-0.00033	Typical concentrations
0.01-1.5	Rotten egg smell, firstly noticeable
2.0-5.0	Nausea, eyes tearing, headaches in prolonged exposure
20	Exhaustion, headache, irritability, dizziness
50-100	Inflammation of eyes, respiratory tract irritation, digestive problems
100	Loss of smell after 2-15 minutes, changes in breathing, throat irritation, increase in severe symptoms after some hours, death after 48 hours
100-150	Loss of smell
200-300	Serious inflammation of the eyes and respiratory tract irritation after 1 hour.
500-700	Collapse after 5 minutes, serious eye problem after 30 minutes, death after 30-60 minutes
700-1000	Unconsciousness, death within minutes
1000-2000	Instant death

Sulfur dioxide can cause acid rain when it is emitted to the atmosphere. It reacts with oxygen and water, forming sulfuric acids, which are then mixed with water or other materials and they fall to the ground as wet or dry deposition, a fact that may be harmful for soil, ponds, forests etc. Wind can contribute to SO_2 travel over long distance and this renders acid rain a worldwide problem. Acid rain has negative effects on ecosystems,

water and soil, because of the leaching of aluminum, which, in combination with acid water, affects fishes, eggs, animals and plants. It has impact on materials as well, because it can damage metal, paint and stone, a fact that affects buildings and monuments. Moreover, It has unfavorable effects on human health, when SO_2 reacts and forms sulfate, which is found, by many studies, to be connected to heart attacks and problematic lung function, especially to people, who suffer from preexisted health problems[3].

As it has been previously mentioned, CO_2 is emitted mainly by combustion of fossil fuels and therefore its removal from flue gases is examined in this work. Furthermore, CO_2 and H_2S removal from natural gas is also examined, because H_2S is corrosive for the equipment and both acid gases reduce its heating value.

2.4. Flue gases composition

Flue gases are the gases, which are derived from combustion plants and they consist of fuel and combustion air, as well as other substances, such as dust, sulfur oxides, carbon dioxide, carbon monoxide, nitrogen oxides, water vapor, oxygen, sulfur dioxide etc. The main constituents of flue gases are presented in Table 2.2. The exact composition of the flue gas depends on the type of fuel and the conditions during combustion. However, generally they consist mainly of nitrogen (60 % v/v), because of the use of air as oxidant in the combustion process. They also contain significant quantities of carbon dioxide, vapor water and oxygen.

Table 2.2: Constituents of flue gases[10]

Components	Remarks
N_2	The main component of combustion air, not produced during combustion
CO_2	Produced during all combustion processes
Vapor water	H_2 in fuel reacts with O_2 and forms water
O_2	Oxygen which was not consumed during combustion
CO	Formed during incomplete combustion
NO_x	Nitrogen of fuel and of air reacts with oxygen of air and forms NO_x
SO_2	Formed through oxidation of the sulfur that is presented in fuel
H_2S	Component of crude oil and natural gas, emitted by some industrial processes
Hydrocarbons	Occur in crude oil, natural gas, and coal; formed through incomplete combustion processes
Hydrocyanic acid	Toxic liquid, exists in flue gases of incineration plants
Ammonia	Component of flue gases in denitrification plants
Hydrogen halides	In flue gases from coal combustion and waste material
Solids	Oxides of silica, Aluminum, Calcium generated from incombustible components of fuels

The main problem of flue gases is that they contain small quantities of pollutants, such as carbon monoxide, nitrogen oxides, and sulfur oxides. For that reason, they are usually treated by some chemical processes[10].

As it has been presented in previous section, electricity generation results to very high CO_2 emissions, hence flue gases from electric power plants are one of the main sources of CO_2 emissions and they should be further examined. Electricity, at most electric power stations, is produced by the use of mechanical energy in order to rotate the shaft of electromechanical generators. This mechanical energy can be produced by converting the chemical energy from fossil fuels combustion, kinetic energy from water, wind etc., thermal or solar energy. The use of fossil fuels has been decreased during the last years in electricity production, but they still remain the main source[11]. The process to generate electricity by burning of fossil fuels can be one of the following:

- The fuel is burned and gases flow through a reboiler, where water is converted to steam, in order its energy to be used to turn a generator of a turbine. Afterwards, steam is condensed and recycled back to the reboiler, in order to repeat the process. This plant is called steam turbine power plant and its disadvantage is the highly pollutant emissions.
- The gases of burning fossil fuels can be directly used, in order to turn the generator of a turbine. This is called gas turbine and the fuel can be either natural gas or another fossil fuel. This method is less energy efficient, but lower amounts of pollutants are emitted.
- In order to combine the advantages of both methods, combined cycle has been proposed. In this process, there is a gas turbine, which operates in the way previously described and the hot gases, which have been produced, are used in order to generate steam and produce electricity, by turning the generator of a second turbine[9].

2.5. Natural gas consumption

For a long period of time, human relied on muscles of human or animals and on combustion of wood. However, after the industrial revolution, fossil fuels, such as oil, coal or gas, play the most important role in energy systems worldwide.

Despite their vital role in our technological, economic and social development, they also have some disadvantages, such as their contribution to air pollution and the production of CO_2, which affects the global climate change. Therefore, in recent years, renewable energy sources have gained increasing attention[4].

In Figure 2.2, the worldwide energy supply by fuel type during the period 1990-2015 is depicted. The energy consumption is increasing worldwide towards the years and there is a low increasing use of wind and solar energy but the dominant role is still being played by fossil fuels, which cover constantly the 75% of the total energy consumption worldwide. Among fossil fuels, the use of natural gas is increasing towards the years[12].

Natural gas is a hydrocarbon mixture, odorless, achromic and non-toxic. It is used for heating, cooking, as a fuel in power stations, as a fuel in some industrial processes, and as an ingredient in paints and plastics.

Natural gas has many advantages, compared to other fossil fuels. Firstly, there is in large quantities. According to the International Energy Agency, there are enough resources for about 230 years. It is flexible. For instance, a gas-fired power station needs less time to start and stop compared to a coal-fired plant, hence it can be easier used in conjunction with renewable energy sources such as solar and wind. Furthermore, it is the cleanest fossil fuel, because it produces the half amount of carbon dioxide and one-tenth of the air pollutants compared to coal, when it is burned to produce electricity. Therefore, it can be used nowadays, in order to reduce CO_2 emissions. The CO_2 emissions in 2018 from the combustion of various fuel types at over 190 countries worldwide are depicted in Figure 2.3[12].
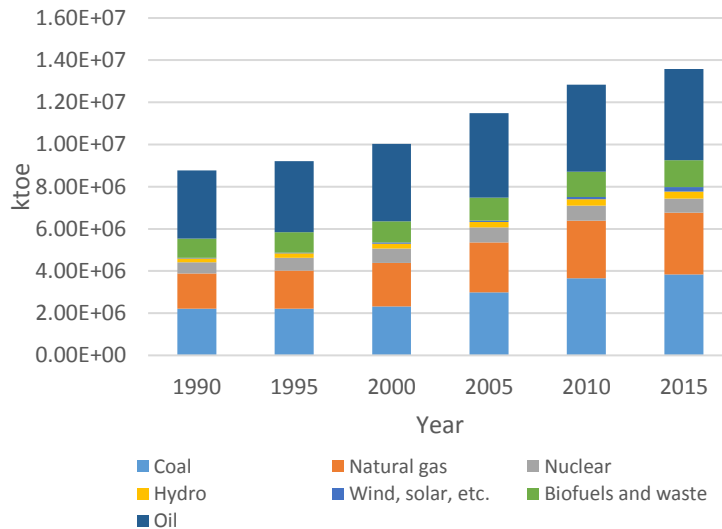
Figure 2.2: Worldwide energy supply by fuel type in 1990-2015[13]

.
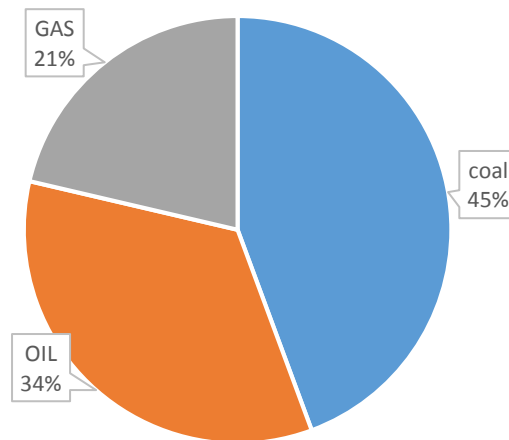
Figure 2.3: CO$_2$ emissions in 2018 from combustion of various fuel types at over 190 countries worldwide[14]

2.6. Origin of natural gas

There are various theories about the origin of fossil fuels. The most widely spread one about the origin of natural gas is that it has been formed by the decomposition of organic matter, such as animals, plants and microorganisms, which were trapped into sediments over a long period of time[15]. According to a theory, fossil fuels are formed, when the organic matter is compressed under the earth shell at high pressure. This is technically named thermogenic methane. The compressed organic matter is decomposed at high temperatures under the earth crust and natural gas is formed[16].

According to another theory, natural gas can be formed closer to the earth surface, because of the action of bacteria and microorganisms[15] and this is called biogenic methane. This kind of methane is usually dissolved into the atmosphere, but in some cases, it can be trapped under the earth surface and recovered as natural gas[16].

In consonance with a third theory, natural gas can be formed without the presence of animals, plants or microorganisms, during processes that take place at deeper depths, where there is gas with high content of hydrogen and carbon molecules. During this process, rising to the surface of earth gas interacts with mineral compounds in absence of oxygen and reactions take place, which result to the formation of nitrogen, carbon dioxide, oxygen, water, argon. This process is called abiogenic and the methane formation will take place at high pressures like thermogenic methane[16].

2.7. Natural gas value chain

The natural gas value chain consists of various processes, which can be classified into three groups: upstream, midstream and downstream. Upstream term refers to exploration and production, which includes searching for potential gas fields, drilling and operating the wells, and bringing the raw natural gas to the surface. Midstream term includes the gas plant, the LNG production and regasification and the transport systems. In midstream processes, the major processing occurs, whereas downstream processes include the refining and distribution of the final product to the consumers[18].

The liquefied natural gas (LNG) value chain is depicted in the Figure 2.4.
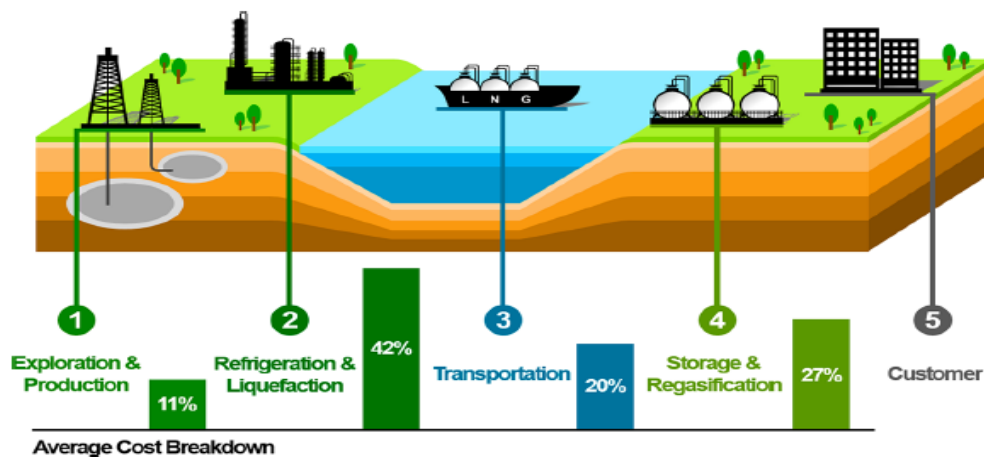
Figure 2.4: Value chain of liquefied natural gas[17].

In case of LNG, refrigeration and liquefaction is the most expensive process, as it is depicted in Figure 2.4, because it takes place under cryogenic conditions[17].

2.8. Natural gas composition

Natural gas consists of hydrocarbon and non-hydrocarbon components and it is a gas at atmospheric temperature and pressure. There are hundreds of different compounds, which may be components of natural gas, but its main compounds are methane, ethane, propane, butane, pentane and traces of hexane or even heavier hydrocarbons. It is also usual for many natural gases to contain nitrogen, carbon dioxide, hydrogen sulfide, mercaptans, carbon disulfide etc. There can be also present several components in trace quantities, such as argon, hydrogen, helium and metallic substances, such as arsenic,

selenium, mercury and uranium. Table 2.3 shows the composition of various natural gas reservoirs in several countries.

According to the composition of natural gas, it can be classified into several categories. Depending on the proportion of hydrocarbons heavier than methane, it can be dry, wet or condensate. Dry natural gas is mainly composed of methane, whereas other hydrocarbons have been removed. Wet natural gas consists of methane and other hydrocarbons and it forms a liquid phase during production at surface conditions. Condensate gas has high quantities of hydrocarbon liquids and forms a liquid phase in the reservoir during production.

Natural gas can also be classified into lean or rich according to the amount of liquids, which can be recovered. These liquids are either ethane and heavier components or propane and heavier components. Lean natural gas has less than 2 GPM (gallons of liquids recoverable per 1000 standard cubic feet) liquid content, whereas rich natural gas has 2-5 GPM and very rich natural gas has >5 GPM liquid content.

Another classification of natural gas is sweet or sour natural gas, according to its H_2S and CO_2 content. Sweet natural gas has usually less than 4 ppmv H_2S, whereas CO_2 is about 3-4 mol %[15].

Table 2.3: Composition of natural gas reservoirs in different parts of the world (volume percent basis)[16]

Components	Laeq (France)	Groningen (Netherlands)	Uthmaniyah (Saudi Arabia)	Ardjuna (Indonesia)	Uch (Pakistan)
Methane	69	81.3	55.5	65.7	27.3
Ethane	3	2.9	18	8.5	0.7
Propane	0.9	0.4	9.8	14.5	0.3
Butane	0.5	0.1	4.5	5.1	0.3
C_5+	0.5	0.1	1.6	0.8	
Nitrogen	1.5	14.3	0.2	1.3	25.2
Hydrogen Sulfide	15.3	-	1.5	-	-
Carbon Dioxide	9.3	0.9	8.9	4.1	46.2

2.9.   Natural gas processing and specifications

In order to be available to the market, natural gas must be processed and transported after its collection. As it has been in section 2.8 mentioned, natural gas gathered from the well, contains hydrocarbon and non-hydrocarbon components, such as water, carbon dioxide, hydrogen sulfide and many other impurities. Therefore, in order to purify natural

gas, it is collected and transmitted through pipelines to the processing plant, even though some processing takes place near the well. The scope of the processing plant is to separate natural gas from associated hydrocarbon liquids, acid gases, and water, in order to satisfy the emission regulations and pipeline specifications. Table 2.4 presents some typical natural gas specifications according to DESFA[19].

Table 2.4: Natural gas specifications[19]

Characteristics	Specification
Wobbe index	13.066-16.328 kWh/Nm^3
Gross Calorific Value (GCV)	10.174-13.674 kWh/Nm^3
Relative density	0.56-0.71
Water Dew Point	+5 °C maximum at 80 bar
Hydrocarbons Dew Point	+3 °C maximum at 80 bar
Components	
Methane	75 % mole minimum
Carbon dioxide	3 % mole maximum
Nitrogen	6 % mole maximum
Oxygen	0.2 % mole maximum
Hydrogen Sulfide	5.4 mg/Nm^3 maximum
Total Sulphur Content	80 mg/Nm^3 maximum

The specifications must be met, in order the natural gas to be of high quality, safe and clean fuel gas for the customers. Furthermore, it has to meet the heating value specifications in order to achieve optimum operation of gas turbines and combustion engines and reduced emissions. A small change on product specifications may have a significant effect on cost and operating conditions of the processing plant[20].

Raw natural gas contains different hydrocarbons, carbon dioxide, hydrogen sulfide, nitrogen, water and others. It can either originate from crude oil reservoirs (associated gas), gas wells or condensate wells (non-associated gas). It can also come from unconventional sources, such as coal seam or offshore wells. The composition of natural gas depends on the origin source. Gas wells usually produce sour gas, while condensate ones produce natural gas condensate and unconventional sources produce rich in CO_2 and nitrogen gas. In order to remove impurities and meet the specifications previously mentioned, raw natural gas must be processed. When natural gas is rich in heavy hydrocarbons, they must be removed in order to meet the heating value specifications. Propane and butane can be sold as liquefied petroleum gas (LPG), whereas C_5+ can be used as a stock for gasoline.

The treatment process of natural gas differs according to the composition of raw gas and the components needed to be recovered. For instance, Figure 2.5 depicts the treatment process of a lean natural gas with a small amount of C_2+ hydrocarbons.
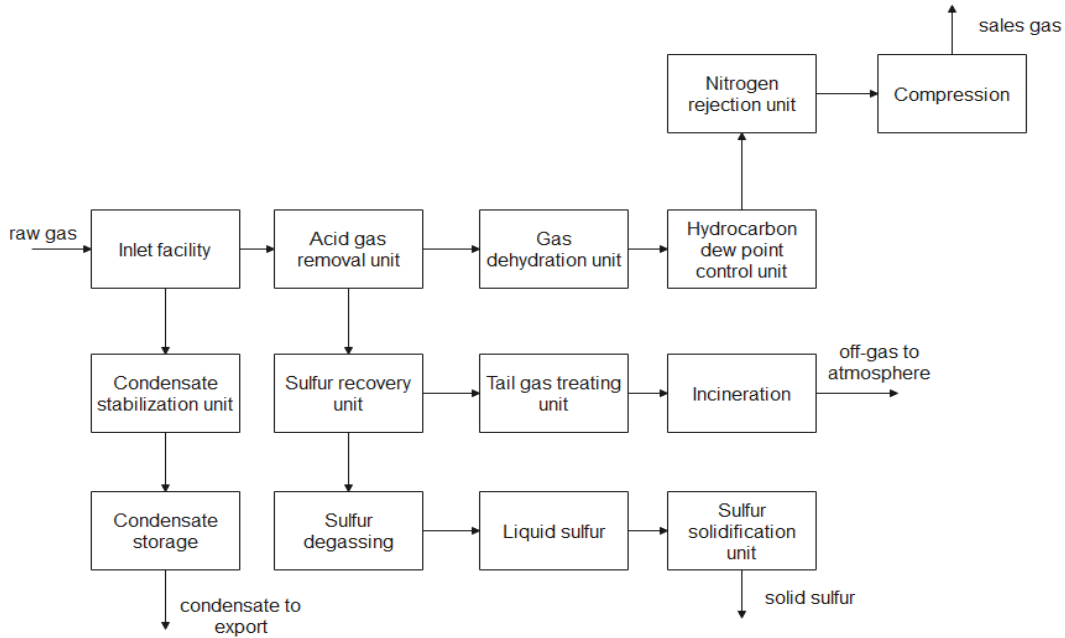
Figure 2.5: Treatment process of a lean natural gas with a small amount of C2+ hydrocarbons[15].

Inlet facility includes slug catcher, separation equipment, and pressure protection system in order to protect the gas plant from emergency conditions. Specifically, the gas produced by the slug catcher, which includes a phase separator and a liquid storage vessel, is fed to a high-pressure separator and then to a sour water stripper unit, where the water content of the liquids is sent to. The water contains monoethylene glycol, which is used for hydrate control and can be recovered in a MEG reclamation unit. The condensate stabilization unit is used to remove light hydrocarbons and H_2S, in order to meet the export condensate specifications. Acid gas removal unit is used to remove acid gases, in order to meet the sales specification values for CO_2 and H_2S. In case of non-existence of a facility of sulfur injection to reinjection wells, acid gas is processed in a sulfur recovery unit, in order to achieve H_2S removal and to meet the emission target. The sweet gas from the acid gas removal unit enters the gas dehydration unit, in order to meet the water dew point specification. Then, it enters the hydrocarbon dew point control unit and nitrogen rejection unit and finally it enters the compression unit to meet the pressure pipeline requirements[15].

2.10. Conclusions

Fossil fuels and flue gases from industrial plants are two of the main sources of hydrogen sulfide and carbon dioxide. Acid rain and global warming are the major environmental problems caused by them. In addition, the toxicity of hydrogen sulfide, the danger for human health and the corrosion to the equipment caused by both substances make their removal to be an imperative need. Therefore, the main removal processes used nowadays and the ones examined in this work are analyzed in next chapter.

2.11. References

1.	Yang, H.; Xu, Z.; Fan, M.; Gupta, R.; Slimane, R. B.; Bland, A. E.; Wright, I., Progress in carbon dioxide separation and capture: A review. *Journal of Environmental Sciences* **2008,** *20* (1), 14-27.

2.	University Corporatioon for Atmospheric Research. https://scied.ucar.edu/carbon-cycle.

3.	Enviromental Protection Agency. https://www.epa.gov/ghgemissions/overview-greenhouse-gases.

4.	https://earthobservatory.nasa.gov/.

5.	United Nations Framework Convention on Climate Change. https://unfccc.int/process-and-meetings/the-paris-agreement/the-paris-agreement.

6.	Ausma, T.; De Kok, L. J., Atmospheric H2S: Impact on Plant Functioning. *Frontiers in Plant Science* **2019,** *10* (743).

7.	Speight, J. G.; El-Gendy, N. S., *Introduction to petroleum biotechnology*. Gulf Professional Publishing: 2017.

8.	Shah, M. S.; Tsapatsis, M.; Siepmann, J. I., Hydrogen sulfide capture: From absorption in polar liquids to oxide, zeolite, and metal–organic framework adsorbents and membranes. *Chemical reviews* **2017,** *117* (14), 9755-9803.

9.	U.S. Department of Labor. https://www.osha.gov/SLTC/hydrogensulfide/hazards.html.

10.	Speight, J. G., 3 - Unconventional gas. In *Natural Gas (Second Edition)*, Speight, J. G., Ed. Gulf Professional Publishing: Boston, 2019; pp 59-98.

11.	Agency, U., Available and emerging technologies for reducing greenhouse gas emissions from coal-fired electric generating units. 2012; pp 33-86.

12.	Shell. https://www.shell.com/energy-and-innovation/natural-gas/natural-gas-and-its-advantages.html.

13.	International Energy Agency. https://www.iea.org/world-energy-balances-and-statistics.

14.	Agency, I. E. CO2 Emissions from Fuel Combustion: Overview. https://www.iea.org/reports/co2-emissions-from-fuel-combustion-overview.

15.	Mokhatab, S.; Poe, W. A., *Handbook of natural gas transmission and processing*. Gulf professional publishing: 2012.

16.	Shimekit, B.; Mukhtar, H., Natural gas purification technologies-major advances for CO2 separation and future directions. *Advances in natural gas technology* **2012,** *2012*, 235-270.

17.	Lee, I.; Park, J.; Moon, I., Key issues and challenges on the liquefied natural gas value chain: a review from the process systems engineering point of view. *Industrial & Engineering Chemistry Research* **2017,** *57* (17), 5805-5818.

18.	Devold, H., Oil and gas production handbook. *An introduction to oil and gas production, transport, refining and petrochemical industry. Oslo* **2013**, 152.

19. Hellenic Gas Transmission System Operator S.A. https://www.desfa.gr/en/regulated-services/transmission/pliroforisimetaforas-page/natural-gas-quality-specification.

20. Poe, W. A.; Mokhatab, S., *Modeling, control, and optimization of natural gas processing plants*. gulf professional publishing: 2016.

3. Acid gas removal processes

In this chapter, the various processes for acid gas removal are discussed and emphasis is given to chemical absorption with use of aqueous alkanolamines and physical absorption with use of methanol, whereas a specific reference is given to an innovative process, i.e. physical absorption with use of ionic liquids as solvents, which are beneficial as compared to organic solvents.

3.1. Introduction

In Chapter 2 the main reasons, why CO_2 should be removed from flue gases have been presented in detail. The need for its removal becomes an imperative, due to its negative impact on climate change and global warming. Furthermore, both CO_2 and H_2S should be removed from natural gas, due to their effect on its heating value and the equipment. For the aforementioned reasons, acid gas removal process is a necessary part of an industrial plant.

Various technologies have been proposed towards the years for that purpose. Concerning flue gases, these processes can take place before, during or after the combustion. The most well-known processes are: chemical absorption, physical absorption, hybrid processes, solid bed adsorption, membrane separation and cryogenic fractionation. Nowadays, chemical absorption process in aqueous alkanomamine solutions dominates the market. However, some disadvantages such as the high energy requirements or the solvent losses of this process have as a result the increased research interest in other processes, such as physical absorption process in ionic liquids. Each solvent has benefits and drawbacks and the proper selection of process and solvent is case-dependent.

In this thesis, chemical and physical absorption processes are studied. For each one, various solvents have been proposed and each of them has advantages and disadvantages. In the first case, aqueous alkanolamines, i.e. monoethanolamine (MEA) and methyldiethanolamine (MDEA), have been chosen as solvents, in order to combine the benefits of a primary and a tertiary alkanolamine. In the second case, methanol, due to its wide use, and ionic liquids, as innovative solvents, have been studied and compared to each other.

Much research work has been devoted to chemical absorption in aqueous alkanolamine solutions. Some of the researchers[1-2] have used aqueous methyldiethanolamine as solvent, others[3-4] aqueous monoethanolamine, whereas in some studies[5-6] blends of aqueous alkanolamines have been used. Methanol as a solvent for acid gas physical absorption has also been studied[7-8], whereas ionic liquids in acid gas removal is a recent field of study[9-10]. However, comparative studies of different processes are very rare (for instance the work of Taheri et al[11]), whereas no comparison of the three processes has been found in literature. Therefore, in this thesis, the three processes are compared to each other.

3.2.   Acid gas capture from flue gases

There are three types of processes for CO_2 capture from flue gases, which are represented in the Figure 3.1:
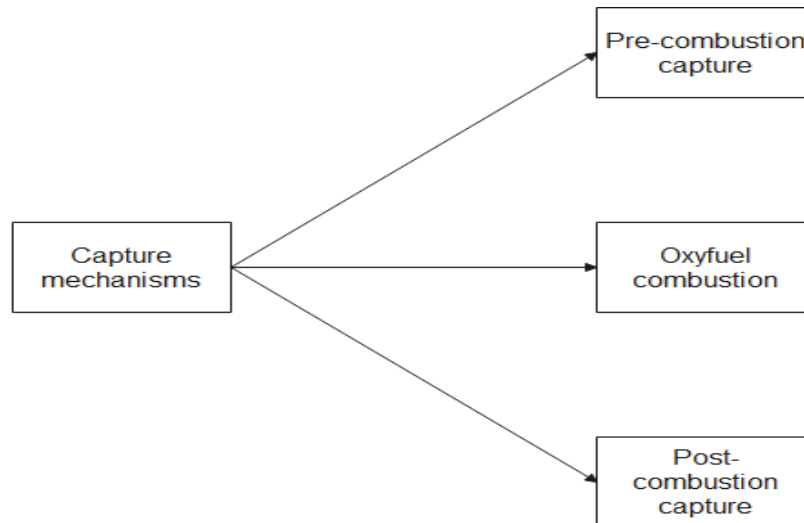
Figure 3.1: Acid gases removal mechanisms from flue gases[12].

- In pre-combustion capture, the carbon, which is contained in the fuel is removed before the combustion. This process includes the reaction of a fuel with air and steam in order to produce a fuel gas, which consists mainly of carbon monoxide and hydrogen. Carbon monoxide reacts with steam in a catalytic reactor in order to produce carbon dioxide and more hydrogen. Carbon dioxide is then captured by physical or chemical absorption and a rich-in-hydrogen fuel is produced[13].
- Oxyfuel combustion is the combustion process with an excess of oxygen, instead of air, a fact that leads to extremely high temperatures. However, these temperatures can be controlled by the recycle of some proportion of flue gases back to the furnace. This process consists mainly of an air separation unit for oxygen production, a boiler or a gas turbine, where the combustion and the generation of power takes place, a flue gas processing unit, where the flue gas is cleaned and sulfur content is removed and finally a CO_2 processing unit. The main advantage of this process is the insignificant production of NO_x, because of the absence of air[14].
- The post-combustion capture involves the acid gas removal after the combustion, i.e. from fuel gases. The technologies used for this purpose are described in the next section.

3.3. Conventional acid gas removal technologies

The acid gas removal technologies, which are traditionally used for natural gas treatment or in post-combustion capture in flue gases treatment, can be categorized as follows:

Chemical absorption process: In this process, acid gas reacts with a solvent and forms chemical dissolved compounds. The most common used solvent is an alkanolamine solution. Afterwards, the solvent is regenerated in a stripper column by the reversal of the chemical reactions at reduced pressures and high temperatures. Chemical solvents are preferred at low partial pressures and low acid gases concentrations[15]. This process is described analytically in next section.

Physical absorption process: In this process, acid gases are absorbed in a solvent physically, without a chemical reaction, due to their solubility. This process is most effective at high pressures and low temperatures, because the solubility of acid gases rises with an increase in pressure and a decrease in temperature, a fact that renders this process more expensive, concerning the capital and operating costs, than chemical absorption process. Physical absorption is used for the removal of high quantities of acid gases in contrast to chemical absorption [15]. Physical solvents are not corrosive and can be regenerated by pressure reduction. However, they absorb a high quantity of hydrocarbons and therefore they are used mainly in cases with low or no concentration of hydrocarbons, such as treating synthesis gas. Commonly used physical solvents are propylene carbonate, dimethyl ether of polyethylene glycol, methanol and N-Methyl-2-pyrrolidone[16]. Ionic liquids have been proposed recently as possible solvents for acid gas physical absorption, due to their unique properties. Their properties and the process of acid gas physical absorption with use of methanol and ionic liquid as solvent are described analytically in next sections.

Hybrid process: It is a common fact, to combine a physical and a chemical solvent in order to acquire the advantages of both processes. This process utilizes the high acid gas solubility in a physical solvent and the reactivity of a chemical solvent in order to achieve extremely low acid gas concentrations[15].

Solid bed adsorption process: In case of physical adsorption, the forces between the adsorbent and the adsorbate are not as strong as in chemical adsorption. In the first case, the adsorbent can be rectified by simple raise of temperature or reduce of partial pressure, whereas in case of chemical adsorbent, the process is called chemisorption and the pressure reduction is not enough for desorption. Therefore, physical adsorption is preferred, due to its low energy consumption in regeneration. Commonly used adsorbents are molecular sieves, silica gels and activated alumina[16].

Membrane separation process: In case of high acid gases concentrations and large flows, the membrane separation process is suggested[15]. This process consists of polymeric membranes and it separates the acid gases by selective penetration. The gas dissolves in membrane and moves under a partial pressure gradient. Membranes installation is not expensive and the operating and maintenance cost is low. However, hydrocarbon losses due to their penetration is a major problem of this process.

Cryogenic fractionation: In this process acid gases are cooled at very low temperatures, in order CO_2 to be liquified and hence separated, which leads to high energy requirements for refrigeration. Furthermore, dehydration of gas is needed in order to avoid hydrates formation[16].

These processes are well depicted in Figure 3.2.
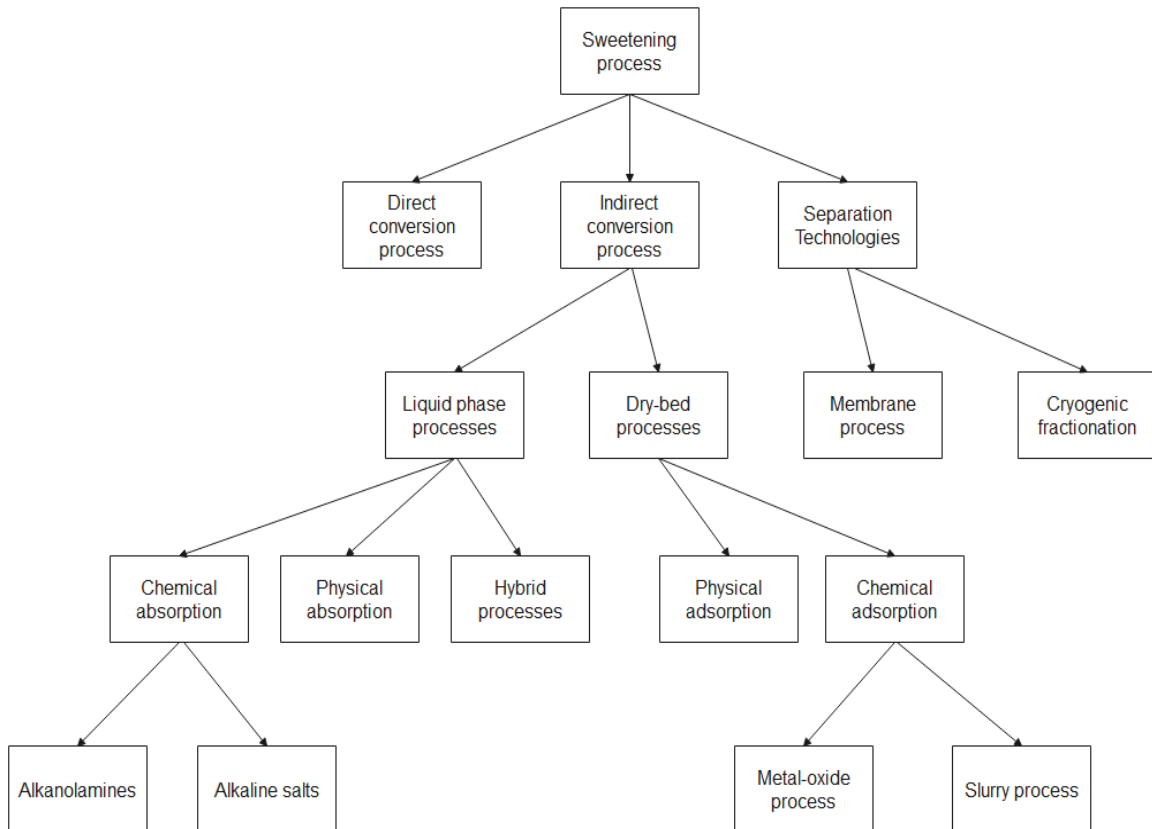
Figure 3.2: Gas sweetening processes[16]

The selection of the process depends on many factors, for instance the composition of the sour gas and the contaminants, the amount of hydrocarbons, the sweet gas purity specifications, the capital and operating cost and the selectivity needed[17].

For instance, in Figure 3.3 acid gas solubility in physical solvents is compared to the one in chemical solvents. Acid gas loading in x-axis denotes the moles of CO_2 per moles of amine, which have been absorbed in liquid phase. As it is depicted, acid gas solubility in liquid phase is higher in chemical solvents in case of low acid gas partial pressures, whereas it is greater in physical ones, in case of high acid gas partial pressure. However, the absorption of hydrocarbon in physical solvents is an issue, which should also be examined, in case of raw gases with high hydrocarbon concentration.
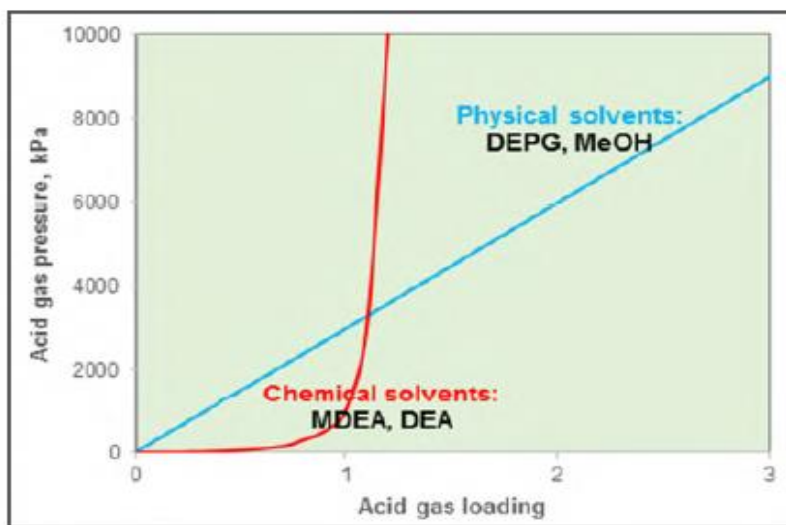
Figure 3.3: Comparison of acid gases solubility in chemical and physical solvents[18]

Therefore, in this thesis both physical and chemical solvents are examined, whereas in case of physical solvents a well-established one (methanol) is compared to an innovative one (ionic liquid) for acid gas treatment. Three acid gases removal processes are examined, which are analytically described in the following sections: chemical absorption with use of aqueous alkanolamines as solvents, physical absorption with use of methanol and physical absorption with use of ionic liquid.

3.3.1. Chemical absorption process

The chemical absorption process can take place by using two different kind of solvents: alkanolamine solutions and potassium carbonate solution. Chemical absorption using aqueous alkanolamine solution is the most common one.

3.3.1.1. Alkanolamines

When inspecting solvents for acid gas absorption, it is important to consider the following important factors:

- Absorption rate: A high absorption rate results to reduced height of the absorption tower and therefore to a reduced capital cost.
- Absorption capacity: A solvent with high acid gas solubility results to lower volume of solvent needed, in order to achieve the predefined gas purity.
- Solvent volatility: The high solvent volatility results to solvent losses, which is undesirable due to economic and environmental reasons.
- Solvent heat of absorption: A low heat of absorption is needed, because it results to lower energy consumption in the reboiler of stripping column.
- Solvent stability: High stability is needed, in terms of thermal decomposition and oxidative degeneration.
- Solvent price: The price of the solvent affects directly the cost of the process.
- Solvent toxicity: The solvent has to be non-toxic for human health and environment[19].

The most common solvent for chemical absorption process is an aqueous alkanolamine solution. More specifically monoethanolamine, diethanolamine and methylidiethanolamine are the most commonly used alkanolamines for the acid gas removal process. Alkanolamines have a weak basicity, which results from the amine function, and it is useful for the removal of the acid gases[17], which dissociate in an aqueous solution forming weak acids.

The alkanolamines can be grouped by the degree of replacement of the central nitrogen atom: a single substitution indicates a primary amine, whereas double and triple substitutions indicate a secondary and a tertiary amine accordingly. Each amine has one or more hydroxyl groups, which reduce vapor pressure and the water solubility, and amine groups, which supply the alkalinity in water and advance the chemical reactions. Primary amines have two hydrogen atoms coupled with the central nitrogen, secondary ones have one and tertiary amines none as they are fully substituted[20].

The amines usually used for acid gases chemical absorption are:

Monoethanolamine (MEA): This amine has a vapor pressure equal to 1.05 mm Hg and 100% relative acid gas capacity. It exhibits good thermal stability, but due to its relatively high vapor pressure, solvent losses occur[17]. Monoethanolamine is a commonly used solvent for acid gas treatment, because it has many advantages, such as the low solvent cost and the high reactivity. However, it has also disadvantages, such as high energy requirements, compared to other alkanolamines[20].

Diethanolamine (DEA): Diethanolamine has a vapor pressure equal to 0.058 mm Hg and a lower relative acid gas capacity (58%), due to its slower reaction[17]. Diethanolamine is possibly the most widely used solvent for acid gas treatment, even though it is less reactive than MEA. It has many benefits, such as the low solvent cost, the resistance to degradation and no solvent losses, due to the low vapor pressure. Furthermore, compared to MEA, it is less corrosive. Nevertheless, it has also drawbacks, such as the non-selectivity in case of mixed acid gases and the higher circulation requirements[20].

Diglycolamine (DGA): DGA is a primary amine, similar to MEA, except for its lower vapor pressure (0.016 mm Hg), which enables the higher amine concentration and the lower circulation rates and energy consumption. It is used for selective removal of H_2S over CO_2 and it has 58 % relative acid gas capacity[17]. DGA has many advantages, such as lower cost due to lower circulation rates, high reactivity and thermal stability, although it appears drawbacks as well, including the higher solvent cost compared to MEA and DEA and the nonselective removal, in case of mixed acid gases[20].

Methyldiethanolamine (MDEA): Recently, methyldiethanolamine has been established as an appealing solvent to the industry for acid gas treatment. It is often used for selective removal of H_2S and has good capacity, good reactivity and very low vapor pressure (0.0061 mm Hg)[17]. The selective H_2S removal is a major advantage, because it can be used in applications, where the purpose is to have very low H_2S concentrations (4 ppmv) and adjustment of CO_2 content. Initially, MDEA was used in tail gas treatment, but nowadays it has replaced primary and secondary amines in refinery treating units. Except for its high H_2S selectivity and low vapor pressure, MDEA has other advantages too, such as the low corrosiveness, the stability to degradation and energy and cost savings. However, it has also disadvantages, which include higher solvent cost and lower reactivity than other solvents[20].

Sterically hindered amines: They have also found application in acid gas treatment. They are not definitely alkanolamines, even though they have similar characteristics in gas purification. This kind of amine is defined as a primary amine, in which the amine group is attached to a tertiary carbon atom or a secondary amine, in which the amine group is attached to a secondary or tertiary carbon atom. They have found application in hot

potassium carbonate systems, organic solvent/amine systems and in aqueous solutions for selective H_2S absorption. Each of these systems uses a different sterically hindered amine. The main advantage of this kind of amines is that their molecular structure can be controlled during their synthetization and hence their properties can be tuned. Examples of these amines are 2-amino-2 methyl-1-propanol, 1-8-p-methanediamine (MDA), 2-piperidine ethanol[21].

The choice of the suitable amine depends on many factors, such as the pressure and temperature of the treated gas, its composition and the desired purity. Another important factor is the need of simultaneous CO_2 and H_2S removal or the selective H_2S removal.

It is a common practice, mixed amines to be applied, in order to combine the advantages of more than one type of amines. For instance, MDEA can be used with a primary amine, such as MEA, in order to combine the low energy requirements and stability of MDEA with the high CO_2 absorption rate of MEA[21].

Piperazine is a cyclic amine, which is also used as an additive, in order to improve the absorption of acid gases by commonly used alkanolamines. It is recommended to be used in combination with MDEA, replacing the primary or secondary amines, because of its less corrosive nature. This solvent blend has been introduced by BASF in 1982 and called "activated MDEA solvent". Piperazine has high capacity of protonation and it increases the CO_2 absorption rate, even though its use increases the heat of absorption[15].

In this thesis, monoethanolamine (MEA) and methyl diethanolamine (MDEA) are examined and their chemical structure is presented in Figure 3.4.
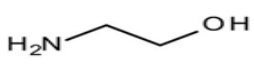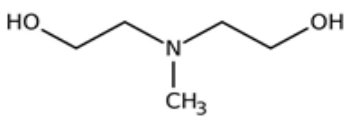
Abbreviation	Name	Structure
MEA	Monoethanolamine	
MDEA	Methyl diethanolamine	

Figure 3.4: Chemical structure of alkanolamines examined in this thesis

A typical flow chart of chemical absorption process is presented in Figure 3.5.

The sour gas is filtered and cleaned of possible liquids, before entering the absorber. The inlet gas may include carbon dioxide, hydrogen sulfide, mercaptans and other gases and its CO_2 and H_2S concentration can range from 0-50% in a molar basis depending on the origin of the gas. The solvent is usually an aqueous alkanolamine solution and the amine concentration depends on the amine type and concentration of acid gases. Typical concentration values are 20-30% w/w for aqueous monoethanolamine solutions, whereas for methyldiethanolamine solutions the corresponding values are 30-50 % w/w.

The sour gas enters the bottom of the absorption column, whereas the solvent enters the top of the column and their flows are countercurrent. When the solvent is exposed to the acid gas, chemical reactions take place and amine solution leaves the bottom of the absorber loaded with acid gases. The sweetened gas leaves the top of the absorber column and continues to further processing.

The absorber is typically a packed or tray column and its operating temperature is usually 40 °C, due to the decrease in acid gases solubility in alkanolamine solutions as temperature increases. The operating pressure is case dependent and it is usually higher in case of natural gas (even 70 bar) than in case of flue gases treatment (around atmospheric pressure).

Rich amine leaves the bottom of the absorber and it enters one or two flash drums, in order the dissolved hydrocarbons to be removed. Subsequently, rich amine is heated by contacting the lean amine solvent in a heat exchanger and then it enters the top of the stripper column, which is heated by a reboiler in order the exothermic reactions to be reversed and the lean solvent regenerated. The stripped gas leaves the top of the stripper and it enters a cooler and then it is sent for further processing. The lean amine solution is filtered, in order heavy hydrocarbons to be removed and then it exchanges heat with the rich amine solution, as it has already been mentioned, whereas afterwards it is further cooled and enters the top of the absorption column[15].

The flash vessels, which are used for the removal of dissolved hydrocarbons from the rich amine solution, operate at low pressure, in order to recover the maximum possible quantity of hydrocarbons. Their removal is necessary, in order to avoid foaming. The operating pressure of these vessels ranges from 0.3-5.2 bar.

Rich amine, which enters the heat exchanger contacting with the lean amine, is usually at 54.4-71.1 °C, whereas the lean amine is at around 115.6-126.7 °C. The lean amine leaving the heat exchanger is cooled at around 82.2 °C. A common problem in this heat exchanger

is the flashing of acid gases at the outlet, which is most probable, when there is reduced circulation rate or low solvent concentration. For that reason, in many applications, stainless steel is used for this heat exchanger.

In the filtration system, both a particulate and a carbon filter are incorporated. The first one is used, in order to remove particles and avoid corrosion. The second one is used to remove active contaminants and hydrocarbons, which result to foaming. When an appropriate inlet gas treatment is preceded, a 10-20 % lean stream filtering is enough, although when it is applicable, total stream filtration is used[20].

The stripper operates at around 120 °C. The high temperature is a result of the reboiler, which is essential for the removal of acid gases from the rich amine solution: it provides heat, which has as a result, the reversal of the exothermic reactions, which have taken place in the absorber column. Higher temperature in stripper column is not recommended due to possible amine degradation. The operating pressure is around 1.2 bar[15].
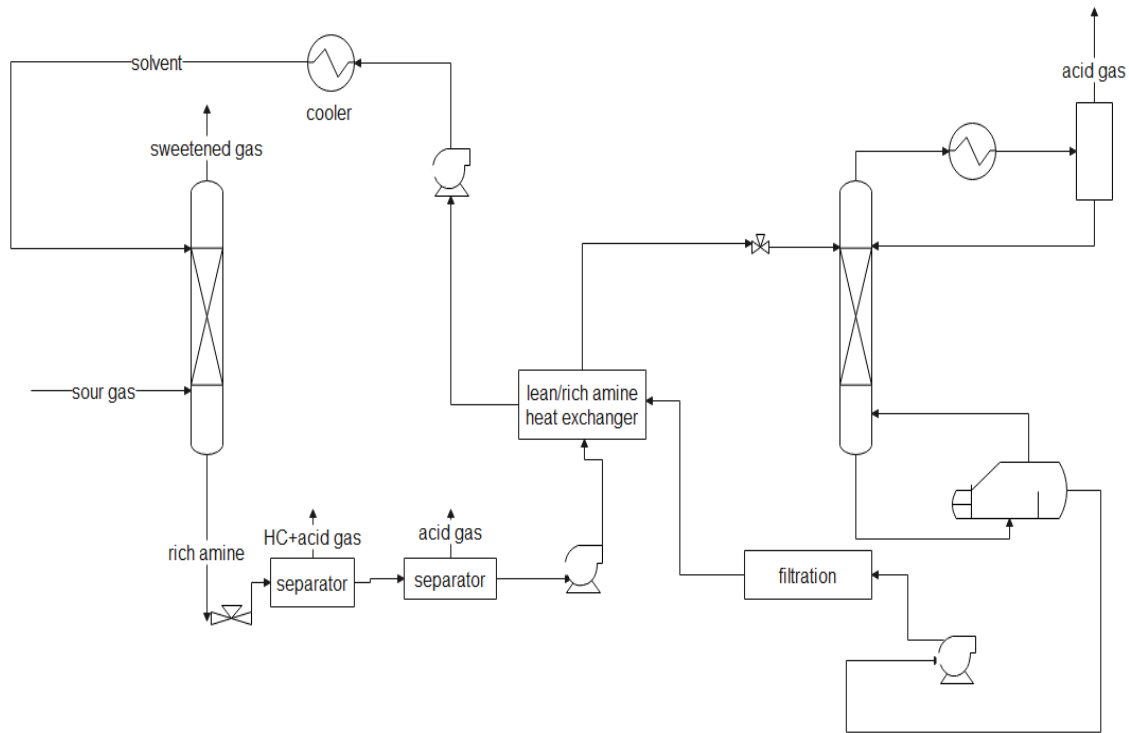
Figure 3.5: Typical flowchart of chemical absorption process for acid gas removal[15].

3.3.2. Physical absorption process

In this thesis two physical absorption processes have been examined: the Rectisol process, which is physical absorption in refrigerated methanol and physical absorption in an ionic liquid.

3.3.2.1. Rectisol Process

Rectisol process is a physical absorption process which uses refrigerated methanol as solvent and it was patented and developed by Lurgi and Linde[22]. This process is the dominant process for syngas purification worldwide and it can be designed in many ways, depending on the composition of the treated gas and the required specifications. Rectisol process is widely used for syngas cleaning, because of the ability to remove trace components, which can be detrimental to downstream processes, such as COS, HCN, NH_3 etc. Furthermore, a wide range of H_2S and CO_2 levels can be reached in this process, while the flexibility of the process layout, in order almost any upstream syngas condition and downstream product specification to be met, is another major advantage.

Methanol is an alcohol and it can be used as a polar protic solvent, able to dissolve H_2S and CO_2. Comparing to other physical solvents, it has a main benefit: the solubilities of H_2S and CO_2 in methanol increase at low temperatures. Methanol can operate at very low temperatures, in order to rise the acid gases solubility, a fact which results to low solvent flow and reduced absorber size. Furthermore, methanol has even more benefits such as the low viscosity, low corrosive nature and non-foaming operation.

In Figure 3.6, Lurgi's scheme[23] is presented. The raw gas is usually firstly cooled and purified from trace components, such as HCN and NH, if they are present, in a prewash unit. Subsequently, the raw gas enters the bottom of an absorption column, which operates at pressure greater than 1 MPa, and a refrigerated methanol stream enters the top of the absorber. Their flows are countercurrent. Methanol stream is at -10 °C to -70 °C and it contacts the acid gas in order to absorb CO_2, H_2S and COS and remove them. Rich methanol leaves the bottom of the absorber column and it enters two contacting columns: the first one is a flash, which operates at atmospheric pressure, in order to regenerate a proportion of methanol and reduce CO_2 content to 5%, while the second is a hot regeneration column in order to reduce the CO_2 content to 3 %[24].
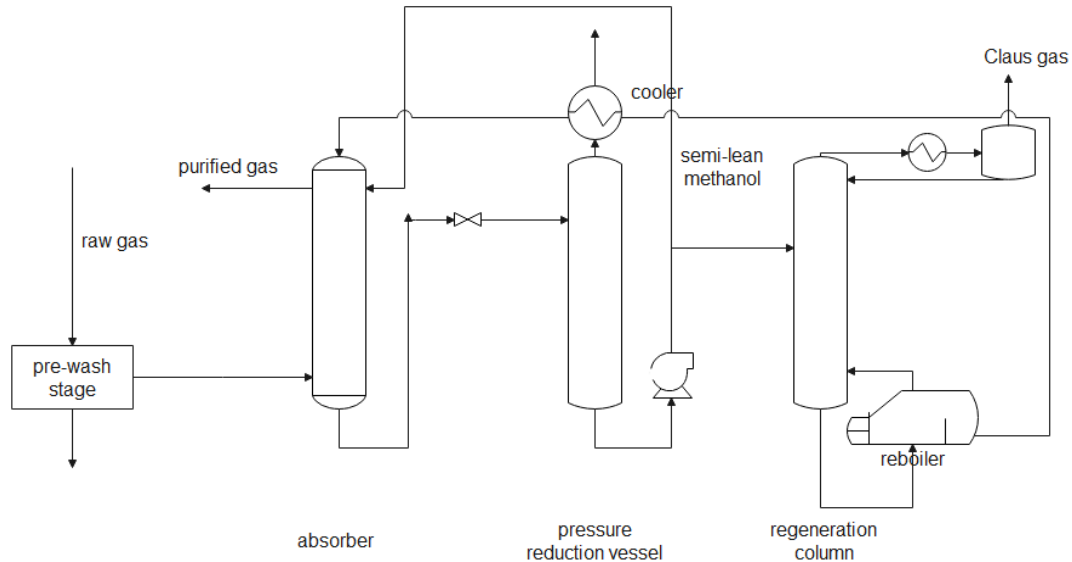
Figure 3.6:Rectisol process[22]

Despite the simplicity of this process, it is not selective and hence unsuitable for CO_2 capture and storage, because the vapor product of the flash column contains a high H_2S quantity. For that purpose, different schemes have been proposed, such as the one presented by Linde[25] or Hochgesand[26] and Weiss[27].

3.3.2.2.   Physical absorption with ionic liquids

Ionic liquids have been recently proposed as solvents in acid gas capture. They are defined as materials, which consist of an organic cation and an organic or inorganic anion. They have melting point below 100 °C and they are tailor made solvents, due to their tunable structure, which enables task-specific optimization. Commonly used cations are imidazolium, pyrrolidinium, pyridinium, quaternary ammonium, tetra alkyl Phosphonium, whereas common anions are tetrafluoroborate, hexafluoroborate, bis(trifluorophoshate)imide, nitrate and acetate.

They have found application in many industrial processes, due to their unique properties: high thermal and chemical stability, low vapor pressure, excellent solvent properties for a wide variety of compounds. These characteristics render them possible solvents for acid gas capture, because in comparison to the widely spread process of chemical absorption with aqueous alkanolamines, they have the following advantages:

- Less energy requirements during regeneration of ionic liquids, due to the physical absorption.

- Their low vapor pressure results to their easier regeneration and reuse with no solvent losses.
- They are not corrosive, because of their high thermal and chemical stability, which prevent their reaction with impurities.
- The ability to combine different cations and anions and design a unique ionic liquid, with ideal physicochemical properties for specific processes, such as heat capacity, thermal decomposition, toxicity, render them as an advantageous solvent for acid gas capture[28].

3.3.2.2.1. Ionic liquids properties

Melting point, viscosity, density, thermal stability, toxicity and vapor pressure are some of the unique properties of ionic liquids, which are analyzed in this section.

Melting point

The melting point of ionic liquids is lower than 100 $^{\circ}$C and it is even lower than that of other salts, due to the non-ideal packing of the ions, a fact which results to lower lattice energy[29].

Melting point is a significant property for the chemical identification of the compounds. Furthermore, it is an even more important property for ionic liquids, because the range, in which they are liquids, is determined by the low melting point and the high decomposition point. Additionally, their solubility in water or organic solvent is correlated with their melting point[30].

This property of ionic liquids can be tuned by the suitable structure of ionic liquids. The intermolecular interactions, van der Walls interactions, the distribution of the ions charge, the volume and the symmetry are factors which affect the melting point. The greater the volume and the asymmetry of the cation and the anion size are, the lower the melting point is[31].

Density

The density of ionic liquids is greater than the one of water and it varies from 1.05 to 1.36 g/cm^3 at ambient temperature. This property also depends on the selection of cation and anion. Generally, density decreases, while the alkyl-chain length of the cation is increasing. However, anion selection is of great importance too[31].

Volatility

Ionic liquids have negligible vapor pressure and for many years it was believed that their vapor pressure cannot be measured. Thus, they are not volatile and can be separated by

simple flash drums. The extremely low volatility is a major advantage of ionic liquids, for environmental and industrial reasons[32].

Ionic liquids have been proposed as green solvents, because of their use instead of volatile organic compounds. Their low vapor pressure makes their recycle and reuse easier and terminates the dangerous exposure and air pollution problems, which may be caused by other solvents[33].

Protic ionic liquids, which have an acidic proton on the cation, are more volatile than aprotic ionic liquids, which have no acidic proton, because the acidic proton can be removed by the basic anion at atmospheric temperature. These reactions have as a result the generation of neutral molecules, which are easily evaporated. Therefore, most studies focus on aprotic ionic liquids, due to their negligible volatility[34].

Volatility measurements are hard, due to the decomposition of many ionic liquids at temperatures, where vapor pressure can be measured. However, it has been concluded, that some ionic liquids with decomposition temperatures greater than 200-300 °C, have vapor pressure lower than 1 Pa[32].

Viscosity

Ionic liquids have high viscosities as a result of their high molecular weights and intermolecular interactions. Compared to organic solvents, which have viscosities from 0.2 to 10 mPa.s, ionic liquids are much more viscous (viscosities ranging from 10 to 10^4 mPa.s). The shape of the anion affects the viscosity of the ionic liquid, while its size has also a significant effect: increasing the size of the anion results to a viscosity increase. Furthermore, a high degree of fluorination of the anion has as a consequence low van der Waals interactions and hence low viscosities. Moreover, the increase in the alkyl group of the cation is followed by an increase in the viscosity of the ionic liquid.

The viscosity is of great importance, because a high one leads to low absorption and desorption rate, in case of acid gases absorption process. However, a higher temperature or water or chloride contaminants result to a lower viscosity[29].

Thermal stability

The majority of ionic liquids are stable even at high temperatures (400 °C). The thermal stability depends more on the anion rather than the nature of the cation. Thermal decomposition increases, when the hydrophilicity of the anions decreases[31], whereas it increases as the anion size increases[29]. The following thermal stability range has been found:

$[PF_6^-] > [Tf_2N^-] > [BF_4^-] >$ halides

Due to the thermal decomposition of the ionic liquids, critical temperatures cannot be specified, because they are greater than the thermal decomposition temperatures.

Toxicity and biodegradability

Even though ionic liquids have been assumed as green solvents, due to their negligible vapor pressure, their toxicology data, presented in literature, are limited. Their low vapor pressure makes it difficult, but not infeasible, for them to enter the environment. For instance, they may enter aquatic environment accidentally and most of them are water soluble, while some (bmim[PF_6] and bmim[BF_4]) decompose in water and form hydrofluoric and phosphoric acids. For this reason, the collection of toxicity data is necessary for their characterization as green solvents[33].

The effect of two commonly used ionic liquids, bmim[PF_6] and bmim[BF_4], on aquatic ecosystem, has been studied, and it was found that they are as toxic as benzene is for ecosystems, but less toxic than ammonia, chlorine and phenol. Furthermore, the effect of the cation in toxicity has been examined and it has been found that as the alkyl chain length is increasing, toxicity increases[29].

Moreover, biodegradability is another physical property, which should be examined. Biodegradable ionic liquids are by definition those that reach a biodegradation level greater than 60 % in 28 days. This property has been studied for imidazolium, phosphonium and pyridinium-based ionic liquids. According to the results of the studies, pyridinium-based ionic liquids have higher biodegradability than the other ones. The effect of the anion in imidazolium based ionic liquids has also been studied and it has been concluded that it is minor, except for octylsulfate anion, which improves remarkably biodegradability[29].

3.3.2.2.2. Categories of ionic liquids used for acid gases capture

During the last decade, the use of ionic liquids has been proposed for a wide range of essential industrial applications and lately they have been suggested as solvents for acid gases absorption, because of their unique properties, in which, among others, high acid gases solubility is included. For instance, it has been mentioned, that CO_2 solubility is exceptionally high in 1-butyl-3-methylimidazolium Hexafluorophosphate, whereas high pressures are usually needed in order to obtain a high CO_2 solubility, because, below the atmospheric pressure, CO_2 solubility in conventional ionic liquids is maximum 0.035 mole fraction[35]. However, the selectivity of ionic liquids in acid gases compared to methane, ethane and other gases, constitutes a major advantage, which makes them ideal solvents for acid gases absorption. Carvahlo And Coutinho[36] have found that CO_2/CH_4 and H_2S/CH_4

ideal selectivities increase as the polarity of ionic liquids increases, because the non-polar methane dissolves in a greater degree in ionic liquids with low polarities. In literature, the most studied binaries gas-ionic liquid mixtures are those containing CO_2[29]. Imidazolium ionic liquids are mainly used for acid gas capture, whereas the acid gas solubility in them can be improved by the addition of an amine in ionic liquid structure or by using mixtures of ionic liquid and alkanolamine.

Imidazolium-based ionic liquids: It is presented in many studies, that, even though acid gases solubility is lower in ionic liquids than in organic solvents, CO_2 solubility is sufficiently high in imidazolium-based ionic liquids. This is, according to Cadena et al[37], due to the filling of intervals of the network of cations and anions by CO_2. It has been found, that the nature of the anion plays the dominant role in CO_2 solubility, whereas the cation plays a secondary role. Moreover, increasing the pressure and decreasing the temperature results to an increase in CO_2 solubility in ionic liquids.

Task-specific ionic liquids: Despite the advantages of ionic liquids, they have basic limitations in order to be used for acid gas absorption, such us the high viscosity, which results to lower CO_2 absorption rate, because it is a function of viscosity of the solvent. Therefore, task-specific ionic liquids have been proposed, in order to overcome the limitation and retain the advantages of ionic liquids. One of the most promising task-specific ionic liquids is amine-functionalized ionic liquid, which can capture 33 mol% CO_2 even at low pressures. However, they have also high viscosities, whereas their formation requires purification and synthesis steps, which increase the cost.

Mixtures of ionic liquids and amines: Instead of amine-functionalized ionic liquids, mixtures of ionic liquids with amines can be used in order to combine the advantages of both of them. Camper et al[38] have used ionic liquid with Tf_2N anion with MEA and DEA and they have found, that these mixtures have lower volatility, low energy requirements and similar efficiency to aqueous alkanolamines. Freire et al[39] have combined bmim[BF_4] with MDEA and even though BF_4^- hydrolysis is notable in acidic solutions, it is not a problem for bmim[BF_4] in aqueous MDEA[35].

Supported ionic liquid membranes: This is a new technology, which consists of two phases, a supporting porous or nonporous membrane and a liquid solvent, which exists in the pores or between two nonporous membranes. The solute diffuses and dissolves into the membrane and it is resorbed at the other side of membrane[40]. Park et al[41] have studied the use of supported ionic liquid membranes for CO_2 and H_2S removal and the results showed high selectivities for CO_2/CH_4 and H_2S/CH_4.

In current thesis CO_2 solubility in imidazolium-based ionic liquids has been studied, because CO_2 solubility in them is high and there are available experimental data in literature. Furthermore, three anions have been selected to be studied, in order to find the anion effect on ionic liquids properties (such as density, vapor pressure and CO_2 solubility) and four cations, in order to study the effect of the cation. The ionic liquids examined in this work are presented in Figure 3.7.
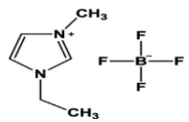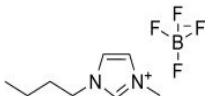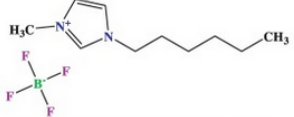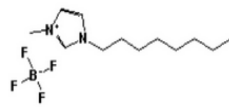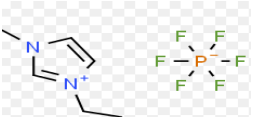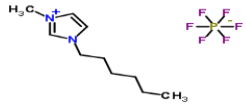
Abbreviation	Name	Structure
emim[BF₄]	1-ethyl-3-methylimidazolium Tetrafluoroborate	
bmim[BF₄]	1-butyl-3-methylimidazolium Tetrafluoroborate	
hmim[BF₄]	1-hexyl-3-methylimidazolium Tetrafluoroborate	
omim[BF₄]	1-octyl-3-methylimidazolium Tetrafluoroborate	
emim[PF₆]	1-ethyl-3-methylimidazolium Hexafluorophosphate	
bmim[PF₆]	1-butyl-3-methylimidazolium Hexafluorophosphate	
hmim[PF₆]	1-hexyl-3-methylimidazolium Hexafluorophosphate	

Figure 3.7: Ionic liquids examined in this work
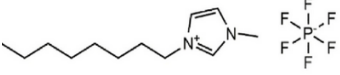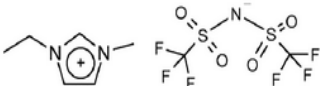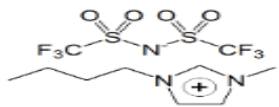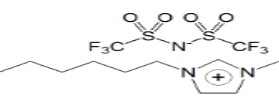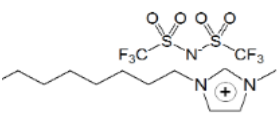
Abbreviation	Name	Structure
omim[PF$_6$]	1-octyl-3-methylimidazolium Hexafluorophosphate	
emim[Tf$_2$N]	1-ethyl-3-methylimidazolium Bis(trifluoromethanesulfonyl)imide	
bmim[Tf$_2$N]	1-butyl-3-methylimidazolium Bis(trifluoromethanesulfonyl)imide	
hmim[Tf$_2$N]	1-hexyl-3-methylimidazolium Bis(trifluoromethanesulfonyl)imide	
omim[Tf$_2$N]	1-octyl-3-methylimidazolium Bis(trifluoromethanesulfonyl)imide	

Figure 3.7 (continued): Ionic liquids examined in this work

3.3.2.3.1. Process description

In this thesis binary mixtures of ionic liquids with CO_2 have been modeled, and CO_2 physical absorption in ionic liquids has been simulated. Thus, the process described in this section includes only CO_2 and not H_2S capture.

In Figure 3.8, the process of physical absorption of acid gases, which are contained in field gas, in ionic liquid is presented. The process consists of five columns: an inlet separator, an absorber and four separators.

Firstly, the gas enters an inlet separator, where liquids and other impurities are removed. The gas leaves the top of the separator and it enters a heater, before entering the absorber. This is necessary, in case of ionic liquids with melting temperature close to the feed temperature, due to the avoidance of solidification of the solvent, whereas in case of ionic liquids with melting points far from feed temperature, heater is not required.

The sour gas enters the bottom of the absorber, whereas ionic liquid enters the top of the absorber and their flows are countercurrent. The pressure of the absorber should be high (even greater than 70 bar), because at high pressure acid gases solubility increases in ionic liquids, whereas methane and ethane solubility does not change notably, a fact which results to higher selectivity of ionic liquid for acid gases. The operating temperature is controlled by the melting point temperature of ionic liquid and their capacity of absorption, which increases when the temperature decreases. Another factor, which is instrumental, is the viscosity of ionic liquids, which decreases as the temperature increases and it affects the efficiency of the absorption column. For these reasons, the temperature of the absorber is 288 K for ionic liquids with low melting points, whereas higher temperatures are selected in case of ionic liquids, with higher melting temperatures. The flow rate of the solvents depends on the composition of the sour gas entering the absorption column.

An upgraded gas, rich in methane, leaves the top of the absorber, whereas rich ionic liquid leaves the bottom of the absorber and enters a series of three flash separators, in order the absorbed methane to be removed, due to depressurization. The pressure of each separator is a result of optimization and case-dependent, in order the recovery of methane to be maximized. The gases leaving the top of the separators are compressed, cooled and recycled back to the absorber.

The fourth flash separator is used in order remove the absorbed CO_2 and recover the ionic liquid, which is recycled to the absorber, after entering a pump and a heater. This flash separator operates at near atmospheric pressure[42].
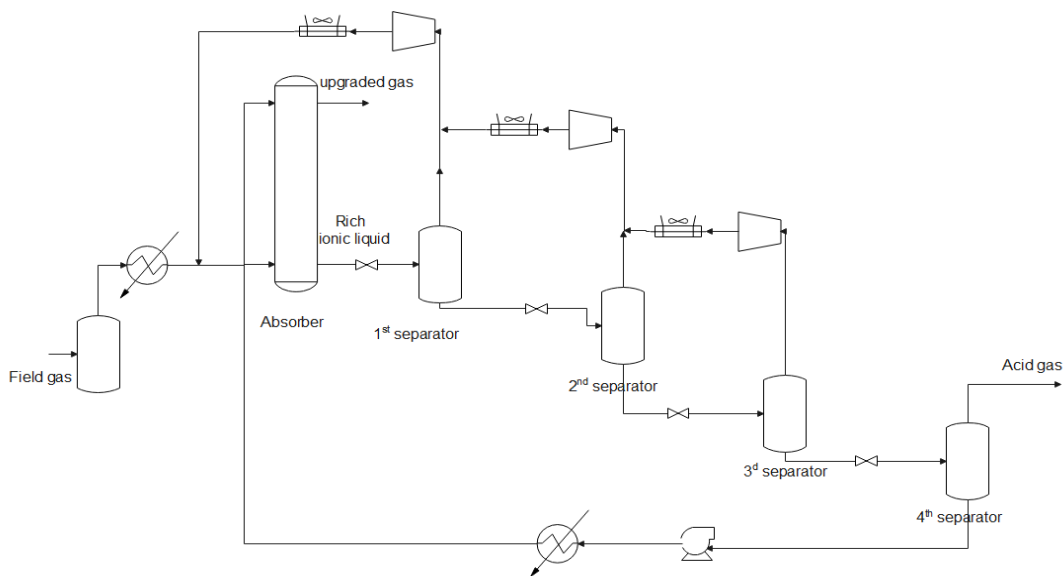
Figure 3.8: Physical absorption of acid gases in ionic liquid[42].

3.4. Conclusions

In this chapter, various technologies have been proposed for acid gases removal from flue gases or natural gas, such as chemical and physical absorption. Each of them has advantages and disadvantages and their appropriateness depends on acid gases concentration in feed gas and the final product specifications. In this thesis, three processes are examined: chemical absorption process in aqueous monoethanolamine solution, physical absorption process in refrigerated methanol and physical absorption in ionic liquids. The description of vapor-liquid equilibrium, and in case of chemical absorption, the description of both chemical and phase equilibrium by thermodynamic models is an essential step, in order to have reliable and validate simulations results. Therefore, the theoretical background of chemical and phase equilibrium is described in next chapter.

3.5.   References

1.   Alfadala, H.; Al-Musleh, E., Simulation of an Acid Gas Removal Process Using Methyldiethanolamine; an Equilibrium Approach. **2009**.

2.   Pacheco, M. A.; Rochelle, G. T., Rate-Based Modeling of Reactive Absorption of CO2 and H2S into Aqueous Methyldiethanolamine. *Industrial & Engineering Chemistry Research* **1998,** *37* (10), 4107-4117.

3.   Dugas, R.; Alix, P.; Lemaire, E.; Broutin, P.; Rochelle, G., Absorber model for CO 2 capture by monoethanolamine — application to CASTOR pilot results. *Energy Procedia* **2009,** *1*, 103-107.

4.   Pellegrini, L. A.; Moioli, S.; Gamba, S., CO2 removal by MEA scrubbing: Process simulation and energy saving study. **2011**.

5.   Rahimpour, M. R.; Saidi, M.; Baniadam, M.; Parhoudeh, M., Investigation of natural gas sweetening process in corrugated packed bed column using computational fluid dynamics (CFD) model. *Journal of Natural Gas Science and Engineering* **2013,** *15*, 127-137.

6.   Glasscock, D.; Rochelle, G., Approximate Simulation of H2S Absorption into Aqueous Alkanolamines. *AIChE Journal* **1993,** *39*, 1389-1397.

7.   Gamba, S.; Pellegrini, L.; Soave, G.; Rossi, P.; Moioli, S., *Acidic gas absorption by methanol: System modeling and simulation*. 2012.

8.   Burr, B.; Lyddon, L. In *A comparison of physical solvents for acid gas removal*, Gas Processors' Association Convention, Grapevine, TX, 2008.

9.   Akinola, T. E.; Oko, E.; Wang, M., Study of CO2 removal in natural gas process using mixture of ionic liquid and MEA through process simulation. *Fuel* **2019,** *236*, 135-146.

10.   Santiago, R.; Lemus, J.; Outomuro, A. X.; Bedia, J.; Palomar, J., Assessment of ionic liquids as H2S physical absorbents by thermodynamic and kinetic analysis based on process simulation. *Separation and Purification Technology* **2020,** *233*, 116050.

11.   Taheri, M.; Dai, C.; Lei, Z., CO2 capture by methanol, ionic liquid, and their binary mixtures: Experiments, modeling, and process simulation. *AIChE Journal* **2018,** *64* (6), 2168-2180.

12.   Kothandaraman, A., *Carbon dioxide capture by chemical absorption: a solvent comparison study*. Citeseer: 2010; Vol. 72.

13.   Jansen, D.; Gazzani, M.; Manzolini, G.; Dijk, E. v.; Carbo, M., Pre-combustion CO2 capture. *International Journal of Greenhouse Gas Control* **2015,** *40*, 167-187.

14.   Stanger, R.; Wall, T.; Spörl, R.; Paneru, M.; Grathwohl, S.; Weidmann, M.; Scheffknecht, G.; McDonald, D.; Myöhänen, K.; Ritvanen, J.; Rahiala, S.; Hyppänen, T.; Mletzko, J.; Kather, A.; Santos, S., Oxyfuel combustion for CO2 capture in power plants. *International Journal of Greenhouse Gas Control* **2015,** *40*, 55-125.

15.   Sadegh, N., *Acid Gas Removal from Natural Gas with Alkanolamines*. Technical University of Denmark (DTU): Kgs. Lyngby, 2013.

16.   Mokhatab, S.; Poe, W. A., *Handbook of natural gas transmission and processing*. Gulf professional publishing: 2012.

17.   Shimekit, B.; Mukhtar, H., Natural gas purification technologies-major advances for CO2 separation and future directions. *Advances in natural gas technology* **2012,** *2012*, 235-270.

18.   Dyment, J.; Watanasiri, S., Acid gas cleaning using DEPG physical solvents: validation with experimental and plant data. *The USA: Aspen Technology Inc* **2015**.

19.   Gabrielsen, J., CO2 capture from coal fired power plants. *Graduate Schools Yearbook 2005* **2005**, 61.

20.   Mitra, S., A Technical Report on Gas Sweetening by Amines. *Petrofac Engineering India Ltd* **2015,** *1*.

21.   Kohl, A. L.; Nielsen, R., *Gas purification*. Elsevier: 1997.

22.   Gatti, M.; Martelli, E.; Marechal, F.; Consonni, S., Review, modeling, Heat Integration, and improved schemes of Rectisol®-based processes for CO2 capture. *Applied thermal engineering* **2014,** *70* (2), 1123-1140.

23.   Herbert, W.; Becker, R.; Danulat, H. G.; Danulat, H. F.; Danulat, D. Process for the purification of gases 1958.

24.   Rackley, S. A., *Carbon capture and storage*. Butterworth-Heinemann: 2017.

25.   Ranke, G.; Weiss, H. Separation of gaseous components from a gaseous mixture by physical scrubbing 1982.

26.   Hochgesand, G., Rectisol and purisol. *Industrial & Engineering Chemistry* **1970,** *62* (7), 37-43.

27.   Weiss, H., Rectisol wash for purification of partial oxidation gases. *Gas Separation & Purification* **1988,** *2* (4), 171-176.

28.   Torralba-Calleja, E.; Skinner, J.; Gutiérrez-Tauste, D., CO2 capture in ionic liquids: a review of solubilities and experimental methods. *Journal of Chemistry* **2013,** *2013*.

29.   Althuluth, M. A., Natural gas sweetening using ionic liquids. *Eindhoven University of Technology* **2014**.

30.   Zhang, S.; Sun, N.; He, X.; Lu, X.; Zhang, X. P., Physical Properties of Ionic Liquids: Database and Evaluation. *Journal of Physical and Chemical Reference Data* **2006,** *35*, 1475.

31.   Singh, G.; Kumar, A., Ionic liquids: Physico-chemical, solvent properties and their applications in chemical processes. **2008**.

32.   Αλεβίζου, Ε., Πειραματική μελέτη και θερμοδυναμική προσομοίωση της ισορροπίας φάσεων συστημάτων που περιέχουν αντιοξειδωτικές ενώσεις και ιοντικά υγρά. **2014**.

33.   Keskin, S.; Kayrak-Talay, D.; Akman, U.; Hortaçsu, Ö., A review of ionic liquids towards supercritical fluid applications. *The Journal of Supercritical Fluids* **2007,** *43* (1), 150-180.

34.   M. S. S. Esperança, J.; Canongia Lopes, J. N.; Tariq, M.; Santos, L. M. N. B. F.; Magee, J. W.; Rebelo, L. P. N., Volatility of Aprotic Ionic Liquids — A Review. *Journal of Chemical & Engineering Data* **2010,** *55* (1), 3-12.

35.   Babamohammadi, S.; Shamiri, A.; Aroua, M. K., A review of CO2 capture by absorption in ionic liquid-based solvents. *Reviews in Chemical Engineering* **2015,** *31* (4), 383-412.

36.   Carvalho, P. J.; Coutinho, J. A., The polarity effect upon the methane solubility in ionic liquids: a contribution for the design of ionic liquids for enhanced CO 2/CH 4 and H 2 S/CH 4 selectivities. *Energy & Environmental Science* **2011,** *4* (11), 4614-4619.

37.   Cadena, C.; Anthony, J. L.; Shah, J. K.; Morrow, T. I.; Brennecke, J. F.; Maginn, E. J., Why is CO2 so soluble in imidazolium-based ionic liquids? *Journal of the American Chemical Society* **2004,** *126* (16), 5300-5308.

38.   Camper, D.; Bara, J. E.; Gin, D. L.; Noble, R. D., Room-temperature ionic liquid– amine solutions: tunable solvents for efficient and reversible capture of CO2. *Industrial & Engineering Chemistry Research* **2008,** *47* (21), 8496-8498.

39.   Freire, M. G.; Neves, C. M.; Marrucho, I. M.; Coutinho, J. A.; Fernandes, A. M., Hydrolysis of tetrafluoroborate and hexafluorophosphate counter ions in imidazolium-based ionic liquids. *The Journal of Physical Chemistry A* **2010,** *114* (11), 3744-3749.

40.   Ramdin, M.; de Loos, T. W.; Vlugt, T. J., State-of-the-art of CO2 capture with ionic liquids. *Industrial & Engineering Chemistry Research* **2012,** *51* (24), 8149-8177.

41.   Park, Y.-I.; Kim, B.-S.; Byun, Y.-H.; Lee, S.-H.; Lee, E.-W.; Lee, J.-M., Preparation of supported ionic liquid membranes (SILMs) for the removal of acidic gases from crude natural gas. *Desalination* **2009,** *236* (1-3), 342-348.

42.   Mortazavi Manesh, S., Application of Ionic Liquids for Gas Sweetening. **2014**.

4. Phase and chemical equilibrium

Solving the problem of phase and chemical equilibrium is vital for process design. According to literature, there are different approaches on solution of chemical and phase equilibrium and they are presented in this chapter. Additionally, the process followed in this work in order to tackle with this problem by using eUMR-PRU model, is described analytically.

4.1. Introduction

"Phase" and "Chemical equilibrium" are two subjects in thermodynamics, which find great practical interest. The design of processes, such as absorption, extraction, distillation or reactors is based on phase equilibrium, chemical equilibrium or both of them[1].

The removal of acid gases from natural gas or flue gases can be achieved by various processes. The most well-known is chemical absorption process of acid gases by using aqueous alkanolamine solutions. These mixtures are thermodynamically described by physical and chemical equilibria. Another process that has been examined during the last decades is the physical absorption of acid gases by ionic liquids. These mixtures are described exclusively by physical equilibrium.

As for the acid gas-water-alkanolamine mixtures, their absorption occurs in two steps. Firstly, the species existing in vapor phase (acid gases) are dissolved into the liquid phase. Secondly, chemical reactions take place in the liquid phase. In this step, the molecular species convert to ions, which exist only in liquid phase, whereas the molecular species exist in both the liquid and vapor phase[2]. From this, it becomes quite clear how complex it is to solve this problem, in which chemical and phase equilibrium coexist.

Concerning the acid gas-water-alkanolamine mixtures, different approaches have been proposed in literature, which are described in this chapter. In the typical acid gas thermodynamic problem variables such as: temperature, amount of acid gas and amine concentration in liquid phase are known, whereas total pressure and composition in gas phase are unknown. The calculations behind solving this issue are described by Smith and Missen[3] as analogous to bubble point pressure calculations, where the temperature and liquid phase composition are known and the purpose is to find the total pressure and the gas phase composition. The liquid phase composition is specified by temperature, total amine concentration and amount of acid gas, while the model calculates the speciation in liquid phase, bubble point pressure and composition of the gas phase[4]. In the present thesis, this problem is presented and solved.

In this chapter, basic concepts and criteria about physical and chemical thermodynamic equilibrium are explained. Furthermore, basic points about the algorithms used to solve the equilibrium problems are discussed.

4.2. Phase equilibrium

Thermodynamic equilibrium is a situation, during which no macroscopic changes occur in a system with time. In an isolated system the entropy is increasing, until equilibrium is achieved, when the entropy has the maximum value[1]. Therefore, in equilibrium:

$$S = maximum$$
<div align="right">eq. 4.1</div>

$$\frac{dS}{dt} = 0$$
<div align="right">eq. 4.2</div>

$$\frac{d^2S}{dt} < 0$$
<div align="right">eq. 4.3</div>

where S denotes the entropy.

In an isolated system with constant temperature and pressure entropy of the system is related to the Gibbs free energy by the following equation:

$$\frac{dG}{dt} = T\frac{-dS}{dt}$$
<div align="right">eq. 4.4</div>

where G denotes the Gibbs free energy and T the temperature of the system.

Therefore, the Gibbs free energy is decreasing with time, until it reaches its lowest value at equilibrium[1]:

$$G = minimum$$
<div align="right">eq. 4.5</div>

$$\frac{dG}{dt} = 0$$
<div align="right">eq. 4.6</div>

$$\frac{d^2G}{dt} > 0$$
<div align="right">eq. 4.7</div>

As far as the phase equilibrium concerns, assuming that there are two phases in an isolated system with controlled temperature and pressure, the minimum value of Gibbs free energy is reached at equilibrium. This condition can be replaced by the equality of the chemical potentials of a substance in two phases[1]:

$$\mu_i(I) = \mu_i(II)$$
<div align="right">eq. 4.8</div>

The chemical potential is related to fugacity by the following equation:

$$\mu_i(II) - \mu_i(I) = RT \ln\frac{\hat{f}_i(II)}{\hat{f}_i(I)}$$
<div align="right">eq. 4.9</div>

where μ refers to chemical potential, $\hat{f}$ refers to fugacity, subscript i denotes the component whereas (I) and (II) denote the phase.

Therefore, the equality of chemical potentials corresponds to the equality of fugacities:

$$\hat{f}_i(I) = \hat{f}_i(II) \qquad \text{eq. 4.10}$$

4.2.1. Low pressures-γ-ɸ approach

This approach is called γ-ɸ approach or the activity coefficient approach. The activity coefficient can be calculated by an activity coefficient model, such as e-NRTL, which is used in this work and presented in Chapter 5.

In this work, only vapor-liquid equilibrium is examined. In case of subcritical fluids, which are liquid in system temperature and pressure the following convention is considered[2]:
$\gamma_i \rightarrow 1$, when $x_i \rightarrow 1$

Equation 4.10 can be replaced in low pressures by:

$$\hat{f}_i^{\,v} = \hat{f}_i^{\,l} \qquad \text{eq. 4.11}$$

$$y_i \hat{\varphi}_i P = x_i \gamma_i f_i^{\,o} \qquad \text{eq. 4.12}$$

$$y_i \hat{\varphi}_i P = x_i \gamma_i P_i^{\,S} \varphi_i^{\,S} e^{\left(\frac{V_i(P-P_i^{\,S})}{RT}\right)} \qquad \text{eq. 4.13}$$

where y_i and x_i are the compositions of component i in vapor and liquid phases respectively

γ_i is the activity coefficient of component i

$\varphi_i^{\,S}$ is the fugacity coefficient of pure component i in liquid phase at system temperature.

$P_i^{\,S}$ is the vapor pressure of pure component i at system temperature.

The exponential factor is the Poynting effect.

In order to use equation 4.13, it is necessary to calculate the vapor pressure of the component. However, in case of supercritical fluids, this is not possible since they cannot exist in liquid phase at the system temperature. Therefore, the asymmetric convention has to be used ($\gamma_i^{\,*} \rightarrow 1$, when $x_i \rightarrow 0$) and the equation 4.11 becomes:

$$\lim_{x_i \rightarrow 0} \frac{\hat{f}_i}{x_i} = f_i^{\,o} = H_i \qquad \text{eq. 4.14}$$

$$\hat{f}_i = x_i \gamma_i^{\,*} H_i \qquad \text{eq. 4.15}$$

where H_i is the Henry's law constant and γ_i^* is the asymmetric normalized activity coefficient of component i.

4.2.2. High pressures-ϕ-ϕ approach

At high pressures ϕ-ϕ approach is preferred. In this case an equation of state is used for both liquid and vapor phases[1].

$$K_i = \frac{y_i}{x_i} = \frac{\widehat{\varphi_i}^l}{\widehat{\varphi_i}^v}$$

eq. 4.16

The fugacity coefficient is calculated by an Equation of State, using the following equation:

$$ln\,\widehat{\varphi_i} = \frac{1}{RT}\int_0^P \left(\overline{V_i} - \frac{RT}{P}\right) dP$$

eq. 4.17

4.2.3. Algorithms for phase equilibrium problems

In order to solve phase equilibrium problems, three types of calculations can be used. The first is called "bubble point calculation", the second "dew point calculation" and the third "isothermal flash". For the first case scenario, the liquid phase composition and either the temperature or pressure are known, while the vapor phase composition and pressure or temperature need to be calculated. For the second case, the vapor phase composition and either the temperature or pressure are defined, while the liquid phase composition and pressure or temperature accordingly need to be calculated. For last case scenario, the compositions of both vapor and liquid phases are unknown, while temperature and pressure are known[1]. All these are summarized in Table 4.1:

Table 4.1: Calculation types, which can be used, in order to solve phase equilibrium problems.

Known	Calculated	Algorithm
Temperature, liquid phase composition	Pressure, vapor phase composition	*Bubble Point Pressure*
Pressure, liquid phase composition	Temperature, vapor phase composition	*Bubble Point Temperature*
Temperature, vapor phase composition	Pressure, liquid phase composition	*Dew Point Pressure*
Pressure, vapor phase composition	Temperature, liquid phase composition	*Dew Point Temperature*
Temperature, Pressure	Liquid and Vapor phase composition	*Isothermal Flash*

In this study, the bubble point calculation was used in order to estimate the model parameters, whereas flash algorithms, which are implemented in process simulators, have been used for the simulations (eg. Isothermal Flash). The bubble point algorithm built for the description of acid gas-water-alkanolamine mixtures by eUMR-PRU model is presented at the end of this chapter.

4.3.   Chemical equilibrium

As far as the chemical equilibrium concerns the equilibrium of a chemical reaction is reached, when it has equal forward and backward rate and it is described by the following equation:

$$\sum v_i \bar{G}_i = 0 \qquad \text{eq. 4.18}$$

$$\sum v_i \left(G_i^o + RT \ln \frac{\hat{f}_i}{f_i^o} \right) = 0 \qquad \text{eq. 4.19}$$

where v_i are stoichiometric coefficients, G_i^o is Gibbs free energy of component i at standard condition and f_i^o is the fugacity of component i at standard condition. Therefore:

$$\ln K = -\frac{\Delta G^o}{RT} \qquad \text{eq. 4.20}$$

where $K = \Pi \left(\frac{\hat{f}_i}{f_i^o} \right)^{v_i} = \Pi \hat{a}_i^{v_i}$ eq. 4.21

$$\Delta G^o = \sum v_i G_i^o \qquad \text{eq. 4.22}$$

$$\hat{a}_i = \frac{\hat{f}_i}{f_i^o} \qquad \text{eq. 4.23}$$

K is called equilibrium constant of the reaction and because $a_i = x_i \gamma_i$, eq.4.20 becomes as follows

$$K = \Pi \hat{a}_i^{v_i} = K_x K_\gamma \qquad \text{eq. 4.24}$$

In activity coefficient models, in order to have consistency with the fugacity reference states, mentioned before, specific limits for activity coefficients have to be set. In most cases, solvent activity coefficients approach one as its mole fraction approach one, whereas solutes activity coefficient approach one as their mole fraction approach zero in pure water. The normalization followed for solutes is called asymmetric, whereas the one followed for solvents is called symmetric. However, in case of acid gases-water-alkanolamine mixtures the solvent is not only water, but also alkanolamines (mixed solvent). Therefore, the activity coefficients of both solvents should follow the symmetric

convention, whereas ions and acid gases, which are the solutes, follow the asymmetric convention[2].

In literature, most equilibrium constants presented are based on the asymmetric convention. Activity and activity coefficients cannot be measured experimentally, but they are identified by vapor-liquid equilibrium experimental data. Compositions can be measured and therefore K_x can be experimentally determined. K_x can have units of molarity, molality or mole fraction. K_x is determined at low concentration of various species, in order to achieve infinite dilution. However, at infinite dilution activity coefficients are unity and therefore $K=K_x$[5]. In this work K_x has mole fraction units and only equilibrium constants that confirm $K=K_x$ have been used. However, when these constants have to be used in low pressure γ-ϕ approach, a conversion of alkanolamine protonation equilibrium constant has to be made, because alkanolamines are symmetrically normalized.

4.3.1. Acid gas chemical reactions

In this section the chemical reactions taking place in liquid phase for acid gases-water-alkanolamines mixtures are presented[6] and categorized according to the amine:

Primary or secondary amines

$$RRNH_2{}^+ + H_2O \leftrightarrow RRNH + H_3O^+ \qquad\qquad \text{eq. 4.25}$$

$$H_2S + H_2O \leftrightarrow HS^- + H_3O^+ \qquad\qquad \text{eq. 4.26}$$

$$HS^- + H_2O \leftrightarrow S^{2-} + H_3O^+ \qquad\qquad \text{eq. 4.27}$$

$$CO_2 + 2H_2O \leftrightarrow HCO_3{}^- + H_3O^+ \qquad\qquad \text{eq. 4.28}$$

$$HCO_3{}^- + H_2O \leftrightarrow CO_3{}^{2-} + H_3O^+ \qquad\qquad \text{eq. 4.29}$$

$$RRNCOO^- + H_2O \leftrightarrow RRNH + HCO_3{}^- \qquad\qquad \text{eq. 4.30}$$

$$2H_2O \leftrightarrow OH^- + H_3O^+ \qquad\qquad \text{eq. 4.31}$$
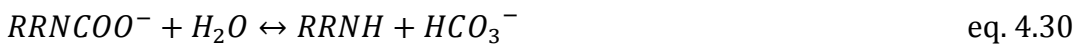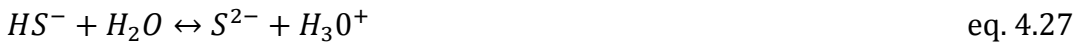
In case of primary amines, the alkyl is replaced with hydrogen.

Tertiary amines

$$R_3NH^+ + H_2O \leftrightarrow R_3N + H_3O^+$$ eq. 4.32

$$H_2S + H_2O \leftrightarrow HS^- + H_3O^+$$ eq. 4.33

$$HS^- + H_2O \leftrightarrow S^{2-} + H_3O^+$$ eq. 4.34

$$CO_2 + 2H_2O \leftrightarrow HCO_3^- + H_3O^+$$ eq. 4.35

$$HCO_3^- + H_2O \leftrightarrow CO_3^{2-} + H_3O^+$$ eq. 4.36

$$2H_2O \leftrightarrow OH^- + H_3O^+$$ eq. 4.37

In case of tertiary amines, the carbamate formation is missing.

4.3.2. Conversions of equilibrium constants

In order to solve the chemical equilibrium, experimental equilibrium constants have to be found in literature. However, some are presented on molality units, while others on mole fraction units. Furthermore, thermodynamic models use different standard states and equilibrium constants- which are presented in literature- have been converted accordingly. Therefore, the correct conversion of equilibrium constants to the required units and standard state is important for the accuracy of chemical equilibrium calculations.

4.3.2.1.   From molality to mole fraction

Equilibrium constants presented in the literature are often given on molality units (moles solute/kg solvent). However, in this work mole fraction units are used. Assuming, for example, water ionization, the equilibrium constant presented in the literature (in molality K) units is:

$$K_m = \frac{a_{OH^-} a_{H_3O^+}}{a_{H_2O}{}^2}$$ eq. 4.38

where α denotes the activity and subscript m refers to molality units.

At infinite dilution in water, the activity of water is one and the activity coefficients of the ions are one:

$$K_m{}^* = m_{OH^-} m_{H_3O^+} \qquad \text{eq. 4.39}$$

where m is the concentration of each species in molality units.

The equilibrium constant in mole fraction units is:

$$K_x{}^* = x_{OH^-} x_{H_3O^+} \qquad \text{eq. 4.40}$$

where x is the concentration of each species in mole fraction.

This form of the equilibrium constants ($K_x{}^*$) is the one used in this work by eUMR-PRU model and it corresponds to the equilibrium constants (4.55-4.62).

Each of the species has to be converted in mole fraction units:

$$x_i = m_i * \left(\frac{M_S}{1000}\right) \qquad \text{eq. 4.41}$$

where M_s is the molecular weight of the solvent (approximately equal to the molecular weight of water: 18 g/mole). Therefore:

$$K_x{}^* = K_m{}^* \left(\frac{M_S}{1000}\right)^2 \qquad \text{eq. 4.42}$$

In logarithmic scale:

$$ln\, K_x{}^* = ln\, K_m{}^* + 2ln\left(\frac{M_S}{1000}\right) \qquad \text{eq. 4.43}$$

In general, in order to convert the equilibrium constant of each reaction from molality to mole-fraction scale, it is necessary to add $\left(\frac{M_S}{1000}\right)$ for each product and to subtract $\left(\frac{M_S}{1000}\right)$ for each reactant, except for water[7].

4.3.2.2. *From asymmetric to symmetric standard state*

In case of alkanolamines, the convention followed in low pressure γ-ϕ approach in this work is the symmetric reference state: $γ_i \rightarrow 1$, when $x_i \rightarrow 1$. However, the equilibrium constants, which are usually reported in the literature follow asymmetric convention: $γ_i{}^* \rightarrow 1$, when $x_i \rightarrow 0$.

The equilibrium constant, normally reported in the literature, is the one used by eUMR-PRU:

$$K_x{}^* = \frac{x_{Am}x_{H_3O^+}}{x_{AmH^+}x_{H2O}} \frac{\gamma^*{}_{Am}\gamma^*{}_{H_3O^+}}{\gamma^*{}_{AmH^+}\gamma_{H2O}} = \frac{x_{Am}x_{H_3O^+}}{x_{AmH^+}x_{H2O}}$$
<div align="right">eq. 4.44</div>

In order to use the symmetric convention for the amines:

$$K_x{}' = \frac{x_{Am}x_{H_3O^+}}{x_{AmH^+}x_{H2O}} \frac{\gamma_{Am}\gamma^*{}_{H_3O^+}}{\gamma^*{}_{AmH^+}\gamma_{H2O}}$$
<div align="right">eq. 4.45</div>

$K_x{}'$ is the constant used by e-NRTL model:

$$K_x{}' = K_x{}^*\gamma^\infty{}_{Am}$$
<div align="right">eq. 4.46</div>

$\gamma^\infty{}_{Am}$ is the symmetrically normalized activity coefficient of alkanolamine at infinite dilution in water[2]. In literature review of equilibrium constants, attention to the convention of the activity coefficient followed should be paid.

4.4. Algorithms for phase and chemical equilibrium

Valid and fast algorithms are essential in phase and chemical equilibrium calculations and in simulations of such processes as those described before. According to literature, there are many algorithms that have been developed to solve this problem and they are classified in two categories, according to Smith and Missen[3]: the Gibbs free energy minimization algorithms and those who solve equilibrium algebraic equations[8].

The first one is a non-stoichiometric approach and it aims to minimize the Gibbs free energy of the system. The second one, is called the law of mass-action approach or the K-value method and it is a stoichiometric approach, which consists of mass balance, chemical and phase equilibrium equations for specified components and reactions. Both methods have advantages and disadvantages. The Gibbs free energy minimization algorithms are able to handle complex-non ideal multiphase systems and determine the stability of the phases. However, they require as input many thermodynamic data (standard chemical potential for all components at different temperatures and pressures), which are hard to find. On the other hand, law of mass-action or K-value approach is simple, convenient and the input thermodynamic data needed are the equilibrium constants of the reaction, which are easier to find compared to the standard chemical potentials[9]. Therefore, when the number of stable phases and the equilibrium constants of the reactions are known this method seems to be the most convenient.

The law of mass-action approach can be further divided in two categories. The first is called SES (simultaneous equation solving), in which all equations are solved simultaneously, using for instance Newton method, Marquardt method, quasi-Newton method or other. In the second category the equations are not solved simultaneously. They are often solved in an inner loop with estimates of equilibrium constants (K-values); the equilibrium constants in their turn change in the outer loop, because of their dependency on phase compositions [10].

In this study the law of mass-action approach is used. As it has already been mentioned in the introduction of this chapter, the electrolyte species will dissociate in the liquid phase in order to form ions. All reactions take place in the liquid phase. The ions will remain in the liquid phase, due to their volatility and there would be no dissociation of them in vapor phase, unless the system temperature is very high. Therefore, equation 4.10 is applied just to molecular components. The composition of ions in liquid phase is of great importance to the phase equilibrium, even though equation 4.10 is applied only to molecular species: the liquid phase composition of the ions affects the composition of molecular species in the same phase and as a result it affects the phase equilibrium[11]. The procedure mainly followed in this work is: Initially, the liquid phase composition is defined by solving the chemical equilibrium as described by equations 4.55-4.68 and then bubble point calculations are performed. In this work one primary (monoethanolamine) and one tertiary (methyldiethanolamine) alkanolamine have been examined. The chemical reactions, mass balance and electroneutrality equations are presented below.

Dissociation of MEAH$^+$

$$MEAH^+ + H_2O \leftrightarrow MEA + H_3O^+ \hspace{4cm} \text{eq. 4.47}$$

Dissociation of MDEAH$^+$

$$MDEAH^+ + H_2O \leftrightarrow MDEA + H_3O^+ \hspace{3cm} \text{eq. 4.48}$$

Dissociation of H$_2$S

$$H_2S + H_2O \leftrightarrow HS^- + H_3O^+ \hspace{4cm} \text{eq. 4.49}$$

Dissociation of HS$^-$

$$HS^- + H_2O \leftrightarrow S^{2-} + H_3O^+ \hspace{4cm} \text{eq. 4.50}$$

Dissociation of CO$_2$

$$CO_2 + 2H_2O \leftrightarrow HCO_3^- + H_3O^+ \qquad \text{eq. 4.51}$$

Dissociation of HCO_3^-

$$HCO_3^- + H_2O \leftrightarrow CO_3^{2-} + H_3O^+ \qquad \text{eq. 4.52}$$

Carbamate reversion to bicarbonate

$$MEACOO^- + H_2O \leftrightarrow MEA + HCO_3^- \qquad \text{eq. 4.53}$$

Ionization of H_2O

$$2H_2O \leftrightarrow OH^- + H_3O^+ \qquad \text{eq. 4.54}$$

The mole-fraction based equilibrium constants are defined as follows:

$$K_1 = \frac{x_{MEA}\, x_{H3O+}}{x_{MEAH+}\, x_{H2O}} \qquad \text{eq.4.55}$$

$$K_2 = \frac{x_{MDEA}\, x_{H3O+}}{x_{MDEAH+}\, x_{H2O}} \qquad \text{eq. 4.56}$$

$$K_3 = \frac{x_{HS^-}\, x_{H3O+}}{x_{H_2S}\, x_{H2O}} \qquad \text{eq. 4.57}$$

$$K_4 = \frac{x_{S^{2-}}\, x_{H3O+}}{x_{HS^-}\, x_{H2O}} \qquad \text{eq. 4.58}$$

$$K_5 = \frac{x_{HCO_3^-}\, x_{H3O+}}{x_{CO_2}\, x_{H2O}^2} \qquad \text{eq. 4.59}$$

$$K_6 = \frac{x_{CO_3^{2-}}\, x_{H3O+}}{x_{HCO_3^-}\, x_{H2O}} \qquad \text{eq. 4.60}$$

$$K_7 = \frac{x_{MEA}\, x_{HCO_3^-}}{x_{MEACOO^-}\, x_{H2O}} \qquad \text{eq. 4.61}$$

$$K_8 = \frac{x_{OH^-}\, x_{H3O+}}{x_{H2O}^2} \qquad \text{eq. 4.62}$$

The eight above equations have to be solved together with mass balance and electroneutrality equations presented below:

$$x_{MDEA} + x_{MDEAH+} = MF_{MDEA,in}$$
<div align="right">eq. 4.63</div>

$$x_{MEA} + x_{MEAH+} + x_{MEACOO-} = MF_{MEA,in}$$
<div align="right">eq. 4.64</div>

$$x_{CO_2} + x_{HCO_3-} + x_{CO_3^{2-}} + x_{MEACOO-} = a_{CO_2} (MF_{MEA,in} + MF_{MDEA,in})$$
<div align="right">eq. 4.65</div>

$$x_{H_2S} + x_{HS-} + x_{S^{2-}} = a_{H_2S} (MF_{MEA,in} + MF_{MDEA,in})$$
<div align="right">eq. 4.66</div>

$$\sum_{j=1}^{NS} x_j = 1$$
<div align="right">eq. 4.67</div>

$$x_{MDEAH+} + x_{MEAH+} + x_{H3O+} - x_{HS-} - 2\,x_{S^{2-}} - x_{HCO_3-} - 2\,x_{CO_3^{2-}} - x_{MEACOO-}$$
$$- x_{OH-}$$
$$= 0$$
<div align="right">eq. 4.68</div>

where x_j is the mole fraction of species i, NS is the number of species, $MF_{MEA,in}$ and $MF_{MDEA,in}$ are the initial mole fractions of MEA and MDEA respectively, and a_{co2} and a_{h2s} are the CO_2 and H_2S loadings, which are defined below:

$$\alpha_{CO_2} = \frac{x_{CO_2tot}}{x_{amine_{tot}}} = \frac{x_{CO_2} + x_{HCO3-} + x_{CO_3^{2-}} + x_{MEACOO-}}{x_{MEA} + x_{MEAH+} + x_{MEACOO-} + x_{MDEA} + x_{MDEAH+}}$$
<div align="right">eq.4.69</div>

$$\alpha_{H_2S} = \frac{x_{H_2Stot}}{x_{amine_{tot}}} = \frac{x_{H_2S} + x_{HS-} + x_{S^{2-}}}{x_{MEA} + x_{MEAH+} + x_{MEACOO-} + x_{MDEA} + x_{MDEAH+}}$$
<div align="right">eq. 4.70</div>

Therefore, there are fourteen unknowns, which are the molecular and ionic species existing at equilibrium in liquid phase: MEA, MDEA, H_2O, H_2S, CO_2, $MEAH^+$, $MDEAH^+$, H_3O^+, OH^-, HS^-, S^{2-}, HCO_3^-, CO_3^{2-} and $MEACOO^-$ and fourteen equations (4.55-4.68), which have to be solved simultaneously[12].

After the solution of chemical equilibrium, the liquid phase composition is used in a bubble point algorithm of eUMR-PRU model, in order to solve phase equilibrium. This procedure is described in the following scheme.
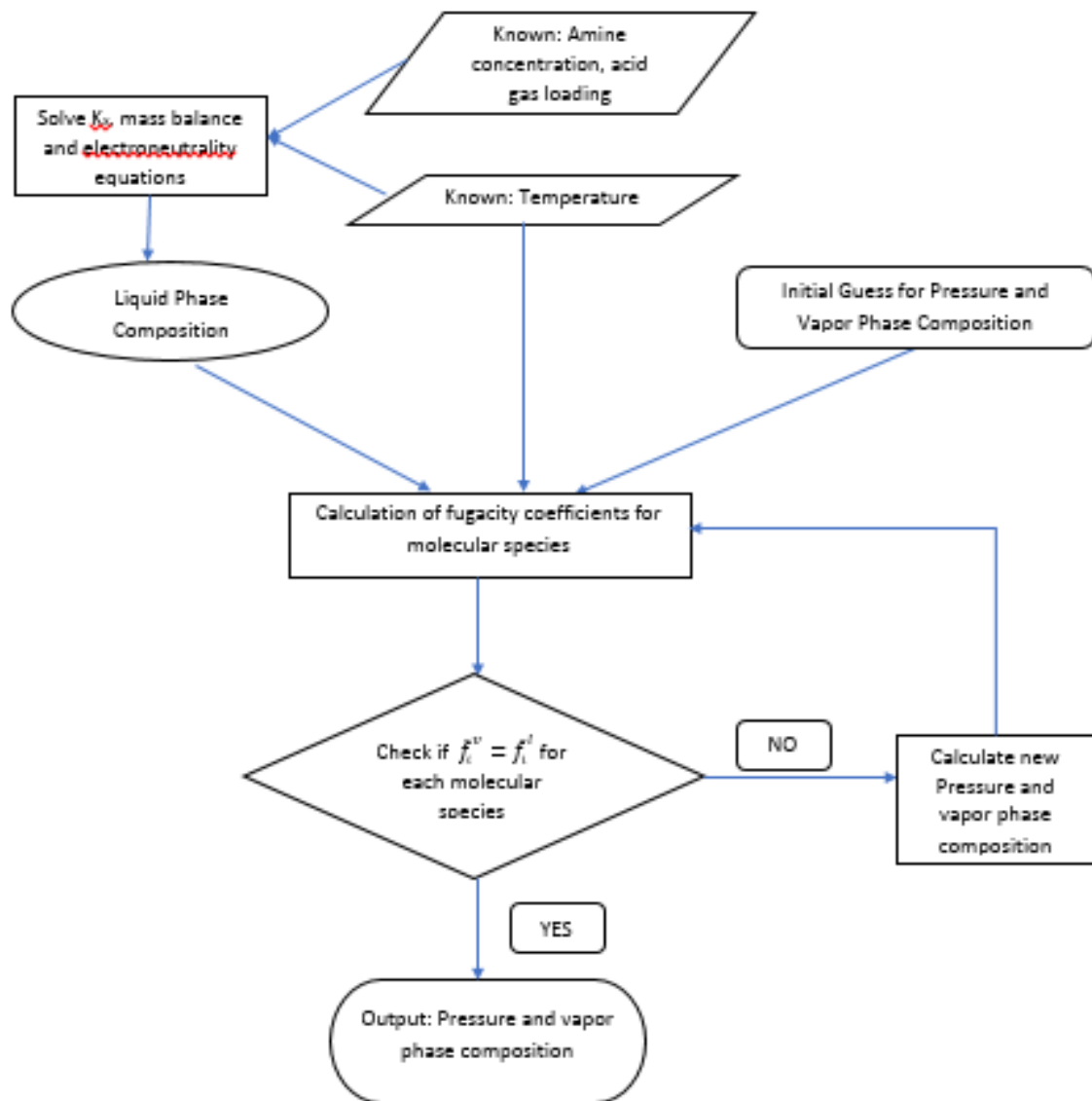
Figure 4.1: Flowchart of bubble point calculation algorithm used in this work

4.5.   Conclusions

Solving the problem of chemical and phase equilibrium is critical in thermodynamics. In this thesis, the mixtures examined are acid gases-water-alkanolamines and acid gas-ionic liquid. In first case, the mixture is described by chemical and phase equilibrium, whereas in second by phase equilibrium only. The problem of "chemical" and "phase equilibrium" is a complex one and therefore different approaches have been proposed in literature on solving it. The law of "mass action" is the most common approach, hence it is used in this work. For that reason, equilibrium constants have been found in literature and they have been used in conjunction with mass balance and electroneutrality equations in order to calculate the liquid phase composition. Subsequently, this composition and the temperature have been used as inputs to a bubble point algorithm, which solves vapor-liquid equilibrium by using a thermodynamic model. The thermodynamic models used in this work are described in next Chapter.

4.6. References

1.   Tassios, D. P., *Applied chemical engineering thermodynamics*. 1993.
2.   Posey, M. L., Thermodynamic model for acid gas loaded aqueous alkanolamine solutions. **1998**.
3.   Smith, W. R.; Missen, R. W., *Chemical reaction equilibrium analysis : theory and algorithms*. New York (N.Y.) : Wiley: 1982.
4.   Sadegh, N., Acid gas removal from natural gas with alkanolamines: a modeling and experimental study. **2013**.
5.   Vrachnos, A. Acid gas absorption in aqueous alkanolamine solutions: Experimental study and thermodynamic modeling. National Technical University of Athens, Athens, 2007.
6.   Barreau, A.; Le Bouhelec, E. B.; Tounsi, K. H.; Mougin, P.; Lecomte, F., Absorption of H2S and CO2 in alkanolamine aqueous solution: experimental data and modelling with the electrolyte-NRTL model. *Oil & Gas Science and Technology-Revue de l'IFP* **2006,** *61* (3), 345-361.
7.   Austgen Jr, D. M. *A model of vapor-liquid equilibria for acid gas-alkanolamine-water systems*; Texas Univ., Austin, TX (USA): 1989.
8.   Tsanas, C. Simultaneous Chemical and Phase Equilibrium Calculations with Non-Stoichiometric Methods. Technical University of Denmark, 2018.
9.   Leal, A. M.; Kulik, D. A.; Kosakowski, G.; Saar, M. O., Computational methods for reactive transport modeling: An extended law of mass-action, xLMA, method for multiphase equilibrium calculations. *Advances in Water Resources* **2016,** *96*, 405-422.
10.   Teh, Y.; Rangaiah, G., A study of equation-solving and Gibbs free energy minimization methods for phase equilibrium calculations. *Chemical Engineering Research and Design* **2002,** *80* (7), 745-759.
11.   Kumar, G. Vapour-liquid Equilibrium of Carbon Dioxide in Newly Proposed Blends of Alkanolamines. 2013.
12.   Plakia, A.; Voutsas, E., Modeling of H2S, CO2 + H2S, and CH4 + CO2 Solubilities in Aqueous Monoethanolamine and Methyldiethanolamine Solutions. *Industrial & Engineering Chemistry Research* **2020,** *59* (24), 11317-11328.

5. Thermodynamic models

In this chapter thermodynamic models used in this work are described. A semiempirical (Kent-Eisenberg), an activity coefficient (electrolyte-NRTL), an equation of state (Peng-Robinson) and an EoS/G^E model (eUMR-PRU in case of acid gases-water-alkanolamines and UMR-PRU in case of acid gas-ionic liquid mixtures) are used in this thesis and their thermodynamic framework is presented.

5.1. Introduction

The simulation and optimization of physical and chemical processes requires the use of either experimental data or thermodynamic models. However, the experimental measurements are expensive and time consuming and they cannot be available at any condition. Last decades, thermodynamic models have been used a lot by process engineers for process design and optimization. For that reason, it is important to have thermodynamic models, which have been regressed to reliable experimental data and describe accurately the studied mixtures at various conditions.

The accurate description of the solubility of acid gases in aqueous alkanolamine solutions is a highly demanding and complex project for the thermodynamic models, because these mixtures are highly non-ideal and they consist of many species, which interact with each other with long-range, short-range and dipole forces[1].

In literature, there are three types of models used for the description of vapor-liquid equilibrium of acid gases in aqueous alkanolamine solutions: semiempirical, activity coefficient and equations of state. Semiempirical models are simple, but they are not based on a theoretical thermodynamic concept. On the other hand, activity coefficient models have an accurate theoretical background and they describe satisfactorily the experimental data especially at low pressures, but they need different equations for the description of the vapor and liquid phases. Equations of state provide a consistent description of the mixture, since they use the same equation for the various phases. Equations of state are often combined with excess Gibbs energy models (EoS/G^E) in order to extend the applicability of activity coefficient models to high pressures.

A well-known semiempirical model is Kent-Eisenberg model[2-3], which assumes ideal vapor and liquid phases. Some of the equilibrium constants of the model are calculated by regression to experimental solubility data of acid gases into aqueous alkanolamines. Many authors have used this model modified[4]. Another semiempirical model is the model of Posey et al[5], which consists of a single reaction which combines the bicarbonate or bisulphide formation with a combined Henry's constant and equilibrium constant and it neglects other reactions.[6]

Widely used activity coefficient models are electrolyte-NRTL[7], extended UNIQUAC[8], Deshmukh-Mather[9] etc. Many authors have used these models to describe the solubility of acid gases in alkanolamines[10-14] coupled with an equation of state for the description of the vapor phase such as Peng-Robinson[15] or Soave-Redlich-Kwong (SRK).

The third type of models are the Equations of State (EoS). These models provide a more consistent description of the mixtures, because the same equation is applied to various phases, but various modifications are required in order to be used in polar, nonideal and

electrolyte mixtures. In order to surpass the disadvantages of EoS, they are often combined with excess Gibbs energy models (EoS/G^E) and they are better than activity coefficient models at high loadings and comparable at medium loadings. Many authors have used equations of state for the description of acid gases solubility in aqueous alkanolamine solutions, such as the electrolyte EoS proposed by Fürst and Renon[16], the electrolyte- LCVM model[6], which combines the translated and modified PR EoS with the extended UNIQUAC[8], the SAFT EoS[17] (Statistical Associating Fluid Theory), which uses the theoretical background of molecular thermodynamics, the PC-SAFT[18-20], the Cubic plus Association (CPA) EoS[21-22], which combines the SRK EoS with the association term obtained from the Wertheim theory.

Recently, ionic liquids have been proposed as potential solvents for acid gases physical absorption and many authors have used models, especially equations of state, in order to describe these mixtures. For example, PR EoS and SRK EoS have been widely used[23-25], because they are simple and accurate. Furthermore, the Group Contribution EoS (GC EoS) presented by Skjord-Jorgensen has been used by some authors[26-28]. This model combines four theories: van der Waals EoS, Carnahan-Starling equations for hard-spheres, NRTL model[29] and the group contribution principle. Cubic plus Association and Statistical Associating Fluid Theory (SAFT) have been also applied in this case[30-31].

In this work, models of all of the above categories are used for the description of vapor-liquid equilibrium of acid gases in aqueous alkanolamines: Kent-Eisenberg[2], electrolyte-NRTL[7] and eUMR-PRU[32], which is an extension of UMR-PRU[33] model to acid gases-water-alkanolamines and it is developed in this thesis. Moreover, PR[15] and UMR-PRU[33] are utilized for the description of vapor-liquid equilibrium of acid gases in ionic liquids.

5.2. Semiempirical model

Semiempirical models are simple, but they are not as preferable as other models nowadays, because the lack precise thermodynamic agreement. The vapor pressure of the gas is related directly to the concentration of the gas in the liquid phase by Henry's constant. It is assumed, that the vapor phase fugacity coefficient is unity and the activity coefficient in the liquid phase is unity. These models can be further classified concerning the type of the equilibrium constant approach (if it is pseudo-equilibrium, fixed or single reaction approach). Models of the first category are not as simple as the rest, because each equilibrium constant is fitted to experimental data. Models of the second approach are simple and rapid, because they use published equilibrium constants for most of the reactions, while the rest, they fit them to experimental data of acid gas solubility in aqueous alkanolamine solutions, in order to account for the non-idealities. Finally, the

last approach is a quick and simple method, because it uses an equilibrium constant, which combines the other constants[1].

5.2.1. Kent-Eisenberg

Kent Eisenberg[2] is a well-known semi-empirical model, because it is simple and describes the experimental data satisfactorily. It belongs to the second approach (fixed equilibrium approach), since it uses mainly published equilibrium constants.

In this work, Kent-Eisenberg model is used for mixtures containing H_2S and MEA or MDEA. The model, presented by Pitsinigos et al[34], is a modified Kent-Eisenberg model and describes the equilibrium through the following equations:

Primary amine: $H_2S + RNH \overset{K_1}{\leftrightarrow} RNH_2{}^+ + HS^-$
$$\text{eq. 5.1}$$

Ternary amine: $H_2S + R_3N \overset{K_1}{\leftrightarrow} R_3NH^+ + HS^-$

$$H_2S \overset{K_2}{\leftrightarrow} HS^- + H^+ \qquad\qquad \text{eq. 5.2}$$

$$HS^- \overset{K_3}{\leftrightarrow} S^{2-} + H^+ \qquad\qquad \text{eq. 5.3}$$

$$H_2O \overset{K_4}{\leftrightarrow} OH^- + H^+ \qquad\qquad \text{eq. 5.4}$$
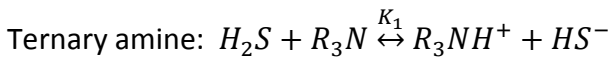
The model consists of eight equations (equilibrium equations for the above reactions plus mass balance equations):

Primary amine:
$$K_1 = \frac{[RR'NH_2{}^+][HS^-]}{[RR'NH][H_2S]} \qquad\qquad \text{eq. 5.5}$$

Ternary amine:
$$K_1 = \frac{[RNH^+][HS^-]}{[R_3N][H_2S]}$$

$$K_2 = \frac{[H^+][HS^-]}{[H_2S]} \qquad\qquad \text{eq. 5.6}$$

$$K_3 = \frac{[H^+][S^{2-}]}{[HS^-]}$$ eq. 5.7

$$K_4 = [H^+][OH^-]$$ eq. 5.8

Primary amine: $[RNH_2{}^+] + [RNH] = M$ eq. 5.9

Ternary amine: $[R_3NH^+] + [R_3N] = M$

$$[H_2S] + [HS^-] + [S^{2-}] = \alpha_{H_2S}M$$ eq. 5.10

$$[RNH_2{}^+] + [H^+] = [OH^-] + [HS^-] + 2[S^{2-}]$$ eq. 5.11

$$P_{H_2S} = H_{H_2S}[H_2S]$$ eq. 5.12

The equilibrium constants and Henry's law constant were estimated by fitting to experimental data and they are presented as a function of temperature in Table 5.1:

Table 5.1: Equilibrium constants of reactions eq. 5.1-5.4 and Henry's constant[34] $(K = e^{A+\frac{B}{T}+\frac{C}{T^2}+\frac{D}{T^3}+\frac{E}{T^4}+F\ln T})$

		Units	A	B	C	D	E	F
K1 (MEA)	T<=363.15	-	-8.3932	4608.71	0	0	0	0
	T>363.15	-	-11.1744	5619.07	0	0	0	0
K1 (MDEA)			-52.1826	-4044.8	0	0	0	7.848
K2		gm ions/kg	218.599	-12995.4	0	0	0	-33.5471
K3		gm ions/kg	-657.965	916311	-490629600	1.15307E+11	-1.01016E+13	0
K4		(gm ions/kg)2	140.932	-13445.9	0	0	0	-22.4773
H_{H2S}		mmHg*kg/(gm moles)	104.518	-136808	73774380	-17472220000	1.52162E+12	0

The eight above equations (eq. 5.5-5.12) can be solved in order to find the concentration of the species. However, the system of equations can be reduced to two equations:

$$\frac{K_4}{[H^+]} + L_{H_2S}M - \frac{P_{H_2S}}{HK} + \left(L_{H_2S}M - \frac{P_{H_2S}}{HK}\right)\frac{K_3}{K_3+[H^+]} - M[H^+]\frac{K_1}{K_2+[H^+]K_1} - [H^+] = 0 \text{ eq. 5.13}$$

$$HK\left(L_{H_2S}M - \frac{P_{H_2S}}{HK}\right)\frac{[H^+]^2}{K_2}K_3\left(1 + \frac{[H^+]}{K_3}\right) - P_{H_2S} = 0 \qquad \text{eq. 5.14}$$

The unknowns are $[H^+]$ and L_{H_2S}, when P_{H_2S} is known, or P_{H_2S}, when L_{H_2S} is known. The two equations are solved using Newton iteration method.

5.3. Activity coefficient model

Activity coefficient models are precise, especially at low and medium loadings, but they are not as simple as semiempirical models, because they need a large amount of interaction parameters to be fitted to an extended database and they use different equations for the description of the various phases. For the representation of the long-range coulombic forces, Debye-Hückel theory is usually preferred. Other theories often used are Fürst and Renon[16], Guggenheim and Turgeon[35] etc. For the short-range forces, models of local composition are mainly used, such as NRTL[29], UNIQUAC, so the new models are electrolyte-NRTL, electrolyte UNIQUAC and extended-UNIQUAC[1]. In this work electrolyte-NRTL (e-NRTL) model has been used.

5.3.1. Electrolyte-NRTL
The e-NRTL model was proposed by Chen et al[7] and it is based on two assumptions: (a) the local composition of cations around cations and anions around anions is zero, and, (b) the ions are distributed in such a way around a molecule that ensures zero net local ionic charge. e-NRTL is based on the following equation:

$$\frac{G^E}{RT} = \frac{G^{E,LC}}{RT} + \frac{G^{E,LR}}{RT} \qquad \text{eq. 5.15}$$

G^E is the excess Gibbs free energy of the electrolyte system, $G^{E,LC}$ is the contribution to the excess Gibbs free energy of the local interactions and it is calculated by NRTL model[29] and $G^{E,LR}$ is the contribution to the excess Gibbs free energy of the long-range interactions.

The activity coefficient, which is derived by the eq. 5.15 needs to be normalized. Therefore, reference states for molecules and ions need to be chosen. The reference

states in a mixed solvent mixture are presented in Table 5.2 and they have been explained in Chapter 4 as well:

Table 5.2: Reference states used in this work for e-NRTL model.

water, amines	Symmetric	$f_i = x_i\gamma_i f^o{}_i$	$\gamma_i \rightarrow 1$, when xi$\rightarrow$1
Ions	asymmetric	$f_i = x_i\gamma^*{}_i f^*{}_i$	$\gamma_i^* \rightarrow 1$, when xi$\rightarrow$0
acid gases	asymmetric	$f_i = x_i\gamma^*{}_i H_i$	$\gamma_i^* \rightarrow 1$, when xi$\rightarrow$0

Pitzer-Debye-Hückel equation is used to calculate the contribution of the long-range interactions to the excess Gibbs free energy:

$$\frac{G^{E,PHD}{}_m}{RT} = \sum_k x_k \left(\frac{1000}{M_s}\right)^{1/2} \left(\frac{4AI}{\rho}\right) ln\left(1 + \rho I^{1/2}\right) \qquad \text{eq. 5.16}$$

where M_s, is the molecular weight of the solvent (kg/kmol)

X_k, is the molecular weight of component k in the liquid phase

A, is the Debye-Hueckel parameter

I, is the ionic strength

ρ, is the closest- approach parameter

The Debye- Hückel parameter is calculated by the following equation:

$$A = \frac{1}{3}\left(\frac{2\pi N_A d_s}{1000}\right)^{1/2} \left(\frac{Q^2{}_e}{e_w k_w T}\right)^{3/2} \qquad \text{eq. 5.17}$$

where N_A, is the Avogadro's number

d_s, is the density of the solvent

Q_e, is the electron charge

k_B, is the Boltzmann constant

e_B, is the dielectric constant of water

T, is the temperature in K

$$I = \frac{1}{2}\sum_i m_i z_i{}^2 \qquad \text{eq. 5.18}$$

where z_i is the charge number of ion i.

The Born equation is used in order to take into account the Gibbs energy of transfer of ions from the infinite dilution in mixed solvent to infinite dilution in aqueous phase:

$$\frac{G^{E,LR}}{RT} = \frac{G^{E,PDH}}{RT} + \frac{G^{E,Born}}{RT}$$

eq. 5.19

where Born term is calculated by the following equation:

$$\frac{G^{E,Born}}{RT} = \left(\frac{Q^2_e}{2k_BT}\right)\left(\frac{1}{e_S} - \frac{1}{e_w}\right)\left(\sum_\iota \frac{x_i z_i^2}{r_k}\right)10^{-2}$$

eq. 5.20

where e_s is the dielectric constant of the solvent mixture

r_k, is the Born radius of species i.

The contribution to the excess Gibbs free energy of the local interactions is calculated by the Non-Random Two Liquid theory:

$$\frac{G^{E,LC}}{RT} = \sum_m n_m \left(\frac{\sum_\iota X_i G_{im}\tau_{im}}{\sum_\iota X_i G_{im}}\right) + \sum_c z_c n_c \left(\frac{\sum_{\iota.ne.c} X_i G_{ic}\tau_{ic}}{\sum_{\iota.ne.c} X_i G_{ic}}\right) + \sum_a z_a n_a \left(\frac{\sum_{\iota.ne.a} X_i G_{ia}\tau_{ia}}{\sum_{\iota.ne.a} X_i G_{ia}}\right)$$

eq. 5.21

where m, is a molecular species

c, is a cation

a, is an anion.

The first term is the contribution of local interactions, when a molecular component is at the center and other molecular components, anions and cations are in its neighborhood. The second term is the contribution when a cation is at the center and the third term is the contribution when an anion is at the center. G and τ are local binary quantities related by the following equation:

$$G = exp(-a\tau)$$

eq. 5.22

$$\tau = -\frac{\ln G}{\alpha}$$

eq. 5.23

where a is the nonrandomness factor parameter and τ is a binary interaction parameter, which is fitted to experimental data and it is usually described by a linear equation with temperature:

$$\tau = a + \frac{b}{T}$$

eq. 5.24

The model adjustable parameters are pure component dielectric constants of nonaqueous solvents, the Born radius of ionic species and the NRTL interaction

parameters between molecule-molecule, molecule-electrolyte, electrolyte-electrolyte. These parameters are temperature-dependent. For example, for a solvent A the dielectric constant is calculated by:

$$e_A(T) = A_A + B_B \left(\frac{1}{T} - \frac{1}{C_A} \right)$$ eq. 5.25

The parameters for equation 5.25 are given in Table A.1 of Appendix_A.

The molecule-molecule binary parameters:

$$\tau_{AA'} = A_{AA'} + \frac{B_{AA'}}{T} + F_{AA'} \ln(T) + G_{AA'}T$$ eq. 5.26

The electrolyte-molecule binary parameters:

$$\tau_{iA} = C_{iA} + \frac{D_{iA}}{T} + E_{iA} \left(\frac{298.15 - T}{T} + \ln\left(\frac{T}{298.15} \right) \right)$$ eq. 5.27

$$\tau_{Ai} = C_{Ai} + \frac{D_{Ai}}{T} + E_{Ai} \left(\frac{298.15 - T}{T} + \ln\left(\frac{T}{298.15} \right) \right)$$ eq. 5.28

where subscript i refers to electrolyte and A to molecule and T is the temperature in Kelvin.

In case of electrolyte-electrolyte parameters, the two electrolytes must share one common anion or one common cation and the temperature dependency is the same as in the electrolyte-molecule binary parameters. The binary interaction parameters are presented in Tables A.2-A.3 of Appendix_A, where E, F, G are set equal to zero and nonrandomness factor is set equal to 0.2. The amine-ion pair/ion pair-amine parameters and CO_2-ion pair/Ion pair-CO_2 parameters were set to 15 and -8 respectively. In this work, the parameters mentioned have been provided by ASPEN PLUS V8.6.

The Henry's constants for CO_2 and H_2S in pure water are presented in Table A.4 of Appendix_A.

The Henry's law constant in the mixed solvent (amine-water) is calculated by the following equation:

$$\ln\left(\frac{H_i}{\gamma_i^{inf}} \right) = \sum_A w_A \ln\left(\frac{H_{iA}}{\gamma_{iA}^{inf}} \right)$$ eq. 5.29

where H_i is the Henry's law constant in amine-water solvent, H_{iA} is the Henry's law constant in pure solvent A (in this case water), γ_i^{inf} is the activity coefficient of i at infinite

dilution in the mixed solvent, whereas $\gamma_{iA}{}^{inf}$ is the activity coefficient of i at infinite dilution in pure solvent A.

$$w_A = \frac{x_A\left(v_{iA}{}^{inf}\right)^{2/3}}{\sum_B x_B\left(v_{iB}{}^{inf}\right)^{2/3}}$$

eq. 5.30

where x_A is the mole fraction of solvent A on a basis free of solutes, $v_{iA}{}^{inf}$ is the partial molar volume of solute I at infinite dilution in pure solvent A.

5.4. Cubic Equations of State

Van der Waals proposed in 1873 the first equation of state, which differed from the equation of ideal gas because he assumed that the real volume, which is available to a molecule's movement, is reduced by the volume which corresponds to the other molecules. Furthermore, he introduced the idea of the intramolecular forces, which result to condensation at high pressures and he concluded, that pressure is analogous to $1/V^2$. Redlich said, that this theory is correct, but van der Waals equation of state lack accuracy in the description of experimental data[36].

Later on, many improvements to this equation have been proposed, leading to new equations of states, such as Redlich-Kwong, Soave-Redlich-Kwong and Peng-Robinson equations of state.

Cubis EoS are used for the calculation of fugacities in vapor and liquid phases. However, they lack accuracy in the description of non-ideal mixtures. Therefore, they are often combined with excess Gibbs energy models resulted to the so-called EoS/G^E models. Equations of state have a poor prediction performance in acid gas-alkanolamine-water mixtures but EoS/G^E appear a good prediction capability to these mixtures[1].

Therefore, in this work the equations of state examined are, PR EoS with classical mixing rules, UMR-PRU, which is an EoS/G^E model and it combines PR EoS with the Universal mixing rules (UMR) [33]. Both of them are used in acid gas-ionic liquid mixtures and they are compared to each other. For the acid gas-alkanolamine-water mixtures, UMR-PRU has been extended with the introduction of the Debye-Hueckel term in the G^E calculation and the new model is named electrolyte-UMR-PRU (eUMR-PRU).

5.4.1. Peng Robinson with classical mixing rules

The models examined in this work are based on PR EoS[15].

$$P = \frac{RT}{v-b} - \frac{a}{v(v+b)+b(v-b)}$$

eq. 5.31

For pure components, the temperature dependent attractive term parameter, a, for non-polar molecules, is calculated by the Soave expressions:

$$a = a_c a(T)$$ eq. 5.32

$$a_c = 0.45724 \frac{R^2 T_c^2}{P_c}$$ eq. 5.33

$$a(T) = [1 + m(1 - T_r^{0.5})]^2$$ eq. 5.34

$$m = 0.37464 + 1.54226\omega - 0.26992\omega^2$$ eq. 5.35

For pure polar molecules, such as water and amines, the attractive term parameter is calculated by the Mathias-Copeman expression:

$$a(T) = [1 + c_1(1 - T_r^{0.5}) + c_2(1 - T_r^{0.5})^2 + c_3(1 - T_r^{0.5})^3]^2 \quad for \quad T \leq T_r$$ eq. 5.36

$$a(T) = [1 + c_1(1 - T_r^{0.5})]^2 \quad for \quad T > T_r$$ eq. 5.37

c_1, c_2, c_3 are pure-component parameters which are determined by fitting pure component vapor pressure data.

The co-volume parameter, b, for pure components is calculated from:

$$b = 0.07780 \frac{RT_c}{P_c}$$ eq. 5.38

For non-ideal mixtures, an interaction parameter k_{ij} or l_{ij} is introduced and α and b are calculated by the van der Waals one fluid mixing rules and the classical combining rules:

$$a = \sum_i \sum_j x_i x_j a_{ij}$$ eq. 5.39

$$b = \sum_i \sum_j x_i x_j b_{ij}$$ eq. 5.40

$$a_{ij} = (a_i a_j)^{1/2}(1 - k_{ij})$$ eq. 5.41

$$b_{ij} = \left(\frac{b_i + b_j}{2}\right)(1 - l_{ij})$$ eq. 5.42

Peng-Robinson EoS has been applied in this work for CO_2 solubility in ionic liquids. The critical properties, acentric factor and Mathias-Copeman parameters are presented in Table A.5 of Appendix A, whereas binary interaction parameters are presented in Table A.10 of Appendix_A.

5.4.2. UMR-PRU model

The basic principle for an EoS/G^E model development is the equality of the calculated, by an equation of state, Gibbs free energy with the Gibbs free energy calculated by an activity coefficient model, according to Huron and Vidal[37]:

$$\left(\frac{G^E}{RT}\right)^{EOS} = \left(\frac{G^E}{RT}\right)^{activity\ coef.model}$$

eq. 5.43

This equality is verified at a reference pressure, which usually is the infinite pressure or zero pressure[38].

UMR-PRU[33] is an EoS/G^E model which combines Peng-Robinson equation of state, presented by equations 5.31-5.38, with UNIFAC[39] via Universal mixing rules.

$$\frac{a}{bRT} = \frac{1}{-0.53}\frac{G_{AC}^E}{RT} + \sum_i x_i \frac{a_i}{b_i RT}$$

eq. 5.44

$$b = \sum_i \sum_j x_i x_j b_{ij}$$

eq. 5.45

$$with \quad b_{ij} = \left(\frac{b_i^{1/2}+b_j^{1/2}}{2}\right)^2 (1-l_{ij})$$

eq. 5.46

In most cases l_{ij} interaction parameter in eq. 5.46 is equal to zero except for the mixtures referred to in Table A.9 of Appendix_A.

In eq. 5.44, $\frac{G_{AC}^E}{RT} = \sum x_i ln\gamma_i$ is calculated by the UNIFAC model[39].

$$ln\,\gamma_n = ln\,\gamma_n^{C,SG} + ln\,\gamma_n^R$$

eq. 5.47

$$ln\,\gamma_n^{C,SG} = -5q_n\left(ln\frac{\varphi_n}{\theta_n}+1-\frac{\varphi_n}{\theta_n}\right)$$

eq. 5.48

$$\varphi_n = \frac{x_n r_n}{\sum_{j=1}^{NS} x_j r_j}$$

eq. 5.49

$$\theta_n = \frac{x_n q_n}{\sum_{j=1}^{NS} x_j q_j}$$

eq. 5.50

$$ln\,\gamma_n^R = q_n\left(1 - ln(\sum_{k=1}^{NS}\theta_k\Psi_{kn}) - \sum_l \frac{\theta_l\Psi_{nl}}{\sum_{k=1}^{NS}\theta_k\Psi_{kn}}\right)$$

eq. 5.51

The interaction parameter Ψ_{nl} between species n and l is given by the following expression:

$$\Psi_{nl} = exp\left[-\frac{A_{nl}+B_{nl}T+C_{nl}T^2}{T}\right]$$

eq. 5.52

where A_{nl}, B_{nl} and C_{nl} are adjustable binary interaction parameters.

UMR-PRU parameters are presented in Tables A.5-A.9 of Appendix_A. Table A.5 includes the critical properties, acentric factors and Mathias-Copeman parameters of PR, UMR-PRU and eUMR-PRU. Table A.7 includes the Van der Waals Volume and Area parameters for UMR-PRU and eUMR-PRU models, whereas Table A.8 includes the binary interaction parameters of eq.5.52 for UMR-PRU and eUMR-PRU models.

5.4.3. Extention of UMR-PRU model (eUMR-PRU model)

Equations of state were initially developed for nonpolar, nonionic and especially ideal mixtures. In order to extend them to polar, electrolyte mixtures, many modifications should be made and, this is the reason why, they are often coupled with activity coefficient models. Equations of state cannot describe sufficiently highly-non-ideal mixtures, such as acid-gases-water-alkanolamines, but EoS/G^E models have been widely applied to these mixtures in literature and they describe them satisfactorily. The ionic species interactions of these mixtures have also been introduced to EoS/G^E model through some modifications[1].

UMR-PRU is an EoS/G^E model, which couples Peng-Robinson EoS with UNIFAC[39] activity coefficient model. In order to extend it to electrolyte mixtures it is necessary to be modified, because of the need of description of more complex phenomena, such as the long-range electrostatic forces between ions. The forces between solvents and ions have a great impact on vapor-liquid equilibrium, because of their effect on temperature, pressure and vapor phase composition at equilibrium. Even though, ions are present only in liquid phase, they affect vapor phase composition, because their presence in liquid phase results to the increase in a volatile component (eg. CO_2) composition in vapor phase. This phenomenon is called "salting-out" effect[40].

In order to describe the long-range electrostatic forces between species, the Debye-Hückel term has been incorporated, so the activity coefficient model is the extended-UNIQUAC, as it is presented by Macedo et al[8]. Therefore:

$$ln\,\gamma_n = ln\,\gamma_n{}^{C,SG} + ln\,\gamma_n{}^{R} + ln\,\gamma_n{}^{DH} \qquad \text{eq. 5.53}$$

The first two terms $ln\,\gamma_n{}^{C,SG}$, $ln\,\gamma_n{}^{R}$ are calculated by eq. 5.47-5.52, while the Debye-Hückel term of the activity coefficient, $ln\,\gamma_n{}^{DH}$, is calculated by:

$$ln\,\gamma_n{}^{DH} = \frac{2AM_n d_s}{B^3 d_n}\left(1 + B\sqrt{I} - \frac{1}{1+B\sqrt{I}} - 2\,ln(1 + B\sqrt{I})\right) \qquad \text{eq. 5.54}$$

$$A = 1.327757 * 10^5 * \frac{d_s{}^{1/2}}{D * T^{3/2}} \qquad \text{eq. 5.55}$$

$$B = 6.359696 * \frac{d_s^{\frac{1}{2}}}{(D\,T)^{\frac{1}{2}}}$$ eq. 5.56

M_n is the molecular weight of pure solvent n (kg/kmol), d_s is the density of the solvent mixture (kg/m³), D is the dielectric constant of the solvent mixture and I is the ionic strength of the mixture.

The ionic strength is calculated through the following equation:

$$I = \frac{1}{2}\sum_i m_i z_i^2$$ eq. 5.57

where z_i is the charge number for ion i and m_i is the molality of the ion.

The dielectric constant of a molecular species is calculated as a function of temperature:

$$D_n = d^{(0)} + \frac{d^{(1)}}{T} + d^{(2)}T + d^{(3)}T^2 + d^{(4)}T^3$$ eq. 5.58

The values of the coefficients $d^{(0)}, d^{(1)}, d^{(2)}, d^{(3)}$ and $d^{(4)}$ for water, MEA and MDEA are given in Table A.6 of Appendix_A.

For mixture containing acid gases, alkanolamine and water the dielectric constant D is calculated between water (1) and alkanolamine (2) by the following expression:

$$D = D_1 + \left[\frac{(D_2-1)(2D_2+1).}{2D_2} - (D_1 - 1)\right] \cdot x_2' \cdot V_2/V$$ eq. 5.59

where $x_{2'}$ is the salt-free mole fraction of alkanolamine and V is the volume of the mixture (m³/kmol).

5.5. References

1.   Suleman, H.; Maulud, A.; Man, Z., Review and selection criteria of classical thermodynamic models for acid gas absorption in aqueous alkanolamines. *Reviews in Chemical Engineering* **2015,** *31*, 599-639.

2.   Kent, R. L.; Elsenberg, B., BETTER DATA FOR AMINE TREATING. *Hydrocarbon Processing* **1976,** *55* (2), 87-90.

3.   Jou, F. Y.; Mather, A. E.; Otto, F. D., Solubility of hydrogen sulfide and carbon dioxide in aqueous methyldiethanolamine solutions. *Industrial & Engineering Chemistry Process Design and Development* **1982,** *21* (4), 539-544.

4.   Jahangiri, A.; Pahlavanzadeh, H.; Mohammadi, A., The Modeling of CO2 Removal From a Gas Mixture by 2-amino-2-methyl-1-propanol (AMP) Using the Modified Kent Eisenberg Model. *Petroleum Science and Technology* **2014,** *32*.

5.   Posey, M. L.; Tapperson, K. G.; Rochelle, G. T., A simple model for prediction of acid gas solubilities in alkanolamines. *Gas Separation & Purification* **1996,** *10* (3), 181-186.

6.   Vrachnos, A.; Kontogeorgis, G.; Voutsas, E., Thermodynamic Modeling of Acidic Gas Solubility in Aqueous Solutions of MEA, MDEA and MEA–MDEA Blends. *Industrial & Engineering Chemistry Research* **2006,** *45* (14), 5148-5154.

7.   Chen, C.-C.; Evans, L. B., A local composition model for the excess Gibbs energy of aqueous electrolyte systems. *AIChE Journal* **1986,** *32* (3), 444-454.

8.   Macedo, E. A.; Skovborg, P.; Rasmussen, P., Calculation of phase equilibria for solutions of strong electrolytes in solvent—water mixtures. *Chemical Engineering Science* **1990,** *45* (4), 875-882.

9.   Deshmukh, R. D.; Mather, A. E., A mathematical model for equilibrium solubility of hydrogen sulfide and carbon dioxide in aqueous alkanolamine solutions. *Chemical Engineering Science* **1981,** *36* (2), 355-362.

10.   Panah, H. S.; Mohammadi, A. H.; Ramjugernath, D., Development of a novel approach for modeling acid gas solubility in alkanolamine aqueous solution. *Journal of Natural Gas Science and Engineering* **2016,** *34*, 112-123.

11.   Sadegh, N.; Thomsen, K.; Solbraa, E.; Johannessen, E.; Rudolfsen, G. I.; Berg, O. J., Solubility of hydrogen sulfide in aqueous solutions of N-methyldiethanolamine at high pressures. *Fluid Phase Equilibria* **2015,** *393*, 33-39.

12.   Austgen, D. M.; Rochelle, G. T.; Chen, C. C., Model of vapor-liquid equilibria for aqueous acid gas-alkanolamine systems. 2. Representation of hydrogen sulfide and carbon dioxide solubility in aqueous MDEA and carbon dioxide solubility in aqueous mixtures of MDEA with MEA or DEA. *Industrial & Engineering Chemistry Research* **1991,** *30* (3), 543-555.

13.   Austgen, D. M.; Rochelle, G. T.; Peng, X.; Chen, C. C., Model of vapor-liquid equilibria for aqueous acid gas-alkanolamine systems using the electrolyte-NRTL equation. *Industrial & Engineering Chemistry Research* **1989,** *28* (7), 1060-1073.

14.   Hessen, E. T.; Haug-Warberg, T.; Svendsen, H. F., The refined e-NRTL model applied to CO2–H2O–alkanolamine systems. *Chemical Engineering Science* **2010,** *65* (11), 3638-3648.

15.   Peng, D.-Y.; Robinson, D. B., A New Two-Constant Equation of State. *Industrial & Engineering Chemistry Fundamentals* **1976,** *15* (1), 59-64.

16.   Fürst, W.; Renon, H., Representation of excess properties of electrolyte solutions using a new equation of state. *AIChE Journal* **1993,** *39* (2), 335-343.

17.   Button, J. K.; Gubbins, K. E., SAFT prediction of vapour-liquid equilibria of mixtures containing carbon dioxide and aqueous monoethanolamine or diethanolamine. *Fluid Phase Equilibria* **1999,** *158-160*, 175-181.

18.   Nasrifar, K.; Tafazzol, A. H., Vapor–Liquid Equilibria of Acid Gas–Aqueous Ethanolamine Solutions Using the PC-SAFT Equation of State. *Industrial & Engineering Chemistry Research* **2010,** *49* (16), 7620-7630.

19.   Pahlavanzadeh, H.; Fakouri Baygi, S., Modeling CO_2 solubility in Aqueous Methyldiethanolamine Solutions by Perturbed Chain-SAFT Equation of State. *The Journal of Chemical Thermodynamics* **2013,** *59*, 214-221.

20.   Uyan, M.; Sieder, G.; Ingram, T.; Held, C., Predicting CO_2 solubility in aqueous N-methyldiethanolamine solutions with ePC-SAFT. *Fluid Phase Equilibria* **2015,** *393*, 91-100.

21.   Kontogeorgis, G. M.; Voutsas, E. C.; Yakoumis, I. V.; Tassios, D. P., An Equation of State for Associating Fluids. *Industrial & Engineering Chemistry Research* **1996,** *35* (11), 4310-4318.

22.   Wang, T.; El Ahmar, E.; Coquelet, C.; Kontogeorgis, G. M., Improvement of the PR-CPA equation of state for modelling of acid gases solubilities in aqueous alkanolamine solutions. *Fluid Phase Equilibria* **2018,** *471*, 74-87.

23.   Freitas, A.; Cunico, L.; Aznar, M.; Guirardello, R., Modeling vapor liquid equilibrium of ionic liquids + gas binary systems at high pressure with cubic equations of state. *Brazilian Journal of Chemical Engineering* **2012**.

24.   Shin, E.-K.; Lee, B.-C.; Lim, J. S., High-pressure solubilities of carbon dioxide in ionic liquids: 1-Alkyl-3-methylimidazolium bis(trifluoromethylsulfonyl)imide. *The Journal of Supercritical Fluids* **2008,** *45* (3), 282-292.

25.   Ren, W.; Sensenich, B.; Scurto, A., High-pressure phase equilibria of {carbon dioxide (CO2) + n-alkyl-imidazolium bis(trifluoromethylsulfonyl)amide} ionic liquids. *Journal of Chemical Thermodynamics* **2010,** *42*, 305-311.

26.   Breure, B.; Bottini, S. B.; Witkamp, G.-J.; Peters, C. J., Thermodynamic Modeling of the Phase Behavior of Binary Systems of Ionic Liquids and Carbon Dioxide with the Group Contribution Equation of State. *The Journal of Physical Chemistry B* **2007,** *111* (51), 14265-14270.

27.   Bermejo, M. D.; Martin, A.; Foco, G.; Cocero, M. J.; Bottini, S. B.; Peters, C. J., Application of a group contribution equation of state for the thermodynamic modeling of the binary systems CO2–1-butyl-3-methyl imidazolium nitrate and CO2–1-hydroxy-1-propyl-3-methyl imidazolium nitrate. *The Journal of Supercritical Fluids* **2009,** *50* (2), 112-117.

28.   Martín, Á.; Méndez, D.; Bermejo, M. D., Application of a group contribution equation of state for the thermodynamic modeling of binary systems (gas+ionic liquids) with bis[(trifluoromethyl)sulfonyl]imide anion. *The Journal of Chemical Thermodynamics* **2010,** *42* (4), 524-529.

29.   Renon, H.; Prausnitz, J. M., Local compositions in thermodynamic excess functions for liquid mixtures. *AIChE Journal* **1968,** *14* (1), 135-144.

30.   Al-fnaish, H.; Lue, L., Modelling the solubility of H2S and CO2 in ionic liquids using PC-SAFT equation of state. *Fluid Phase Equilibria* **2017,** *450*, 30-41.

31.   Kheiri, A.; Afsharpour, A., The CPA EoS application to model CO2 and H2S simultaneous solubility in ionic liquid [C2mim][PF6]. *Petroleum Science and Technology* **2018,** *36* (13), 944-950.

32.   Plakia, A.; Pappa, G.; Voutsas, E., Modeling of CO2 solubility in aqueous alkanolamine solutions with an extended UMR-PRU model. *Fluid Phase Equilibria* **2018,** *478*.

33.   Voutsas, E.; Magoulas, K.; Tassios, D., Universal Mixing Rule for Cubic Equations of State Applicable to Symmetric and Asymmetric Systems: Results with the Peng–Robinson Equation of State. *Industrial & Engineering Chemistry Research - IND ENG CHEM RES* **2004,** *43*.

34.   Pitsinigos, V. D.; Lygeros, A. I., Predicting H/sub 2/S-MEA equilibria. *Hydrocarbon Process.; (United States)* **1989**, Medium: X; Size: Pages: 43-44.

35.   Guggenheim, E.; Turgeon, J., Specific interaction of ions. *Transactions of the Faraday Society* **1955,** *51*, 747-761.

36.   Tassios, D. P., *Applied chemical engineering thermodynamics*. 1993.

37.   Huron, M.-J.; Vidal, J., New mixing rules in simple equations of state for representing vapour-liquid equilibria of strongly non-ideal mixtures. *Fluid Phase Equilibria* **1979,** *3* (4), 255-271.

38.   Michelsen, M. L., A method for incorporating excess Gibbs energy models in equations of state. *Fluid Phase Equilibria* **1990,** *60* (1), 47-58.

39.   Hansen, H. K.; Rasmussen, P.; Fredenslund, A.; Schiller, M.; Gmehling, J., Vapor-liquid equilibria by UNIFAC group contribution. 5. Revision and extension. *Industrial & Engineering Chemistry Research* **1991,** *30* (10), 2352-2355.

40.   Sander, B.; Fredenslund, A.; Rasmussen, P., Calculation of vapour-liquid equilibria in mixed solvent/salt systems using an extended UNIQUAC equation. *Chemical engineering science* **1986,** *41* (5), 1171-1183.

6. Solubility of CO_2 and CH_4+CO_2 in aqueous monoethanolamine and methyldiethanolamine solutions using eUMR-PRU model

In this chapter the results of eUMR-PRU model in CO_2-MEA-H_2O, CO_2-MDEA-H_2O, CO_2-MEA-MDEA-H_2O and CH_4-CO_2-MDEA-H_2O mixtures are presented and compared to those of electrolyte-NRTL model.

6.1. Introduction

The design of the chemical absorption process in aqueous alkanolamines requires proper thermodynamic models capable of describing the solubility of CO_2 in aqueous alkanolamines. In Chapter 4, the typical acid gas thermodynamic problem has been described. According to this, the liquid phase composition (which is calculated by solving the chemical equilibrium) and temperature are defined, whereas pressure and vapor phase composition need to be calculated. The described problem is complex, due to the necessity to solve both chemical and phase equilibrium. In literature, a frequently used method to solve this problem is the law-of mass action, whereas the models used for phase equilibrium calculation can be categorized into three types: semiempirical, activity coefficient or equations of state [1].

In literature, models of all categories have been used for modeling the CO_2 solubility in alkanolamines. For instance, Gabrielsen et al[2] have modeled CO_2 solubility in aqueous MEA, DEA and MDEA assuming only one combined chemical equilibrium reaction and ideal gas and liquid properties. Electrolyte-NRTL[3] and extended UNIQUAC[4] are some examples of activity coefficients models used for modeling the CO_2 solubility in aqueous alkanolamines. For instance, Hessen et al[5] have used the refined eNRTL model proposed by Bollas et al[6] for modeling CO_2 solubility in aqueous MEA and MDEA and the results are improved at high loadings. The use of EoS/G^E models in literature for modeling the CO_2 solubility in alkanolamines is more limited than activity coefficient models. Some examples are the work of Derks et al[7], who have used the electrolyte EoS proposed by Fürst and Renon[8], and Vrachnos et al[9], who have used the electrolyte LCVM[9] model. CPA EoS, proposed by Kontogeorgis et al[10], is another example of equations of state used in these mixtures. Zoghi et al[11] have used CPA EoS for modeling CO_2 solubility in aqueous MDEA.

As far as the CO_2 chemical absorption from natural gas concerns, thermodynamic models should be able to describe the hydrocarbon loss to the amine solution, especially methane loss, which is the major component of natural gas. Furthermore, in experimental measurements of CO_2 solubility in aqueous alkanolamines, methane is often used as a make-up gas at high pressure measurements and it affects the solubility of carbon dioxide. These issues should be examined and sufficiently described by a thermodynamic model. In literature, there are only a few studies about this issue. Solbraa et al[12], Huttenhuis et al[13-14] and Versteeg et al[15] investigated CH_4-CO_2-MDEA-H_2O, H_2S-CH_4-MDEA-H_2O and CO_2-H_2S-CH_4-MDEA-H_2O mixtures by using a modification of Redlich-Kwong-Soave EoS. Other researchers[16-17] studied the effect of methane on acid gas partial

pressure and fugacities in aqueous MDEA solutions with SRK EoS and they have shown that changes in partial pressure of methane affects also the partial pressure of acid gases.

In this thesis, in order to model the CO_2 and CH_4+CO_2 solubility in aqueous alkanolamines, the liquid phase composition is determined by solving the chemical equilibrium and the vapor-liquid equilibrium is solved by an EoS/G^E model (eUMR-PRU), which is a modification of UMR-PRU including the Debye-Hückel term, in order to take the long-range electrostatic forces into account.

In this chapter the results of eUMR-PRU model in CO_2-MEA-H_2O, CO_2-MDEA-H_2O, CO_2-MEA-MDEA-H_2O and CO_2-CH_4-MDEA-H_2O mixtures are presented. Firstly, a literature review is performed, in order to find the accurate equilibrium constants and solve the chemical equilibrium. Secondly, a literature review of CO_2 experimental solubilities, in aqueous MEA and MDEA solutions is performed, in order to use it for the fitting procedure of eUMR-PRU parameters. After the evaluation of the databases, chemical and phase equilibrium are solved and the results are compared with electrolyte-NRTL. It has to be noted, that due to the high number of intercorrelated model parameters of eUMR-PRU, which are UNIQUAC interaction parameters and van der Waals Volume and Area parameters of the ions, the fitting procedure has been very demanding.

6.2. Database
6.2.1. Chemical equilibrium constants
The chemical equilibrium reactions are presented in detail in Chapter 4. The chemical equilibrium constants used in this thesis are presented in Table 6.1:

Table 6.1: Equilibrium constants for reactions 4.47-4.54 expressed as: $\ln K_x = A + \frac{B}{T} + C \ln T + DT$, where K_x is the mole-fraction based equilibrium constant, and T is the temperature in K.

Reaction	A	B	C	D	References
4.47	-4.90737	-6166.12	0	-0.00099	18
4.48	-83.4914	-819.7	10.9756	0	18
4.49	214.582	-12995.4	-33.5471	0	19
4.50	-32	-3338	0	0	20
4.51	231.465	-12092.1	-36.7816	0	19
4.52	216.049	-12431.7	-35.4819	0	19
4.53	0.03669	-2275.19	0	0	18
4.54	132.899	-13445.9	-22.4773	0	19

Specifically, the reactions 4.47-4.48, 4.51-4.54 are needed to describe CO_2-MEA-H_2O, CO_2-MDEA-H_2O, CO_2-MEA-MDEA-H_2O and CO_2-CH4-MDEA-H_2O mixtures. A literature review is performed, in order to find accurate experimental chemical equilibrium constants of these reactions, which must be mole fraction-based (eq. 4.55-4.56, 4.59-4.62 of Chapter 4). For reactions 4.51, 4.52, 4.54 most authors use the same equilibrium constants, proposed by Edwards et al[19], while for the rest those of Jakobsen et al[18] are selected. Jakobsen et al[18] have performed NMR studies and they have presented measurements of liquid phase composition independently from thermodynamic models, a fact that is not common in literature. The most common is to evaluate ionic concentrations using equilibrium constants and a thermodynamic model and not solely from NMR data. After the determination of liquid phase composition, Jakobsen et al[18] have compared these compositions with those derived by a thermodynamic model, which combines Peng-Robinson EoS and extended UNIFAC[4] using equilibrium constants taken from literature. These equilibrium constants are selected in this work, because they are closer to experimental data than any other equilibrium constants. They are checked for their accuracy in Figure 6.1.
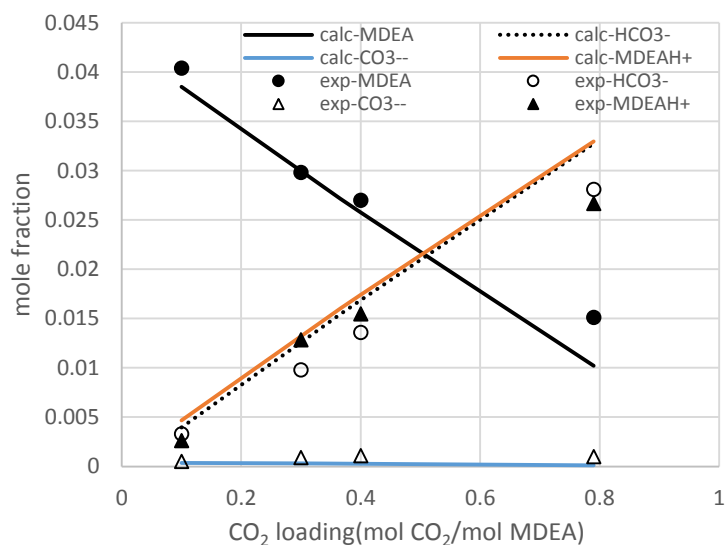
Figure 6.1: Comparison of calculated liquid phase speciation of CO_2-MDEA-H_2O mixture at 313.15 K, as it was determined by solving equilibrium, mass balance and electro-neutrality equations, with experimental liquid phase speciation measured by Jakobsen et al[18] .

In this figure the calculated liquid phase composition, as it is determined by solving eq. 4.55-4.56 and 4.59-4.68, is compared with the experimental liquid phase speciation of

several species, as it has been measured by Jakobsen et al[18]. As it is shown, the calculated and experimental values are in a great agreement.

6.2.2. Vapor-Liquid equilibrium data

In order to create an appropriate database of experimental vapor-liquid data, a literature review is performed. The evaluation of the experimental data is performed by the examination of trends followed with respect to amine concentration and temperature.

Concerning CO_2-H_2O-MEA mixture, Jou et al[21] have mentioned, that data of Lee et al[22] show higher CO_2 partial pressures than other authors, due to the methods employed in order to determine the liquid phase composition. That is also confirmed by the evaluation of the data in this thesis, but since the differences are small it is decided to keep them in database. The overall experimental database used is presented in Table B.1 of Appendix B, whereas the fitting database and prediction database are presented in section 6.3.

Concerning CO_2-H_2O-MDEA mixture, data of Ali et al[23] and Bishnoi et al[24] differ significantly from all other sources at the same conditions, and they are excluded from database. For example, a comparison of data of Bishnoi et al[24] with other sources is presented in Figure 6.2, where CO_2 solubility at 48.9 % w/w aqueous MDEA solution at 313 K is depicted. Furthermore, data of Rho et al[25] are excluded from database as well, because they follow a problematic trend compared to all other sources, a fact that it is also raised by Chunxi et al[26]. The overall experimental database used is presented in Table B.2 of Appendix B, whereas the fitting database and prediction database are presented in section 6.3.
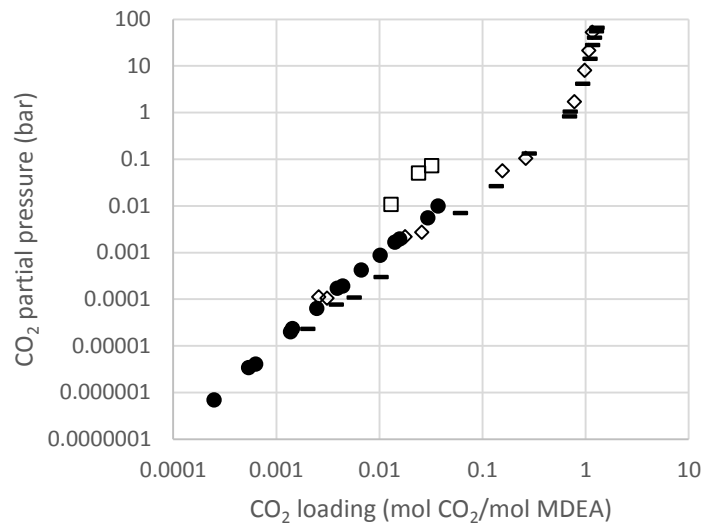
Figure 6.2: Comparison of experimental data (symbols: – Jou et al[27], ● Rogers et al[28], □ Bishnoi et al[24] and ◊ Huang et al[29]) at 48.9 % w/w MDEA at 313 K.

Finally, the database for the CH_4-MDEA, CH_4-MDEA-H_2O and CO_2-CH_4-MDEA-H_2O mixtures is presented in Table B.3 of Appendix B.

6.3. Results

In this section the results of CO_2-MEA-H_2O, CO_2-MDEA-H_2O and CO_2-MEA-MDEA-H_2O and CO_2-CH_4-MDEA-H_2O are presented.

The number of parameters required to be estimated for eUMR-PRU model is very high, due to the number of species (eleven in this case). Some parameters are taken from literature such as critical properties and acentric factor[30], Mathias-Copeman parameters for water[31], MDEA[9], and MEA[9]. Furthermore, van der Waals Volume and Area parameters for MEA, MDEA and water and UNIQUAC interaction parameters for mixtures MEA-H_2O and MDEA-H_2O are also taken from literature[9, 32]. Van der Waals Volume and Area parameters of CO_2 are taken from Voutsas et al[33]. The dielectric constants for all molecular components are taken from Vrachnos et al[9]. Binary interaction parameters of CH_4-H_2O are taken from Petropoulou et al[34] and those of CO_2-CH_4 from Louli et al [35] .

The rest parameters, which are van der Waals Volume and Area parameters of ionic species (MEAH+, MDEA+, HCO_3-, CO_3--, OH-, H_3O+, MEACOO-) and UNIQUAC interaction parameters, except for those taken from literature, are estimated in this work by fitting to experimental data of ternary CO_2-MEA-H_2O, CO_2-MDEA-H_2O and CH_4-MDEA-H_2O or quaternary CO_2-MEA-MDEA-H_2O and CH_4-CO_2- MDEA-H_2O mixtures.

The objective function used for the regression procedure of CH_4-MDEA-H_2O mixture is:

$$OF = \frac{1}{NP1} \sum_{i=1}^{NP1} abs\left(\frac{P_{tot,exp} - P_{tot,calc}}{P_{tot,exp}} \cdot 100\right)$$

eq. 6.1

The objective function used for the regression procedure of CO_2-MEA-H_2O, CO_2-MDEA-H_2O or quaternary CO_2-MEA-MDEA-H_2O and CO_2-CH_4-MDEA-H_2O mixtures is:

$$OF = \frac{1}{NP1} \sum_{i=1}^{NP1} \left(log\, P_{CO2,calc} - log\, P_{CO2,exp}\right) + \frac{1}{NP2} \sum_{j=1}^{NP2} \left(log\, P_{tot,calc} - log\, P_{tot,exp}\right)$$

eq. 6.2

Pure component parameters of eUMR-PRU are presented in Tables A.5, A.6 of Appendix A, whereas van der Waals Volume and Area and eUMR-PRU binary interaction parameters are presented in Tables A.7, A.8 of Appendix A accordingly. The rest binary interaction parameters (eg. CO_2-H_3O^+), that are required for the mixtures presented in this Chapter and are not presented in Table A.8 are equal to zero.

Concerning electrolyte-NRTL model, the parameters needed are taken from ASPEN PLUS V8.6 and they are presented in Tables A.1-A.4 of Appendix A. For the description of vapor phase Redlich-Kwong EoS is used.

6.3.1. Binary mixtures: MEA-H_2O, MDEA-H_2O

The parameters of MEA-H_2O and MDEA-H_2O are taken from literature as it is mentioned Section 6.3. However, the experimental data of CO_2 solubility in aqueous alkanolamines at low loadings are not accurate enough, but they resemble to binaries MEA-H_2O and MDEA-H_2O because CO_2 concentration is very low. Therefore, eUMR-PRU is evaluated to freezing point depression predictions, which are calculated by the following equation:

$$\ln(a_w) = -\frac{\Delta H_{fus}}{RT_m^2} \Delta T_f - \left(\frac{\Delta H_{fus}}{RT_m} - \frac{\Delta C_p}{2R}\right) \frac{\Delta T_f^2}{T_m^2}$$

eq. 6.3

where a_w is the activity of water calculated by eUMR-PRU

ΔH_{fus}=6008 J/mol is the heat of fusion of water

$T_m = 273.15\, K$ is the freezing point temperature of water

ΔT_f is the freezing point depression of water

ΔC_p=37.6 J/(mol K) is the heat capacity difference between liquid and solid states of water

In Figure 6.3a the results for freezing point depression for MEA-H_2O mixture are presented, whereas in Figure 6.3b the results for freezing point depression for MDEA-H_2O mixture are presented. eUMR-PRU predictions agree satisfactorily with the experimental data, which implies the accurate predictions at low acid gas loadings in ternary mixtures.
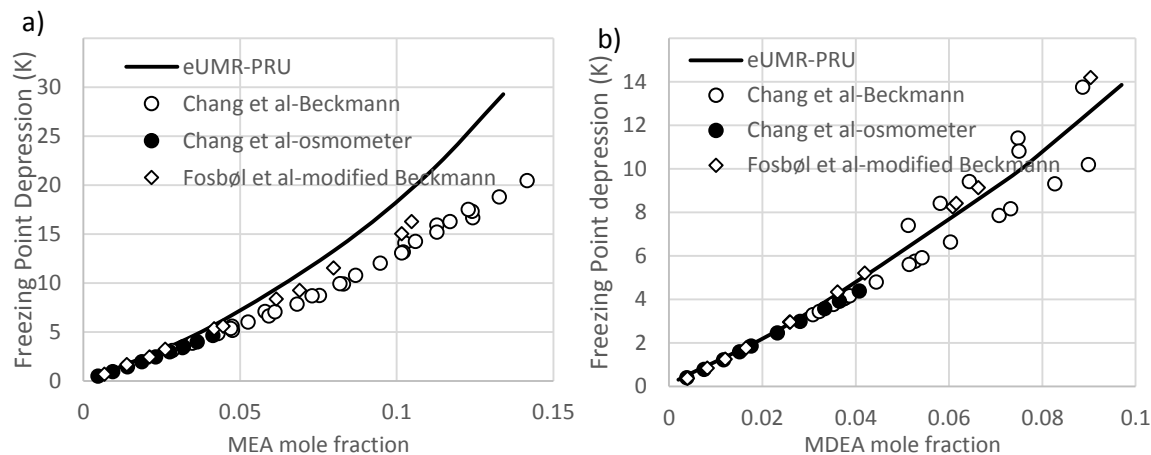
Figure 6.3: Freezing point depression predictions with eUMR-PRU model for mixtures: a) MEA-H_2O, b) MDEA-H_2O[36-37]

6.3.2. CO_2-H_2O-MEA

The results of eUMR-PRU model for CO_2-H_2O-MEA mixture are presented in Table 6.2. The model is evaluated to correlation and prediction results and it is in accordance with the experimental data in both cases. More specifically, eUMR-PRU has average absolute relative deviation in pressure equal to 39.2 % in a total of 132 experimental data, which are used in correlation procedure, whereas the corresponding value for 730 data points used for prediction is 36.2 %. The sufficient performance of eUMR-PRU in prediction results indicates the good extrapolation behavior of the model.

The performance of the model is compared with: a) results of other models presented in literature and b) with results obtained in this work using electrolyte-NRTL in some typical figures. In the first case, the results of eUMR-PRU are compared to those of SAFT-HR, PC-SAFT and e-NRTL, presented by Najaflloo et al[38]. The average absolute relative deviations are 33.4 %, 35.6 % and 42.2 % of SAFT-HR, PC-SAFT and e-NRTL respectively, whereas eUMR-PRU yields an AARDP% equal to 36.6 % in a similar database. This indicates that the results of eUMR-PRU are comparable or even better than those of other models.

In the second case, eUMR-PRU is compared to e-NRTL proposed by ASPEN PLUS V8.6 in some typical figures. In Figure 6.4a, the experimental data presented are those of Hilliard

et al[39] at 313.15 K and 333.15 K at 40 % w/w MEA and the performance of eUMR-PRU is in a greater agreement with the experimental data than the one of e-NRTL especially at higher loadings, with average absolute relative deviation of eUMR-PRU equal to 26.7 % and that of e-NRTL greater than 100 % due to the overestimation of the experimental data. In Figure 6.4b the experimental data presented are those of Aronu et al[40] at 313.15, 333.15 and 353.15 K at 30 % w/w MEA. In this case, where the concentration of MEA is lower, the results of the two models are closer to each other, but eUMR-PRU yields still a better performance, with an average absolute relative deviation in pressure equal to 23.6 %, whereas the corresponding value of e-NRTL is 31.6 %.

Table 6.2: eUMR-PRU model results for CO_2-MEA-H_2O mixtures.

Reference	NP[a]	T range (K)	% w/w MEA	AARDP%[b]
Correlation results				
22	53	313.15-393.15	15	38.4%
21	79	313.15-423.15	30	39.7%
Overall	132	313.15-423.15	15-30	39.2%
Prediction results				
22	159	313.15-393.15	6.2-30	41.8%
41	13	313.15	15.3	32.8%
42	8	313.15-353.15	15.3	29.4%
43	62	373.15-443.15	30	21.5%
39	55	313-333	17-40.8	39.9%
44	20	313.15-413.15	15.2	25.9%
45	15	353.15-373.15	15.7	36.1%
46	7	353.15	15.7	38.3%
47	53	313.15-413.15	15.3	37.3%
48	8	313.2	15.3	43.2%
49	45	313.15-373.15	15.2-30.2	37.4%
50	11	373.15	26.8	43.8%
51	16	393	30	40.6%
52	7	313.2	15.3	36.4%
40	212	313.15-393.15	15-60	34.9%
53c	9	313.15-393.15	30	36.7%
29	30	313.15-393.15	20-30	37%
Overall	730	313.15-443.15	6.2-60	36.2%

[a] NP: number of experimental data points; [b] $AARDP\% = \frac{1}{NP}\sum \frac{abs(P_{exp}-P_{calc})}{P_{exp}} * 100$

[c] AARDP% refers to total pressures
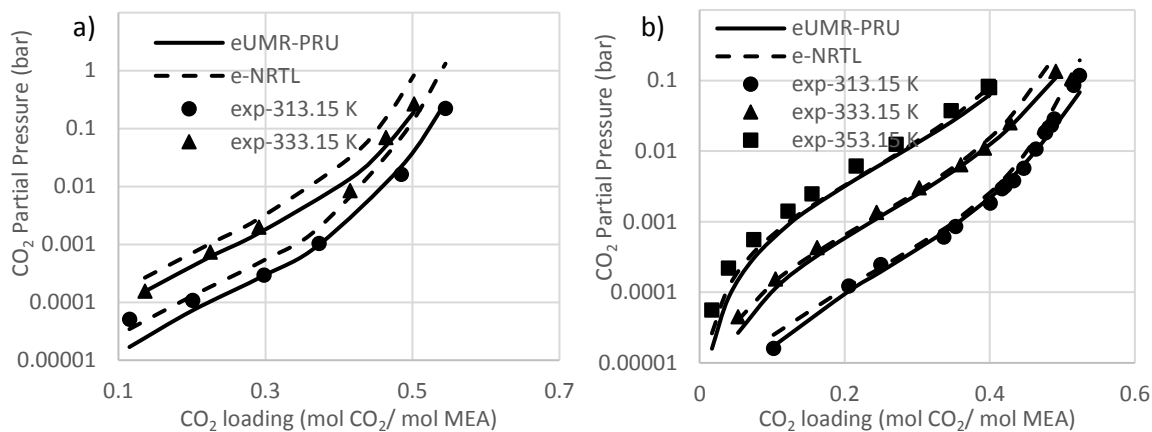
Figure 6.4: Comparison of eUMR-PRU results and e-NRTL results for the mixture CO_2-MEA-H_2O a) with experimental data of Hilliard et al[39] at 313.15 K and at 333.15 K at 40 % w/w MEA and b) with experimental data of Aronu et al[40] at 313.15, 333.15 and 353.15 K at 30% w/w MEA.

6.3.3. CO_2-H_2O-MDEA

In this section eUMR-PRU results for CO_2-H_2O-MDEA mixture are presented. In Table 6.3 the fitting and prediction databases are presented and the results of eUMR-PRU are given out analytically. In a total of 161 data points the correlation results have an average absolute relative deviation in pressure equal to 37.6 %, whereas the prediction results have average absolute relative deviation in pressure equal to 29.9 % in 598 data points, a fact which implies the predictive capability of the model.

The performance of the model is evaluated again in two ways: by comparison to literature results and by comparison to electrolyte-NRTL with ASPEN PLUS V8.6 parameters. Concerning the first case, Zhang et al[54] have used e-NRTL in a similar database. To make the evaluation fair, eUMR-PRU is evaluated in the same database used by Zhang et al[54]. The average absolute relative deviation in pressure for their model is 57.7 %, whereas that of eUMR-PRU for the same database is 30.8 %, including correlation and prediction results.

Concerning the second case, some typical prediction results of eUMR-PRU and e-NRTL are presented in Figure 6.5. In Figure 6.5a, the experimental data depicted are those of Sidi-Boumedine et al[55] at 313.15, 348.15 K and at 46.8 % w/w MDEA, whereas in Figure 6.5b the experimental data of Dawodu et al[50] at 373.15, 393.15 K at 52 % w/w MDEA are used for comparison purposes. As it is shown, the performance of eUMR-PRU is the most satisfactory in Figure 6.5a, whereas e-NRTL predicts more accurately the experimental

data of Figure 6.5b, which indicates the better performance of this model at higher temperatures. The overall absolute deviations in pressure in Figure 6.5a, are 28.2 % and 32.7 % for eUMR-PRU and e-NRTL accordingly, whereas in Figure 6.5b, the overall absolute deviations in pressure are 14.7 % and 10.5 % for eUMR-PRU and e-NRTL accordingly.

Table 6.3: eUMR-PRU model results for CO_2-MDEA-H_2O mixtures.

Reference	NP	T range (K)	% w/w MDEA	AARDP%
Correlation results				
[27]	90	313.15-393.15	23.3-48.9	35.5%
[29]	66	313.15-393.15	23-50	40.7%
[56]	5	313.15	18.8	34.3%
Overall	161	313.15-393.15	18.8-50	37.6%
Prediction results				
[27]	7	298.15	48.9	49.6%
[57]	36	313.15-373.15	35	34.9%
[58]	44	298.15-393.15	30	31.8%
[59a]	11	313.15	23.8	26.2%
[55a]	58	313.15-348.06	25.7-46.8	26.9%
[28]	24	313.15	23-50	29.1%
[60a]	79	313.15-413.15	18.8-32.1	26.1%
[61a]	28	313.15-393.15	32-48.7	29.4%
[51]	34	328-358	50	17.7%
[62a]	4	313.15	23.8	39.1%
[63]	5	313.15	23.3	27.5%
[64]	27	373.15-413.15	21.9-52.8	32.9%
[50]	12	37.15-393.15	52.8	14.7%
[65a]	9	313.15-393.15	30	28.4%
[66]	12	313.15	30	51.8%
[42]	14	313.15	23.3-50	28.4%
[67]	65	313-373	36.5-50	20.7%
[68]	30	298-373	50	42.2%
[69]	99	298-388	11.9-23.7	36.2%
Overall	598	298-413.15	11.9-52.8	29.9%

[a] The AARDP% refers to total pressures
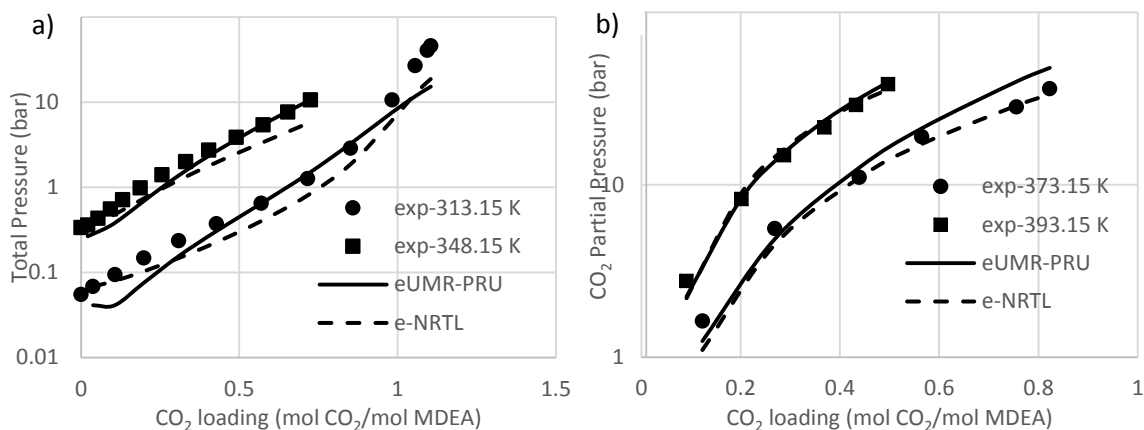
Figure 6.5: Comparison of eUMR-PRU results and e-NRTL results for the mixture CO_2-MDEA-H_2O a) with experimental data of Sidi-Boumedine et al[55] at 313.15 K and at 348.15 K at 46.8 % w/w MDEA and b) with experimental data of Dawodu et al[50] at 373.15 K and at 393.15 K at 52% w/w MDEA.

6.3.4. CO_2-H_2O-MEA-MDEA

In Chapter 3, it has been mentioned that amine blends are commonly used, in order to combine the advantages of different types of alkanolamines (in this case of a primary and a tertiary alkanolamine). Therefore, the accurate description of acid gases solubility in such mixtures is a crucial issue. In this section the results of eUMR-PRU in such mixtures are presented and compared with those of e-NRTL. It is worth mentioning, that eUMR-PRU results in CO_2-H_2O-MEA-MDEA mixtures are predictions, because no extra parameters have been fitted to these mixtures. The unknown parameters, for example UNIFAC interaction parameters between ions of an alkanolamine and ions of the other alkanolamine, have been set to zero, in order the extrapolation capability of the model to other mixtures to be checked.

In Figure 6.6, the results of the two models are compared to each other and with experimental data. The experimental data presented in the four figures are those of Jou et al[58], Dawodu et al[50] and Austgen et al[42]. The overall average absolute relative deviation in pressure for eUMR-PRU is 38.5 %, 22.9 %, 40.9 % and 40% moving towards from Figure 6.6a to 6.6d, whereas the corresponding values for e-NRTL are 25.3 %, 27.2 %, 36.4 % and 33.9 %. eUMR-PRU predictions in these mixtures are sufficient, but e-NRTL describes more accurately the experimental data, especially at high pressures.
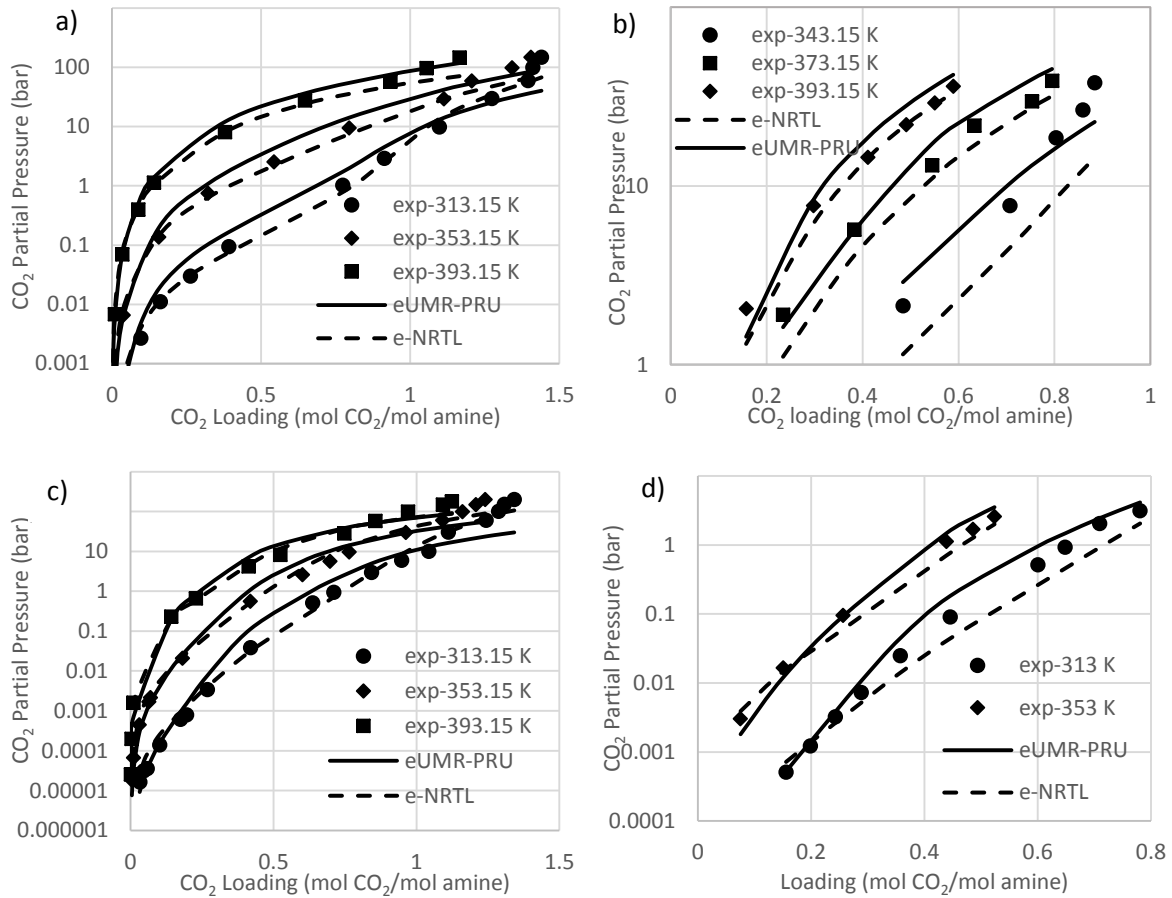
Figure 6.6: Comparison of eUMR-PRU results and e-NRTL results for the mixture CO_2-MEA-MDEA-H_2O a) with experimental data of Jou et al[58] at 1.5 % w/w MEA and 28.5 % w/w MDEA, b) with experimental data of Dawodu et al[50] at 4.7 % w/w MEA and 39.1 % w/w MDEA, c) with experimental data of Jou et al[58] at 10% w/w MEA and 20 % w/w MDEA, d) with experimental data of Austgen et al[42] at 12.2 % w/w MEA and 23.3 % w/w MDEA.

6.3.5. CH_4-CO_2-MDEA-H_2O

In this section the effect of methane on vapor-liquid equilibria of CO_2-MDEA-H_2O mixture is examined by using eUMR-PRU model. Binary interaction parameters between CH_4-MDEA have been calculated by fitting to ternary CH_4-MDEA-H_2O mixture and not to binary CH_4-MDEA mixture, because of the inadequate description of ternary CH_4-MDEA-H_2O and multicomponent CH_4-CO_2-MDEA-H_2O mixtures. For CH_4-CO_2-MDEA-H_2O mixture, one extra parameter is calculated- the one between MDEAH$^+$ and CH_4^- by fitting to experimental data of Addicks et al[62]. The results are presented in Table 6.4 and in Figures

6.7-6.8, in which the adequate description of both ternary CH_4-MDEA-H_2O and quaternary CH_4-CO_2-MDEA-H_2O mixtures is depicted.

Table 6.4: Results of eUMR-PRU in mixtures containing methane.

CH_4 with	References	NP	T (K)	AARDP%
MDEA-H_2O	[70], [71]	85	298.15-4232.15	5.5
CO_2-MDEA-H_2O	[62]	31	313.15-353.15	12.1
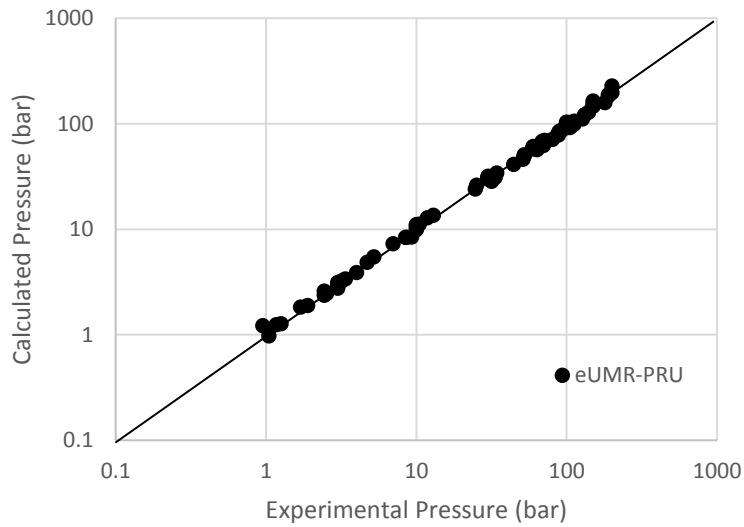
Figure 6.7: Comparison of eUMR-PRU results with experimental data[70-71] for CH_4-MDEA-H_2O mixtures at 298.15-423.15 K.
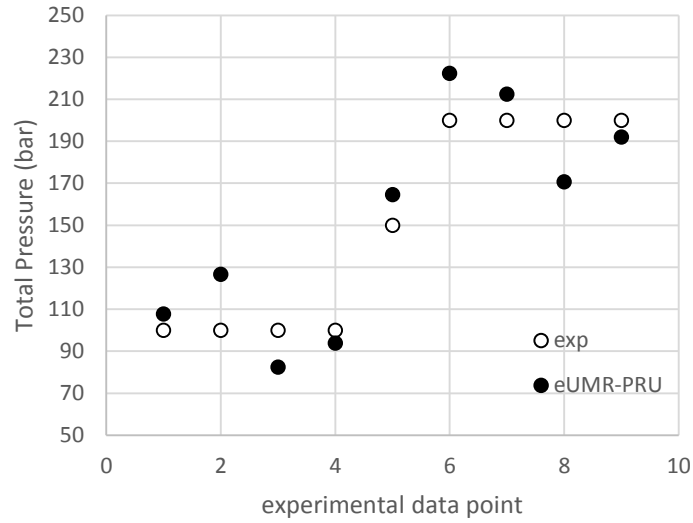
Figure 6.8: Comparison of eUMR-PRU results with experimental data[62] at 353.15 K at 50 % w/w MDEA for CO_2- CH_4-MDEA-H_2O.

The decrease in a gas solubility in a salt solution comparing with salt-free water, is called salting-out effect[12]. eUMR-PRU describes this effect precisely as shown in Figure 6.9, in which CH_4 solubility decreases as CO_2 loading increases.
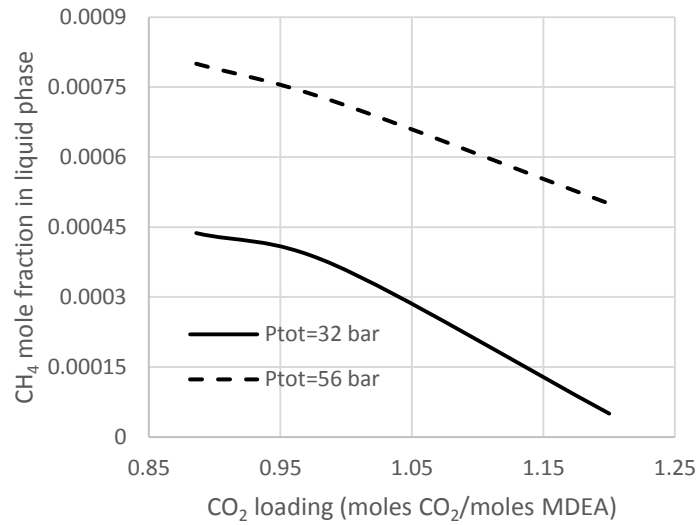
Figure 6.9: CH_4 salting-out effect in mixture CH_4-CO_2-MDEA-H_2O at 323.15 K and 50 % w/w MDEA.

Concerning the effect of methane on acid gas solubility in aqueous alkanolamine mixtures, Sadegh et al[17], performed a study and they have shown that, an increase in the concentration of methane results to decrease in acid gas solubility. This is well depicted in Figures 6.10-6.11, in which it is demonstrated that as the partial pressure of methane increases, the partial pressure of CO_2 increases as well and therefore the solubility of CO_2 in liquid phase decreases.
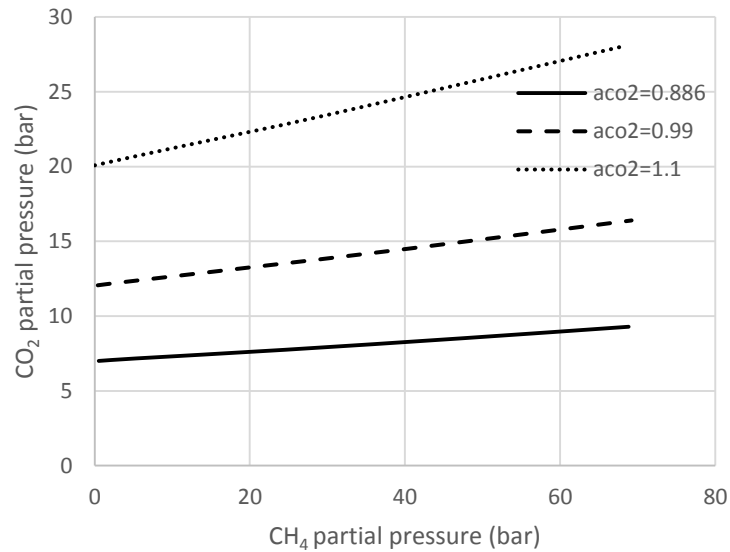
Figure 6.10: eUMR-PRU description of methane effect on CO_2 partial pressure for the CO_2-CH_4-MDEA-H_2O mixtures at 323.15 K and 50 % w/w MDEA, for different CO_2 loadings (aCO2).
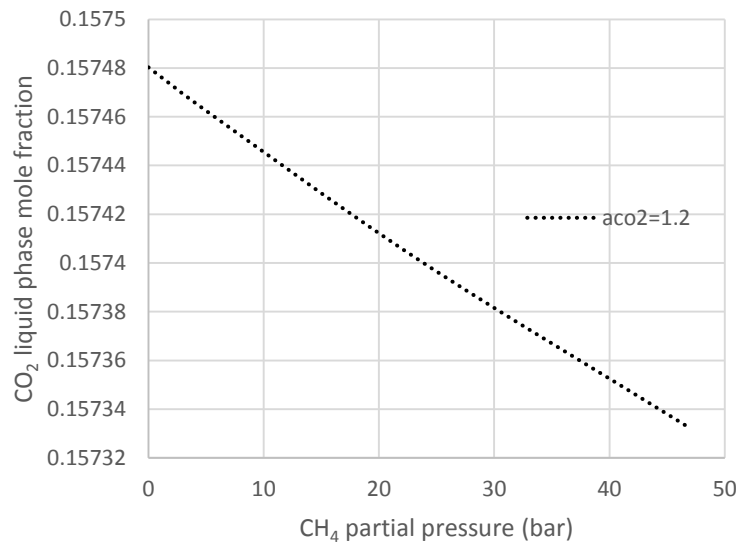
Figure 6.11: UMR-PRU prediction of methane effect on CO_2 solubility for the CO_2-CH_4-MDEA-H_2O mixture at 323.15 and 50 % w/w MDEA, for CO_2 loading equal to 1.2.

6.4. Conclusions

CO_2 chemical absorption by alkanolamines is the most common method for CO_2 removal in industry. The alkanolamines examined in this work are monoethanolamine and methyldiethanolamine. UMR-PRU model has been extended to CO_2-MEA-H_2O, CO_2-MDEA-H_2O and CO_2-MEA-MDEA-H_2O mixtures, by the addition of Debye- Hückel term in G^E calculation and the estimation of the missing parameters by fitting to experimental vapor-liquid equilibrium data. The model has been tested in a wide variety of temperatures (298-443 K), amine concentrations (5-60 % w/w) and acid gas loadings (0.0003-2.1) and its performance has been found to be satisfactory. eUMR-PRU has been compared in some cases indicatively with electrolyte-NRTL, which is a widely used -for this kind of mixtures- model, and the results were comparable to each other. Furthermore, the effect of methane on CO_2 solubility in aqueous MDEA mixture has been examined and it has been concluded that an increase in methane concentration results to a decrease in CO_2 solubility. Methane salting-out effect has also been proven by using eUMR-PRU model. In conclusion, eUMR-PRU has been successfully extended to CO_2-alkanolamines-water and CO_2-CH_4-MDEA-H_2O mixtures and the new thermodynamic framework, which is proposed in this work, is able to describe explicitly phase and chemical equilibrium.

6.5. References

1. Suleman, H.; Maulud, A.; Man, Z., Review and selection criteria of classical thermodynamic models for acid gas absorption in aqueous alkanolamines. *Reviews in Chemical Engineering* **2015,** *31*, 599-639.

2. Gabrielsen, J.; Michelsen, M. L.; Stenby, E. H.; Kontogeorgis, G. M., A model for estimating CO2 solubility in aqueous alkanolamines. *Industrial & engineering chemistry research* **2005,** *44* (9), 3348-3354.

3. Chen, C.-C.; Evans, L. B., A local composition model for the excess Gibbs energy of aqueous electrolyte systems. *AIChE Journal* **1986,** *32* (3), 444-454.

4. Macedo, E. A.; Skovborg, P.; Rasmussen, P., Calculation of phase equilibria for solutions of strong electrolytes in solvent—water mixtures. *Chemical Engineering Science* **1990,** *45* (4), 875-882.

5. Hessen, E. T.; Haug-Warberg, T.; Svendsen, H. F., The refined e-NRTL model applied to CO2–H2O–alkanolamine systems. *Chemical Engineering Science* **2010,** *65* (11), 3638-3648.

6. Bollas, G.; Chen, C.-C.; Barton, P., Refined electrolyte-NRTL model: Activity coefficient expressions for application to multi-electrolyte systems. *AIChE Journal* **2008,** *54* (6), 1608-1624.

7. Derks, P.; Hogendoorn, J.; Versteeg, G., Experimental and theoretical study of the solubility of carbon dioxide in aqueous blends of piperazine and N-methyldiethanolamine. *The Journal of Chemical Thermodynamics* **2010,** *42* (1), 151-163.

8. Fürst, W.; Renon, H., Representation of excess properties of electrolyte solutions using a new equation of state. *AIChE Journal* **1993,** *39* (2), 335-343.

9. Vrachnos, A.; Kontogeorgis, G.; Voutsas, E., Thermodynamic Modeling of Acidic Gas Solubility in Aqueous Solutions of MEA, MDEA and MEA–MDEA Blends. *Industrial & Engineering Chemistry Research* **2006,** *45* (14), 5148-5154.

10. Kontogeorgis, G. M.; Voutsas, E. C.; Yakoumis, I. V.; Tassios, D. P., An Equation of State for Associating Fluids. *Industrial & Engineering Chemistry Research* **1996,** *35* (11), 4310-4318.

11. Zoghi, A. T.; Feyzi, F.; Dehghani, M. R., Modeling CO2 solubility in aqueous N-methyldiethanolamine solution by electrolyte modified Peng–Robinson plus association equation of state. *Industrial & engineering chemistry research* **2012,** *51* (29), 9875-9885.

12. Solbraa, E., Equilibrium and non-equilibrium thermodynamics of natural gas processing. **2002**.

13. Huttenhuis, P.; Agrawal, N.; Versteeg, G., The solubility of hydrogen sulfide in aqueous N-methyldiethanolamine solutions. *International Journal of Oil, Gas and Coal Technology* **2008,** *1*.

14. Huttenhuis, P. J. G.; Agrawal, N. J.; Solbraa, E.; Versteeg, G. F., The solubility of carbon dioxide in aqueous N-methyldiethanolamine solutions. *Fluid Phase Equilibria* **2008,** *264* (1), 99-112.

15. Versteeg, G.; Agrawal, N.; Huttenhuis, P., Solubility of Carbon Dioxide and Hydrogen Sulfide in Aqueous N-Methyldiethanolamine Solutions. *Industrial & Engineering Chemistry Research* **2009,** *48*.

16.	Dicko, M.; Coquelet, C.; Jarne, C.; Northrop, S.; Richon, D., Acid gases partial pressures above a 50wt% aqueous methyldiethanolamine solution: Experimental work and modeling. *Fluid Phase Equilibria* **2010,** *289* (2), 99-109.

17.	Sadegh, N., *Acid Gas Removal from Natural Gas with Alkanolamines*. Technical University of Denmark (DTU): Kgs. Lyngby, 2013.

18.	Jakobsen, J. P.; Krane, J.; Svendsen, H. F., Liquid-phase composition determination in CO2– H2O– alkanolamine systems: An NMR study. *Industrial & engineering chemistry research* **2005,** *44* (26), 9894-9903.

19.	Edwards, T.; Maurer, G.; Newman, J.; Prausnitz, J., Vapor-liquid equilibria in multicomponent aqueous solutions of volatile weak electrolytes. *AIChE Journal* **1978,** *24* (6), 966-976.

20.	Austgen, D. M.; Rochelle, G. T.; Peng, X.; Chen, C. C., Model of vapor-liquid equilibria for aqueous acid gas-alkanolamine systems using the electrolyte-NRTL equation. *Industrial & engineering chemistry research* **1989,** *28* (7), 1060-1073.

21.	Jou, F.-Y.; Mather, A. E.; Otto, F. D., The solubility of CO2 in a 30 mass percent monoethanolamine solution. *The Canadian Journal of Chemical Engineering* **1995,** *73* (1), 140-147.

22.	Lee, J. I.; Otto, F. D.; Mather, A. E., Equilibrium between carbon dioxide and aqueous monoethanolamine solutions. *Journal of Applied Chemistry and Biotechnology* **1976,** *26* (1), 541-549.

23.	Ali, B. S.; Aroua, M. K., Effect of Piperazine on CO 2 Loading in Aqueous Solutions of MDEA at Low Pressure. *International Journal of Thermophysics* **2004,** *25* (6), 1863-1870.

24.	Bishnoi, S.; Rochelle, G. T., Thermodynamics of Piperazine/Methyldiethanolamine/Water/Carbon Dioxide. *Industrial & Engineering Chemistry Research* **2002,** *41* (3), 604-612.

25.	Rho, S.-W.; Yoo, K.-P.; Lee, J. S.; Nam, S. C.; Son, J. E.; Min, B.-M., Solubility of CO2 in Aqueous Methyldiethanolamine Solutions. *Journal of Chemical & Engineering Data* **1997,** *42* (6), 1161-1164.

26.	Chunxi, L.; Fürst, W., Representation of CO2 and H2S solubility in aqueous MDEA solutions using an electrolyte equation of state. *Chemical Engineering Science* **2000,** *55* (15), 2975-2988.

27.	Jou, F. Y.; Mather, A. E.; Otto, F. D., Solubility of hydrogen sulfide and carbon dioxide in aqueous methyldiethanolamine solutions. *Industrial & Engineering Chemistry Process Design and Development* **1982,** *21* (4), 539-544.

28.	Rogers, W. J.; Bullin, J. A.; Davison, R. R., FTIR measurements of acid-gas– methyldiethanolamine systems. *AIChE journal* **1998,** *44* (11), 2423-2430.

29.	Huang, S.; Ng, H., Solubility of H2S and CO2 in Alkanolamines: GPA Research Report RR-155. **1998**.

30.	Daubert, T. E.; Danner, R. P., *Data compilation tables of properties of pure compounds*. Design Institute for Physical Property Data, American Institute of Chemical …: 1985.

31.	Boukouvalas, C.; Spiliotis, N.; Coutsikos, P.; Tzouvaras, N.; Tassios, D., Prediction of vapor-liquid equilibrium with the LCVM model: a linear combination of the Vidal and

Michelsen mixing rules coupled with the original UNIF. *Fluid Phase Equilibria* **1994,** *92*, 75-106.

32.   Voutsas, E.; Vrachnos, A.; Magoulas, K., Measurement and thermodynamic modeling of the phase equilibrium of aqueous N-methyldiethanolamine solutions. *Fluid Phase Equilibria* **2004,** *224* (2), 193-197.

33.   Voutsas, E. C.; Boukouvalas, C. J.; Kalospiros, N. S.; Tassios, D. P., The performance of EoS/GE models in the prediction of Vapor-Liquid Equilibria in asymmetric systems. *Fluid Phase Equilibria* **1996,** *116* (1), 480-487.

34.   Petropoulou, E. G.; Voutsas, E. C., Thermodynamic Modeling and Simulation of Natural Gas Dehydration Using Triethylene Glycol with the UMR-PRU Model. *Industrial & Engineering Chemistry Research* **2018,** *57* (25), 8584-8604.

35.   Louli, V.; Pappa, G.; Boukouvalas, C.; Skouras, S.; Solbraa, E.; Christensen, K.; Voutsas, E., Measurement and prediction of dew point curves of natural gas mixtures. *Fluid Phase Equilibria* **2012,** *334*, 1–9.

36.   Chang, H. T.; Posey, M.; Rochelle, G. T., Thermodynamics of alkanolamine-water solutions from freezing point measurements. *Industrial & Engineering Chemistry Research* **1993,** *32* (10), 2324-2335.

37.   Fosbøl, P. L.; Pedersen, M. G.; Thomsen, K., Freezing Point Depressions of Aqueous MEA, MDEA, and MEA– MDEA Measured with a New Apparatus. *Journal of Chemical & Engineering Data* **2011,** *56* (4), 995-1000.

38.   Najafloo, A.; Zarei, S., Modeling solubility of CO2 in aqueous monoethanolamine (MEA) solution using SAFT-HR equation of state. *Fluid Phase Equilibria* **2018,** *456*, 25-32.

39.   Hilliard, M., A Predictive Thermodynamic Model for an Aqueous Blend of Potassium Carbonate, Piperazine, and Monoethanolamine for Carbon Dioxide Capture from Flue Gas. **2008**.

40.   Aronu, U.; Gondal, S.; Hessen, E.; Haug-Warberg, T.; Hartono, A.; Hoff, K.; Svendsen, H., Solubility of CO2 in 15, 30, 45 and 60 mass% MEA from 40 to 120 °C and model representation using the extended UNIQUAC framework. *Chemical Engineering Science* **2011,** *66*, 6393–6406.

41.   Shen, K. P.; Li, M. H., Solubility of carbon dioxide in aqueous mixtures of monoethanolamine with methyldiethanolamine. *Journal of Chemical & Engineering Data* **1992,** *37* (1), 96-100.

42.   Austgen, D. M.; Rochelle, G. T.; Chen, C. C., Model of vapor-liquid equilibria for aqueous acid gas-alkanolamine systems. 2. Representation of hydrogen sulfide and carbon dioxide solubility in aqueous MDEA and carbon dioxide solubility in aqueous mixtures of MDEA with MEA or DEA. *Industrial & Engineering Chemistry Research* **1991,** *30* (3), 543-555.

43.   Xu, Q.; Rochelle, G., Total pressure and CO2 solubility at high temperature in aqueous amines. *Energy Procedia* **2011,** *4*, 117-124.

44.   Lawson, J. D.; Garst, A., Gas sweetening data: equilibrium solubility of hydrogen sulfide and carbon dioxide in aqueous monoethanolamine and aqueous diethanolamine solutions. *Journal of Chemical and Engineering Data* **1976,** *21* (1), 20-30.

45.   Isaacs, E. E.; Otto, F. D.; Mather, A. E., Solubility of mixtures of hydrogen sulfide and carbon dioxide in a monoethanolamine solution at low partial pressures. *Journal of Chemical and Engineering Data* **1980,** *25* (2), 118-120.

46.   Jane, I.-S.; Li, M.-H., Solubilities of mixtures of carbon dioxide and hydrogen sulfide in water+ diethanolamine+ 2-amino-2-methyl-1-propanol. *Journal of Chemical & Engineering Data* **1997,** *42* (1), 98-105.

47.   Jones, J.; Froning, H.; Claytor Jr, E., Solubility of Acidic Gases in Aqueous Monoethanolamine. *Journal of chemical and engineering data* **1959,** *4* (1), 85-92.

48.   Song, J.-H.; Yoon, J.-H.; Lee, H.; Lee, K.-H., Solubility of carbon dioxide in monoethanolamine+ ethylene glycol+ water and monoethanolamine+ poly (ethylene glycol)+ water. *Journal of Chemical & Engineering Data* **1996,** *41* (3), 497-499.

49.   Lee, J.; Otto, F. D.; Mather, A. E., The solubility of H2S and CO2 in aqueous monoethanolamine solutions. *The Canadian Journal of Chemical Engineering* **1974,** *52* (6), 803-805.

50.   Dawodu, O. F.; Meisen, A., Solubility of carbon dioxide in aqueous mixtures of alkanolamines. *Journal of Chemical and Engineering Data* **1994,** *39* (3), 548-552.

51.   Ma'mun, S.; Nilsen, R.; Svendsen, H. F.; Juliussen, O., Solubility of carbon dioxide in 30 mass% monoethanolamine and 50 mass% methyldiethanolamine solutions. *Journal of Chemical & Engineering Data* **2005,** *50* (2), 630-634.

52.   Park, S.-B.; Lee, H.; Lee, K.-H., Solubilities of carbon dioxide in aqueous potassium carbonate solutions mixed with physical solvents. *International journal of thermophysics* **1998,** *19* (5), 1421-1428.

53.   Mathonat, C.; Majer, V.; Mather, A.; Grolier, J.-P., Use of flow calorimetry for determining enthalpies of absorption and the solubility of CO2 in aqueous monoethanolamine solutions. *Industrial & engineering chemistry research* **1998,** *37* (10), 4136-4141.

54.   Zhang, Y.; Chen, C.-C., Thermodynamic modeling for CO2 absorption in aqueous MDEA solution with electrolyte NRTL model. *Industrial & engineering chemistry research* **2011,** *50* (1), 163-175.

55.   Sidi-Boumedine, R.; Horstmann, S.; Fischer, K.; Provost, E.; Fürst, W.; Gmehling, J., Experimental determination of carbon dioxide solubility data in aqueous alkanolamine solutions. *Fluid phase equilibria* **2004,** *218* (1), 85-94.

56.   Kamps, Á. P. S.; Rumpf, B.; Maurer, G.; Anoufrikov, Y.; Kuranov, G.; Smirnova, N. A., Solubility of CO2 in H2O+ N-methyldiethanolamine+(H2SO4 or Na2SO4). *AIChE Journal* **2002,** *48* (1), 168-177.

57.   Jou, F. Y.; Carroll, J. J.; Mather, A. E.; Otto, F. D., The solubility of carbon dioxide and hydrogen sulfide in a 35 wt% aqueous solution of methyldiethanolamine. *The Canadian Journal of Chemical Engineering* **1993,** *71* (2), 264-268.

58.   Jou, F.-Y.; Otto, F. D.; Mather, A. E., Vapor-liquid equilibrium of carbon dioxide in aqueous mixtures of monoethanolamine and methyldiethanolamine. *Industrial & engineering chemistry research* **1994,** *33* (8), 2002-2005.

59.   Silkenbäumer, D.; Rumpf, B.; Lichtenthaler, R. N., Solubility of Carbon Dioxide in Aqueous Solutions of 2-Amino-2-methyl-1-propanol and N-Methyldiethanolamine and

Their Mixtures in the Temperature Range from 313 to 353 K and Pressures up to 2.7 MPa. *Industrial & engineering chemistry research* **1998,** *37* (8), 3133-3141.

60.   Kuranov, G.; Rumpf, B.; Smirnova, N. A.; Maurer, G., Solubility of single gases carbon dioxide and hydrogen sulfide in aqueous solutions of N-methyldiethanolamine in the temperature range 313– 413 K at pressures up to 5 MPa. *Industrial & engineering chemistry research* **1996,** *35* (6), 1959-1966.

61.   Kamps, Á. P.-S.; Balaban, A.; Jödecke, M.; Kuranov, G.; Smirnova, N. A.; Maurer, G., Solubility of single gases carbon dioxide and hydrogen sulfide in aqueous solutions of N-methyldiethanolamine at temperatures from 313 to 393 K and pressures up to 7.6 MPa: new experimental data and model extension. *Industrial & engineering chemistry research* **2001,** *40* (2), 696-706.

62.   Addicks, J.; Owren, G. A.; Fredheim, A. O.; Tangvik, K., Solubility of carbon dioxide and methane in aqueous methyldiethanolamine solutions. *Journal of Chemical & Engineering Data* **2002,** *47* (4), 855-860.

63.   Macgregor, R. J.; Mather, A. E., Equilibrium solubility of H2S and CO2 and their mixtures in a mixed solvent. *The Canadian Journal of Chemical Engineering* **1991,** *69* (6), 1357-1366.

64.   Chakma, A.; Meisen, A., Solubility of carbon dioxide in aqueous methyldiethanolamine and N,N-bis(hydroxyethyl)piperazine solutions. *Industrial & Engineering Chemistry Research* **1987,** *26* (12), 2461-2466.

65.   Mathonat, C.; Majer, V.; Mather, A.; Grolier, J.-P., Enthalpies of absorption and solubility of CO2 in aqueous solutions of methyldiethanolamine. *Fluid phase equilibria* **1997,** *140* (1-2), 171-182.

66.   Baek, J.-I.; Yoon, J.-H., Solubility of carbon dioxide in aqueous solutions of 2-amino-2-methyl-1, 3-propanediol. *Journal of Chemical & Engineering Data* **1998,** *43* (4), 635-637.

67.   Xu, G.-W.; Zhang, C.-F.; Qin, S.-J.; Gao, W.-H.; Liu, H.-B., Gas– liquid equilibrium in a CO2– MDEA– H2O system and the effect of piperazine on it. *Industrial & engineering chemistry research* **1998,** *37* (4), 1473-1477.

68.   Park, M. K.; Sandall, O. C., Solubility of carbon dioxide and nitrous oxide in 50 mass methyldiethanolamine. *Journal of Chemical & Engineering Data* **2001,** *46* (1), 166-168.

69.   Bhairi, A. M. Experimental equilibrium between acid gases and ethanolamine solutions. Oklahoma State University, 1984.

70.   Jou, F.-Y.; Carroll, J. J.; Mather, A. E.; Otto, F. D., Solubility of Methane and Ethane in Aqueous Solutions of Methyldiethanolamine. *Journal of Chemical & Engineering Data* **1998,** *43* (5), 781-784.

71.   Schmidt, K. A. G.; Jou, F.-Y.; Mather, A. E., Solubility of Methane in an Aqueous Methyldiethanolamine Solution (Mass Fraction 50 %). *Journal of Chemical & Engineering Data* **2008,** *53* (8), 1725-1727.

7. Modeling of mixtures containing H_2S: H_2S, CO_2+H_2S, in aqueous MEA and MDEA solutions using eUMR-PRU model and H_2S-hydrocarbon mixtures using UMR-PRU model

In this chapter, the extension of the eUMR-PRU model to H_2S-MEA-H_2O, H_2S-MDEA-H_2O, CO_2-H_2S-MEA-H_2O and CO_2-H_2S-MDEA-H_2O is presented and the results are compared to those of electrolyte-NRTL and Kent-Eisenberg models. Furthermore, the results of UMR-PRU in H_2S-gases and in H_2S-hydrocarbon mixtures are also displayed.

7.1. Introduction

The simulation and optimization of the chemical absorption process of hydrogen sulfide from natural gas requires the availability of thermodynamic models capable of describing accurately the solubility of hydrogen sulfide in aqueous alkanolamines solutions. In literature three categories of models are used for this purpose: semiempirical, activity coefficient and equations of state. For instance, recently used models are the following: Deshmuck-Mather model[1] has been used to describe the solubility of H_2S and CO_2 in five different amines[2]. Extended-UNIQUAC[3] has been used for modeling the solubility of H_2S in aqueous MDEA solution and Soave-Redlich-Kwong EoS has been used for the description of the vapor phase[4]. Electrolyte cubic square-well equation of state has been used for modeling CO_2 and H_2S solubility in aqueous MDEA solution[5], whereas electrolyte-SRK plus association equation of state[6] has also been used for modeling these mixtures[7].

In this chapter eUMR-PRU is extended to H_2S-MEA-H_2O, H_2S-MDEA-H_2O, CO_2-H_2S-MEA-H_2O and CO_2-H_2S-MDEA-H_2O. As described in Chapter 4, the liquid phase composition is determined by solving chemical equilibrium, mass balance and electroneutrality equations and then vapor-liquid equilibrium is calculated by eUMR-PRU model. The eUMR-PRU model results are compared to those of other widely used models (Kent-Eisenberg[8] and e-NRTL[9]), in order to evaluate its performance.

Another principal issue for H_2S removal from natural gas process design is the accurate knowledge of phase behavior of acid gases with light gases (nitrogen, methane, ethane) and with hydrocarbons. Therefore, a thermodynamic model should be capable of describing the phase behavior of such mixtures. For this reason, in this chapter the description of vapor-liquid equilibrium of mixtures containing H_2S and gases and H_2S and hydrocarbons by UMR-PRU model is also examined.

7.2. Solubility of H_2S, CO_2+H_2S, in aqueous MEA and MDEA Solutions using eUMR-PRU model

In this section the results of eUMR-PRU in H_2S-MEA-H_2O, H_2S-MDEA-H_2O, CO_2-H_2S-MEA-H_2O and CO_2-H_2S-MDEA-H_2O mixtures are presented. A literature review and the fitting procedure are performed and discussed in detail. The results of eUMR-PRU are compared to those of Kent-Eisenberg and e-NRTL models.

7.2.1. Database
7.2.1.1. Chemical equilibrium constants

The chemical equilibrium reactions describing the mixtures of this chapter are eq. 4.47-4.54, whereas the equilibrium constants used in this work are presented in Table 6.1 of Chapter 6. The equilibrium constants for reactions eq. 4.49-4.50 are those proposed by Edwards et al[10] and Austgen et al[11], while for the rest, the correlations employed in Chapter 6 are used in this Chapter as well. In this case too, chemical equilibrium constants must be mole fraction-based (eq. 4.55-4.62 of Chapter 4) and their evaluation has been performed by comparison of equilibrium constants of different authors and by comparison of calculated with the experimental measured values presented by other authors. For instance, as far as the dissociation of H_2S concerns, the comparison of different equilibrium constants is presented in Figure 7.1:
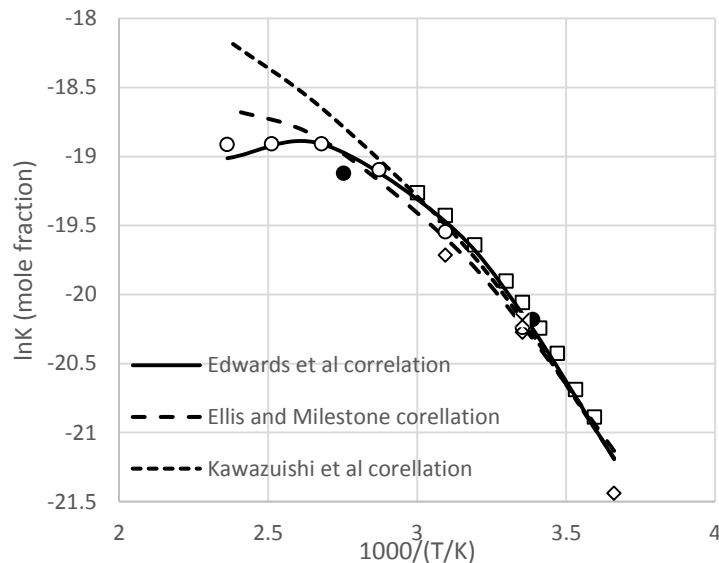
Figure 7.1: Comparison of correlations proposed in the literature (Edwards et al[10], Ellis and Milestone[12], Kawazuishi et al[13]) for chemical equilibrium constant of first dissociation of H_2S with experimental values (○ Tsonopoulos et al[14], ● Ellis and Milestone[12], ◊ Loy et al[15], □ Wright and Maas[16], X Ellis and Golding[17])

The correlation of Edwards et al[10] is the only one which describes both high and low temperatures sufficiently well. Furthermore, many other authors use the correlations of Edwards et al[10]. Posey et al[18] have concluded after the evaluation of equilibrium constants, that those of Edwards et al[10] are sufficient in order to be used by a thermodynamic model.

7.2.2.1. Vapor-Liquid equilibrium data

In order to calculate eUMR-PRU model parameters, an appropriate database of experimental vapor-liquid equilibrium data should be developed. Therefore, a literature review is performed and the database is evaluated by the same way as the one presented in previous chapter.

Firstly, binary UNIQUAC interaction parameters between H_2S-H_2O and CO_2-H_2S should be calculated, before modeling ternary mixtures (H_2S-MEA-H_2O, H_2S-MDEA-H_2O). For this reason, the data selected for the two binary mixtures are presented in Table B.4 of Appendix B.

For the ternary mixture H_2S-MEA-H_2O the database is presented in Table B.5 of Appendix B. Among the data found in literature, those of Isaacs et al[19] are excluded, because of their lower partial pressures than other authors and their wrong trend in some cases. This is well depicted in Figure 7.2. For similar reasons, data of Rieger et al[20] and Li et al[21] are also excluded from database.

For the ternary mixture H_2S-MDEA-H_2O the database is presented in Table B.6. In this mixture, the total pressure data of Huang et al[22] differ remarkably from any other author, so they are excluded from database. Data of Li et al[21] are excluded from database in this mixture as well.

As far as the H_2S-MEA-MDEA-H_2O mixture concerns, no experimental data have been found, except for those of Li et al[21]. However due to their problematic trend in H_2S-MEA-H_2O and H_2S-MDEA-H_2O mixtures they are not considered as trustworthy and that is the reason why this mixture is not modeled. The database for the quaternary mixtures CO_2-H_2S-MEA-H_2O and CO_2-H_2S-MDEA-H_2O is presented in Tables B.7-B.8 of Appendix B.
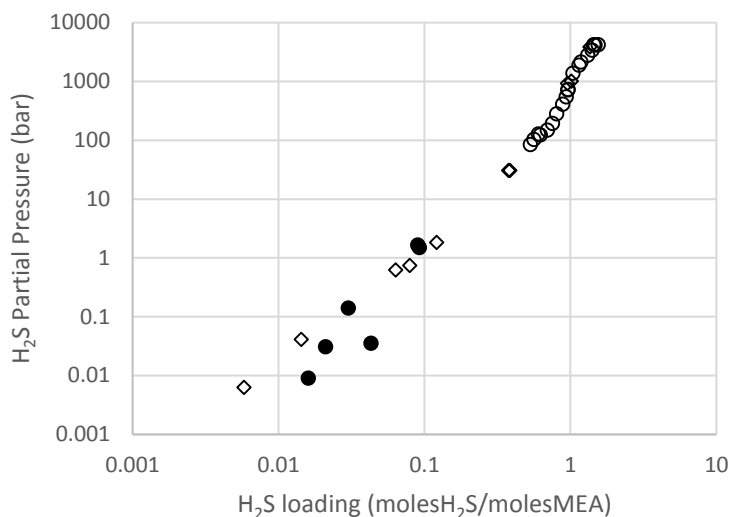
Figure 7.2: Comparison of experimental data of H_2S-MEA-H_2O mixture at 15.3 % w/w MEA at 373.15 K (○ Lee at al[23], ◊ Lawson et al[24], ● Isaacs et al[19])

7.2.2. Results

In this section the results of H_2S-MEA-H_2O, H_2S-MDEA-H_2O, CO_2-H_2S-MEA-H_2O, CO_2-H_2S-MDEA-H_2O mixtures with eUMR-PRU, Kent-Eisenberg and e-NRTL models are presented.

In order to extend eUMR-PRU to these mixtures, the necessary pure component parameters and binary interaction parameters should be determined. Most of the pure component parameters are taken from literature. Critical properties and acentric factors for all molecular species are taken from Daubert and Danner [25]. Mathias-Copeman parameters for water are taken from Boukouvalas et al[26], for MDEA and MEA from Vrachnos et al[27]. Dielectric constants of all molecular species are taken from Vrachnos et al[27]. Mathias-Copeman parameters for H_2S are estimated in this work by fitting to vapor pressure experimental data. Pure component parameters are presented in Tables A.5, A.6 of Appendix_A.

Van der Waals Volume and Area parameters for all species are presented in Table A.7 of Appendix A. Van der Waals Volume and Area parameters for all molecular species are taken from Vrachnos et al[27], whereas those of ions: $MEAH^+$, $MDEA^+$, HCO_3^-, CO_3^{--} and $MEACOO^-$, OH^-, H_3O^+ are calculated in this work by fitting to vapor-liquid equilibrium data of mixtures presented in previous chapter, whereas for HS^- and S^{2-} are calculated by fitting to experimental data of H_2S solubility in aqueous MEA and MDEA solutions.

Binary UNIQUAC interaction parameters MEA-H_2O are taken from Vrachnos et al[27], whereas those of MDEA-H_2O from Voutsas et al[28] and of CO_2-H_2O from Petropoulou et

al[29]. Binary UNIQUAC interaction parameters for H_2S-H_2O, CO_2-H_2S are calculated in this work by fitting to binary vapor-liquid equilibrium data. The rest binary interaction parameters are calculated by fitting to ternary H_2S-MEA-H_2O, H_2S-MDEA-H_2O or quaternary CO_2-H_2S-MEA-H_2O, CO_2-H_2S-MDEA-H_2O mixtures. All of them are presented in Table A.8 of Appendix A. The rest binary interaction parameters (eg. H_2S-H_3O^+), that are required for the mixtures presented in this Chapter and are not presented in Table A.8 are equal to zero.

For the calculation of the missing interaction parameters, two objective functions are used for the fitting procedure. For the H_2S-H_2O, CO_2-H_2S mixtures it is:

$$OF = \frac{1}{NP} \sum_{i=1}^{NP1} abs\left(\frac{P_{tot,exp} - P_{tot,calc}}{P_{tot,exp}} \cdot 100\right)$$

eq. 7.1

For the H_2S-MEA-H_2O, H_2S-MDEA-H_2O, CO_2-H_2S-MEA-H_2O and CO_2-H_2S-MDEA-H_2O mixtures it is:

$$OF = \frac{1}{NP1} \sum_{i=1}^{NP1} abs\left(\log P_{CO2,calc} - \log P_{CO2,exp}\right) + \frac{1}{NP2} \sum_{i=1}^{NP2} abs\left(\log P_{H2S,calc} - \log P_{H2S,exp}\right) + \frac{1}{NP3} \sum_{i=1}^{NP3} abs\left(\log P_{tot,calc} - \log P_{tot,exp}\right)$$

eq. 7.2

In Eqs 7.1 and 7.2 subscript tot refers to total pressures, calc to calculated values and exp to experimental values, CO_2 and H_2S to CO_2 and H_2S partial pressures accordingly.

Kent-Eisenberg[8] and e-NRTL[9] are used as well to describe the ternary H_2S-MEA-H_2O, H_2S-MDEA-H_2O mixtures for comparison purposes, whereas in quaternary CO_2-H_2S-MDEA-H_2O, electrolyte-NRTL model is compared with eUMR-PRU. Kent-Eisenberg model parameters are taken from Pitsinigos et al[30] and they are presented in Table 5.1 of Chapter 5, whereas those of e-NRTL have been taken from ASPEN PLUS V 8.6 and they are presented in Tables A.1 to A.4 of Appendix A.

7.2.2.1. *Mathias-Copeman parameters of H_2S*

Mathias-Copeman parameters of H_2S are estimated in this thesis by fitting experimental vapor pressure data of H_2S. The data are taken from Daubert and Danner[25] and they are described by the following correlation:

$$P_{H_2S}{}^{S}(bar) = e^{\left(85.584 - \frac{3839.9}{T} - 11.199\,ln(T) + 0.018848\,T^1\right)} \Big/ 100000$$

eq. 7.3

The overall absolute deviation in vapor pressure, in the temperature range of 186.8 to 351.1 K, is 0.02%.

7.2.2.2. Binary H_2S-H_2O and H_2S-CO_2 UNIQUAC interaction parameters

Binary interaction parameters H_2S-H_2O and H_2S-CO_2 are calculated by fitting the binary VLE experimental data presented in Table B.4 of Appendix B. The correlation results are presented in Table 7.1.

Table 7.1: UMR-PRU model results in binary H_2S-H_2O and H_2S-CO_2 mixtures.

					UMR-PRU		
	NP	T-range (K)	x_{H2S}	P-range (bar)	AARDP%[a]	AARDy%[b]	Ref
H_2S-H_2O	137	298.17-423.15	0.0005-0.111	0.5-206.8	9.3%	1.3%	[31-35]
H_2S-CO_2	122	283.15-360.9	0.033-0.99	20.27-82.74	0.9%	2.2%	[36-38]

[a] $AADP\% = \frac{1}{NP}\sum \frac{abs(P_{exp}-P_{calc})}{P_{exp}} * 100$, [b] $AADy\% = \frac{1}{NP}\sum \frac{abs(y_{exp}-y_{calc})}{y_{exp}} * 100$

7.2.2.3. H_2S-MEA-H_2O and H_2S-MDEA-H_2O mixtures

The results of eUMR-PRU, Kent-Eisenberg[8] and e-NRTL[9] models in H_2S-MEA-H_2O mixture are presented in Table 7.2. In a wide range of temperatures (298.15 to 413.15 K) and MEA concentrations (15.2-30.5 % w/w), eUMR-PRU has an average absolute relative deviation in pressure 25.9 % in a total of 148 correlation data points, whereas the corresponding values for Kent-Eisenberg model is 19.2 % and for e-NRTL 22.4 %. The prediction capability of the models is checked in 100 data points, in which eUMR-PRU has 35 % average absolute relative deviation in partial pressure, whereas the average absolute relative deviation in total pressure is 34.2 %. The corresponding values for e-NRTL are 34.9 % for partial and 42.8 % for total pressures, whereas for Kent-Eisenberg 29.4% for partial pressures in 97 data points. The results of this mixture indicate that the performance of eUMR-PRU is comparable to other widely used models and even better in case of total pressure prediction.

References	%w/w MEA	T-range (K)	KE model		e-NRTL		eUMR-PRU	
			NP	AARDP%	NP	AARDP%	NP	AARDP%
			Correlation					
39	15.3-30.5	298.15-393.15	92	18.3%	96	22.4%	96	26.5%
24	15.2-30.5	313.15-413.15	52	20.8%	52	22.3%	52	24.9%
Overall			**144**	**19.2%**	**148**	**22.4%**	**148**	**25.9%**
			Prediction					
23	15.3-30.5	313.15-373.15	54	28.8%	56	34.6%	56	34.4%
22	20	313.15-393.15	27	37.7%	28	34.8%	28	38.5%
40	15.3	298.15	16	17.3%	16	36.2%	16	30.8%
40a	15.3	298.15	-	-	16	42.8%	16	34.2%
Overall (in H$_2$S partial pressures)			**97**	**29.4%**	**100**	**34.9%**	**100**	**35.0%**
Overall (in total pressures)			**-**	**-**	**16**	**42.8%**	**16**	**34.2%**

^{a} The results refer to total pressures.

The results of eUMR-PRU, Kent-Eisenberg and e-NRTL models in H$_2$S-MDEA-H$_2$O mixture are presented in Table 7.3. In a wide range of temperatures 298.15-413.15 K and amine concentrations 11.94-50.42 % w/w MDEA, eUMR-PRU model yields an average absolute relative deviation in pressure in a total of 158 correlation data points of partial pressure equal to 35.9 %, while for total pressure (71 data points) is 25.4%. The corresponding values for e-NRTL are 25.9 % and 12.6 % accordingly. Kent-Eisenberg predicts only H$_2$S partial pressure and in a total of 144 data points has an average absolute relative deviation equal to 57.1 %. Checking the predictive capability of the models, in a total of 152 data points, eUMR-PRU yields an average absolute relative deviation in partial pressure 37.6 %, while the corresponding values for e-NRTL and Kent-Eisenberg are 22.9 % and 44.2 % respectively. In 100 data points of total pressures, eUMR-PRU has 20.4 % average absolute relative deviation in pressure, whereas e-NRTL has 14.8 %. The results indicate that eUMR-PRU describes satisfactorily this mixture and it is comparable to e-NRTL and more accurate than Kent-Eisenberg, which has the highest average absolute relative deviation in partial pressure.

Table 7.3: VLE results for the system H₂S-MDEA-H₂O system with the eUMR-PRU, KE model and e-NRTL models.

References	%w/w MDEA	T-range (K)	KE model		e-NRTL		eUMR-PRU	
			NP	AARDP%	NP	AARDP%	NP	AARDP%
Correlation								
[41]	23.6	313.15	13	59.9%	13	37.0%	13	35.6%
[42a]	18.7-32.2	313.15-413.15	-	-	71	12.6%	71	25.4%
[43]	11.94-50.42	298.15-393.15	131	56.8%	145	24.9%	145	35.9%
Overall (in H₂S partial pressures)			**144**	**57.1%**	**158**	**25.9%**	**158**	**35.9%**
Overall (in total pressures)			**-**	**-**	**71**	**12.6%**	**71**	**25.4%**
Prediction								
[44a]	46.8	313.15-373.15	-	-	25	21.3%	25	14.6%
[45a]	48.8	313.15-393.15	-	-	26	15.7%	26	14.2%
[46]	35-50	313.15-373.15	40	44.8%	40	22.3%	40	30.7%
[47]	23.9	313.15	26	39.7%	27	22.7%	27	47.0%
[22]	23.1-50	313.15-393.15	36	63.4%	36	35.8%	36	51.1%
[40]	12-20	298.15-388.65	49	32.1%	49	14.0%	49	28.2%
[40a]	12-20	298.15-388.65			49	10.9%	49	26.7%
Overall (in H₂S partial pressures)			**151**	**44.2%**	**152**	**22.9%**	**152**	**37.6%**
Overall (in total pressures)			**-**	**-**	**100**	**14.8%**	**100**	**20.4%**

[a] The results refer to total pressures.

Some typical figures for H₂S-MEA-H₂O and H₂S-MDEA-H₂O mixtures are presented. In Figure 7.3, Kent-Eisenberg, e-NRTL and eUMR-PRU results for H₂S-MEA-H₂O mixture are compared to each other and with experimental data at 298.15-373.15 K and at 15.2-30.5 % w/w MEA. Kent-Eisenberg has the best results, whereas e-NRTL predicts lower H₂S solubility at high pressures (higher partial pressure than the experimental data) and eUMR-PRU overestimates H₂S solubility in aqueous MEA solutions (lower H₂S partial pressure).
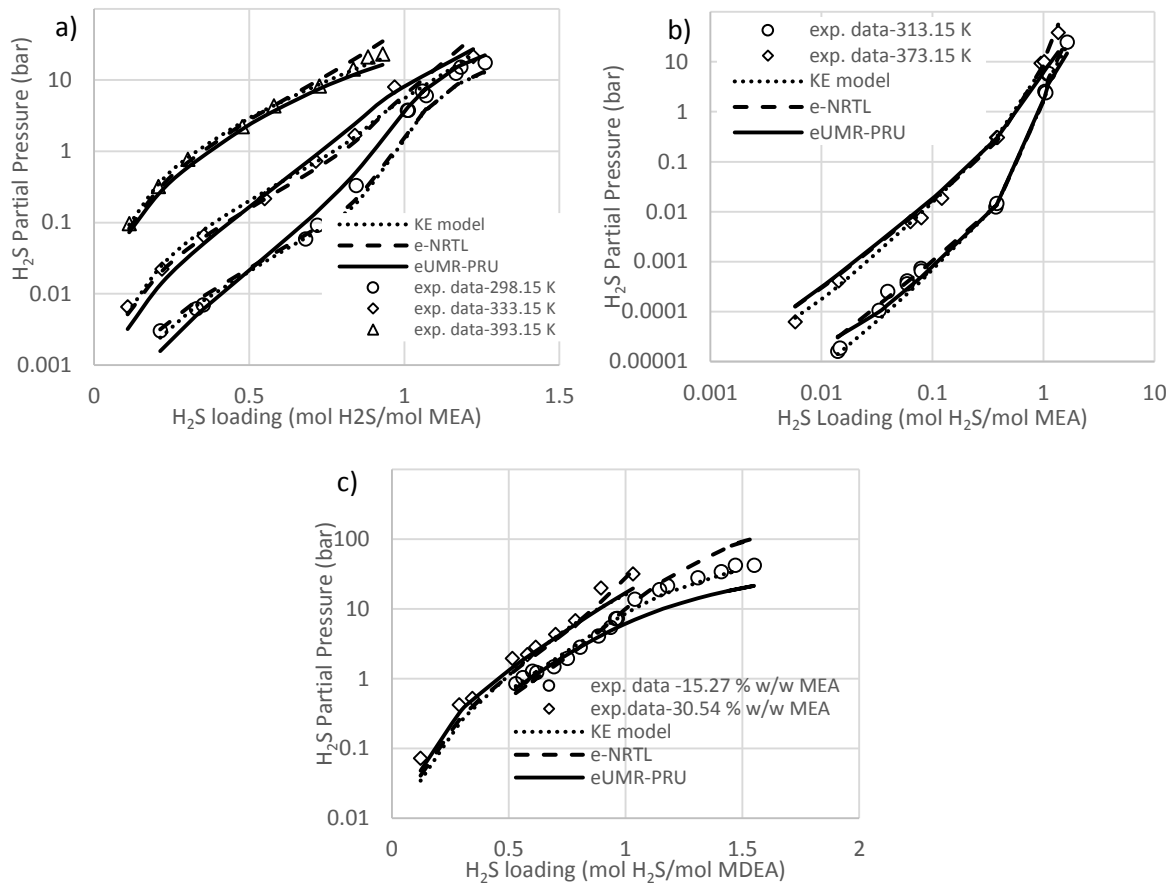
Figure 7.3 *Comparison of Kent-Eisenberg, e-NRTL and eUMR-PRU model results for H_2S-MEA-H_2O with a) experimental data[39] at 298.15, 333.15 and 393.15 K and 30.5 % w/w MEA, b) with experimental data[24] at 313.15, 373.15 and 15.2 % w/w MEA, c) with experimental data[23] at 373.15 K and 15.2 % w/w MEA and 30.5 % w/w MEA.*

In Figure 7.4, Kent-Eisenberg, e-NRTL and eUMR-PRU results for H_2S-MDEA-H_2O mixture are presented along with the experimental data at 11.9-46.8 % w/w MDEA and at 313-373 K. The results of eUMR-PRU are in a greater agreement with the experimental data than those of the other models, except for the case of high loadings at 11.94 % w/w MDEA. Kent-Eisenberg has poor prediction capability especially at 35 % w/w MDEA and at 373.15 K.
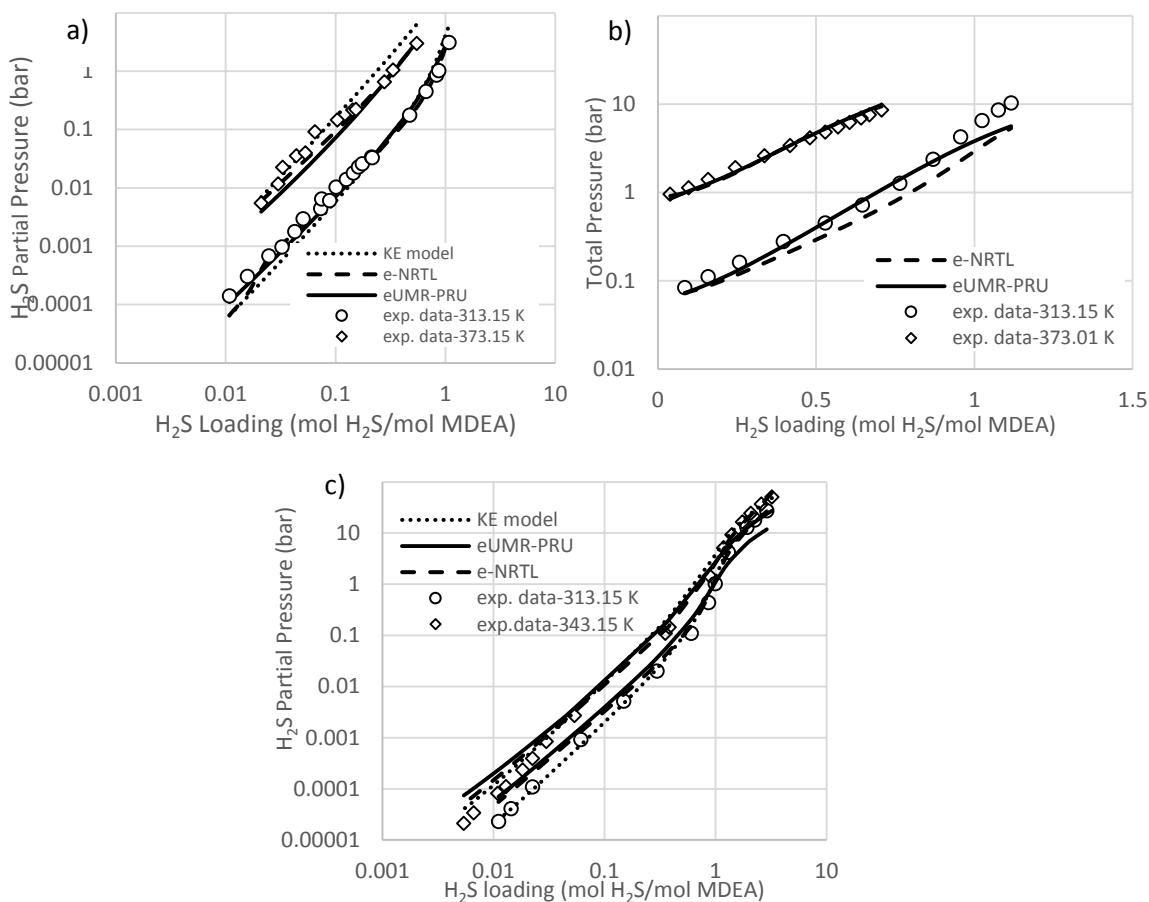
Figure 7.4: *Comparison of KE, e-NRTL and eUMR-PRU model results for H_2S-MDEA-H_2O mixture a) with experimental data[46] at 313.15 K, 373.15 K and 35 % w/w MDEA, b) with experimental data[44] at 313.15 K and at 373.01 K and 46.8 % w/w MDEA, c) with experimental data[43] at 313.15 K and 343.15 K and 11.9 % w/w MDEA*

7.2.2.4. CO_2-H_2S-MEA-H_2O and CO_2-H_2S-MDEA-H_2O mixtures

In order to extend eUMR-PRU to mixtures of acid gases-alkanolamine-water, the parameters between CO_2 and ionic species of H_2S and H_2S and ionic species of CO_2 should be determined, as all the others have already been calculated from the previous mixtures. These parameters are calculated by simultaneous fitting to experimental data of CO_2-H_2S-MEA-H_2O and CO_2-H_2S-MDEA-H_2O mixtures.

Some typical results are presented in Figures 7.5-7.6. The results are presented as parity plot figures comparing the calculated acid gas partial pressure with the experimental. In Figures 7.5a to d the calculated by eUMR-PRU and e-NRTL solubilities of acid gases in aqueous monoethanolamine solutions are compared with the experimental data. eUMR-PRU predicts more accurately the experimental data at low and medium partial pressures

H₂S, whereas e-NRTL is more accurate than eUMR-PRU at high pressures and at CO_2 solubility predictions.
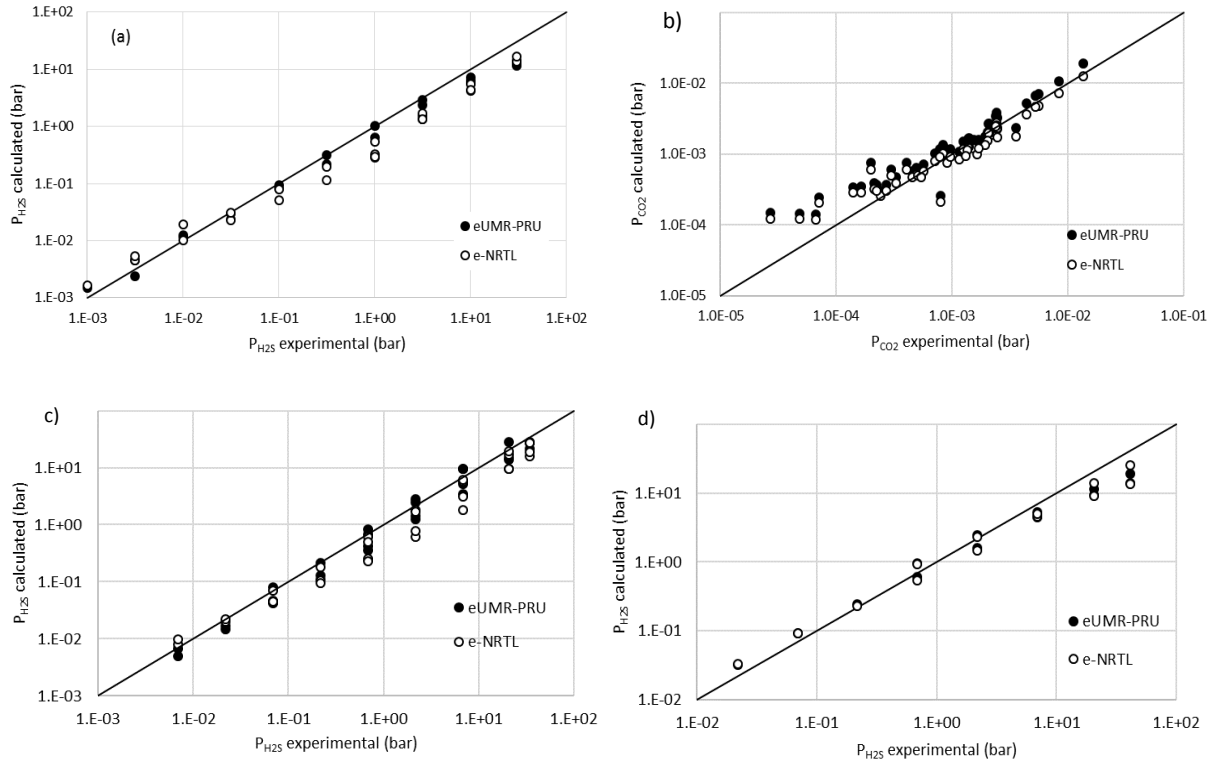
Figure 7.5: Comparison of e-NRTL and eUMR-PRU results with experimental data for CO_2-H_2S-MEA-H_2O mixtures: (a) 313.15 K and 15.3 % w/w MEA[48], (b) 373.15 K and 15.3 % w/w MEA[19], (c) 313.15 K and 30.5 % w/w MEA[49], (d) 373.15 K and 30.5 % w/w MEA[49]

In Figure 7.6a to d, the results of e-NRTL and eUMR-PRU in CO_2-H_2S-MDEA-H_2O mixture are compared to each other and to the experimental data. In this mixture, the results of e-NRTL are better in H_2S solubility prediction than eUMR-PRU, especially at low and medium pressures, whereas at high pressures the performance of the two models is similar. Furthermore, eUMR-PRU predicts more accurately CO_2 solubility in aqueous methyldiethanolamine solutions, especially at low and medium pressures.
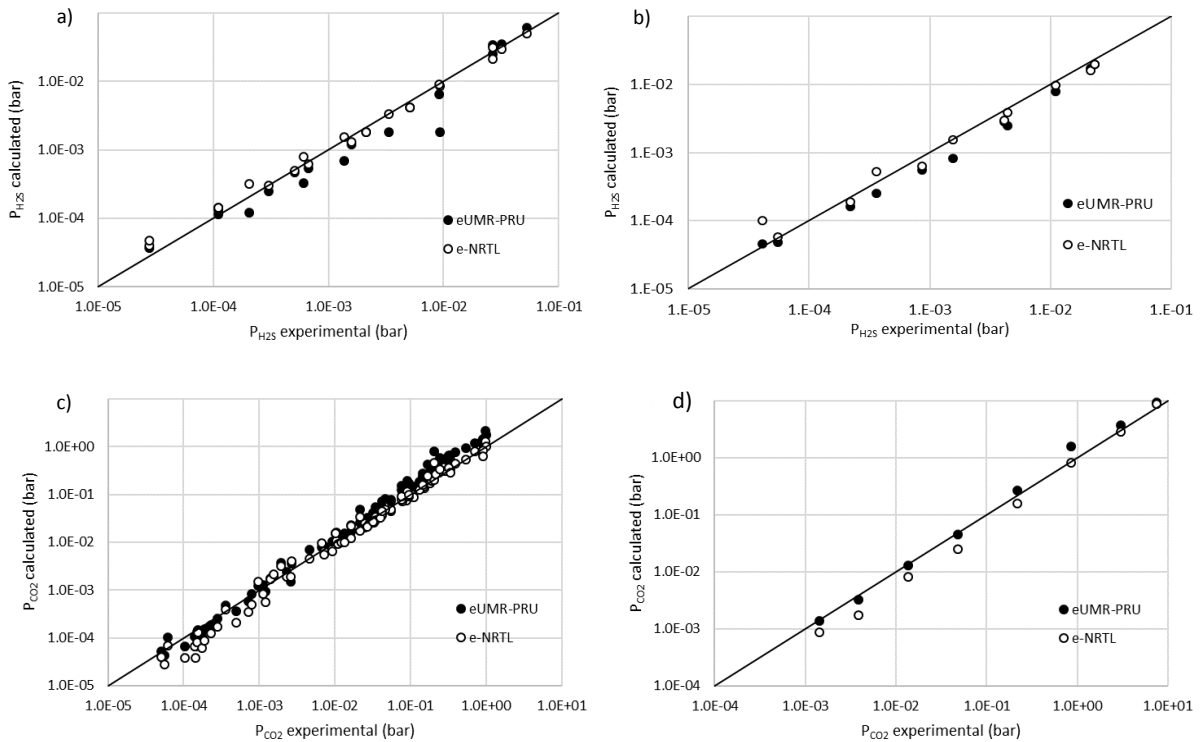
Figure 7.6: Comparison of e-NRTL and UMR-PRU results with experimental data for CO_2-H_2S-MDEA-H_2O mixtures: (a) 313.15 K and 23 % w/w MDEA[50], (b) 323.15 K and 23 % w/w MDEA[50], (c) 313.15 K and 35 % w/w MDEA[51], (d) 313.15 K and 50 % w/w MDEA[22].

7.3. Modeling of H_2S-hydrocarbon mixtures using UMR-PRU model

The correct description of vapor-liquid equilibrium of mixtures containing H_2S and hydrocarbons (HC) by a thermodynamic model is a crucial issue for H_2S removal from natural gas process design. For that reason, UMR-PRU has been extended to these mixtures.

The critical properties and Mathias-Copeman parameters of H_2S are calculated in this work and they are presented in Table A.5 of Appendix A. The critical properties and acentric factors of gases (CH_4, N_2, C_2H_6) and of hydrocarbons are taken from literature[25] and they are presented in Table A.5 of Appendix A as well. The Van der Waals Volume and Area parameters are taken from literature[52] and they are presented in Table A.7 of Appendix A. The binary interaction parameters between H_2S and C_2H_6, CH_2, ACH, $ACCH_2$, N_2 and CH_4 are calculated in this work by fitting to experimental data.

The database used for the fitting procedure of H_2S-HC mixtures with UMR-PRU model, is presented in Table B.9 of Appendix B. The selected experimental data cover a wide range of temperatures (182-523 K) and pressures (0.06-213 bar). The parameters of H_2S-N_2, H_2S-CH_4 and H_2S-C_2H_6 are calculated by fitting to the corresponding binary mixtures, whereas those between H_2S and CH_2 groups are calculated by fitting to binary mixtures of H_2S with normal alkanes, isoalkanes and cycloalkanes presented in Table B.9. The parameters between H_2S and ACH and $ACCH_2$ groups are calculated by fitting to binary mixtures of H_2S with the aromatic hydrocarbons. The objective function is eq.7.1.

The binary interaction parameters of UMR-PRU for these mixtures are presented in Table A.8 of Appendix A. The results of UMR-PRU are presented in Table 7.4. The AARDP % and AARDy % (5.1 and 5.2 accordingly) indicate the successful extension of UMR-PRU to these mixtures.

Table 7.4: UMR-PRU model results in H_2S-HC mixtures

Hydrogen Sulfide with	Ref	AARDP%[a]	AARDy%[b]
Nitrogen	[53 54]	5.9	6.4
Methane	[55 56]	4.1	4.6
Ethane	[57 58]	0.9	4.9
Propane	[58 59]	5.8	4.5
n-butane	[58 60]	4.4	12.6
isobutane	[61]	3.2	5.1
n-pentane	[62]	5.4	7.6
neopentane	[63]	5.7	15.1
isopentane	[63]	6.1	9.5
n-hexane	[64]	5.3	1.4
n-heptane	[65]	8.3	2.7
isooctane	[66]	11.9	
n-nonane	[67]	5.9	1.0
n-decane	[68 66]	5.5	0.2
n-dodecane	[69]	5.3	
n-tridecane	[66]	3.7	
n-pentadecane	[64]	5.6	0.1
n-hexadecane	[70 66]	5.7	
n-eicosane	[71]	7.9	
cyC6	[64]	2.3	0.4
mcyC6	[72]	4.4	2.2
ecyC6	[73]	6.0	1.8
pcyC6	[73]	8.4	0.5
Benzene	[64 74]	1.4	0.9

m-xylene	75	6.2	1.8
Toluene	65	4.5	0.9
Propyl-benzene	76	4.9	0.4
Mesitylene	75	5.9	1.3
Overall		**5.1**	**5.2**

$$^a\,AARDP\% = \frac{1}{NP}\sum\frac{abs(P_{exp}-P_{calc})}{P_{exp}}*100,\ ^b\,AARDy\% = \frac{1}{NP}\sum\frac{abs(y_{exp}-y_{calc})}{y_{exp}}*100$$

7.4. Conclusions

The removal of H_2S from natural gas and flue gases is essential for environmental and health reasons, as well as for the protection of process equipment from corrosion. The most common process used, is chemical absorption with use of aqueous alkanolamines as solvents. Thermodynamic models should be capable of describing H_2S solubility in aqueous alkanolamines, in order to design the process properly. For this reason, eUMR-PRU has been extended to H_2S-MEA-H_2O, H_2S-MDEA-H_2O, CO_2-H_2S-MEA-H_2O and CO_2-H_2S-MDEA-H_2O mixtures in this chapter. Firstly, the binary H_2S-H_2O and CO_2-H_2S parameters have been estimated by fitting to binary experimental data. Secondly, the unknown parameters have been fitted to multicomponent mixtures (acid gas(es)-alkanolamine-water). The model has been evaluated in a wide range of temperatures (298.15-413.15 K) and amine concentrations (12-50 % w/w), as well as acid gas loadings (0-3.23) and its performance has been compared to those of other models, commonly used for such systems, i.e. Kent-Eisenberg and e-NRTL. eUMR-PRU describes satisfactorily the aforementioned mixtures and its results are comparable to those of the other models. Furthermore, UMR-PRU has been extended to H_2S-gases and H_2S-HC mixtures, which are important for natural gas industry. In conclusion, eUMR-PRU is capable to accurately predict the solubility of acid gases in aqueous alkanolamines and UMR-PRU has successfully been extended to mixtures containing H_2S and gases and H_2S and hydrocarbons.

7.5. References

1.   Deshmukh, R. D.; Mather, A. E., A mathematical model for equilibrium solubility of hydrogen sulfide and carbon dioxide in aqueous alkanolamine solutions. *Chemical Engineering Science* **1981,** *36* (2), 355-362.

2.   Panah, H. S.; Mohammadi, A. H.; Ramjugernath, D., Development of a novel approach for modeling acid gas solubility in alkanolamine aqueous solution. *Journal of Natural Gas Science and Engineering* **2016,** *34*, 112-123.

3.   Sadegh, N., *Acid Gas Removal from Natural Gas with Alkanolamines*. Technical University of Denmark (DTU): Kgs. Lyngby, 2013.

4.   Sadegh, N.; Thomsen, K.; Solbraa, E.; Johannessen, E.; Rudolfsen, G. I.; Berg, O. J., Solubility of hydrogen sulfide in aqueous solutions of N-methyldiethanolamine at high pressures. *Fluid Phase Equilibria* **2015,** *393*, 33-39.

5.   Haghtalab, A.; Izadi, A., Solubility and thermodynamic modeling of hydrogen sulfide in aqueous (diisopropanolamine+2-amino-2-methyl-1-propanol+piperazine) solution at high pressure. *The Journal of Chemical Thermodynamics* **2015,** *90*, 106-115.

6.   Kontogeorgis, G.; Folas, G., *Thermodynamic Models for Industrial Applications*. Wiley: 2010.

7.   Afsharpour, A.; Haghtalab, A., Implementation of electrolyte CPA EoS to model solubility of CO2 and CO2 + H2S mixtures in aqueous MDEA solutions. *Chinese Journal of Chemical Engineering* **2019**.

8.   Kent, R. L.; Elsenberg, B., BETTER DATA FOR AMINE TREATING. *Hydrocarbon Processing* **1976,** *55* (2), 87-90.

9.   Renon, H.; Prausnitz, J. M., Local compositions in thermodynamic excess functions for liquid mixtures. *AIChE Journal* **1968,** *14* (1), 135-144.

10.   Edwards, T.; Maurer, G.; Newman, J.; Prausnitz, J., Vapor-liquid equilibria in multicomponent aqueous solutions of volatile weak electrolytes. *AIChE Journal* **1978,** *24* (6), 966-976.

11.   Austgen, D. M.; Rochelle, G. T.; Peng, X.; Chen, C. C., Model of vapor-liquid equilibria for aqueous acid gas-alkanolamine systems using the electrolyte-NRTL equation. *Industrial & engineering chemistry research* **1989,** *28* (7), 1060-1073.

12.   Ellis, A.; Milestone, N., The ionization constants of hydrogen sulphide from 20 to 90° C. *Geochimica et Cosmochimica Acta* **1967,** *31* (4), 615-620.

13.   Kawazuishi, K.; Prausnitz, J. M., Correlation of vapor-liquid equilibria for the system ammonia-carbon dioxide-water. *Industrial & engineering chemistry research* **1987,** *26* (7), 1482-1485.

14.   Tsonopoulos, C.; Coulson, D. M.; Inman, L. B., Ionization constants of water pollutants. *Journal of chemical and engineering data* **1976,** *21* (2), 190-193.

15.   Loy, H.; Himmelblau, D., The first ionization constant of hydrogen sulfide in water. *The Journal of Physical Chemistry* **1961,** *65* (2), 264-267.

16.   Wright, R.; Maass, O., The electrical conductivity of aqueous solutions of hydrogen sulphide and the state of the dissolved gas. *Canadian Journal of Research* **1932,** *6* (6), 588-595.

17.   Ellis, A.; Golding, R., 25. Spectrophotometric determination of the acid dissociation constants of hydrogen sulphide. *Journal of the Chemical Society (Resumed)* **1959**, 127-130.

18.   Posey, M. L., Thermodynamic model for acid gas loaded aqueous alkanolamine solutions. **1998**.

19.   Isaacs, E. E.; Otto, F. D.; Mather, A. E., Solubility of mixtures of hydrogen sulfide and carbon dioxide in a monoethanolamine solution at low partial pressures. *Journal of Chemical & Engineering Data* **1980,** *25* (2), 118-120.

20.   Riegger, E.; Tartar, H. V.; Lingafelter, E. C., Equilibria between Hydrogen Sulfide and Aqueous Solutions of Monoethanolamine at 25°, 45° and 60°. *Journal of the American Chemical Society* **1944,** *66* (12), 2024-2027.

21.   Li, M. H.; Shen, K. P., Solubility of hydrogen sulfide in aqueous mixtures of monoethanolamine with N-methyldiethanolamine. *Journal of Chemical & Engineering Data* **1993,** *38* (1), 105-108.

22.   Huang, S. H.; Ng, H. J.; Ltd, D. B. R. R.; Gas Processors, A.; Gas Research, I., *Solubility of H2S and CO2 in alkanolamines*. Gas Processors Association: Tulsa, OK, 1998.

23.   Lee, J. I.; Otto, F. D.; Mather, A. E., The solubility of H2S and CO2 in aqueous monoethanolamine solutions. *The Canadian Journal of Chemical Engineering* **1974,** *52* (6), 803-805.

24.   Lawson, J. D.; Garst, A. W., Gas sweetening data: equilibrium solubility of hydrogen sulfide and carbon dioxide in aqueous monoethanolamine and aqueous diethanolamine solutions. *Journal of Chemical & Engineering Data* **1976,** *21* (1), 20-30.

25.   Daubert, T. E.; Danner, R. P., *Data compilation tables of properties of pure compounds*. Design Institute for Physical Property Data, American Institute of Chemical …: 1985.

26.   Boukouvalas, C.; Spiliotis, N.; Coutsikos, P.; Tzouvaras, N.; Tassios, D., Prediction of vapor-liquid equilibrium with the LCVM model: a linear combination of the Vidal and Michelsen mixing rules coupled with the original UNIF. *Fluid Phase Equilibria* **1994,** *92*, 75-106.

27.   Vrachnos, A.; Kontogeorgis, G.; Voutsas, E., Thermodynamic Modeling of Acidic Gas Solubility in Aqueous Solutions of MEA, MDEA and MEA–MDEA Blends. *Industrial & Engineering Chemistry Research* **2006,** *45* (14), 5148-5154.

28.   Voutsas, E.; Vrachnos, A.; Magoulas, K., Measurement and thermodynamic modeling of the phase equilibrium of aqueous N-methyldiethanolamine solutions. *Fluid Phase Equilibria* **2004,** *224* (2), 193-197.

29.   Petropoulou, E. G.; Voutsas, E. C., Thermodynamic Modeling and Simulation of Natural Gas Dehydration Using Triethylene Glycol with the UMR-PRU Model. *Industrial & Engineering Chemistry Research* **2018,** *57* (25), 8584-8604.

30.   Pitsinigos, V. D.; Lygeros, A. I., Predicting H/sub 2/S-MEA equilibria. *Hydrocarbon Process.; (United States)* **1989**, Medium: X; Size: Pages: 43-44.

31.   Clarke, E. C. W.; Glew, D. N., Aqueous Nonelectrolyte Solutions. Part VIII. Deuterium and Hydrogen Sulfides Solubilities in Deuterium Oxide and Water. *Canadian Journal of Chemistry* **1971,** *49* (5), 691-698.

32.   Burgess, M. P.; Germann, R. P., Physical properties of hydrogen sulfide-water mixtures. *AIChE Journal* **1969,** *15* (2), 272-275.

33.   Gillespie, P. C.; Wilson, G. M.; Gas Processors, A., *Vapor-liquid and liquid-liquid equilibria : water-methane, water-carbon dioxide, water-hydrogen sulfide, water-npentane, water-methane-npentane*. Gas Processors Association: Tulsa, Okla., 1982.

34.   Selleck, F. T.; Carmichael, L. T.; Sage, B. H., Phase Behavior in the Hydrogen Sulfide-Water System. *Industrial & Engineering Chemistry* **1952,** *44* (9), 2219-2226.

35.   Yu, Q. L., D.; Liu, R.; Zhou, H.; Chen, M.; Chen, G.; Chen, Y.; Hu, Y.; Xu, X.; Shen, L.; Han, S.-J., , VLE OF H2S-H2O System. *Chemical Engineering (China)* **1980,** *4*.

36.   Bierlein, J. A.; Kay, W. B., Phase-Equilibrium Properties of System Carbon Dioxide-Hydrogen Sulfide. *Industrial & Engineering Chemistry* **1953,** *45* (3), 618-624.

37.   Chapoy, A.; Coquelet, C.; Liu, H.; Valtz, A.; Tohidi, B., Vapour–liquid equilibrium data for the hydrogen sulphide (H2S)+carbon dioxide (CO2) system at temperatures from 258 to 313K. *Fluid Phase Equilibria* **2013,** *356*, 223-228.

38.   Sobocinski, D. P.; Kurata, F., Heterogeneous phase equilibria of the hydrogen sulfide–carbon dioxide system. *AIChE Journal* **1959,** *5* (4), 545-551.

39.   Lee, J. I.; Otto, F. D.; Mather, A. E., Equilibrium in hydrogen sulfide-monoethanolamine-water system. *Journal of Chemical & Engineering Data* **1976,** *21* (2), 207-208.

40.   Maddox, R. N. B., A. H.; Diers, J. R.; Thomas, P. A. , Equilibrium Solubility of Carbon Dioxide or Hydrogen Sulfide in Aqueous Solutions of Monoethanolamine, Diglycolamine, Diethanolamine and Methyldiethanolamine. *Gas Processors, A.; Gas Research, I* **1987**.

41.   Lemoine, B.; Li, Y.-G.; Cadours, R.; Bouallou, C.; Richon, D., Partial Vapor Pressure of CO2 and H2S Over Aqueous Methyldiethanolamine Solutions. *Fluid Phase Equilibria* **2000,** *172*, 261-277.

42.   Kuranov, G.; Rumpf, B.; Smirnova, N. A.; Maurer, G., Solubility of Single Gases Carbon Dioxide and Hydrogen Sulfide in Aqueous Solutions of N-Methyldiethanolamine in the Temperature Range 313–413 K at Pressures up to 5 MPa. *Industrial & Engineering Chemistry Research* **1996,** *35* (6), 1959-1966.

43.   Jou, F. Y.; Mather, A. E.; Otto, F. D., Solubility of hydrogen sulfide and carbon dioxide in aqueous methyldiethanolamine solutions. *Industrial & Engineering Chemistry Process Design and Development* **1982,** *21* (4), 539-544.

44.   Sidi-Boumedine, R.; Horstmann, S.; Fischer, K.; Provost, E.; Fürst, W.; Gmehling, J., Experimental determination of hydrogen sulfide solubility data in aqueous alkanolamine solutions. *Fluid Phase Equilibria* **2004,** *218*, 149-155.

45.   Kamps, Á. P.-S.; Balaban, A.; Jödecke, M.; Kuranov, G.; Smirnova, N. A.; Maurer, G., Solubility of Single Gases Carbon Dioxide and Hydrogen Sulfide in Aqueous Solutions of N-Methyldiethanolamine at Temperatures from 313 to 393 K and Pressures up to 7.6 MPa: New Experimental Data and Model Extension. *Industrial & Engineering Chemistry Research* **2001,** *40* (2), 696-706.

46.   Jou, F.-Y.; Carroll, J. J.; Mather, A. E.; Otto, F. D., The solubility of carbon dioxide and hydrogen sulfide in a 35 wt% aqueous solution of methyldiethanolamine. *The Canadian Journal of Chemical Engineering* **1993,** *71* (2), 264-268.

47.   Macgregor, R. J.; Mather, A. E., Equilibrium solubility of H2S and CO2 and their mixtures in a mixed solvent. *The Canadian Journal of Chemical Engineering* **1991,** *69* (6), 1357-1366.

48.   Lee, J. I.; Otto, F. D.; Mather, A. E., The measurement and prediction of the solubility of mixtures of carbon dioxide and hydrogen sulphide in a 2.5 N monoethanolamine solution. *The Canadian Journal of Chemical Engineering* **1976,** *54* (3), 214-219.

49.   Lee, J. I.; Otto, F. D.; Mather, A. E., Solubility of mixtures of carbon dioxide and hydrogen sulfide in 5.0N monoethanolamine solution. *Journal of Chemical & Engineering Data* **1975,** *20* (2), 161-163.

50.   Rogers, W. J.; Bullin, J. A.; Davison, R. R., FTIR measurements of acid-gas–methyldiethanolamine systems. *AIChE Journal* **1998,** *44* (11), 2423-2430.

51.   Jou, F. Y.; Carroll, J. J.; Mather, A. E.; Otto, F. D., Solubility of mixtures of hydrogen sulfide and carbon dioxide in aqueous N-methyldiethanolamine solutions. *Journal of Chemical & Engineering Data* **1993,** *38* (1), 75-77.

52.   Petropoulou, E., Development of a group–contribution equation of state for the thermodynamic modelling of associating mixtures. **2018**.

53.   Kalra, H.; Krishnana, T. R.; Robinson, D. B., Equilibrium-phase properties of carbon dioxide-butane and nitrogen-hydrogen sulfide systems at subambient temperatures. *Journal of Chemical and Engineering Data* **1976,** *21* (2), 222-225.

54.   Besserer, G. J.; Robinson, D. B., Equilibrium-phase properties of nitrogen-hydrogen sulfide system. *Journal of Chemical and Engineering Data* **1975,** *20* (2), 157-161.

55.   Reamer, H.; Sage, B.; Lacey, W., Phase equilibria in hydrocarbon systems-volumetric and phase behavior of the methane-hydrogen sulfide system. *Industrial & Engineering Chemistry* **1951,** *43* (4), 976-981.

56.   Kohn, J. P.; Kurata, F., Heterogeneous phase equilibria of the methane—hydrogen sulfide system. *AIChE Journal* **1958,** *4* (2), 211-217.

57.   Kalra, H.; Robinson, D. B.; Krishnan, T. R., The equilibrium phase properties of the ethane-hydrogen sulfide system at subambient temperatures. *Journal of Chemical and Engineering Data* **1977,** *22* (1), 85-88.

58.   Lobo, L.; Ferreira, A.; Fonseca, I.; Senra, A., Vapour pressure and excess Gibbs free energy of binary mixtures of hydrogen sulphide with ethane, propane, and n-butane at temperature of 182.33 K. *The Journal of Chemical Thermodynamics* **2006,** *38* (12), 1651-1654.

59.   Von Steckel, F., Dampf-Flussigkeits-Gleichgewichte einiger binarer, schwefelwasserstoffhaltiger systeme unter Druck. *Svensk Kemisk Tidskrift* **1945,** *9*, 209-216.

60.   Leu, A. D.; Robinson, D. B., Equilibrium phase properties of the n-butane-hydrogen sulfide and isobutane-hydrogen sulfide binary systems. *Journal of Chemical and Engineering Data* **1989,** *34* (3), 315-319.

61.   Knapp, H.; Döring, R.; Oellrich, L.; Plöcker, U.; Prausnitz, J., Chemistry Data Series, Vol. VI. *VLE for Mixtures of Low Boiling Substances, D. Behrens and R. Eckerman, eds., Frankfurt AM, DECHEMA, Germany* **1982**.

62.   Reamer, H.; Sage, B.; Lacey, W., Phase equilibria in hydrocarbon systems-volumetric and phase behavior of n-pentane–hydrogen sulfide system. *Industrial & Engineering Chemistry* **1953,** *45* (8), 1805-1809.

63.   Leu, A. D.; Robinson, D. B., High-pressure vapor-liquid equilibrium phase properties of the isopentane-hydrogen sulfide and neopentane-hydrogen sulfide binary systems. *Journal of Chemical and Engineering Data* **1992,** *37* (1), 14-17.

64.   Laugier, S.; Richon, D., Vapor-liquid equilibria for hydrogen sulfide+ hexane,+ cyclohexane,+ benzene,+ pentadecane, and+(hexane+ pentadecane). *Journal of Chemical and Engineering Data* **1995,** *40* (1), 153-159.

65.   Ng, H.-J.; Kalra, H.; Robinson, D. B.; Kubota, H., Equilibrium phase properties of the toluene-hydrogen sulfide and heptane-hydrogen sulfide binary systems. *Journal of Chemical and Engineering Data* **1980,** *25* (1), 51-55.

66.   Yokoyama, C.; Usui, A.; Takahashi, S., Solubility of hydrogen sulfide in isooctane, n-decane, n-tridecane, n-hexadecane and squalane at temperatures from 323 to 523 K and pressures up to 1.6 MPa. *Fluid phase equilibria* **1993,** *85*, 257-269.

67.   Eakin, B.; De Vaney, W., Vapor-liquid equilibria in hydrogen-hydrogen sulfide-C9 hydrocarbon systems. **1974**.

68.   Reamer, H.; Selleck, F.; Sage, B.; Lacey, W., PHASE EQUILIBRIA IN HYDROCARBON SYSTEMS-Volumetric and Phase Behavior of Decane–Hydrogen Sulfide System. *Industrial & Engineering Chemistry* **1953,** *45* (8), 1810-1812.

69.   Feng, G.-X.; Mather, A. E., Solubility of H2S in n-dodecane. *Fluid phase equilibria* **1993,** *87* (2), 341-346.

70.   Feng, G. X.; Mather, A. E., Solubility of H2S in n-hexadecane at elevated pressure. *The Canadian Journal of Chemical Engineering* **1993,** *71* (2), 327-328.

71.   Feng, G. X.; Mather, A. E., Solubility of hydrogen sulfide in n-eicosane at elevated pressure. *Journal of Chemical and Engineering Data* **1992,** *37* (4), 412-413.

72.   Ng, H.-J.; Robinson, D. B., The equilibrium phase properties of selected naphthenic binary systems: carbon dioxide-methylcyclohexane, hydrogen sulfide-methylcyclohexane. *Fluid Phase Equilibria* **1979,** *2* (4), 283-292.

73.   Huang, S. S.; Robinson, D. B., Equilibrium phase properties of the ethylcyclohexane-hydrogen sulfide and n-propylcyclohexane-hydrogen sulfide binary systems. *Journal of Chemical and Engineering Data* **1985,** *30* (2), 154-157.

74.   Fischer, K.; Chen, J.; Petri, M.; Gmehling, J., Solubility of H2S and CO2 in N-octyl-2-pyrrolidone and of H2S in methanol and benzene. *AIChE journal* **2002,** *48* (4), 887-893.

75.   Huang, S. S.-S.; Robinson, D. B., Vapor-liquid equilibrium in selected aromatic binary systems: m-xylene-hydrogen sulfide and mesitylene-hydrogen sulfide. *Fluid phase equilibria* **1984,** *17* (3), 373-382.

76.   Richon, D.; Laugier, S.; Renon, H., High-pressure vapor-liquid equilibrium data for binary mixtures containing molecular nitrogen, carbon dioxide, hydrogen sulfide and an aromatic hydrocarbon or propylcyclohexane in the range 313-473 K. *Journal of Chemical and Engineering Data* **1992,** *37* (2), 264-268.

8. Ionic liquids

UMR-PRU is extended to CO_2-ionic liquid mixtures and it is compared to Peng-Robinson EoS. The database and the results of the two models are presented in this chapter.

8.1. Introduction

Ionic liquids consist of an organic cation and an inorganic anion and they have attracted a lot of attention last decades, due to their unique thermodynamic properties, such as liquid state in room temperature, very low vapor pressure, nonflammability, chemical and thermal stability, and the fact that they offer the capability of being recycled by using simple flash drums[1]. Because of these properties, ionic liquids have been recently proposed as green solvents in many processes, such as the acid gas absorption from natural gas or flue gases.

In order to design and simulate the absorption process with ionic liquids as solvents, it is necessary to have proper thermodynamic models, able to describe the solubility of acid gases in ionic liquids. In literature there are several models used to model acid gas solubility in ionic liquids. According to Vega et al[2] the models used for these mixtures can be classified in the following categories: cubic equations, activity coefficient models, quantum mechanics-based methods, and statistical mechanics-based molecular approaches. Peng-Robinson[3-6] and Soave-Redlich-Kwong EoS[4] have been used to model mixtures of acid gases in ionic liquids. They usually lack accuracy at high pressures[7]. NRTL[8] is an example of activity coefficient models used to describe such mixtures. Group contribution methods such as UNIFAC[9-11] and the Group Contribution EoS (GC EoS)[12-14] have also been used by some authors to describe the phase-equilibria of acid gases-ionic liquid mixtures. Statistical mechanics-based models[7, 15] have also been employed by some authors and they describe sufficiently these mixtures.

Cubic equations of state usually appear inability to describe high pressures of acid gas-ionic liquid mixtures. Therefore, the use of EoS/G^E models is a better suggestion than cubic EoS for these mixtures. For that reason, in this thesis UMR-PRU is extended to CO_2-ionic liquid mixtures and it is compared to Peng-Robinson EoS with two interaction parameters, k_{ij} and l_{ij}, calculated as group contribution functions.

For both models, critical properties, acentric factor, Mathias-Copeman parameters of the components are necessary properties. The critical properties of ionic liquids cannot be determined experimentally, since most ionic liquids start to decompose at the normal boiling point temperature. Therefore, in literature, several methods, usually group contribution ones, can be found, in order to determine these properties of ionic liquids[16]. According to these methods, the critical properties of a component are estimated by a correlation, which sums the contribution of the groups appearing in this molecule. Due to the lack of experimental critical properties, their calculated values are usually checked for their accuracy in predicting the liquid density of the ionic liquid, as such data are available in literature. However, the accuracy of the critical properties in estimating the vapor

pressure of ionic liquids is not tested, even though it is crucial for the models to predict very low vapor pressure for such components. This lack of testing is usually due to the limited number of experimental vapor pressure measurements of ionic liquids.

In this thesis, twelve ionic liquids are examined, which derived from the combination of imidazolium-based cations (1-Ethyl-3-methylimidazolium, 1-Butyl-3-methylimidazolium, 1-Hexyl-3-methylimidazolium, 1-octyl-3-methylimidazolium) with three type of anions, i.e. tetrafluoroborate, hexafluorophosphate, bis(trifluoromethylsulfonyl)imide. UMR-PRU is extended to CO_2-ionic liquid mixtures and it is compared to Peng-Robinson EoS. Their critical properties are estimated in this thesis, while Mathias-Copeman parameters are employed for all ionic liquids for which vapor-pressure data were available. The critical properties and Mathias-Copeman parameters are estimated by fitting them to experimental vapor-pressure and liquid density data. Additionally, critical properties and Soave parameter for the temperature dependency of the attractive term of PR EoS are also estimated, because in process simulators no Mathias-Copeman parameters can be applied.

After the estimation of pure component parameters, the binary CO_2-ionic liquids mixtures are modelled. In order UMR-PRU to be extended to CO_2-ionic liquid binary mixtures, ionic liquids are decomposed in groups and UNIFAC interaction parameters and van der Waals volume and area parameters are estimated by fitting to experimental data. Furthermore, l_{ij} binary interaction parameter is calculated as a function of carbon number of the alkyl-chain of ionic liquid. For comparison purposes, Peng-Robinson EoS is extended to these mixtures with use of k_{ij} interaction parameters as a function of carbon number of the alkyl chain and the temperature, whereas l_{ij} parameters are also used as a function of carbon number of the alkyl chain.

In the first part of this chapter the database developed for pure components and binary mixtures is presented, while in the second part, the results of UMR-PRU and Peng-Robinson EoS are shown.

8.2. Database

8.2.1. Pure components

In order to determine the critical properties, Soave and Mathias-Copeman parameters for pure components, it is necessary to gather the appropriate data. These are liquid density and vapor pressure data. Concerning the liquid density data, the database is very extended, because there are plenty of experimental data published in literature. Therefore, data from different authors for the same ionic liquid and at the same conditions are compared to each other, in order to define incompatible data and exclude

them from the database. Furthermore, the selected data are examined, in order to ascertain, whether or not, specific thermodynamic trends are followed. As far as the vapor pressure data concerns, the database is very limited due to the lack of published experimental data. Therefore, in most cases it is not applicable to compare data from different sources. However, these data are also examined for thermodynamic trends. The selected for fitting procedure databases are presented in Tables B.11-B.12 of Appendix B and the thermodynamic trends are presented through figures and discussed below.

As far as the liquid density concerns, the following thermodynamic trends should be followed:

- As the molecular weight of the cation increases, the liquid density decreases[17].
- As the size of the anion increases, the liquid density increases[18]

These trends are followed by the data selected for the fitting database. Two typical figures are presented below. Figure 8.1 confirms that the experimental data chosen follow correctly the trend of the liquid density as a function of the cation molecular weight.
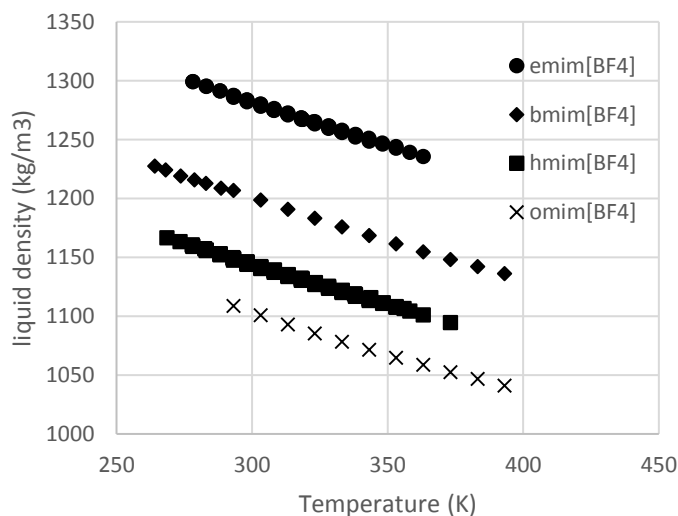
Figure 8.1: Effect of the cation size on liquid density of ionic liquids (experimental data: emim[BF4] [19-22], bmim[BF4] [23-24], hmim[BF4] [25-29], omim[BF4] [23].

Figure 8.2 confirms, that the experimental data chosen follow correctly the trend of the liquid density, which increases as the anion size increases.
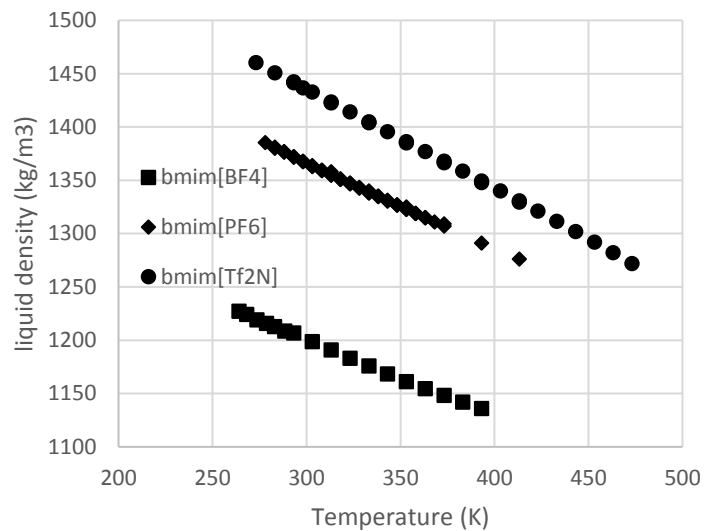
Figure 8.2: Effect of the anion size on liquid density of ionic liquids (experimental data: bmim[BF4][23-24], bmim[PF6] [30-31] [32-34], bmim[Tf2N] [35-36]).

Concerning the vapor pressure of ionic liquids, Zaitsau et al[37] stated, that enthalpies of vaporization of ionic liquids, depend on the Coulomb interactions within the liquid and gas phase ion pair and that van der Waals interactions increase with increasing alkyl chain length. Rocha et al[38] stated, that the vapor pressure of ionic liquids decreases as the alkyl chain length increases. This is confirmed by the experimental data chosen in this work, as it is presented in Figure 8.3.
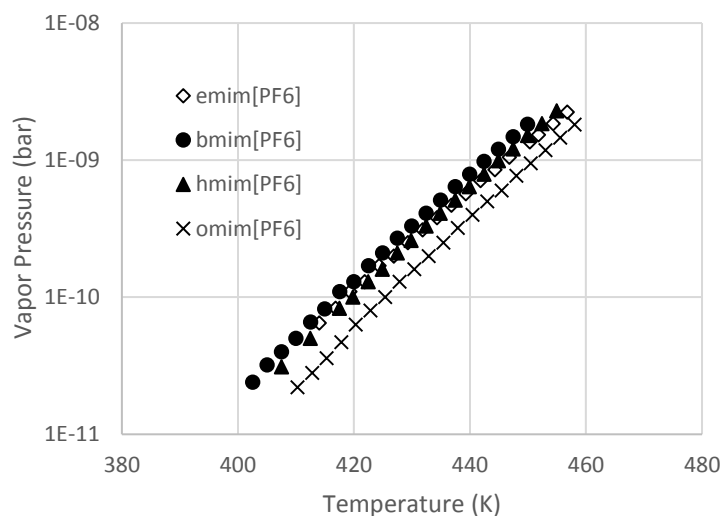
Figure 8.3: Effect of the alkyl chain length on vapor pressure of ionic liquids (experimental data: emim[PF6] [37], bmim[PF6] [37], hmim[PF6] [37], omim[PF6] [37]).

8.2.2. Binary mixtures

Thermodynamic modeling of the solubility of acid gases in ionic liquids is of particular importance for design and simulation of acid gas physical absorption processes with the use of ionic liquids as solvents. For this purpose, it is necessary to have proper thermodynamic models, which are developed by fitting to experimental data. Therefore, it is crucial to create an appropriate database of experimental solubility data of acid gases in ionic liquids. In this thesis the CO_2 solubility in ionic liquids mentioned before is modeled and the experimental data found in literature are evaluated in order to define, whether or not, specific thermodynamic trends are followed and if there is data agreement for the same binary mixture from different researchers.

In most cases, there are not data for the same binary mixture from many different sources. An exception is the binary system of CO_2/bmim[PF$_6$], which has been measured by many authors leading to data, that are not always in good agreement with each other, as it is shown in Figure 8.4.
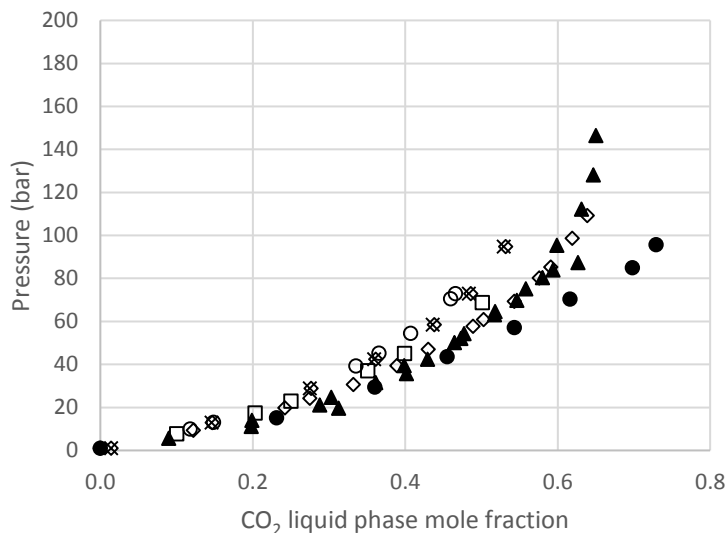
Figure 8.4: Comparison of experimental data for CO_2 solubility in bmim[PF_6] at 313 K (● Blanchard et al[39],○ Zhang et al[40], ◊ Liu et al[41], □ Shariati et al[42], X Kamps et al[43], ◊Kumelan et al[44], ▲ Aki et al[45])

Figure 8.4 depicts the pressure effect on the CO_2 solubility in bmim[PF_6] at 313 K. The maximum depicted pressure is 200 bar for clear display of the data at low pressures. The data discrepancy can easily be drawn as a conclusion from this figure: Data of Aki et al[45] are similar to those of Liu et al[41], whereas they differ from data of Kamps et al[43], Kumelan et al[44], Zhang et al[41] and Shariati et al[42], which are close to each other. Finally, data of Blanchard et al[39] differ from all other literature sources. Measurements of Aki et al[45] follow a problematic trend, since the pressure does not always increase as the CO_2 mole fraction increases, and therefore they are excluded from the database, as well as those of Liu et al[41]. Data of Blanchard et al[39] differ from all other sources, so they are also excluded from the database. This procedure is followed for each binary mixture.

As far as the thermodynamic trends which should be followed two basic conclusions have been drawn from literature review:

- As the length of the alkyl chain of the cation increases, the solubility of CO_2 in the ionic liquid increases as well, especially at high pressures[46].
- The fluorination of the anion results to higher CO_2 solubility in the ionic liquid. Concerning the ionic liquids with anions BF_4, PF_6, Tf_2N, the CO_2 solubility is the highest at Tf_2N ionic liquids and the lowest at BF_4 ionic liquids[47].

Thus, the previously selected data are also checked if they follow the aforementioned described thermodynamic trends. For instance, the CO_2 solubility in ionic liquids with anion Tf_2N is depicted in Figure 8.5:
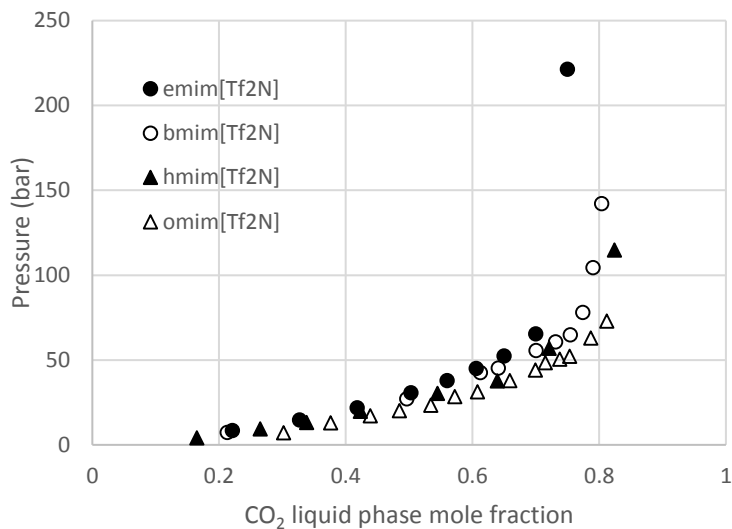
Figure 8.5: Effect of the alkyl chain length of the cation on CO_2 solubility in ionic liquids at 303 K (experimental data:emim[Tf2N][48], bmim[Tf2N] [49], hmim[Tf2N][50], omim[Tf2N][5]).

From this figure, it can be concluded that the data selected in this work confirm that the increase in the alkyl chain length of the cation results to higher CO_2 solubility in the ionic liquid. Furthermore, from Figure 8.6 it can be concluded that the fluorination of the anion results to higher CO_2 solubility in the ionic liquid.

The data selected for the fitting procedure are presented in Table B.13 of Appendix B.
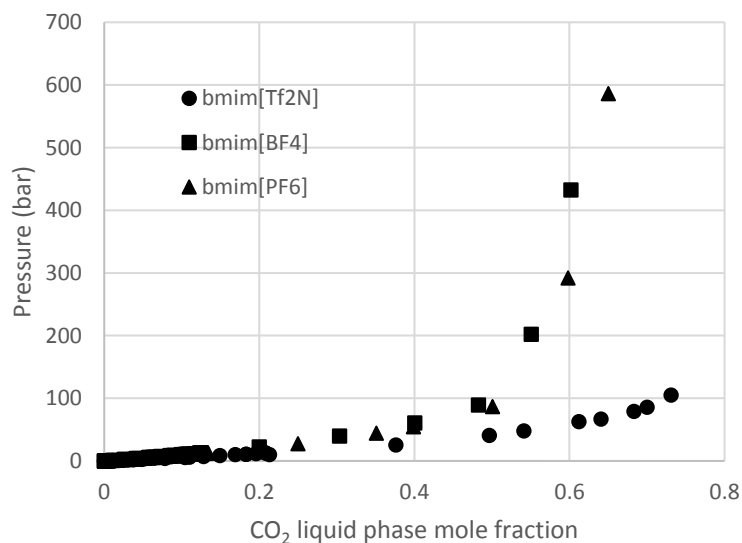
Figure 8.6: Effect of the fluorination of the anion on CO_2 solubility in ionic liquids at 323.15 K.(experimental data: bmim[Tf2N][49, 51], bmim[BF4][51-52], bmim[PF6][51, 53])

8.3. Results

In this section, UMR-PRU and PR EoS description of liquid density and vapor pressure of ionic liquids and CO_2 solubility in them is presented.

8.3.1. Pure components

As stated before, critical temperature and pressure, Soave (m) and Mathias-Copeman (c_1, c_2, c_3) parameters for ionic liquids are estimated in order to enable the application of a cubic equation of state equation to ionic liquids systems.

Since the experimental liquid densities of ionic liquids are measured at lower temperatures, whereas the experimental vapor pressures are measured at higher temperatures, the following procedure is followed: the critical temperature, pressure and Mathias-Copeman parameters of ionic liquids are fitted at low temperatures only to liquid density data, while at higher temperatures only to vapor pressure data. For each ionic liquid critical temperature, pressure and Soave parameter are estimated for comparison purposes and due to the fact that Mathias-Copeman parameters are inapplicable in process simulators. In case of the absence of vapor pressure data, only Soave and no Mathias-Copeman parameter is estimated so as the model to correctly predict the liquid density and describe the effect of the alkyl chain length on vapor pressure. The same fitting procedure is followed for the critical temperature and pressure and Soave parameter as well. Therefore, two objective functions are used (one for the fitting to the density data, another one for fitting to vapor pressure data), as shown below.

Fitting to experimental liquid volume

$$OF = \frac{1}{NP} \sum_{i=1}^{NP} \left(\frac{V_{i,exp} - V_{i,calc}}{V_{i,exp}} \right)^2 * 100 \qquad \text{eq. 8.1}$$

Fitting to experimental vapor pressure:

$$OF = \frac{1}{NP} \sum_{i=1}^{NP} abs\left(ln\left(P_{i,exp}\right) - ln(P_{i,calc}) \right) \qquad \text{eq. 8.2}$$

As far as the critical properties of CO_2 concerns, they were taken from literature[54]. In Table 8.1 the calculated properties are presented with the average absolute percentage deviation in liquid density and in natural logarithm of vapor pressure, whereas the fitting to experimental vapor pressures is also presented in Figure 8.7, where the use of Soave

parameter is compared with the use of Mathias-Copeman parameters. It is concluded that the results are similar, with a slightly better description of the trend of experimental vapor pressure data by Mathias-Copeman parameters, a fact which results to the lower average absolute relative deviation in vapor pressures compared to the one of Soave parameter. The same result is concluded by the comparison of liquid densities as well.

In literature, the most common methods presented, to calculate the critical properties and the acentric factor of ionic liquids, are group contribution methods. For instance, Valderrama et al[55] used Lydersen-Joback-Reid method, in which it is necessary the structure of the molecule and the molecular weight to be known. They used a correlation, in order to calculate the liquid densities of the ionic liquids and compare them to experimental values. They calculate the densities at low temperatures (295-313 K) for all of the ionic liquids examined in the present work and the average absolute deviations in liquid densities are always higher than the ones calculated with the present critical properties and Peng-Robinson EoS, except for the average absolute deviation in liquid densities of hmim[BF_4], hmim[PF_6] and bmim[Tf_2N] which are about 0.5 % for Valderrama et al[55] with their correlation, whereas in present work they are about 3% at the same temperatures with Peng-Robinson EoS.

Another, group contribution method (Joback method) was used by Shin et al[5], in order to estimate the critical properties of ionic liquids with anion Tf_2N, whereas Shariati et al[56], used fitted the critical properties and acentric factor of ionic liquids to binary vapor-liquid equilibrium data of CO_2-ionic liquid mixtures with Peng-Robinson EoS. Shariati et al[56] have also used a correlation to calculate liquid densities and they have lower average absolute deviations in liquid densities than Valderrama et al[55] and even lower than the one presented in this work in some cases. However, they have not checked the accuracy of their critical properties in vapor pressure estimation.

Table 8.1: Correlation results of Peng-Robinson EoS in liquid density and vapor pressure of ionic liquids.

	T-range	Tc (K)	Pc(bar)	c1	c2	c3	AARDρ%[a]	AARDlnPs%[b]	Tc (K)	Pc(bar)	m	AARDρ%[a]	AARDlnPs%[b]%
emimPF₆	278.15-370.15	1050.4	38.9	3.136093	-2.05341	-0.64425	1.6	2.6	1040.354	39.8957	2.351621	2.3	3.7
bmimPF₆	280.15-400.15	1120.1	35.6	3.201632	-2.68354	-0.97883	1.9	0.3	1121.004	35.49735	2.089044	1.8	3.5
hmimPF₆	280.15-380.15	1353.5	35.6	1.812754	-1.43593	1.213973	3.6	0.4	1330.847	35.18214	1.478291	2.3	1.1
omimPF₆	280.15-390.15	1425.7	34.6	1.802544	-1.28732	0.400907	2.4	0.1	1440.231	34.68694	1.29924	2.0	1.4
emimTf₂N	280.15-460.15	1110.9	27.3	1.66641	0.968509	-1.81562	2.5	2.0	1169.06	29.19092	1.57214	2.3	1.3
bmimTf₂N	280.15-460.15	1150.9	24.9	1.589483	0.839271	-1.7997	2.6	1.9	1193.898	26.88286	1.55236	3.1	2.9
hmimTf₂N	260-470	1186.6	23.4	1.792688	-0.95482	0.637446	2.7	1.2	1197.712	23.13224	1.500786	2.8	1.6
omimTf₂N	280-460	1298.3	23.2	0.722688	1.654825	-0.83745	2.3	1.0	1200.325	20.81564	1.45822	3.0	2.8
emimBF₄	280-365	1050	45.8	2.081709	0	0	2.6	-	1050	45.8	2.081709	2.6	-
bmimBF₄	273.15-393.15	1123.9	39.5	2.687917	-1.60576	0.048637	1.8	2.9	1147.406	40.83743	2.008709	2.8	3.3
hmimBF₄	273.15-363.15	1160.5	33.5	2.00556	0	0	2.3	-	1160.5	33.5	2.00556	2.3	-
omimBF₄	293.15-393.15	1270.9	32	1.850509	0	0	1.3	-	1270.9	32	1.850509	1.3	-

[a]$AARD\rho \% = \frac{1}{NP}\sum abs\left(\frac{\rho_{exp}-\rho_{calc}}{\rho_{exp}}\right)*100$

[b]$AARDlnP_s \% = \frac{1}{NP}\sum abs\left(\frac{lnP_{s\,exp}-lnP_{s\,calc}}{lnP_{s\,exp}}\right)*100$

Figure 8.7:Comparison of vapor pressure results by PR EoS using Soave and MC expression with experimental data: (a) [bmim]BF$_4$[57], b) [emim]PF$_6$[37], c) [bmim]PF$_6$[37], d) [hmim]PF$_6$[37], e) [omim]PF$_6$[37], f) [emim]Tf$_2$N[38, 58], g) [bmim]Tf$_2$N[38, 58], h) [hmim]Tf$_2$N[38, 58], i) [omim]Tf$_2$N[38, 58]

8.3.2. Binary mixtures

Lots of studies about the solubility of acid gases in ionic liquids have been presented in literature, but their majority is experimental. However, for process design of absorption columns thermodynamic models capable of describing the solubility are necessary, and therefore the interaction parameters between acid gases and ionic liquids need to be determined.

Group contribution methods are based on the assumption that a property of a component can be determined as a function of the individual properties of the various groups, which compose the component. Knowing these functions, someone can easily calculate properties of other components or mixtures, when the structure of the

164

components is known. This indicates the predictive capability of the group contribution methods, which makes them valuable tools for process designers.

In this section the modeling of the CO_2 solubility in ionic liquids with UMR-PRU model is presented. The G^E part of the model is calculated with UNIFAC, which implies that functional groups of ionic liquids must be determined. In literature[59] three approaches for the application of UNIFAC to ionic liquids have been presented:

- The ionic liquid is divided into two groups: one cation and one anion
- The ionic liquid is divided into cation core, one anion and some CH_2, CH_3 groups.
- The ionic liquid is divided into one cation-anion skeleton and CH_2, CH_3 groups, which appear in the alkyl chain.

In the first approach the structure of the alkyl chain is not reflected. In the second approach there are many groups and as a consequence many parameters need to be determined, which makes the fitting procedure more complex. In the last approach the groups are electrically neutral and therefore the Debye-Hueckel term is not needed. In this work the last approach is adopted by UMR-PRU model. The groups of the ionic liquids are presented in Table 8.2.

Table 8.2: UNIFAC groups considered for UMR-PRU in this work.

PF_6 ionic liquids	Tf_2N ionic liquids	BF_4 ionic liquids
mim[PF_6]	mim[Tf_2N]	mim[BF_4]
CH_3	CH_3	CH_3
CH_2	CH_2	CH_2

For example, hmim[PF_6] ionic liquid has 1 CH_3 group, 5 CH_2 group and 1 mim[PF_6] group.

Concerning, UMR-PRU model, the UNIFAC interaction parameters calculated through fitting in this work are those between mim[PF_6] and CO_2, mim[Tf_2N] and CO_2, mim[BF_4] and CO_2 and those between mim[PF_6] and CH_2, mim[Tf_2N] and CH_2, mim[BF_4] and CH_2, whereas those between CO_2 and CH_2 are taken from literature[60]. Furthermore, the van der Waals volume and Area parameters of mim[PF_6], mim[Tf_2N] and mim[BF_4] are calculated in this work, whereas those of CO_2 and CH_2 are taken from literature[61]. The l_{ij} binary interaction parameters between the two components (CO_2 and ionic liquid) were also estimated as a function of carbon number in the alkyl chain (Eq. 8.3) via fitting to experimental data. The parameters D_1-D_2 for UMR-PRU model are presented in Table A.9 of Appendix_A.

$$l_{ij} = D_1 + D_2\ CN \qquad\qquad \text{eq. 8.3}$$

For comparison purposes, Peng-Robinson EoS with classical van der Waals one fluid mixing rules is also examined. However, in order to obtain a fair comparison with UMR-PRU, a group contribution method for Peng-Robinson is developed. Therefore, the k_{ij} interaction parameters are presented as a function of temperature and carbon number in the alkyl chain (eq.8.4), whereas l_{ij} interaction parameters are presented as a function of the carbon number in the alkyl chain (eq.8.3).

$$k_{ij} = A_1 + B_1\ CN + (A_2 + B_2\ CN)\ T + (A_3 + B_3\ CN)\ T^2 \qquad\qquad \text{eq. 8.4}$$

The A_1-A_3, B_1-B_3 and D_1-D_2 parameters for Peng Robinson EoS are presented in Table A.10 of Appendix_A.

The objective function for both models is:

$$OF = \frac{1}{NP} \sum_{i=1}^{NP} abs\left(ln\ P_{calc} - ln\ P_{exp}\right) \qquad\qquad \text{eq. 8.5}$$

The results of the fitting procedure are presented in Table 8.3.

Table 8.3: Peng-Robinson and UMR-PRU correlation results in CO_2 solubility in ionic liquids.

	References	NP	AARDP%[a]	
			PR	UMR-PRU
[emim]PF$_6$	[62]	62	29.6	9.2
[bmim]PF$_6$	[43, 51, 53, 63]	298	7.8	4.6
[hmim]PF$_6$	[64-65]	108	19.6	9.1
[omim]PF$_6$	[39]	15	31.4	33.0
[emim]Tf$_2$N	[48, 66-68]	174	6.2	9.2
[bmim]Tf$_2$N	[49, 51, 69-70]	160	15.9	11.5
[hmim]Tf$_2$N	[50, 71-72]	125	12.6	13.7
[omim]Tf$_2$N	[73, 5]	123	17.2	6.3
[emim]BF$_4$	[74-76]	36	11.1	12.01
[bmim]BF$_4$	[51-53]	216	9.1	8.6
[hmim]BF$_4$	[64, 77]	111	9.8	6.3
[omim]BF$_4$	[39]	86	13.6	4.1
Overall		1514	12.3	8.4

[a]$AADP\ \% = \frac{1}{NP} \sum abs\left(\frac{P_{exp} - P_{calc}}{P_{exp}}\right) * 100$

UMR-PRU describes satisfactorily the experimental data, used for the correlation procedure, whereas Peng-Robinson EoS has a slightly higher average absolute relative deviation in pressure. Furthermore, both models describe sufficiently the CO_2 solubility at high pressures, but UMR-PRU describes more accurately the trend of experimental data at medium and high pressures, as it is concluded by Figures 8.8-8.10.

In literature, there are many models used for calculation of CO_2 solubility in ionic liquids. Some of them are based on group contribution methods and they are comparable with the group contribution method proposed in this work. For example, Hizaddin et al[78] used the predictive SRK model, which combines a cubic equation of state with UNIFAC activity coefficient model. For CO_2-emim[Tf_2N] mixture, the average absolute deviation in pressure is 6.8% and 6.1% for PSRK and 12.8 % and 3.4 % for UMR-PRU for data of Carvalho et al[48] and Schilderman et al[67] accordingly. In CO_2-bmim[Tf_2N] mixture Hizaddin et al[78] and present work have used data of Oh et al[49] and the average absolute deviation in pressure is 16.14 % and 6.7 % for PSRK and UMR-PRU respectively. In CO_2-bmim[BF_4] mixture PSRK has about 5.7 % average absolute deviation in data of Shiflett and Yokozeki[79] and Kroon et al[52], whereas the AADP% of UMR-PRU is 8.6 %. In CO_2-bmim[PF_6] the AADP% of PSRK is 3.6 % and 14.7 % for data of Anthony et al and Kamps et al[43] respectively, whereas the corresponding values for UMR-PRU are 3.4 % and 8.3 % respectively. In another work, Kheiri and Afsharpour[80] have used CPA EoS and they have AADP% in CO_2-bmim[PF_6] mixture 10.4 % in data of Kamps et al[43], whereas the corresponding value for UMR-PRU is 8.3%, as it has been mentioned. It can be concluded, that UMR-PRU gives very satisfactory results comparable with other models presented in literature and in most cases, they are in a greater agreement with the experimental data.
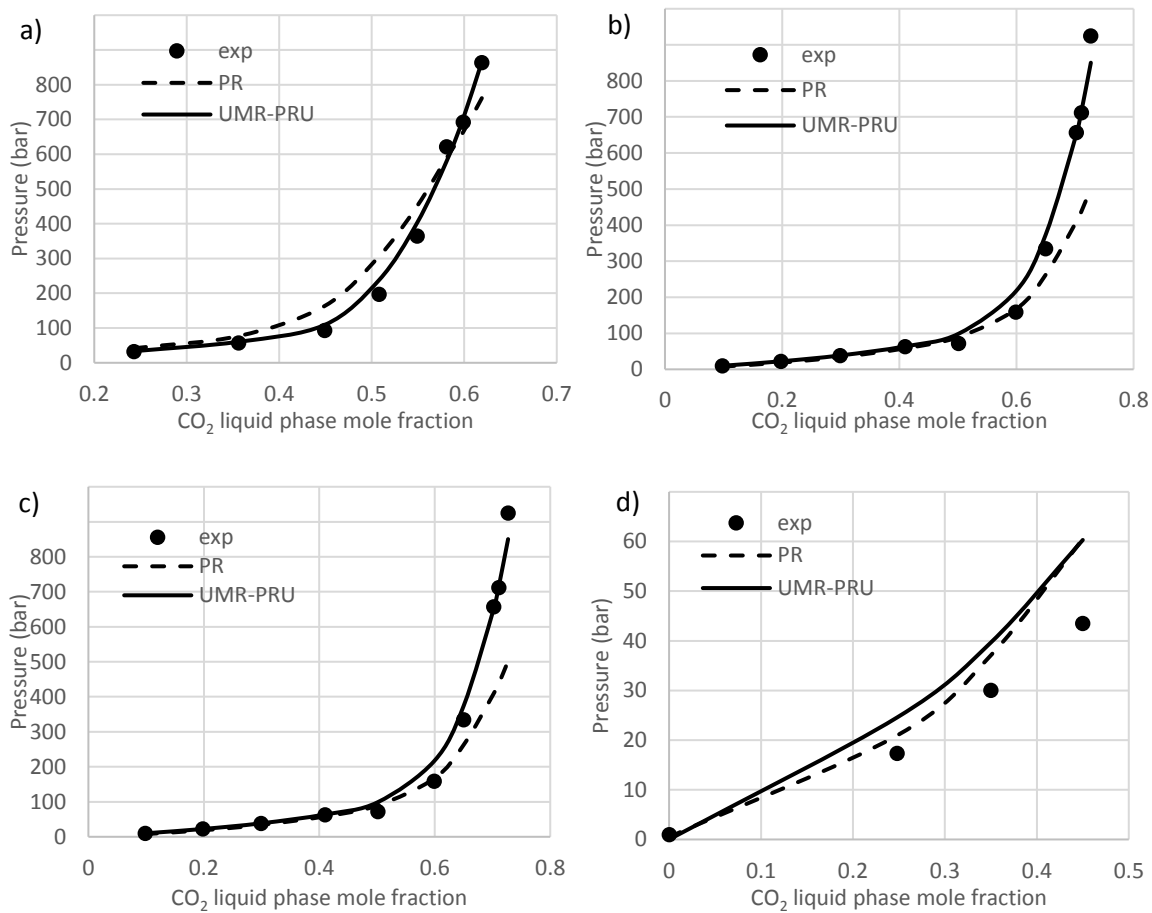
Figure 8.8:Comparison of UMR-PRU and Peng-Robinson EoS results with the experimental solubilities of CO_2 in a) [emim]PF_6 at 323 K^{62}, b) [bmim]PF_6 at 353.3 K^{53}, c) [hmim]PF_6 at 338.2 K^{65} and d) [omim]PF_6 at 333.15 K^{39}.
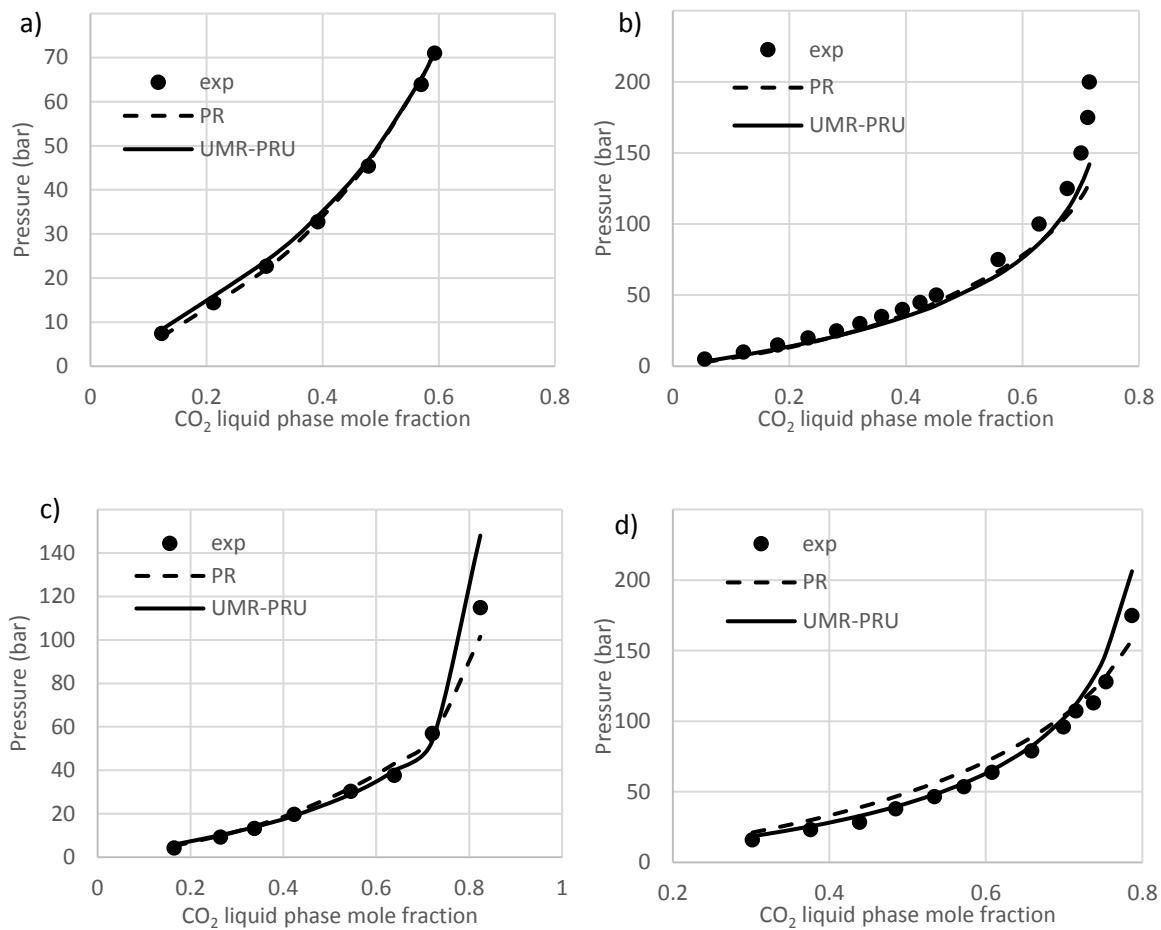
Figure 8.9: Comparison of UMR-PRU and Peng-Robinson EoS results with the experimental solubilities of CO_2 in a) [emim]Tf$_2$N at 322 K[67], b) [bmim]Tf$_2$N at 338 K[69], c) [hmim]Tf$_2$N at 303.15 K[50] and d) [omim]Tf$_2$N at 344.55 K[5].
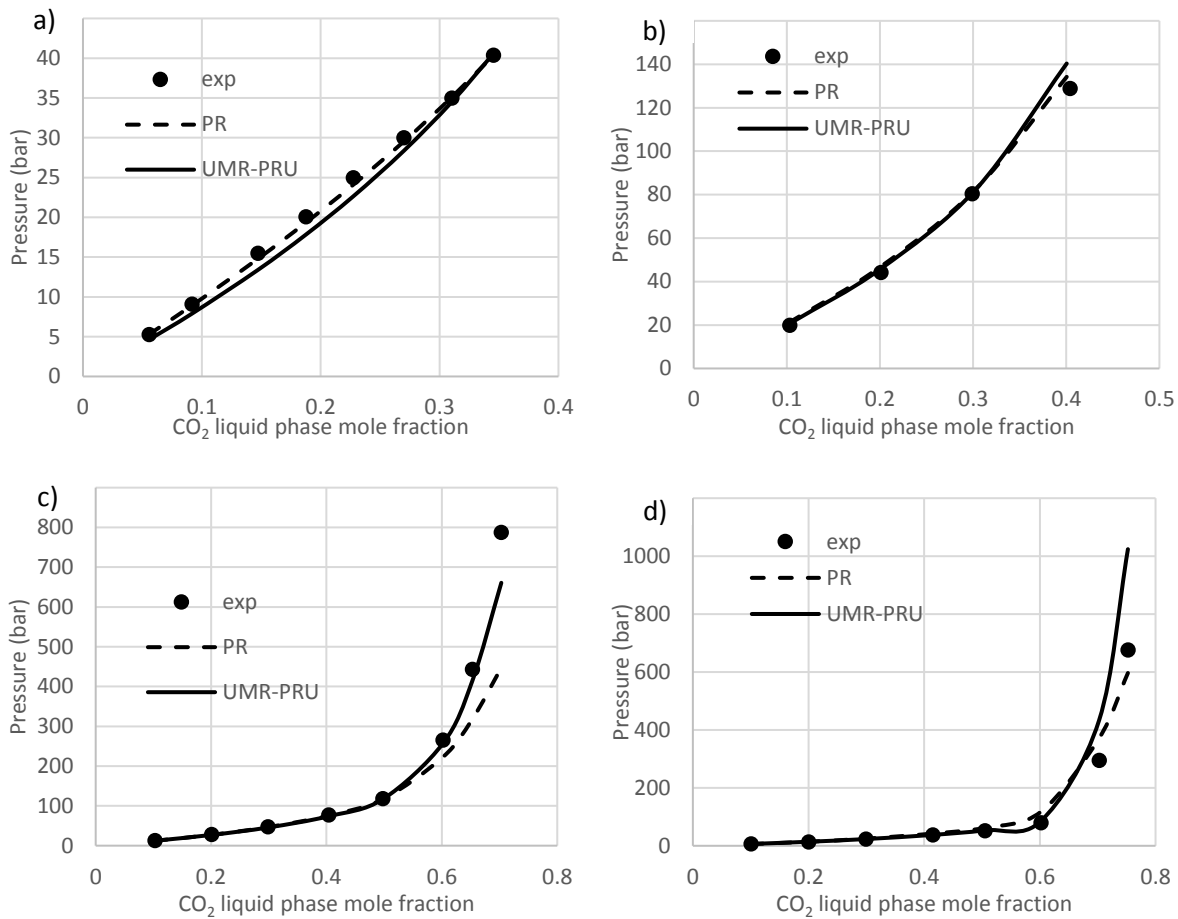
Figure 8.10: Comparison of UMR-PRU and Peng-Robinson EoS results with the experimental solubilities of CO_2 in a) [emim]BF4 at 298 K[74], b) [bmim]BF4 at 368 K[52], c) [hmim]BF4 at 348 K[77] and d) [omim]BF4 at 313 K[39].

8.4. Conclusions

In this chapter UMR-PRU is extended to CO_2-ionic liquid mixtures and it is compared to Peng-Robinson EoS. The correct description of liquid density and vapor pressure of ionic liquids is a prerequisite for the correct description of vapor-liquid equilibrium of binary mixtures. Thus, the critical properties and Mathias-Copeman or Soave parameter are fitted to vapor pressure and liquid density experimental data in a wide range of temperatures 278.15 to 460.15 K. The results obtained either by using Soave parameter or Mathias-Copeman parameters are similar to each other with a slight advantage of Mathias-Copeman parameters. UMR-PRU describes more sufficiently the vapor-liquid equilibrium of binary CO_2-ionic liquid mixtures with an average absolute relative deviation in pressure 8.4 % in 1514 number of data points, whereas the corresponding value for

Peng-Robinson EoS is 12.3 %. The performance of the two models in low and medium pressures is similar, whereas UMR-PRU describes more precisely the high pressures.

8.5. References

1.   Lei, Z.; Dai, C.; Liu, X.; Xiao, L.; Chen, B., Extension of the UNIFAC Model for Ionic Liquids. *Industrial & Engineering Chemistry Research* **2012,** *51* (37), 12135-12144.

2.   Vega, L. F.; Vilaseca, O.; Llovell, F.; Andreu, J. S., Modeling ionic liquids and the solubility of gases in them: Recent advances and perspectives. *Fluid Phase Equilibria* **2010,** *294* (1), 15-30.

3.   Shariati, A.; Peters, C. J., High-pressure phase behavior of systems with ionic liquids: measurements and modeling of the binary system fluoroform+1-ethyl-3-methylimidazolium hexafluorophosphate. *The Journal of Supercritical Fluids* **2003,** *25* (2), 109-117.

4.   Freitas, A.; Cunico, L.; Aznar, M.; Guirardello, R., Modeling vapor liquid equilibrium of ionic liquids + gas binary systems at high pressure with cubic equations of state. *Brazilian Journal of Chemical Engineering* **2012**.

5.   Shin, E.-K.; Lee, B.-C.; Lim, J. S., High-pressure solubilities of carbon dioxide in ionic liquids: 1-alkyl-3-methylimidazolium bis (trifluoromethylsulfonyl) imide. *The Journal of Supercritical Fluids* **2008,** *45* (3), 282-292.

6.   Ren, W.; Sensenich, B.; Scurto, A. M., High-pressure phase equilibria of {carbon dioxide (CO2)+n-alkyl-imidazolium bis(trifluoromethylsulfonyl)amide} ionic liquids. *The Journal of Chemical Thermodynamics* **2010,** *42* (3), 305-311.

7.   Al-fnaish, H.; Lue, L., Modelling the solubility of H2S and CO2 in ionic liquids using PC-SAFT equation of state. *Fluid Phase Equilibria* **2017,** *450*, 30-41.

8.   Domańska, U.; Marciniak, A., Phase behaviour of 1-hexyloxymethyl-3-methyl-imidazolium and 1,3-dihexyloxymethyl-imidazolium based ionic liquids with alcohols, water, ketones and hydrocarbons: The effect of cation and anion on solubility. *Fluid Phase Equilibria* **2007,** *260* (1), 9-18.

9.   Kato, R.; Gmehling, J., Systems with ionic liquids: Measurement of VLE and γ^∞ data and prediction of their thermodynamic behavior using original UNIFAC, mod. UNIFAC (Do) and COSMO-RS (Ol). *The Journal of Chemical Thermodynamics* **2005,** *37* (6), 603-619.

10.   Nebig, S.; Bölts, R.; Gmehling, J., Measurement of vapor‑liquid equilibria (VLE) and excess enthalpies (HE) of binary systems with 1-alkyl-3-methylimidazolium bis(trifluoromethylsulfonyl)imide and prediction of these properties and γ^∞ using modified UNIFAC (Dortmund). *Fluid Phase Equilibria* **2007,** *258* (2), 168-178.

11.   Alevizou, E. I.; Pappa, G. D.; Voutsas, E. C., Prediction of phase equilibrium in mixtures containing ionic liquids using UNIFAC. *Fluid Phase Equilibria* **2009,** *284* (2), 99-105.

12.   Breure, B.; Bottini, S. B.; Witkamp, G.-J.; Peters, C. J., Thermodynamic Modeling of the Phase Behavior of Binary Systems of Ionic Liquids and Carbon Dioxide with the Group Contribution Equation of State. *The Journal of Physical Chemistry B* **2007,** *111* (51), 14265-14270.

13.	Bermejo, M. D.; Martin, A.; Foco, G.; Cocero, M. J.; Bottini, S. B.; Peters, C. J., Application of a group contribution equation of state for the thermodynamic modeling of the binary systems CO2–1-butyl-3-methyl imidazolium nitrate and CO2–1-hydroxy-1-propyl-3-methyl imidazolium nitrate. *The Journal of Supercritical Fluids* **2009,** *50* (2), 112-117.

14.	Martín, Á.; Méndez, D.; Bermejo, M. D., Application of a group contribution equation of state for the thermodynamic modeling of binary systems (gas+ionic liquids) with bis[(trifluoromethyl)sulfonyl]imide anion. *The Journal of Chemical Thermodynamics* **2010,** *42* (4), 524-529.

15.	Rahmati-Rostami, M.; Behzadi, B.; Ghotbi, C., Thermodynamic modeling of hydrogen sulfide solubility in ionic liquids using modified SAFT-VR and PC-SAFT equations of state. *Fluid Phase Equilibria* **2011,** *309* (2), 179-189.

16.	Valderrama, J.; Robles, P., Critical properties, normal boiling temperatures, and acentric factors of fifty ionic liquids. *Industrial & Engineering Chemistry Research* **2007,** *46* (4), 1338-1344.

17.	Singh, G.; Kumar, A., Ionic liquids: Physico-chemical, solvent properties and their applications in chemical processes. **2008**.

18.	Gomes de Azevedo, R.; Esperança, J. M.; Najdanovic-Visak, V.; Visak, Z. P.; Guedes, H. J.; Nunes da Ponte, M.; Rebelo, L. P., Thermophysical and thermodynamic properties of 1-butyl-3-methylimidazolium tetrafluoroborate and 1-butyl-3-methylimidazolium hexafluorophosphate over an extended pressure range. *Journal of Chemical & Engineering Data* **2005,** *50* (3), 997-1008.

19.	Neves, C. M.; Kurnia, K. A.; Coutinho, J. o. A.; Marrucho, I. M.; Lopes, J. N. C.; Freire, M. G.; Rebelo, L. P. N., Systematic study of the thermophysical properties of imidazolium-based ionic liquids with cyano-functionalized anions. *The Journal of Physical Chemistry B* **2013,** *117* (35), 10271-10283.

20.	Klomfar, J.; Součková, M.; Pátek, J., Buoyancy density measurements for 1-alkyl-3-methylimidazolium based ionic liquids with tetrafluoroborate anion. *Fluid phase equilibria* **2009,** *282* (1), 31-37.

21.	Jia-zhen, Y.; Jing-Bin, L.; Jing, T.; Mei, H., Study on the density and surface tension of ionic liquid EMIBF4 in terms of standard addition method. **2007**.

22.	Zarei, H.; Keley, V., Density and speed of sound of binary mixtures of ionic liquid 1-ethyl-3-methylimidazolium tetrafluoroborate, N, N-dimethylformamide, and N, N-dimethylacetamide at temperature range of 293.15–343.15 K: measurement and PC-SAFT modeling. *Journal of Chemical & Engineering Data* **2017,** *62* (3), 913-923.

23.	Gardas, R. L.; Freire, M. G.; Carvalho, P. J.; Marrucho, I. M.; Fonseca, I. M.; Ferreira, A. G.; Coutinho, J. A., High-pressure densities and derived thermodynamic properties of imidazolium-based ionic liquids. *Journal of Chemical & Engineering Data* **2007,** *52* (1), 80-88.

24.	Součková, M.; Klomfar, J.; Pátek, J., Surface tension and 0.1 MPa density of 1-alkyl-3-methylimidazolium tetrafluoroborates in a homologous series perspective. *The Journal of Chemical Thermodynamics* **2016,** *100*, 79-88.

25.	Sanmamed, Y.; González-Salgado, D.; Troncoso, J.; Romani, L.; Baylaucq, A.; Boned, C., Experimental methodology for precise determination of density of RTILs as a

function of temperature and pressure using vibrating tube densimeters. *The Journal of Chemical Thermodynamics* **2010,** *42* (4), 553-563.

26.	Sanmamed, Y.; González-Salgado, D.; Troncoso, J.; Cerdeirina, C.; Romani, L., Viscosity-induced errors in the density determination of room temperature ionic liquids using vibrating tube densitometry. *Fluid phase equilibria* **2007,** *252* (1-2), 96-102.

27.	Klomfar, J.; Součková, M.; Pátek, J., Temperature dependence measurements of the density at 0.1 MPa for 1-alkyl-3-methylimidazolium-based ionic liquids with the trifluoromethanesulfonate and tetrafluoroborate anion. *Journal of Chemical & Engineering Data* **2010,** *55* (9), 4054-4057.

28.	Navia, P.; Troncoso, J.; Romaní, L., Excess magnitudes for ionic liquid binary mixtures with a common ion. *Journal of Chemical & Engineering Data* **2007,** *52* (4), 1369-1374.

29.	Vakili-Nezhaad, G.; Vatani, M.; Asghari, M.; Ashour, I., Effect of temperature on the physical properties of 1-butyl-3-methylimidazolium based ionic liquids with thiocyanate and tetrafluoroborate anions, and 1-hexyl-3-methylimidazolium with tetrafluoroborate and hexafluorophosphate anions. *The Journal of Chemical Thermodynamics* **2012,** *54*, 148-154.

30.	Currás, M. R.; Mato, M. M.; Sanchez, P. B.; Garcia, J., Experimental densities of 2, 2, 2-trifluoroethanol with 1-butyl-3-methylimidazolium hexafluorophosphate at high pressures and modelling with PC-SAFT. *The Journal of Chemical Thermodynamics* **2017,** *113*, 29-40.

31.	Qiao, Y.; Yan, F.; Xia, S.; Yin, S.; Ma, P., Densities and viscosities of [Bmim][PF6] and binary systems [Bmim][PF6]+ ethanol,[Bmim][PF6]+ benzene at several temperatures and pressures: determined by the falling-ball method. *Journal of chemical & engineering data* **2011,** *56* (5), 2379-2385.

32.	Salgado, J.; Regueira, T.; Lugo, L.; Vijande, J.; Fernández, J.; García, J., Density and viscosity of three (2, 2, 2-trifluoroethanol+ 1-butyl-3-methylimidazolium) ionic liquid binary systems. *The Journal of Chemical Thermodynamics* **2014,** *70*, 101-110.

33.	Almeida, H. F.; Canongia Lopes, J. N.; Rebelo, L. P.; Coutinho, J. o. A.; Freire, M. G.; Marrucho, I. M., Densities and viscosities of mixtures of two ionic liquids containing a common cation. *Journal of Chemical & Engineering Data* **2016,** *61* (8), 2828-2843.

34.	Rocha, M. A.; Ribeiro, F. M.; Ferreira, A. I. L.; Coutinho, J. A.; Santos, L. M., Thermophysical properties of [CN− 1C1im][PF6] ionic liquids. *Journal of Molecular Liquids* **2013,** *188*, 196-202.

35.	Nieto de Castro, C. A.; Langa, E.; Morais, A. L.; Lopes, M. L. M.; Lourenço, M. J. V.; Santos, F. J. V.; Santos, M. S. C. S.; Lopes, J. N. C.; Veiga, H. I. M.; Macatrão, M.; Esperança, J. M. S. S.; Marques, C. S.; Rebelo, L. P. N.; Afonso, C. A. M., Studies on the density, heat capacity, surface tension and infinite dilution diffusion with the ionic liquids [C4mim][NTf2], [C4mim][dca], [C2mim][EtOSO3] and [Aliquat][dca]. *Fluid Phase Equilibria* **2010,** *294* (1), 157-179.

36.	Hamidova, R.; Kul, I.; Safarov, J.; Shahverdiyev, A.; Hassel, E., Thermophysical properties of 1-butyl-3-methylimidazolium bis (trifluoromethylsulfonyl) imide at high temperatures and pressures. *Brazilian Journal of Chemical Engineering* **2015,** *32* (1), 303-316.

37.   Zaitsau, D. H.; Yermalayeu, A. V.; Emel'yanenko, V. N.; Butler, S.; Schubert, T.; Verevkin, S. P., Thermodynamics of Imidazolium-Based Ionic Liquids Containing PF6 Anions. *The Journal of Physical Chemistry B* **2016,** *120* (32), 7949-7957.

38.   Rocha, M. A. A.; Lima, C. F. R. A. C.; Gomes, L. R.; Schröder, B.; Coutinho, J. A. P.; Marrucho, I. M.; Esperança, J. M. S. S.; Rebelo, L. P. N.; Shimizu, K.; Lopes, J. N. C.; Santos, L. M. N. B. F., High-Accuracy Vapor Pressure Data of the Extended [CnC1im][Ntf2] Ionic Liquid Series: Trend Changes and Structural Shifts. *The Journal of Physical Chemistry B* **2011,** *115* (37), 10919-10926.

39.   Blanchard, L. A.; Gu, Z.; Brennecke, J. F., High-pressure phase behavior of ionic liquid/CO2 systems. *The Journal of Physical Chemistry B* **2001,** *105* (12), 2437-2444.

40.   Zhang, S.; Yuan, X.; Chen, Y.; Zhang, X., Solubilities of CO_2 in 1-butyl-3-methylimidazolium hexafluorophosphate and 1, 1, 3, 3-tetramethylguanidium lactate at elevated pressures. *Journal of Chemical & Engineering Data* **2005,** *50* (5), 1582-1585.

41.   Liu, Z.; Wu, W.; Han, B.; Dong, Z.; Zhao, G.; Wang, J.; Jiang, T.; Yang, G., Study on the phase behaviors, viscosities, and thermodynamic properties of CO2/[C4mim][PF6]/methanol system at elevated pressures. *Chemistry–A European Journal* **2003,** *9* (16), 3897-3903.

42.   Shariati, A.; Gutkowski, K.; Peters, C. J., Comparison of the phase behavior of some selected binary systems with ionic liquids. *AIChE Journal* **2005,** *51* (5), 1532-1540.

43.   Perez-Salado Kamps, A.; Tuma, D.; Xia, J.; Maurer, G., Solubility of CO_2 in the ionic liquid [bmim][PF6]. *Journal of Chemical & Engineering Data* **2003,** *48* (3), 746-749.

44.   Kumełan, J.; Pérez-Salado Kamps, Á.; Tuma, D.; Maurer, G., Solubility of CO_2 in the ionic liquids [bmim][CH3SO4] and [bmim][PF6]. *Journal of Chemical & Engineering Data* **2006,** *51* (5), 1802-1807.

45.   Aki, S. N.; Mellein, B. R.; Saurer, E. M.; Brennecke, J. F., High-pressure phase behavior of carbon dioxide with imidazolium-based ionic liquids. *The Journal of Physical Chemistry B* **2004,** *108* (52), 20355-20365.

46.   Muldoon, M. J.; Aki, S. N.; Anderson, J. L.; Dixon, J. K.; Brennecke, J. F., Improving carbon dioxide solubility in ionic liquids. *The Journal of Physical Chemistry B* **2007,** *111* (30), 9001-9009.

47.   Lei, Z.; Dai, C.; Chen, B., Gas Solubility in Ionic Liquids. *Chemical Reviews* **2014,** *114* (2), 1289-1326.

48.   Carvalho, P. J.; Álvarez, V. H.; Machado, J. J.; Pauly, J.; Daridon, J.-L.; Marrucho, I. M.; Aznar, M.; Coutinho, J. A., High pressure phase behavior of carbon dioxide in 1-alkyl-3-methylimidazolium bis (trifluoromethylsulfonyl) imide ionic liquids. *The Journal of Supercritical Fluids* **2009,** *48* (2), 99-107.

49.   Oh, D.-J.; Lee, B.-C., High-pressure phase behavior of carbon dioxide in ionic liquid 1-butyl-3-methylimidazolium bis (trifluoromethylsulfonyl) imide. *Korean Journal of Chemical Engineering* **2006,** *23* (5), 800-805.

50.   Yim, J.-H.; Lim, J. S., CO2 solubility measurement in 1-hexyl-3-methylimidazolium ([HMIM]) cation based ionic liquids. *Fluid Phase Equilibria* **2013,** *352*, 67-74.

51.   Anthony, J. L.; Anderson, J. L.; Maginn, E. J.; Brennecke, J. F., Anion effects on gas solubility in ionic liquids. *The Journal of Physical Chemistry B* **2005,** *109* (13), 6366-6374.

52.   Kroon, M. C.; Shariati, A.; Costantini, M.; van Spronsen, J.; Witkamp, G.-J.; Sheldon, R. A.; Peters, C. J., High-pressure phase behavior of systems with ionic liquids: Part V. The binary system carbon dioxide+ 1-butyl-3-methylimidazolium tetrafluoroborate. *Journal of Chemical & Engineering Data* **2005,** *50* (1), 173-176.

53.   Shiflett, M. B.; Yokozeki, A., Solubilities and diffusivities of carbon dioxide in ionic liquids:[bmim][PF6] and [bmim][BF4]. *Industrial & Engineering Chemistry Research* **2005,** *44* (12), 4453-4464.

54.   Vrachnos, A.; Kontogeorgis, G.; Voutsas, E., Thermodynamic modeling of acidic gas solubility in aqueous solutions of MEA, MDEA and MEA– MDEA blends. *Industrial & engineering chemistry research* **2006,** *45* (14), 5148-5154.

55.   Valderrama, J. O.; Robles, P. A., Critical Properties, Normal Boiling Temperatures, and Acentric Factors of Fifty Ionic Liquids. *Industrial & Engineering Chemistry Research* **2007,** *46* (4), 1338-1344.

56.   Shariati, A.; Ashrafmansouri, S.-S.; Osbuei, M. H.; Hooshdaran, B., Critical properties and acentric factors of ionic liquids. *Korean Journal of Chemical Engineering* **2013,** *30* (1), 187-193.

57.   Krannich, M.; Heym, F.; Jess, A., Characterization of Six Hygroscopic Ionic Liquids with Regard to Their Suitability for Gas Dehydration: Density, Viscosity, Thermal and Oxidative Stability, Vapor Pressure, Diffusion Coefficient, and Activity Coefficient of Water. *Journal of Chemical & Engineering Data* **2016,** *61* (3), 1162-1176.

58.   Zaitsau, D. H.; Kabo, G. J.; Strechan, A. A.; Paulechka, Y. U.; Tschersich, A.; Verevkin, S. P.; Heintz, A., Experimental Vapor Pressures of 1-Alkyl-3-methylimidazolium Bis(trifluoromethylsulfonyl)imides and a Correlation Scheme for Estimation of Vaporization Enthalpies of Ionic Liquids. *The Journal of Physical Chemistry A* **2006,** *110* (22), 7303-7306.

59.   Lei, Z.; Dai, C.; Wang, W.; Chen, B., UNIFAC model for ionic liquid-CO2 systems. *AIChE Journal* **2014,** *60* (2), 716-729.

60.   Louli, V.; Pappa, G.; Boukouvalas, C.; Skouras, S.; Solbraa, E.; Christensen, K. O.; Voutsas, E., Measurement and prediction of dew point curves of natural gas mixtures. *Fluid Phase Equilibria* **2012,** *334*, 1-9.

61.   Petropoulou, E.; Pappa, G. D.; Voutsas, E., Modelling of phase equilibrium of natural gas mixtures containing associating compounds. *Fluid Phase Equilibria* **2017,** *433*, 135-148.

62.   Shariati, A.; Peters, C., High-pressure phase behavior of systems with ionic liquids: II. The binary system carbon dioxide+ 1-ethyl-3-methylimidazolium hexafluorophosphate. *The Journal of supercritical fluids* **2004,** *29* (1-2), 43-48.

63.   Kim, J. E.; Lim, J. S.; Kang, J. W., Measurement and correlation of solubility of carbon dioxide in 1-alkyl-3-methylimidazolium hexafluorophosphate ionic liquids. *Fluid phase equilibria* **2011,** *306* (2), 251-255.

64.   Kim, Y.; Choi, W.; Jang, J.; Yoo, K.-P.; Lee, C., Solubility measurement and prediction of carbon dioxide in ionic liquids. *Fluid Phase Equilibria* **2005,** *228*, 439-445.

65.   Shariati, A.; Peters, C. J., High-pressure phase behavior of systems with ionic liquids: Part III. The binary system carbon dioxide+ 1-hexyl-3-methylimidazolium hexafluorophosphate. *The Journal of supercritical fluids* **2004,** *30* (2), 139-144.

66.   Moya, C.; Gonzalez-Miquel, M.; Rodriguez, F.; Soto, A.; Rodriguez, H.; Palomar, J., Non-ideal behavior of ionic liquid mixtures to enhance CO2 capture. *Fluid Phase Equilibria* **2017,** *450*, 175-183.

67.   Schilderman, A. M.; Raeissi, S.; Peters, C. J., Solubility of carbon dioxide in the ionic liquid 1-ethyl-3-methylimidazolium bis (trifluoromethylsulfonyl) imide. *Fluid Phase Equilibria* **2007,** *260* (1), 19-22.

68.   Jacquemin, J.; Husson, P.; Majer, V.; Gomes, M. F. C., Influence of the cation on the solubility of CO 2 and H 2 in ionic liquids based on the bis (trifluoromethylsulfonyl) imide anion. *Journal of solution chemistry* **2007,** *36* (8), 967-979.

69.   Karadas, F.; Köz, B.; Jacquemin, J.; Deniz, E.; Rooney, D.; Thompson, J.; Yavuz, C. T.; Khraisheh, M.; Aparicio, S.; Atihan, M., High pressure CO2 absorption studies on imidazolium-based ionic liquids: Experimental and simulation approaches. *Fluid Phase Equilibria* **2013,** *351*, 74-86.

70.   Lee, B.-C.; Outcalt, S. L., Solubilities of Gases in the Ionic Liquid 1-n-Butyl-3-methylimidazolium Bis(trifluoromethylsulfonyl)imide. *Journal of Chemical & Engineering Data* **2006,** *51* (3), 892-897.

71.   Shiflett, M. B.; Yokozeki, A., Solubility of CO2 in room temperature ionic liquid [hmim][Tf2N]. *The Journal of Physical Chemistry B* **2007,** *111* (8), 2070-2074.

72.   Kumełan, J.; Kamps, A. P.-S.; Tuma, D.; Maurer, G., Solubility of CO2 in the ionic liquid [hmim][Tf2N]. *The Journal of Chemical Thermodynamics* **2006,** *38* (11), 1396-1401.

73.   Jalili, A. H.; Safavi, M.; Ghotbi, C.; Mehdizadeh, A.; Hosseini-Jenab, M.; Taghikhani, V., Solubility of CO2, H2S, and their mixture in the ionic liquid 1-octyl-3-methylimidazolium bis (trifluoromethyl) sulfonylimide. *The Journal of Physical Chemistry B* **2012,** *116* (9), 2758-2774.

74.   Lei, Z.; Yuan, J.; Zhu, J., Solubility of CO2 in propanone, 1-ethyl-3-methylimidazolium tetrafluoroborate, and their mixtures. *Journal of Chemical & Engineering Data* **2010,** *55* (10), 4190-4194.

75.   Lei, Z.; Han, J.; Zhang, B.; Li, Q.; Zhu, J.; Chen, B., Solubility of CO2 in binary mixtures of room-temperature ionic liquids at high pressures. *Journal of Chemical & Engineering Data* **2012,** *57* (8), 2153-2159.

76.   Watanabe, M.; Kodama, D.; Makino, T.; Kanakubo, M., CO2 absorption properties of imidazolium based ionic liquids using a magnetic suspension balance. *Fluid Phase Equilibria* **2016,** *420*, 44-49.

77.   Costantini, M.; Toussaint, V. A.; Shariati, A.; Peters, C. J.; Kikic, I., High-pressure phase behavior of systems with ionic liquids: Part IV. Binary system carbon dioxide+ 1-hexyl-3-methylimidazolium tetrafluoroborate. *Journal of Chemical & Engineering Data* **2005,** *50* (1), 52-55.

78.   Hizaddin, H. F.; Hadj-Kali, M. K.; AlNashef, I. M.; Mjalli, F. S.; Hashim, M. A., Prediction of CO2 solubility in ionic liquids using the PSRK model. *The Journal of Supercritical Fluids* **2015,** *100*, 184-193.

79.   Shiflett, M. B.; Yokozeki, A., Solubilities and Diffusivities of Carbon Dioxide in Ionic Liquids: [bmim][PF6] and [bmim][BF4]. *Industrial & Engineering Chemistry Research* **2005,** *44* (12), 4453-4464.

80.	Kheiri, A.; Afsharpour, A., The CPA EoS application to model CO2 and H2S simultaneous solubility in ionic liquid [C2mim][PF6]. *Petroleum Science and Technology* **2018,** *36* (13), 944-950.

9. Process simulations

In this chapter, eUMR-PRU model is incorporated in a commercial process simulator and it is tested in physical, chemical and simultaneous physical and chemical equilibrium calculations. Furthermore, acid gas model of HYSYS V8.6 is used for simulation of CO_2 absorption in an aqueous monoethanolamine solution, whereas UMR-PRU model is used for simulation of CO_2 absorption in refrigerated methanol and in hmim[Tf_2N] ionic liquid as solvent and it is compared with Peng-Robinson EoS. Finally, the three processes are compared to each other and suggestions are made, in order to have an effective process with low energy requirements.

9.1.   Introduction

As it has been stated in Chapter 2, acid gases, existing in flue gases and natural gas, can cause significant problems both in equipment and the environment. Therefore, they should be removed from flue gases especially for environmental and health reasons, whereas it is important to be removed from natural gas, because they reduce its heating value and can cause corrosion to the equipment.

In Chapter 3, different processes, which can be employed for CO_2 removal, are described. The post-combustion capture processes from flue gases are the same with those used for CO_2 removal from natural gas. Chemical absorption in aqueous alkanolamine is the dominant process nowadays. However, it has significant drawbacks, such as the volatility of some alkanolamines, a fact which results to solvent losses, and the high energy requirements in solvent regeneration. Physical absorption in methanol, known as Rectisol process, can be an alternative solution, due to its low corrosive nature and non-foaming operation (Chapter 3). However, its high energy requirements and high volatility are significant drawbacks, which justify the focus on ionic liquids as alternative solvents, on the condition that their high viscosity is overcome.

In literature, many simulation studies about CO_2 chemical absorption in aqueous alkanolamine solutions, have been found. Aqueous monoethanolamine as solvent has been used in some of them[1-2], whereas amine blends are often a good alternative, in order to combine the advantages of different amines[3-4].   Methanol as a solvent has also been used a lot[5-6], whereas ionic liquids in acid gas removal is a recent field of study[7-8]. An interesting recent research, which is not commonly found in literature, has been presented by Taheri et al[9], who use methanol and ionic liquid mixtures and compare the results of CO_2 captures, solvent losses and energy requirements.

Therefore, in this chapter, a comparative study of three processes (CO_2 chemical absorption in a 30% w/w MEA solution, CO_2 physical absorption in refrigerated methanol and CO_2 physical absorption in hmim[Tf_2N]) is presented, whereas mixtures of methanol and hmim[Tf_2N] are also proposed as possible solvents, in order to combine the advantages of these solvents and reduce the viscosity of ionic liquid.

9.2. Incorporation of UMR-PRU in process simulators

Although, UMR-PRU model is not a built-in model in commercial process simulators, it can be incorporated in them via the Computer Aided Process Engineering (CAPE-OPEN) protocol. CO-Lan is the organization responsible for management CAPE-OPEN standard, which defines rules and interfaces that allow applications or components to be incorporated. Therefore, UMR-PRU by using the calculated parameters in this work, can be used for simulations. The way that a thermodynamic model can be incorporated in a process simulator is presented in Figure 9.1.
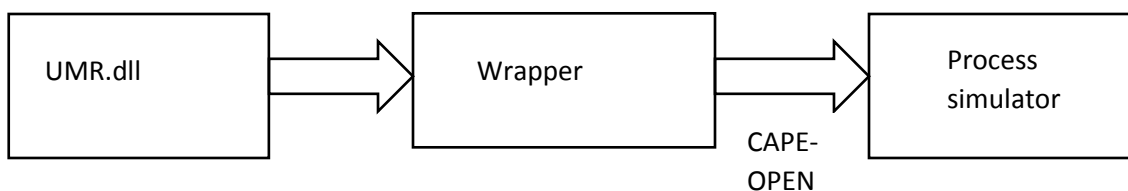
Figure 9.1: Incorporation of UMR-PRU in process simulators.

UMR.dll is a Fortran Library for thermodynamic calculations and Wrapper is a C# Library, which acts as a medium between UMR.dll and process simulator, in this case Aspen HYSYS v8.6.

eUMR-PRU (i.e. UMR-PRU with the Debye-Hückel term for electrolytes) has not been previously implemented in process simulators. Therefore, it is incorporated in this thesis by adding the Debye-Hückel term and doing other appropriate changes in the already existing UMR.dll. For the calculation of fugacity and specific properties, such as enthalpy, heat capacities etc. the first and second derivative of activity coefficient with respect to temperature and the first derivative of activity coefficient with respect to moles must be defined. The first and second derivative of the Debye-Hückel activity coefficient with respect to temperature and the first derivative of Debye-Hückel activity coefficient with respect to moles have been calculated in this thesis and they are presented in APPENDIX C.

The incorporation of eUMR-PRU in HYSYS, has been tested in phase equilibrium calculations, in chemical equilibrium calculations and in simultaneous physical and chemical calculations, a fact which implies the successive implementation of the model. Some indicative chemical equilibrium and simultaneous physical and chemical equilibrium results for H_2S-MEA-H_2O mixture are presented in Figure 9.2. Despite the successful implementation of the model, it was not possible to use it in simulations, because significant difficulties have been found in solving the simultaneous phase and chemical equilibrium in an absorption column by the simulator.
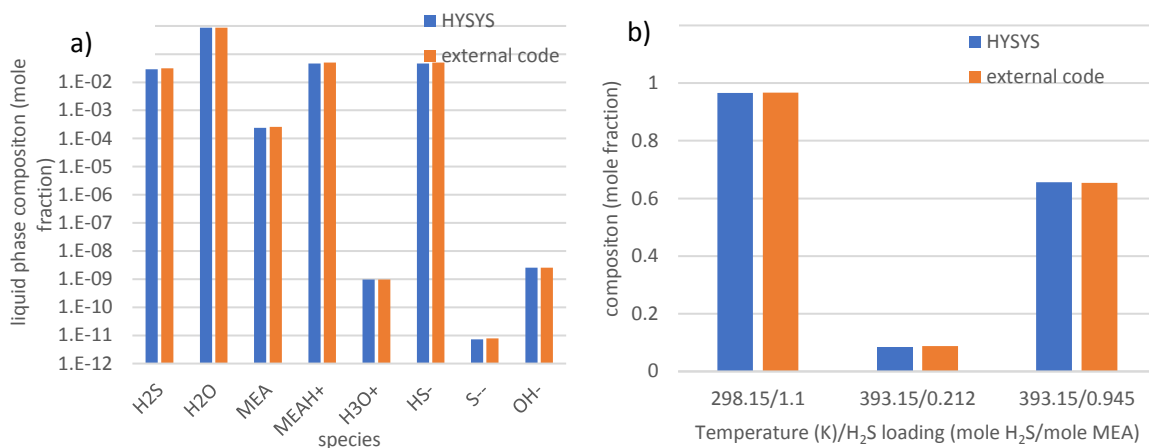
Figure 9.2: Comparison of a) chemical equilibrium (25 °C,, 15 % w/w MEA and 1.61 H₂S loading) and b) phase and chemical equilibrium (15.27 % w/w MEA) calculations by HYSYS V8.6 and external code in H₂S-MEA-H₂O mixture.

9.3. CO_2 chemical absorption from natural gas using an aqueous alkanolamine solution

In this section, the CO_2 chemical absorption process is presented. The solvent used is a 30% w/w aqueous monoethanolamine solution and the thermodynamic package used for the simulation is Acid Gas in HYSYS.

9.3.1. Base Case

The process flowchart is presented in Figure 9.3. The acid gas, after its compression enters the bottom of an absorption column, which operates at higher pressure than atmospheric, whereas the solvent, which consists of 30% w/w MEA, enters the top of the absorption column and their flows are countercurrent. Sweet natural gas leaves the top of the absorber, whereas the rich-in-CO_2 solvent leaves the bottom of the absorber.

Rich solvent must be heated, in order to enter the regeneration column. Therefore, before entering a heat exchanger, rich solvent is pressurized via a pump, in order to remain in liquid state, when exiting the heat exchanger and subsequently entering the regeneration column. The CO_2 stream leaves the top of the regeneration column, whereas lean solvent leaves the bottom of the column and its energy content is used to heat the rich solvent in the heat exchanger, mentioned before.

The natural gas, after leaving the top of the absorber, enters a scrubber, where it contacts water, in order to regenerate and reuse any solvent quantity remained. Even though, this column is not always used, it is of great importance in case of MEA, because of its

volatility. Purified gas leaves the top of this column, whereas a make-up stream, rich in water leaves the bottom of the column and it is mixed with the lean solvent from the regeneration column. The produced by the mixer stream enters a heater and it is recycled back to the absorber.
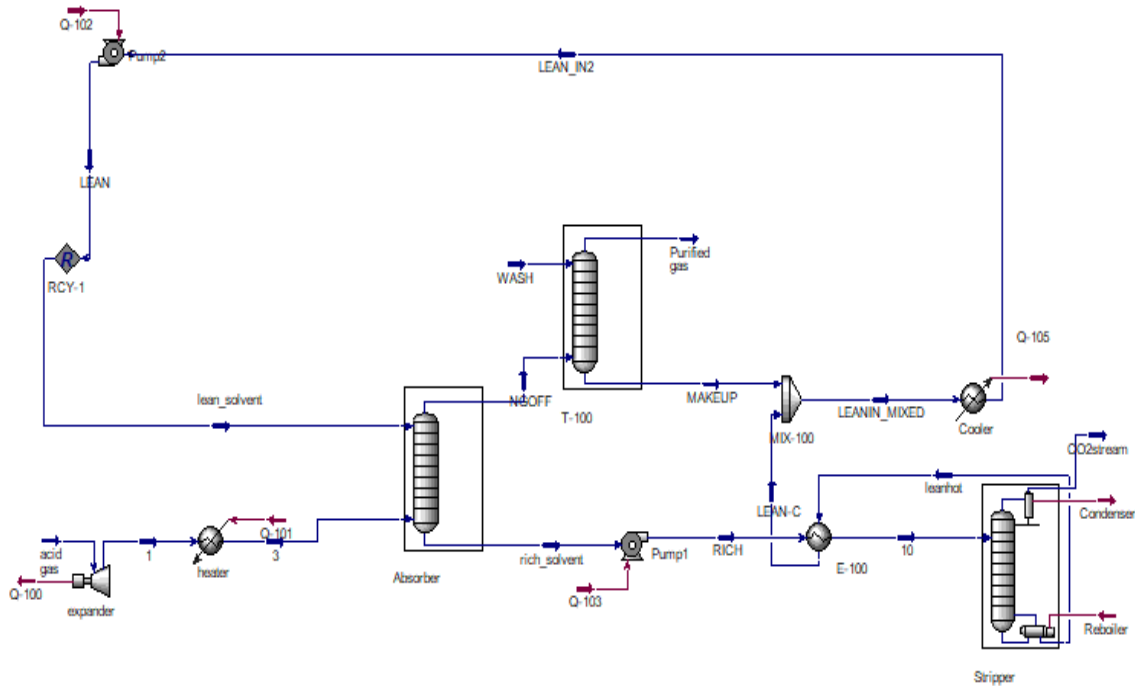
Figure 9.3: Flowchart for CO₂ absorption in aqueous monoethanolamine solution

The operating conditions of the process and the composition of the solvent and acid gas are presented in Tables 9.1-9.2.

Table 9.1: Operating conditions of the process

	Absorber	Stripper	Scrubber
Number of stages	6	6	2
Pressure (bar)	4	1.723	1

Table 9.2: Streams of the absorption column

	Lean_solvent	Acid gas	3	NG-OFF	Rich_solvent
Mass Flow (kg/hr)	474973.46	99786.26	99786.26	72779.35	501980.37
Pressure (bar)	4	30	4	4	4
Temperature (°C)	46.15	40.00	37.78	46.37	75.91
Composition (mass fraction)					
MEA	2.90E-01	0	0	7.91E-05	2.75E-01
H_2O	6.78E-01	0.00E+00	0.00E+00	2.60E-02	6.38E-01
CO_2	3.14E-02	2.90E-01	2.90E-01	8.63E-05	8.72E-02
N_2	2.27E-09	2.84E-02	2.84E-02	3.89E-02	7.40E-07
CH_4	1.15E-07	6.82E-01	6.82E-01	9.35E-01	3.15E-05

The solvent is an aqueous solution of 30 % w/w MEA with acid gas loading equal to 0.15. The acid gas loading of the solvent is usually preferred to be 0.1-0.3. In Table 9.3 the streams of the scrubber are presented.

Table 9.3: Streams of the scrubber

	Wash	Purified gas	Make up
Mass Flow (kg/hr)	3904.00	73908.30	2775.05
Pressure (bar)	1	1	1
Temperature (°C)	25.00	27.55	27.62
Composition (mass fraction)			
MEA	0	5.95E-23	2.08E-03
H_2O	1	4.10E-02	9.98E-01
CO_2	0	8.41E-05	2.45E-05
N_2	0	3.83E-02	2.45E-05
CH_4	0	9.21E-01	1.96E-05

The wash flow is selected to be 3904 kg/hr, in order to be able to remove the whole amount of MEA, which is contained in NG-OFF stream and in order to replace the water loss. The streams of the stripper column are presented in Table 9.4.

	10	leanhot	CO$_2$ stream
Mass Flow (kg/hr)	501980.37	472197.71	29782.66
Pressure (bar)	8.5	1.723	1.723
Temperature (ºC)	107.00	118.22	48.91
Composition (mass fraction)			
MEA	2.75E-01	2.92E-01	3.28E-12
H$_2$O	6.38E-01	6.76E-01	2.95E-02
CO$_2$	8.72E-02	3.16E-02	9.70E-01
N$_2$	7.40E-07	6.89E-31	1.25E-05
CH$_4$	3.15E-05	1.09E-27	5.31E-04

The purity of CO_2 in CO_2 stream is 97 % in mass fraction and the CO_2 recovery (mass of CO_2 in CO_2 stream/mass of CO_2 in acid gas stream) is 99.8%.

The energy requirements of the process per kg of recovered CO_2 is presented in Table 9.5.

Table 9.5: Energy requirements of the process

Equipment	Energy/mass of recovered CO$_2$ (kJ/kg)
Expander	507.87
Pump1	9.72
Pump2	6.35
Cooler	2533.97
Heater	576.44
Condenser	3000.84
Reboiler	5813.11

9.3.2. Sensitivity analysis

A sensitivity analysis is performed, in order to detect the most important parameters for the energy requirements of the process.

The variables, that are considered to be of great importance to the total energy requirements of the process, are: the energy requirements of the reboiler and condenser of the stripper and the ones of the Cooler, which ensures the desired temperature of the solvent in the absorber column.

Three parameters remain constant in each step of sensitivity analysis: the CO_2 mass fraction of the CO_2 stream (97 %), the CO_2 recovery of the whole process, which is 99.8 % and the MEA concentration in solvent, which is 30 % w/w.

9.3.2.1.   Number of stages of the absorption column

Changes in the stages of the absorption column results to changes in CO_2 recovery. In order the same CO_2 recovery to be remained, changes in solvent mass flow are necessary, as it is depicted in Figure 9.4a.
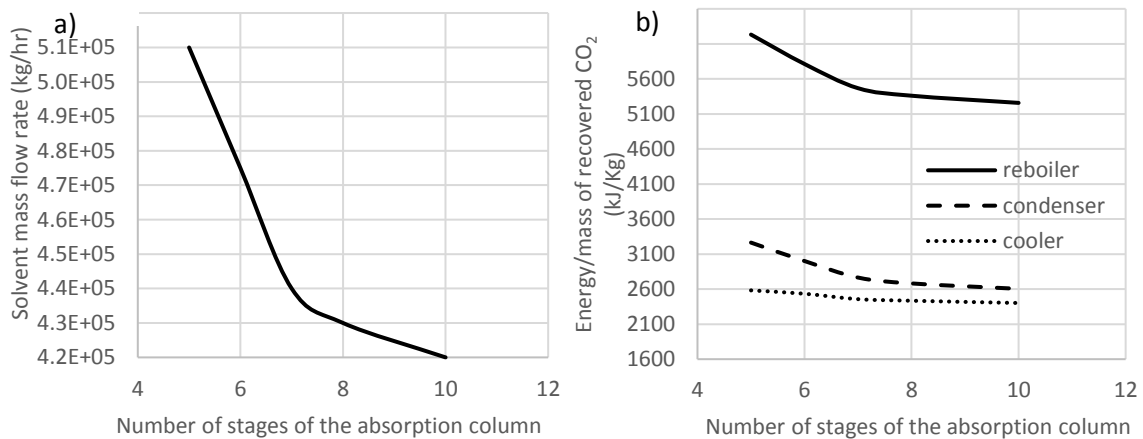
Figure 9.4: Effect of number of stages of the absorption column on solvent mass flow and energy requirements

An increase in the number of stages of the absorber results to lower solvent mass flow rate in order to obtain the same CO_2 recovery. However, for more than 7 stages, the effect of stages number on the solvent mass flow is not so pronounced.

The lower solvent mass flow results to a decrease in energy requirements, as it is depicted in Figure 9.4b.

9.3.2.2.   Solvent mass flow

The solvent mass flow affects the CO_2 recovery as it is well depicted in Figure 9.5a.

As it is expected, an increase in the solvent flow rate, results to an increase in CO_2 recovery, whereas as CO_2 recovery becomes higher than 98%, great changes in solvent mass flow are required in order to obtain a further increase of the CO_2 recovery.
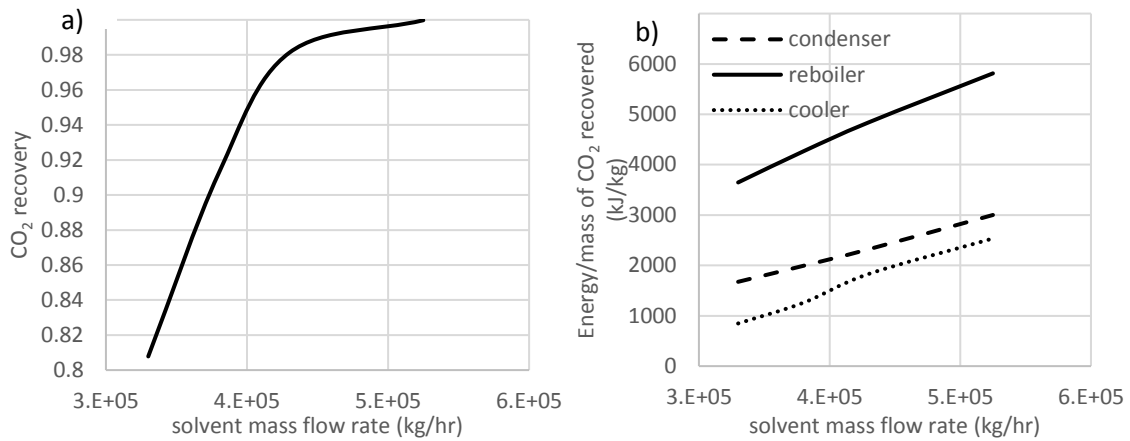
Figure 9.5: Effect of solvent mass flow on CO_2 recovery and energy requirements

The higher solvent flow rate results to higher energy requirements per kg of recovered CO_2, as it is shown in Figure 9.5b.

9.3.2.3.   Number of stages of stripping column

The increase in the number of stages of the stripping column results to a lower reflux ratio and energy requirements of the condenser and reboiler, in order to achieve the same recovery and purity, as shown in Figure 9.6.
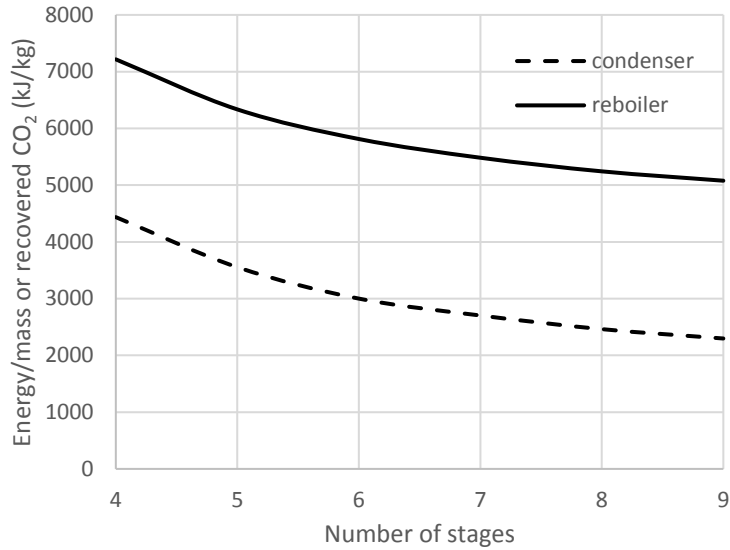
Figure 9.6: Effect of number of stages on reboiler and condenser energy requirements.

9.3.2.4. Pressure of the absorption column

An increase in pressure of the absorption column results to higher CO_2 absorption. Thus, lower solvent mass flow rate is needed in order the same CO_2 recovery and purity to be achieved. The lower solvent mass flow rate results to lower energy requirements per kg of recovered CO_2 in the whole process. The energy requirements of cooler, condenser and reboiler are depicted in Figure 9.7.
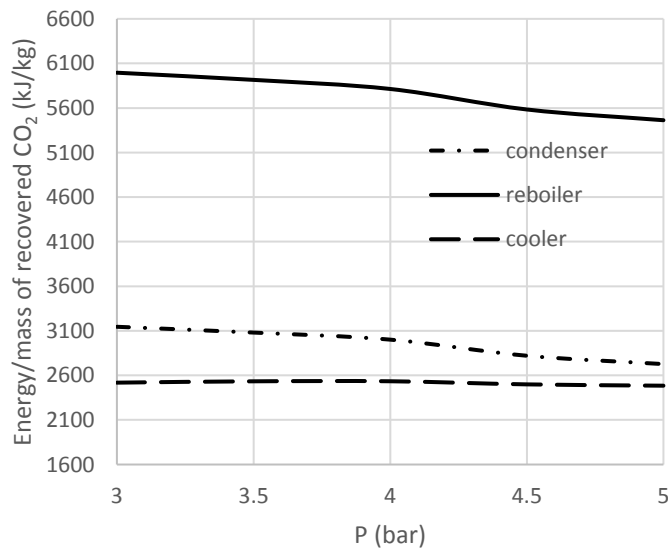
Figure 9.7: Effect of the pressure of the absorber on the energy requirements of condenser, reboiler and cooler.

9.3.2.5.   Pressure of the distillation column

Increasing the pressure of the distillation column results to higher temperatures of reboiler and condenser, a fact which results to the shift of equilibrium of reactions to the left and facilitates the CO_2 recovery. Therefore, a decreased reflux ratio and lower energy requirements of the reboiler and the condenser are required, in order to have the same CO_2 purity and recovery, as it is presented in Figure 9.8.
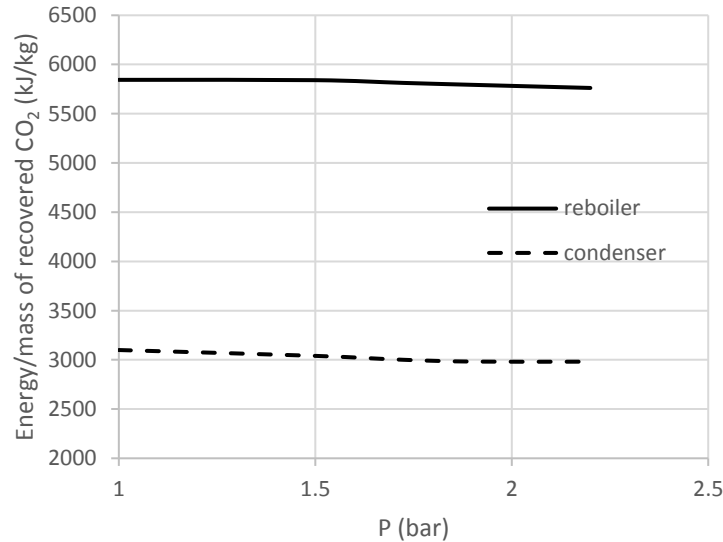
Figure 9.8: Effect of pressure of distillation column on reboiler and condenser energy requirements.

As the pressure of the column increases the temperature of the reboiler increases and hence the energy requirements of the cooler increase. However, the reduction of reboiler energy requirements results to total reduction of the energy requirements of this process. The increase in temperature in the regeneration column results to higher CO_2 solubility in vapor phase, a fact which renders the CO_2 recovery easier. The further increase in the pressure of regeneration column is not recommended, due to the increase in the reboiler temperature, a fact that provokes the degradation of MEA, if the temperature rises up to 130 °C.

9.3.2.6.   Reflux ratio

An increase in reflux ratio results to an increase in CO_2 recovery and as it is expected, the higher the reflux ratio, the higher the energy of the condenser and the reboiler.
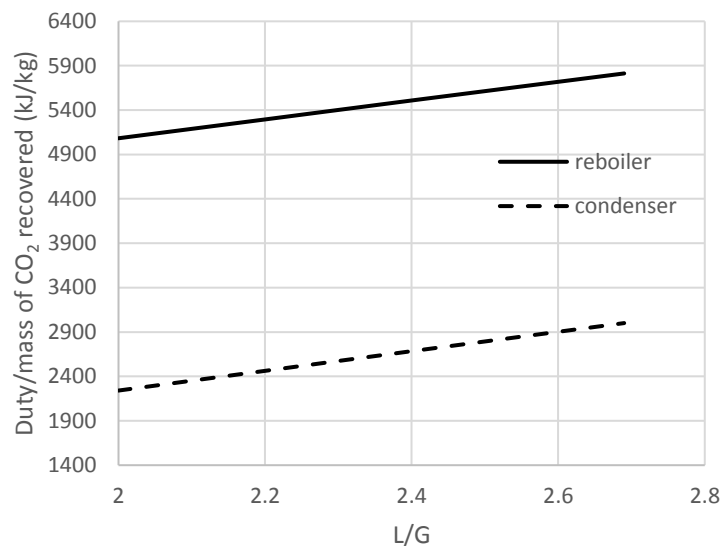
Figure 9.9: Effect of reflux ratio on reboiler and condenser energy requirements.

9.4.   Physical absorption process

In this section CO_2 physical absorption process is examined. Two solvent have been studied: methanol and hmim[Tf_2N] ionic liquid by using two thermodynamic models: UMR-PRU and Peng-Robinson. Firstly, the parameters of the two models are presented and secondly some indicative VLE results of the two models are compared to each other.

9.4.1.   Parameters for UMR-PRU and Peng-Robinson EoS

In this section the parameters used for UMR-PRU and Peng-Robinson EoS are presented. The critical properties and Mathias-Copeman parameters used are the ones presented in Table A.5 of Appendix A for UMR-PRU, whereas for Peng-Robinson, the critical properties and Soave parameter used are those of UNISIM R451. An exception is hmim[Tf_2N], because it is introduced as a pseudocomponent in UNISIM and hence the critical properties and Soave parameter used for PR EoS are those presented in Table 8.1 of Chapter 8 .Concerning UMR-PRU model, the whole hmim[Tf_2N] molecule is assumed as a UNIFAC group for convenience in calculation of the missing binary interaction parameters (N_2-hmim[Tf_2N], CH_4-hmim[Tf_2N], CH_3OH-hmim[Tf_2N]). Therefore, van der Waals Volume and Area parameters of hmim[Tf_2N] are estimated as a summation of the parameters of the groups considered in Chapter 8 (1 CH_3, 5 CH_2 and 1 mim[Tf_2N]), while the rest are taken from Petropoulou et al[10]. The binary interaction parameters between N_2, CH_4, CO_2 and CH_3OH are from literature[10], whereas those between these components and hmim[Tf_2N] are calculated in this work by fitting to experimental vapor-liquid equilibrium

data taken from literature[11-16]. Van der Waals Volume and Area parameters are presented in Table A.7 of Appendix A, whereas binary interaction parameters are presented in Table A.8 of Appendix A.

Peng-Robinson interaction parameters as a function of temperature and carbon number could not be used in UNISIM. Therefore, the default values for k_{ij} interaction parameters between N_2, CH_4, CO_2 and CH_3OH have been used, whereas the rest have been estimated in this thesis by fitting to experimental data[11-16] and they are presented in Table 9.6.

Table 9.6: Binary interaction parameters of PR EoS estimated in this work (used for simulation purposes).

i	j	k_{ij}
CO_2	hmim[Tf_2N]	-0.097
CH_4	hmim[Tf_2N]	-0.1017
CH_3OH	hmim[Tf_2N]	-0.0005
N_2	hmim[Tf_2N]	0.8942

9.4.2. Comparison of UMR-PRU and Peng-Robinson VLE results

Possible difference in the results of UMR-PRU and PR EoS of CO_2 absorption in methanol and in ionic liquid processes are to some degree due to the difference in VLE results of the two models. Therefore, these results are compared in this section.

In case of methanol, at -45 °C, the VLE calculations of the two models for CO_2-MeOH mixtures are presented in Figure 9.10a. UMR-PRU predicts higher CO_2 solubility at low pressures than Peng-Robinson. However, no conclusion can be drawn for the results of the models in the process, since methanol enters the absorption column, at -50 °C, whereas the operating pressure of the column is 60 bar and there are not such available data.

Figure 9.10b presents CO_2 solubility in hmim[Tf_2N] at 20 °C, which is the temperature at which the ionic liquid enters the absorption column. In this case, also UMR-PRU predicts more accurately the experimental data and its results imply lower CO_2 solubility and thus absorption than Peng-Robinson does.

Methane solubility in the solvent is of great importance, because the greater it is, the more difficult it is to recover methane in purified gas and to have a high CO_2 purity in the recovered CO_2 stream. UMR-PRU predicts lower CH_4 solubility in ionic liquid than Peng-Robinson does a fact which can be verified by 9.10c.

In conclusion, UMR-PRU seems to be the most accurate model for process simulations.
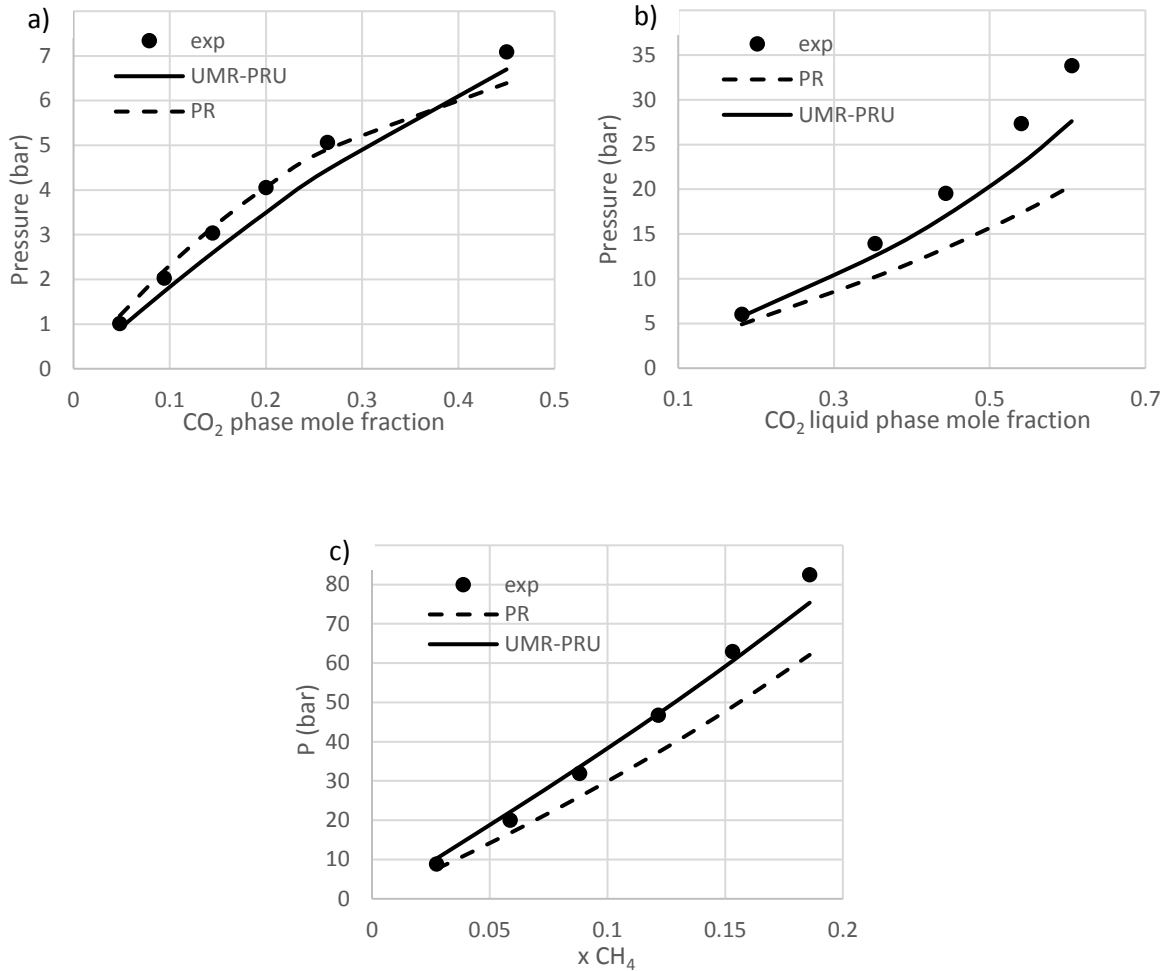
Figure 9.10: UMR-PRU and Peng-Robinson EoS calculations for a) the solubility of carbon dioxide in methanol at -45 °C, b) the solubility of carbon dioxide in hmim[Tf₂N] at 20 °C and c) the solubility of methane in hmim[Tf₂N] at 20 °C.

9.4.3. CO$_2$ absorption from natural gas using refrigerated methanol

Even though acid gas chemical absorption process in aqueous alkanolamines dominates the market, it is not definite that this is the most efficient and energy-effective process. According to an economic analysis of physical, chemical and hybrid absorption processes for CO$_2$ capture from flue gases at low pressure, presented by Zhang et al[17], at CO$_2$ mole fraction in feed greater than 33%, physical absorption has the lowest cost, whereas in lower CO$_2$ mole fractions chemical absorption is the most cost-effective process. The capital costs of both processes are similar to each other, whereas the lowest capital cost is the one of chemical absorption at low CO$_2$ mole fractions in feed and the one of physical

absorption is the lowest at higher CO_2 mole fractions in feed. At high pressure in acid gas stream, hybrid physical and chemical process is economically preferred.

In this process, CO_2 mole fraction in feed is lower than 33 % and the pressure is high. According to Zhang et al[17] the selection of the suitable process is case dependent, and thus in this thesis physical absorption process is studied as well.

In this section CO_2 physical absorption process is presented. The solvent used is refrigerated methanol and the process is a variation of the well-known Rectisol. The results of UMR-PRU and Peng-Robinson EoS are presented.

9.4.3.1. Prediction of heat capacities

The accurate description of heat capacities by a thermodynamic model is essential for reliable energy requirements calculations. UMR-PRU predicts sufficiently the heat capacities of pure methanol. However, in order to obtain even more accurate predictions, Mathias-Copeman parameters of pure methanol are fitted both in heat capacity data and in vapor pressure data. The results on vapor pressures are almost the same as the ones calculated by using the previous parameters. Small changes are found on heat capacities and they are presented in Figure 9.11.
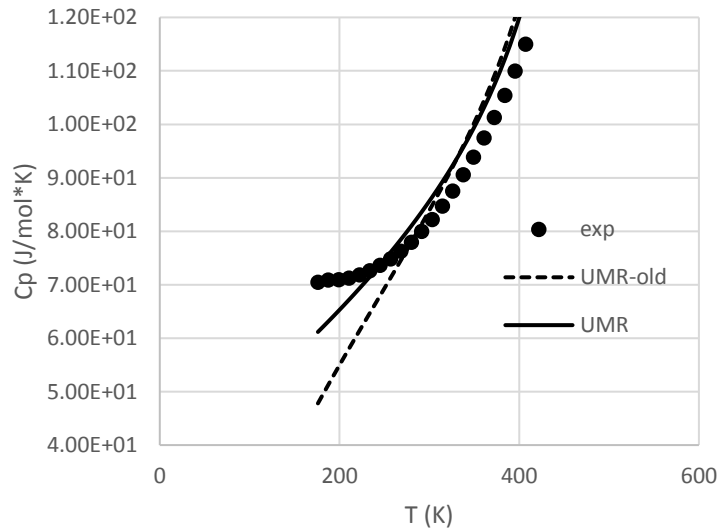
Figure 9.11: Heat capacity calculations of pure methanol by UMR-PRU model, using the fitted-to-heat-capacity-Mathias-Copeman parameters (UMR) and old Mathias-Copeman parameters (UMR-old)

The new Mathias-Copeman parameter set is: c1=1.22031, c2=-0.413779, c3=-0.084285. The new parameter set is used for UMR-PRU in Rectisol process and the results are presented in Section 9.4.3.2., whereas the results with the old parameter set (UMR-old) are presented in Appendix D. Any difference between the two models (UMR and UMR-old) is due to the changes in heat capacity predictions and not due to different VLE predictions.

As it has been expected the new Mathias-Copeman parameters, which result to higher heat capacity predictions in the temperature range of interest result to higher energy requirements. Nevertheless, the differences in energy requirements are very small (about 1.2% increase in energy requirements with new Mathias-Copeman parameters), a fact that can be explained by the small change in heat capacity predictions.

9.4.3.2. Base Case-1

In this section, the use of refrigerated methanol as solvent for CO_2 absorption is examined. A typical flowchart of this process has been presented in Chapter 3. The process flowchart used for the simulation is presented in Figure 9.12.
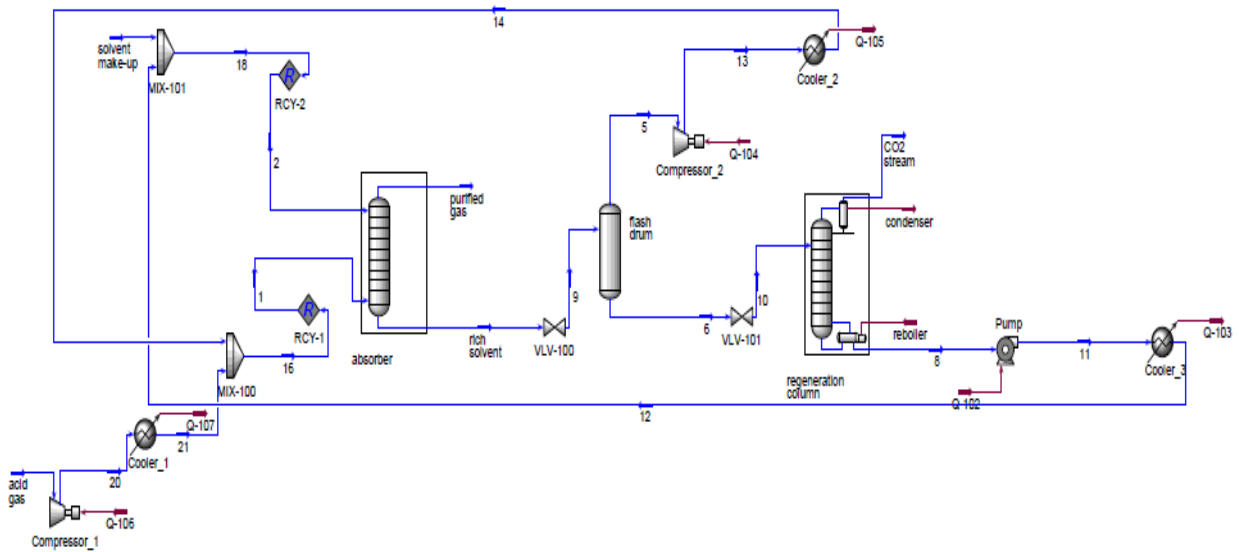
Figure 9.12: Flowchart for CO_2 absorption in refrigerated methanol

The acid gas enters the process at 20 °C, whereas methanol is at -50 °C. Both of them enter the absorption column, whereas purified gas leaves the top of this column and rich-in-CO_2 methanol leaves the bottom of the column. The rich solvent, after its pressure reduction, enters a flash drum, in order any other dissolved gases, except for CO_2, to be removed. The vapor product, which leaves the top of the flash drum is compressed and cooled and it is recycled back to the absorption column. The liquid product of the flash drum, which is the rich-in-CO_2-solvent enters the regeneration column (distillation column), which operates at 1 bar, in order CO_2 to be recovered as the vapor product and methanol to be regenerated as the liquid product. Methanol enters a pump and a cooler and it is recycled back to the absorption column.

It should be noted, that solvent make-up is necessary in case of methanol, due to solvent losses during the process, because of the volatility of methanol.

In Table 9.7 the operating conditions of the absorption and the regeneration column are presented, whereas in Tables 9.8-9.10, the streams of this process are presented, as they have been calculated by UMR-PRU and Peng-Robinson EoS.

Table 9.7: Operating conditions of the process

	Absorption column	Flash	Regeneration column
Number of stages	6		6
Pressure (bar)	60	1.01325	1

The pressure of the absorber is chosen to be high enough, because of the increased solubility of CO_2 in methanol at high pressures. 60 bar for the absorber column have been suggested for Rectisol Process[18].

Table 9.8: Results of the absorption column

Model	Acid gas	1		Solvent make-up		2		Purified gas		Rich solvent	
		UMR	PR	UMR	PR	UMR	PR	UMR	PR	UMR	PR
T ºC	40	15.49	16.26	-50	-50	-50.00	-50.00	-46.32	-50.40	-0.02	-11.74
P (bar)	30	60	60	60	60	60	60	60	60	60	60
Mass flow (kg/h)	99786	392011	452251	759	773	768956	769005	70801	70782	1090166	1150473
Composition (mass fraction)											
Nitrogen	2.84E-02	7.77E-03	7.36E-03	0.00E+00	0.00E+00	7.46E-21	8.21E-24	4.00E-02	4.00E-02	2.00E-04	4.32E-04
CO_2	2.90E-01	7.54E-01	7.64E-01	0.00E+00	0.00E+00	6.34E-10	2.72E-14	6.09E-04	1.74E-04	2.71E-01	3.00E-01
Methane	6.82E-01	2.37E-01	2.28E-01	0.00E+00	0.00E+00	1.28E-15	1.36E-19	9.59E-01	9.60E-01	2.28E-02	3.04E-02
Methanol	0.00E+00	1.85E-03	7.67E-04	1.00E+00	1.00E+00	1.00E+00	1.00E+00	1.52E-04	1.88E-04	7.06E-01	6.69E-01

The methane recovery in the process is 99.8%, whereas its purity in purified gas is 96% in mass fraction. The results of both models are really close to each other.

Table 9.9: Results of the flash drum

stream	9		5		6	
Model	UMR	PR	UMR	PR	UMR	PR
T ºC	-36.02	-40.34	-36.02	-40.34	-36.02	-40.34
P (bar)	1.01325	1.01325	1.01325	1.01325	1.01325	1.01325
Mass flow (kg/h)	1090166.46	1150473.71	292224.83	352466.51	797941.63	798007.21
Composition (mass fraction)						
Nitrogen	2.00E-04	4.32E-04	7.47E-04	1.41E-03	2.42E-07	7.24E-07
CO_2	2.71E-01	3.00E-01	9.12E-01	8.99E-01	3.62E-02	3.62E-02
Methane	2.28E-02	3.04E-02	8.47E-02	9.90E-02	1.80E-04	1.66E-04
Methanol	7.06E-01	6.69E-01	2.49E-03	9.84E-04	9.64E-01	9.64E-01

The differences between the two models in flash drum are mainly due to the different temperature of the inlet stream calculated by the two models.

Table 9.10: Results of the distillation column

Model	10		CO_2 stream		8	
	UMR	PR	UMR	PR	UMR	PR
T ºC	-36.04	-40.35	-3.83	0.99	63.12	66.05
P (bar)	1	1	1	1	1	1
Mass flow (kg/h)	797941.63	798007.21	29744.70	29775.38	768196.93	768231.82
Composition (mass fraction)						
Nitrogen	2.42E-07	7.24E-07	6.49E-06	1.94E-05	7.47E-21	2.66E-19
CO_2	3.62E-02	3.62E-02	9.70E-01	9.70E-01	6.35E-10	1.48E-09

Methane	1.80E-04	1.66E-04	4.82E-03	4.44E-03	1.29E-15	4.61E-15
Methanol	9.64E-01	9.64E-01	2.52E-02	2.55E-02	1.00E+00	1.00E+00

The CO_2 recovery is greater than 99 % and the purity of CO_2 is 97 % in mass fraction.

The energy requirements of the process are presented in Table 9.11.

Table 9.11: Energy requirements of the process

Equipment	Energy/mass of recovered CO_2 (kJ/kg)	
	UMR	PR
Cooler_1	6.73E+02	6.73E+02
Cooler_2	2.72E+03	5.60E+03
Cooler_3	7.78E+03	1.08E+04
Compressor_1	4.26E+02	4.26E+02
Compressor_2	2.53E+03	5.44E+03
Condenser	5.22E+02	5.52E+02
Reboiler	7.76E+03	1.07E+04
Pump	3.27E+02	3.60E+02

9.4.3.3.   Sensitivity analysis

In this process it is common to have a lower pressure in flash drum than in absorber and near atmospheric pressure in the regeneration column. These two pressures have significant effect on the composition and the flow rates of the streams and thus on the energy requirements of the process. The effect of these pressures, the one of the solvent mass flow and the number of stages of absorption and regeneration columns are examined and presented in this section. For the sensitivity analysis Peng-Robinson EoS has been used.

9.4.3.3.1.   Solvent mass flow rate

Changing the circulation rate affects significantly the CO_2 recovery, that has also a significant effect on the calculated energy requirements (Figure 9.13). As it is expected, for high CO_2 recovery a high solvent flow rate is required, and thus higher energy requirements of the reboiler and cooler_3. However, the energy of compressor_2 and cooler_2 decrease as the solvent mass flow increases due to the mass flow rate reduction of the vapor stream of flash.
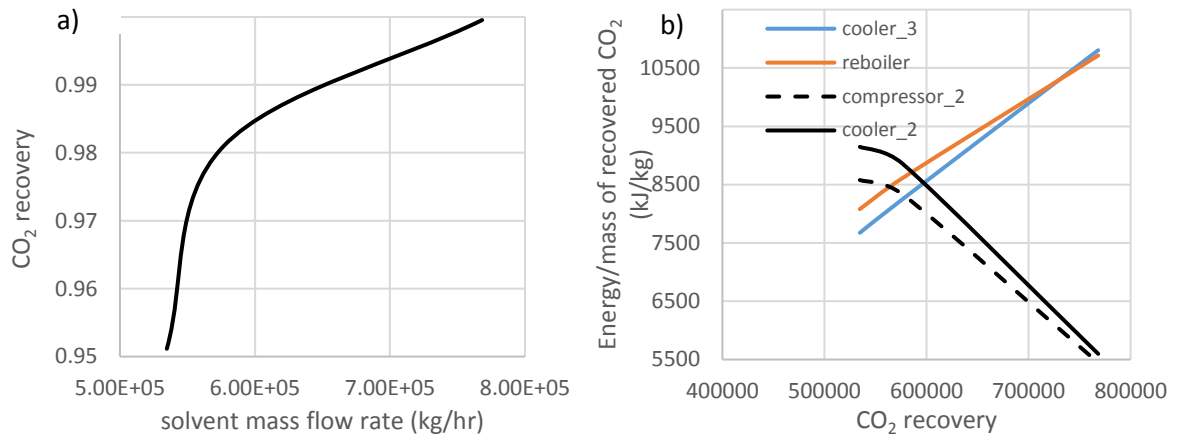
Figure 9.13: Effect of solvent mass flow rate on CO_2 recovery and energy requirements.

9.4.3.3.2. Number of stages of absorption column

The increase in the number of stages of the absorber provokes the decrease in solvent mass flow rate, in order the same CO_2 recovery to be achieved. This has as a result the decrease in most energy requirements, except for those of cooler_2 and compressor_2, which increase, due to the mass flow rate increase in the vapor product of flash drum (Figure 9.14).
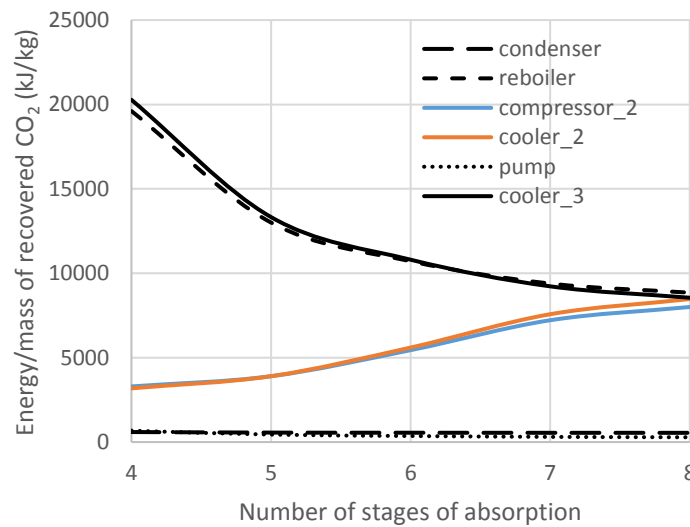
Figure 9.14: Effect of number of stages of absorption column on energy requirements.

9.4.3.3.3.   Number of stages of regeneration column

An increase in the number of stages of regeneration column results in a decrease in the reflux ratio and thus in a decrease in the energy requirements of the reboiler and condenser.
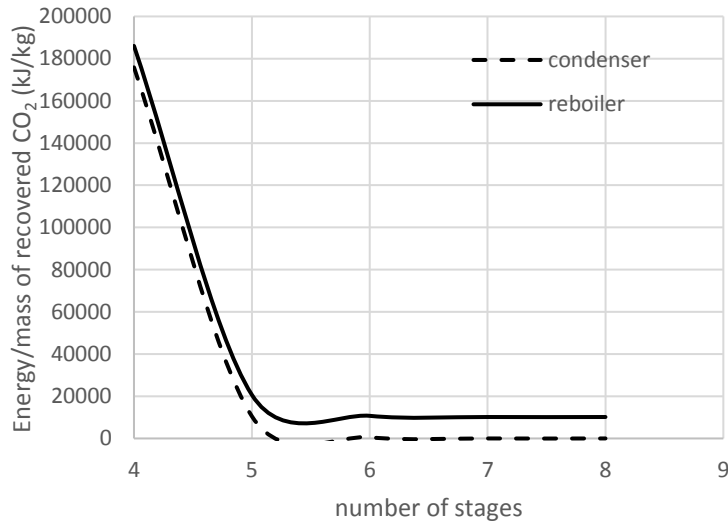
Figure 9.15: Effect of number of stages of regeneration column on energy requirements of condenser and reboiler.

9.4.3.3.4.   Pressure of absorption column

As the pressure of the absorber increases, the solvent mass flow rate required decreases, in order to have the same CO_2 recovery. Therefore, the energy requirements of pump, cooler_3, condenser and reboiler decrease, whereas those of cooler_2 and compressor_2 increase due to the pressure increase and temperature decrease required (Figure 9.16).

198
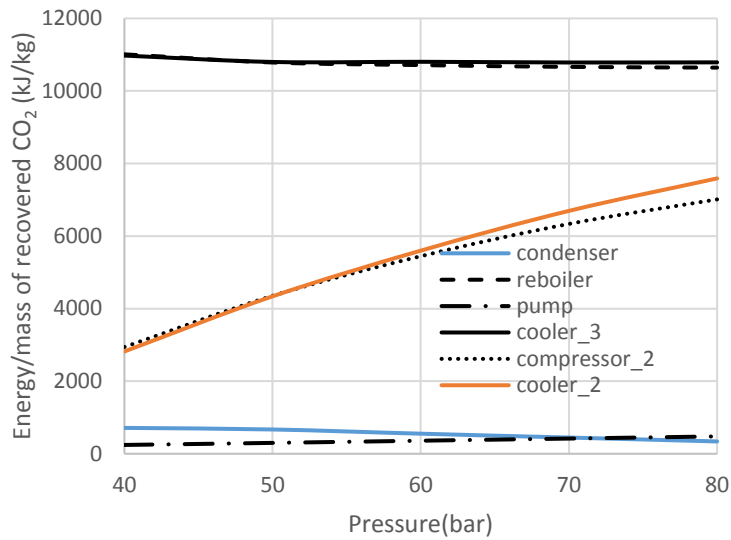
Figure 9.16: Effect of pressure of absorption column on energy requirements.

9.4.3.3.5. Pressure of flash drum

The pressure of the flash drum is an important design parameter, because it has a huge effect on the composition and flow rate of the vapor product of the flash drum and thus on the input in the absorption column. Furthermore, it also plays an important role in purity of CO_2 in CO_2 stream because it affects the methane flow rate, which enters the regeneration column.

The increase in pressure in flash drum results to increase in methane and CO_2 entering in distillation column and therefore less solvent mass flow is required, in order the same CO_2 recovery to be achieved. The decrease in solvent mass flow rate in combination with the decrease in vapor product mass of the flash drum results to decrease in the energy requirements (Figure 9.17).
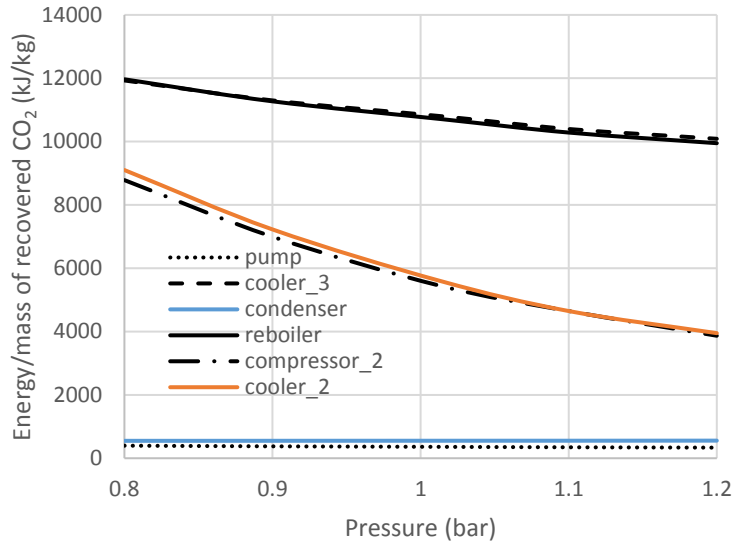
Figure 9.17: Effect of pressure of flash drum on energy requirements.

9.4.3.3.6. Pressure of regeneration column

The increase in the pressure of the regeneration column results to higher temperature at condenser and reboiler and thus higher energy requirements. These are depicted in Figure 9.18. Condenser energy requirements are almost constant.
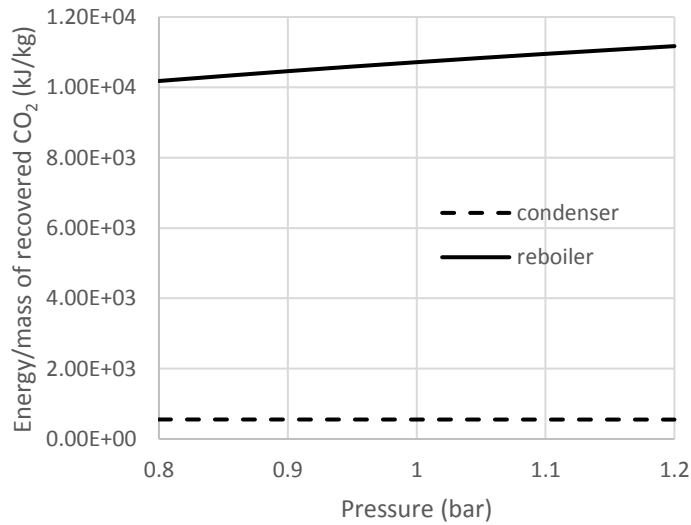
Figure 9.18: Effect of pressure of distillation column on energy requirements of condenser and reboiler.

9.4.3.3.7.   Reflux ratio

As the reflux ratio of regeneration column increases, the energy requirements of the condenser and the reboiler increase. This is depicted in Figure 9.19.
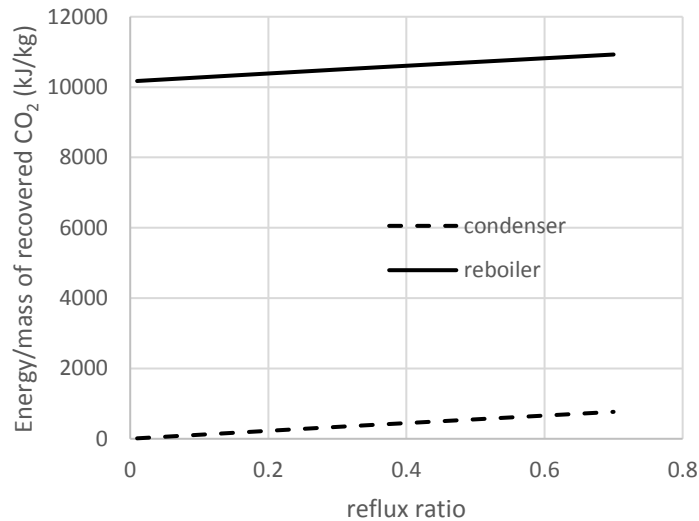
Figure 9.19: Effect of reflux ratio on energy requirements of condenser and reboiler.

It should be noted that in Figure 9.19, changes in reflux ratio do not affect CO_2 purity and recovery. Therefore, even 0.01 reflux ratio is adequate for the same CO_2 purity and recovery.

9.4.3.4.   Base Case-2

A modification of Base Case-1 is examined by utilizing a reboiled absorber for the solvent regeneration instead of a distillation column.

The detailed results are presented in Appendix D and they show that those of the absorption column and the flash drum are almost identical to the ones presented in 9.4.3.2. section. The methane recovery is 99.8 % and the methane purity in purified gas is 96 % in mass fraction.

Differences are found in the results of the regeneration columns of both processes. In order to regenerate almost the total amount of methanol in the liquid product of the absorber a high purity in CO_2 in CO_2 stream is achieved.

The main advantage of this process, as compared to the one with the distillation column, is the absence of the condenser and its corresponding energy requirement. The energy requirements of Base Case-2 process are presented in Table D.8 of Appendix D. It is concluded that the only differences in energy requirements in both cases, appear only on those of the condenser and the reboiler. As it is expected in case of reboiled absorber the energy requirements of the process are lower -about 3.4 % less- than in case of distillation-, because there are no energy requirements for the condenser and the energy requirements of the reboiler are lower, due to the absence of reflux. For that purpose, the reboiled absorber is suggested as an energy-effective variation for this process.

9.4.4. CO_2 absorption using ionic liquid

In this section CO_2 absorption process in ionic liquid (hmim[Tf_2N]) is simulated using UMR-PRU model and Peng-Robinson EoS.

9.4.4.1.   Base Case

Ionic liquids are an energy-effective suggestion for CO_2 absorption. Because of their low volatility, there are no solvent losses and therefore there is no need for solvent make up. Furthermore, their low volatility makes their regeneration possible by using simple flash drums and no distillation column is needed. Actually, three flash drums are employed; the first two are used for the removal of the dissolved methane and nitrogen in the solvent, while the last one is used for the separation of CO_2 from the ionic liquid. The temperature of the solvent entering the absorption column is higher than in previous cases and the pressure of the absorber is lower, a fact that, in combination with the absence of the distillation column, results to lower energy requirements.

The process flowchart is presented in Figure 9.20. Acid gas after its compression and cooling, enters the bottom of the absorption column, whereas ionic liquid enters the top of the absorption column. Purified gas, rich in methane, is the top product of the absorber, whereas rich solvent is its liquid product, which is used for further processing. The pressure decreases towards the flash drums. The rich solvent enters the first flash at 9 bar, the second at 1.8 bar and the third at 0.3 bar. The vapor products of the first two flash drums are rich in methane and they are recycled back to the absorber, whereas the vapor product of the third flash drum is rich in CO_2. The bottom product of the third flash drum is the lean solvent, which is recycled back to the absorption column.
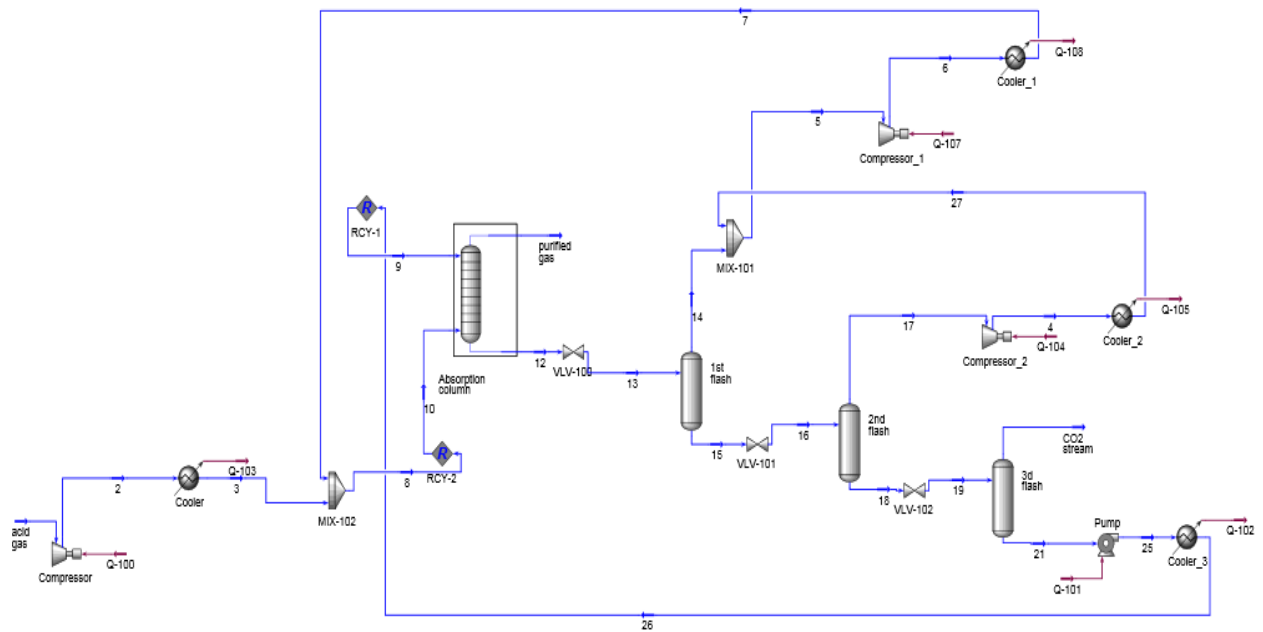
Figure 9.20: Process flowchart of CO$_2$ absorption in ionic liquid

The operating conditions of the process and the results obtained with UMR-PRU and Peng-Robinson models, are presented in Tables 9.12 to 9.17.

Table 9.12: Operating conditions of the process

	Absorption column	1st Flash Drum	2nd Flash Drum	3^{d} Flash Drum
Number of stages	6			
Pressure (bar)	40	9	1.8	0.3

Table 9.13: Results of the absorption column

	Acid gas	10		9		Purified gas		12	
Model		UMR	PR	UMR	PR	UMR	PR	UMR	PR
T ºC	40	18.98	18.76	19.97	20	21.22	27.32	23.57	38.05
P (bar)	30	40	40	40	40	40	40	40	40
Mass flow (kg/h)	99786	193664	222183	10652682	10654974	71644	71696	10774702	10805462
				Composition (mass fraction)					
Nitrogen	0.02836	1.47E-02	1.28E-02	1.06E-15	7.47E-16	3.95E-02	3.95E-02	1.29E-06	1.20E-06
CO_2	0.28957	4.24E-01	4.77E-01	9.01E-04	8.78E-04	2.05E-02	2.27E-02	8.38E-03	1.05E-02
Methane	0.68207	5.61E-01	5.10E-01	1.91E-06	2.85E-06	9.40E-01	9.38E-01	3.84E-03	4.26E-03
hmimTf$_2$N	0.00000	5.96E-16	1.81E-15	9.99E-01	9.99E-01	5.70E-15	7.15E-15	9.88E-01	9.85E-01

The purity of methane is 94% in mass fraction in purified gas and the methane recovery is about 99 %.

Table 9.14: Results of the first flash drum

Stream	13		14		15	
Model	UMR	PR	UMR	PR	UMR	PR
T ºC	24.07	36.02	24.07	36.02	24.07	36.02
P (bar)	9	9	9	9	9	9
Mass flow (kg/h)	10774702.51	10805462.07	59008.04	77692.35	10715694.47	10727770
			Composition (mass fraction)			
Nitrogen	1.29E-06	1.20E-06	2.34E-04	1.67E-04	3.19E-09	2.66E-09
CO_2	8.38E-03	1.05E-02	4.26E-01	5.15E-01	6.08E-03	6.87E-03
Methane	3.84E-03	4.26E-03	5.74E-01	4.84E-01	7.00E-04	7.87E-04
hmimTf$_2$N	9.88E-01	9.85E-01	1.09E-15	3.68E-15	9.93E-01	9.92E-01

The vapor product (14) of the first flash drum is rich in methane (57.4 % mass fraction with UMR-PRU model) and thus it is recycled back to the absorber, in order to be recovered.

Stream	16		17		18	
Model	UMR	PR	UMR	PR	UMR	PR
T °C	23.45	32.00	23.45	32.00	23.45	32.00
P (bar)	1.8	1.8	1.8	1.8	1.8	1.8
Mass flow (kg/h)	10715694.47	10727769.72	34870.00	44707.15	10680824.47	10683062.57
Composition (mass fraction)						
Nitrogen	3.19E-09	2.66E-09	9.79E-07	6.38E-07	3.67E-12	2.57E-12
CO_2	6.08E-03	6.87E-03	8.06E-01	8.30E-01	3.47E-03	3.43E-03
Methane	7.00E-04	7.87E-04	1.94E-01	1.70E-01	6.90E-05	7.96E-05
hmimTf$_2$N	9.93E-01	9.92E-01	1.47E-15	2.58E-15	9.96E-01	9.96E-01

The vapor product of the second flash drum (17) has less methane than the previous one (19.4 % mass fraction calculated by UMR-PRU model), but still enough to be recovered.

Table 9.16: Results of the third flash drum

	19		CO_2 stream		21	
Model	UMR	PR	UMR	PR	UMR	PR
T °C	22.59	28.64	22.59	28.64	22.59	28.64
P (bar)	0.3	0.3	0.3	0.3	0.3	0.3
Mass flow (kg/h)	10680824.47	10683062.57	28142.15	28087.77	10652682.32	10654974.80
Composition (mass fraction)						
Nitrogen	3.67E-12	2.57E-12	1.39E-09	9.79E-10	1.06E-15	7.47E-16
CO_2	3.47E-03	3.43E-03	9.75E-01	9.71E-01	9.01E-04	8.78E-04
Methane	6.90E-05	7.96E-05	2.55E-02	2.92E-02	1.91E-06	2.85E-06
hmimTf$_2$N	9.96E-01	9.96E-01	4.89E-15	5.21E-15	9.99E-01	9.99E-01

The purity of CO_2 in CO_2 stream is more than 97 % mass fraction and the CO_2 recovery is about 95%.

The energy requirements of the process per kg of recovered CO_2 are presented in Table 9.17.

Table 9.17: Energy requirements of the process

Equipment	Energy/mass of recovered CO_2 (kJ/kg)	
	UMR	PR
Cooler	3.60E+02	3.63E+02
Cooler_1	9.18E+02	1.48E+03
Cooler_2	2.48E+02	1.57E+02
Cooler_3	1.36E+03	1.38E+03
Compressor	1.77E+02	1.78E+02
Compressor_1	7.74E+02	1.07E+03
Compressor_2	2.43E+02	3.11E+02
Pump	1.55E+03	1.59E+03

9.4.4.2. Sensitivity analysis

In the current process, the operating conditions of the flash drums are not predefined. The decreasing pressure towards the flash drums was the only known information and the pressures presented before have been chosen, in order to obtain the appropriate purity and recovery of CO_2 in CO_2 stream. The solvent circulation rate is also of great importance for CO_2 recovery and purity. The purity and recovery of CO_2 is defined by the combination of circulation rate and the pressures of flash drums and thus none of them has been kept constant, because it is very difficult to find the proper combinations. For the sensitivity analysis Peng-Robinson EoS has been used.

9.4.4.2.1. Solvent circulation rate

The circulation rate of the solvent defines in a great degree the CO_2 recovery and CO_2 purity, as it is presented in Figure 9.21a.
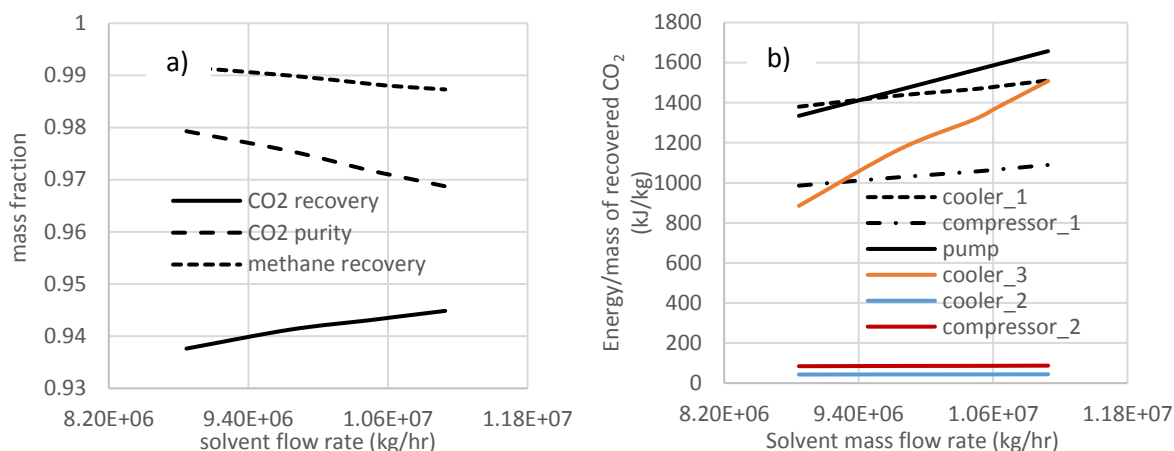
Figure 9.21: Effect of solvent mass flow on CO_2 recovery, purity and CH_4 recovery and on energy requirements.

Increase in the solvent circulation rate results to higher CO_2 recovery, as it is expected. However, it has as a result the decrease in CO_2 purity. This can be explained by the methane flow entering the third flash drum, which increases as the solvent mass flow rate increases, due to its increase in rich solvent.

Figure 9.21b presents the effect of solvent mass flow on energy requirements of the process, which increase. The increase in the energy requirements of pump and cooler_3 is expected, due to the increase in the circulation rate. The increase in the rest energy requirements can be explained by the increase in the methane flow in the whole process, due to the decrease of its recovery in purified gas (Figure 9.21a).

9.4.4.2.2. Pressure of the absorption column

As the pressure of the absorption column increases, the CO_2 recovery increases while the CO_2 purity in CO_2 stream decreases, due to the increase in methane absorption in ionic liquid. Nevertheless, the changes in CO_2 recovery and purity are very small and they can be assumed as constant. As it is expected, the higher pressure in absorption column combined with the fact that the solvent mass flow remains constant, results to higher energy requirements of compressor_1, cooler_1 and pump (Figure 9.22).
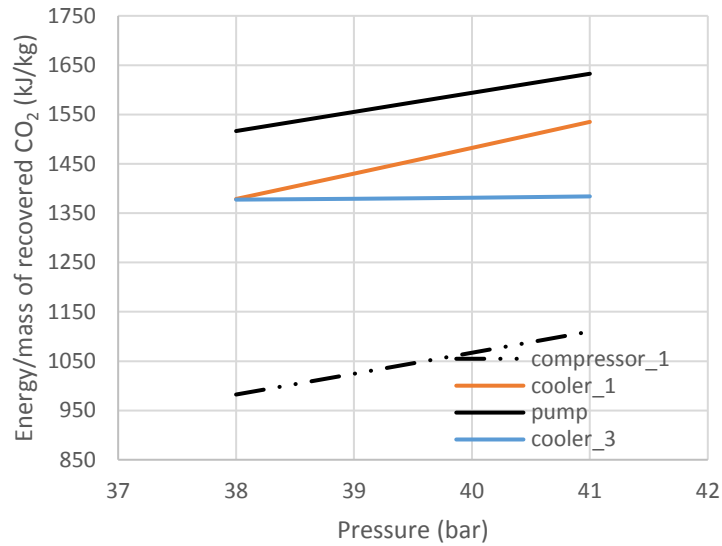
Figure 9.22: Effect of absorber pressure on energy requirements.

9.4.4.2.3.   Pressure of the first flash drum

The pressure of the first flash drum has significant effect both on CO_2 recovery and CO_2 purity. Increasing the pressure of the first flash drum results to lower CO_2 purity and CO_2 recovery. The decrease in the CO_2 purity is explained by the increase in the methane mass flow in the stream entering the third flash drum.
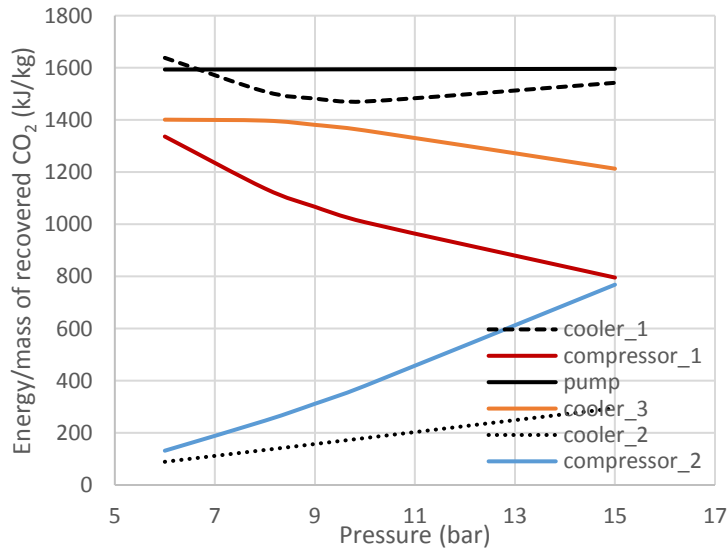
Figure 9.23: Effect of pressure of first flash drum on energy requirements.

The increase in pressure of first flash drum results to lower mass flow of its vapor product and a higher mass flow of vapor product of second flash drum. Thus, the energy requirements of compressor_2 and cooler_2 increase, whereas those of compressor_1 decrease (Figure 9.23).

9.4.4.2.4. Pressure of second flash drum

Changes in pressure of the second flash drum results to changes in CO_2 recovery and purity in CO_2 stream.
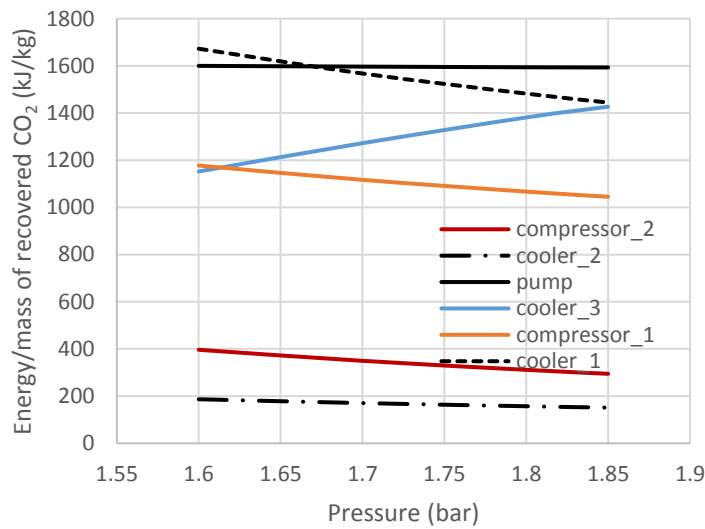
Figure 9.24: Effect of pressure of 2nd flash drum on energy requirements.

By increasing the pressure, the recovery of CO_2 increases, whereas the purity decreases, a fact that can be explained by the increasing mass flow rate of methane entering the third flash drum.

The increasing pressure results to a decrease in mass flow of the second flash drum's vapor product. The decreasing total flow entering the compressor and the decreasing change in pressure and temperature needed, result in the decrease of energy requirements of compressor_2 and cooler_2 (Figure 9.24).

9.4.4.2.5.   Pressure of third flash drum

Changing the pressure of third flash drum results to changes in CO_2 recovery and purity. Figure 9.25a shows that the increase in pressure results to higher CO_2 purity and lower CO_2 recovery. The lower CO_2 recovery results to higher mass flow of lean solvent leaving the bottom of the flash drum. However, this fact does not compensate the decreasing need of temperature change and thus the decrease in energy requirements of cooler_3 (Figure 9.25b).
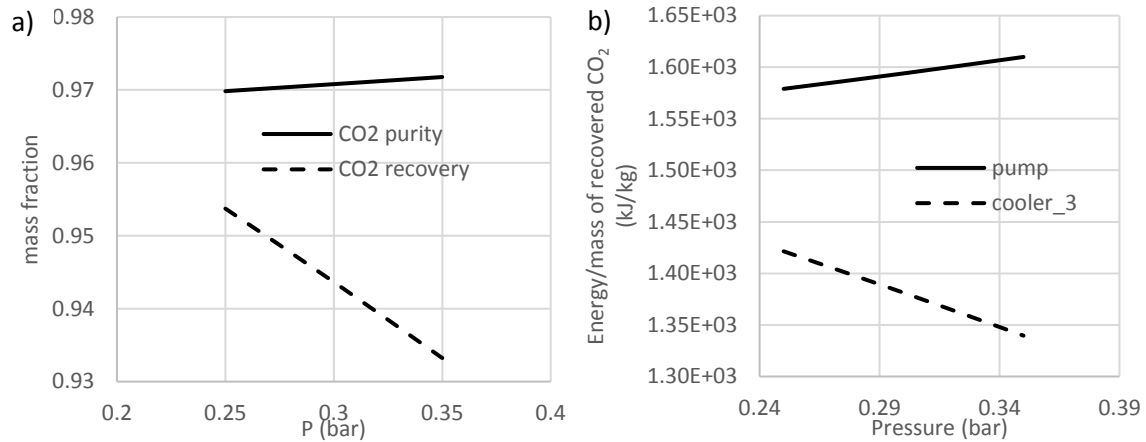
Figure 9.25: Effect of pressure of 3ᵈ flash drum on CO_2 purity and recovery and on energy requirements of pump and cooler_3.

9.4.5.   Mixtures of methanol-ionic liquid

The use of ionic liquids in physical absorption process is an energy effective solution with no solvent losses and therefore no need for solvent make-up. However, their use as solvents for CO_2 absorption is not a practical application, due to their high viscosities. Therefore, the use of hmim[Tf$_2$N] and methanol mixture is examined, in order to reduce the energy requirements compared to those of methanol and the viscosity compared to the one of pure hmim[Tf$_2$N].

The results obtained with PR EoS are presented in Figure 9.26. As it is expected, the more ionic liquid in the solvent, the less the energy requirements. It should be noted, that in each analogy of solvents, different circulation rates have been used in order to have the same CO_2 recovery and purity in CO_2 stream.
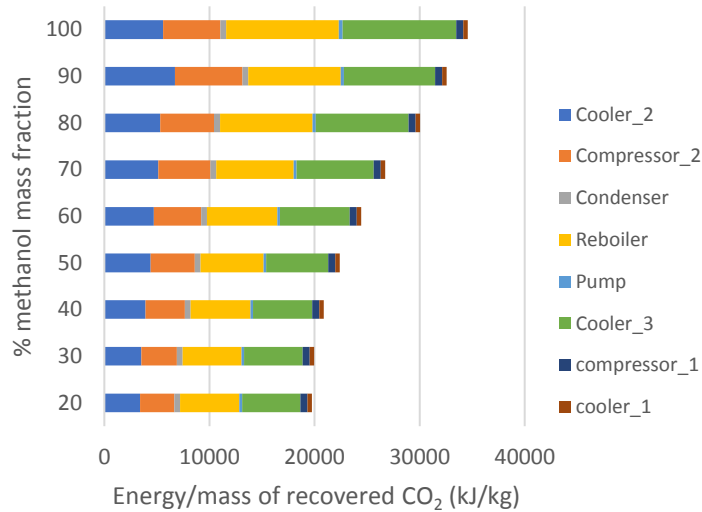
Figure 9.26: Energy requirements of different analogy of solvent in methanol-hmim[Tf₂N] mixture.

9.5. Comparison of the three processes

Chemical absorption in aqueous alkanolamine solution, physical absorption in refrigerated methanol and physical absorption in ionic liquid are different processes used for the removal of CO_2 from a natural gas stream. It is of great interest for the industry to know, which process requires the least energy. Therefore, a comparison of the energy requirements of these processes is presented in this section, targeting a high CO_2 purity (97%) and CO_2 recovery (95%). It should be noticed, that the operating conditions for each process are those presented in sensitivity analysis, which result to the lowest energy requirements.

The comparison of the three base cases is presented in Figure 9.27. The mechanical energy is negative, when energy is needed, whereas it is positive when energy is produced. Although, the acid gas chemical absorption has significant energy requirements due to the chemical reactions, the process with refrigerated methanol appears to have the highest energy requirements due to the extremely low temperature and high pressure needed. The process with ionic liquid seems to be the most energy effective solution, but it should be further examined, because it is not applicable due to its high viscosity. The mixture of 20% methanol and 80% ionic liquid in mass fraction, which has been presented in previous section and it has the least energy requirements compared to the other mixtures, is a promising solution, but the energy requirements are still high compared to those of MEA.
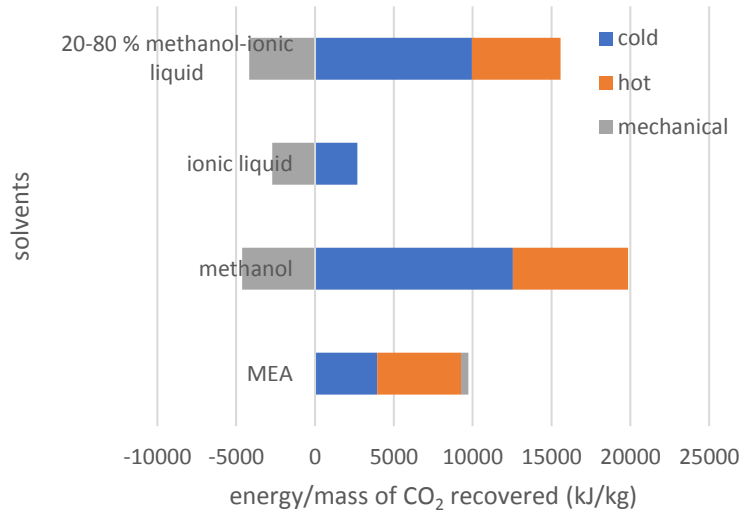
Figure 9.27: Comparison of different solvents

9.6.   Conclusions

In this chapter, eUMR-PRU has been incorporated in commercial process simulators by using a CAPE-OPEN protocol. The implementation has been proven to be successful, after the testing results of physical, chemical and simultaneous physical and chemical equilibrium in the simulator. Furthermore, three different processes for CO_2 removal from natural gas have been simulated. The first one is chemical absorption in aqueous monoethanolamine solution, which has been modeled with Acid Gas thermodynamic package in HYSYS V8.6, whereas the second is physical absorption in refrigerated methanol, and the third regards physical absorption in ionic liquid. The last two processes have been modeled by Peng-Robinson EoS and UMR-PRU and it is proven that, concerning the VLE results, UMR-PRU calculations are more accurate. All processes resulted to similarly high CO_2 recovery and purity but with different energy requirements. Sensitivity analysis, which has been performed in all cases, has been focused on the effect, that different parameters have, on energy requirements of the process. Furthermore, a comparison of the three processes concerning the energy requirements has been performed, and it has been concluded, that the energy requirements of physical absorption in methanol are the highest. Ionic liquid is much more energy effective, because there is no need for distillation unit, due to its extremely low vapor pressure. However, its use is not applicable, especially due to its main disadvantage, which is the high viscosity. For that purpose, the use of a mixture of ionic liquid and methanol has been proposed in this work as a possible application with lower energy requirements than methanol and lower viscosity than

the pure ionic liquid. However, this suggestion should be further examined and other solvent mixtures should be tested as well. Nevertheless, ionic liquids seem to be a promising solvent for acid gas absorption.

9.7. References

1.   Dugas, R.; Alix, P.; Lemaire, E.; Broutin, P.; Rochelle, G., Absorber model for CO 2 capture by monoethanolamine — application to CASTOR pilot results. *Energy Procedia* **2009,** *1*, 103-107.

2.   Pellegrini, L. A.; Moioli, S.; Gamba, S., CO2 removal by MEA scrubbing: Process simulation and energy saving study. **2011**.

3.   Rahimpour, M. R.; Saidi, M.; Baniadam, M.; Parhoudeh, M., Investigation of natural gas sweetening process in corrugated packed bed column using computational fluid dynamics (CFD) model. *Journal of Natural Gas Science and Engineering* **2013,** *15*, 127-137.

4.   Glasscock, D.; Rochelle, G., Approximate Simulation of H2S Absorption into Aqueous Alkanolamines. *AIChE Journal* **1993,** *39*, 1389-1397.

5.   Gamba, S.; Pellegrini, L.; Soave, G.; Rossi, P.; Moioli, S., *Acidic gas absorption by methanol: System modeling and simulation*. 2012.

6.   Burr, B.; Lyddon, L. In *A comparison of physical solvents for acid gas removal*, Gas Processors' Association Convention, Grapevine, TX, 2008.

7.   Akinola, T. E.; Oko, E.; Wang, M., Study of CO2 removal in natural gas process using mixture of ionic liquid and MEA through process simulation. *Fuel* **2019,** *236*, 135-146.

8.   Santiago, R.; Lemus, J.; Outomuro, A. X.; Bedia, J.; Palomar, J., Assessment of ionic liquids as H2S physical absorbents by thermodynamic and kinetic analysis based on process simulation. *Separation and Purification Technology* **2020,** *233*, 116050.

9.   Taheri, M.; Dai, C.; Lei, Z., CO2 capture by methanol, ionic liquid, and their binary mixtures: Experiments, modeling, and process simulation. *AIChE Journal* **2018,** *64* (6), 2168-2180.

10.   Petropoulou, E., Development of a group–contribution equation of state for the thermodynamic modelling of associating mixtures. **2018**.

11.   Shiflett, M. B.; Yokozeki, A., Solubility of CO2 in room temperature ionic liquid [hmim][Tf2N]. *The Journal of Physical Chemistry B* **2007,** *111* (8), 2070-2074.

12.   Kumełan, J.; Kamps, A. P.-S.; Tuma, D.; Maurer, G., Solubility of CO2 in the ionic liquid [hmim][Tf2N]. *The Journal of Chemical Thermodynamics* **2006,** *38* (11), 1396-1401.

13.   Yim, J.-H.; Lim, J. S., CO2 solubility measurement in 1-hexyl-3-methylimidazolium ([HMIM]) cation based ionic liquids. *Fluid Phase Equilibria* **2013,** *352*, 67-74.

14.   Kim, Y.; Jang, J.; Lim, B.; Kang, J. W.; Lee, C., Solubility of mixed gases containing carbon dioxide in ionic liquids: Measurements and predictions. *Fluid phase equilibria* **2007,** *256* (1-2), 70-74.

15.   Kumełan, J.; Pérez-Salado Kamps, Á.; Tuma, D.; Maurer, G., Solubility of the single gases methane and xenon in the ionic liquid [hmim][Tf2N]. *Industrial & engineering chemistry research* **2007,** *46* (24), 8236-8240.

16.   Kato, R.; Gmehling, J., Systems with ionic liquids: Measurement of VLE and γ∞ data and prediction of their thermodynamic behavior using original UNIFAC, mod. UNIFAC (Do) and COSMO-RS (Ol). *The Journal of Chemical Thermodynamics* **2005,** *37* (6), 603-619.

17.   Zhang, X.; Song, Z.; Gani, R.; Zhou, T., Comparative economic analysis of physical, chemical, and hybrid absorption processes for carbon capture. *Industrial & Engineering Chemistry Research* **2020,** *59* (5), 2005-2012.

18.   Gatti, M.; Martelli, E.; Marechal, F.; Consonni, S., Review, modeling, Heat Integration, and improved schemes of Rectisol®-based processes for CO2 capture. *Applied thermal engineering* **2014,** *70* (2), 1123-1140.

10.Conclusions

Acid gases exist in flue gases and fossil fuels can cause significant problems to human health, environment and equipment and thus their removal is necessary. The accurate thermodynamic description of acid gases solubility in different solvents is essential, in order to select and design the proper acid gas removal process from natural gas or flue gases, whereas the simulation of the process is the next step required.

In this thesis, the CO_2 and H_2S removal processes from natural gas and CO_2 removal from flue gases have been modeled and simulated. For the thermodynamic modeling, an EoS/G^E model, i.e. UMR-PRU, has been extended to the mixtures examined in this work and it has been compared to other widely used models.

The most commonly used process for acid gas removal is chemical absorption in aqueous alkanolamines. In this process, physical and chemical equilibria coexist and ionic species are formed by the reactions taking place only in liquid phase and they remain in liquid phase, whereas the molecular species exist in both liquid and vapor phases. UMR-PRU has been extended to such mixtures by the addition of Debye-Hückel term in order to account for the long-range electrostatic forces (eUMR-PRU). The parameters required to be estimated include the binary interaction parameters between all species and van der Waals Volume and Area parameters. The algorithm used for the solution of this problem is analogous to bubble point algorithm, because temperature is defined and the liquid phase composition is known by the solution of chemical equilibrium. Thus, pressure and vapor phase mole fractions are calculated by the model.

Two alkanolamines have been examined: monoethanolamine (MEA) and methyldiethanolamine (MDEA). Firstly, the CO_2 solubility in aqueous MEA, MDEA and in aqueous MEA-MDEA blends has been modeled. Therefore, a wide database of experimental data points, taken from the literature, has been used, in order to take into consideration a wide range of temperatures (298-443 K), amine concentrations (5-60 % w/w) and acid gas loadings (0.0003-2.1). Some of these data have been used for the fitting procedure (training data set), whereas others for the model predictions (test data set). In all cases, eUMR-PRU has an average absolute relative deviation in pressure greater than 30 %. However, this deviation is comparable to that of other models found in literature, such as electrolyte-NRTL, a fact which implies a successful extension of the model to these mixtures. Furthermore, the effect of methane in CO_2-H_2O-MDEA mixture has also been examined by eUMR-PRU model and it has been concluded that by increasing the methane concentration, the acid gas solubility in liquid phase decreases.

Moreover, H_2S and CO_2+H_2S solubility in aqueous monoethanolamine and methyldiethanolamine has been modeled by eUMR-PRU. In this case too, a wide variety

of temperatures (298-413.15 K), amine concentrations (12-50 % w/w) and acid gas loadings (0-3.229) have been included in experimental database. eUMR-PRU has a satisfactory performance, comparable or even better in some cases to that of electrolyte-NRTL and Kent-Eisenberg models. UMR-PRU has also been successfully extended to H_2S-gases and H_2S-hydrocarbon mixtures and it yields an average absolute relative deviation in pressure equal to 5.1% and in vapor phase composition 5.2 %.

Except for acid gas chemical absorption in aqueous alkanolamine solution, physical absorption is also a possible process for acid gas removal. In this thesis, two physical solvents have been examined: methanol and ionic liquids. In order ionic liquids to be used in process simulations, UMR-PRU model should be extended to CO_2-ionic liquid mixtures. The ionic liquids examined in this work are imidazolium-based with an alkyl-chain. Firstly, pure ionic liquids have been modelled and specific emphasis has been given on the correct prediction of their densities and extremely low vapor pressures, because they are of great importance, in order to correctly simulate the absence of solvent losses of the process. Furthermore, UMR-PRU has been used for the description of binary CO_2-ionic liquid mixtures. The results are in a great agreement with the experimental data and the average absolute relative deviation in pressure is less than 9 %. Furthermore, Peng-Robinson EoS has been used in these mixtures for comparison purposes. For that purpose, k_{ij} and l_{ij} binary interaction parameters have been expressed as a function of temperature and carbon number and the average absolute relative deviation in pressure is about 12 % in 1514 data points.

After the extension of UMR-PRU (or eUMR-PRU) to these mixtures, it has been considered to be necessary to be used in a more applied task. Therefore, UMR-PRU, which had already been incorporated in process simulators, has been used for simulations, whereas eUMR-PRU has been implemented in process simulators through a CAPE-OPEN protocol in this thesis. This implementation has been checked in physical, chemical and simultaneous physical and chemical equilibrium calculations and it has been concluded that the implementation was successful. Furthermore, three processes have been simulated and compared to each other: CO_2 chemical absorption from natural gas using an aqueous 30% w/w MEA solution, CO_2 physical absorption from natural gas using refrigerated methanol as solvent and CO_2 physical absorption from natural gas using hmim[Tf_2N] as solvent. For the first one, acid gas thermodynamic package in HYSYS has been used, while for the rest two, UMR-PRU and Peng-Robinson EoS have been employed. The results indicate, that the use of ionic liquid is the most energy effective solution, whereas methanol process has higher energy requirements than chemical absorption for the specific feed and operating conditions used. The use of ionic liquids in CO_2 removal has been proven to be promising, but due to their high viscosity, it is not

applicable. Therefore, mixtures of methanol and ionic liquid, have been suggested as an energy effective solution, in order to make the use of ionic liquids more applicable and to overcome the problems caused by their high viscosity, although this process should be further examined.

In conclusion, eUMR-PRU has been successfully extended to CO_2-H_2O-MEA, CO_2-H_2O-MDEA, CO_2-H_2O-MEA-MDEA, H_2S-H_2O-MEA, H_2S-H_2O-MDEA, CO_2-H_2S-H_2O-MEA, CO_2-H_2S-H_2O-MDEA and to CH_4-CO_2-H_2O-MDEA mixtures and it has been incorporated in process simulators. Furthermore, UMR-PRU has been successfully extended to H_2S-gases, H_2S-hydrocarbon, CO_2-ionic liquid mixtures, and it has been used in simulation of CO_2 absorption in refrigerated methanol and in ionic liquid. All these, comprises the fulfillment of the scope of this work, which is the extension of the model to these mixtures, in order to develop a simple and accurate thermodynamic model applicable to the whole natural gas processing.

11. Future Work

The subject of this thesis is modeling and simulation of CO_2 and H_2S removal processes from natural gas and flue gases. However, the scope of a work is not to fill in all the gaps of scientific research in this subject, but to offer the next step in the specific research field, in order other researchers to continue this work.

Concerning the eUMR-PRU model, the huge number of intercorrelated parameters made it difficult to find the optimal solution. Therefore, it would be helpful, if other methods instead of Newton's method are used, in order to generate the possible solutions. A good alternative might be a genetic algorithm. Furthermore, in acid gases-water-alkanolamines mixtures, except for the vapor-liquid equilibria, properties such us enthalpies of absorption, heat capacities, heat of vaporization should be examined, and may be included in the fitting procedure, in order more accurate energy requirements calculations to be predicted by eUMR-PRU model in simulation of a chemical absorption process.

UMR-PRU model, which has been extended to CO_2-ionic liquid mixtures, can be further extended to H_2S-ionic liquid mixtures. In this case also, heat capacities of ionic liquids can be examined and included in fitting procedure, in order more accurate energy requirements to be predicted by the model in simulations. Moreover, different UNIFAC groups than the ones presented in this work, can be used, in order to check if there is any improvement to the results. UMR-PRU predictive capability in CO_2-ionic liquid and H_2S-ionic liquid mixtures can be further tested, by examining other binary mixtures which have not been included in the fitting procedure (for instance 1-butyl-2,3-dimethylimidazolium tetrafluoroborate, or 1-butyl-2,3-dimethylimidazoliumbis ((trifluoromethyl)sulfonyl) amide).

Regarding the simulations, the absence of use of eUMR-PRU model in CO_2 chemical absorption in an aqueous monoethanolamine solution is an important issue, which is due to the difficulty of the process simulators used (HYSYS, UNISIM) to solve the simultaneous physical and chemical equilibrium with the presence of electrolytes. Therefore, other simulators can also be examined such as ASPEN PLUS or PRO/II, a fact which probably requires changes in UMR.dll or even in the CAPE-OPEN protocol used. Furthermore, concerning the simulations of physical absorption, a more detailed study of the prediction of energy requirements of the process by a thermodynamic model can be performed. Moreover, different mixtures of ionic liquids with other solvents, except for ionic liquid-methanol, which has been examined in this thesis, can be studied, in order the use of ionic liquids in acid gas removal to be applicable. For instance, mixtures of ionic liquid-alkanolamine or an amine-functionalized ionic liquid have been proven to be efficient.

Finally, the work presented in this thesis can be used as part of an integrated process, such as an integrated gasification combined cycle, in which the sour syngas exiting the gasifier, enters a sweetening process, such as the ones presented.

A. APPENDIX: Parameters for e-NRTL, UMR-PRU, eUMR-PRU models and Peng Robinson EoS

A.1. Parameters for e-NRTL model taken from Aspen Plus V8.6

The parameters for e-NRTL used in this thesis are presented.

Table A.1: Dielectric constant of molecular species (eq. 5.25).

	CO_2	H_2S	WATER	MDEA
A_A	1.449	5.93	78.51	21.9957
B_A	0	0	31989.4	8992.68
C_A	296.15	283.15	298.15	298.15

Table A.2: Molecule-molecule binary interaction parameters (eq. 5.26) (non-randomness factor equal to 0.2).

A	A'	$A_{AA'}$	$B_{AA'}$	$A_{A'A}$	$B_{A'A}$
CO_2	H_2O	10.064	-3268.14	10.064	-3268.14
H_2S	H_2O	-3.674	1155.9	-3.674	1155.9
WATER	MEA	1.438498	99.02104	-1.0466	-337.546

Table A.3: Electrolyte-molecule and electrolyte-electrolyte binary interaction parameters (eq.5.27-5.28).

				C	D
WATER		MEA+	HS-	4.849272	1215.54
MEA+	HS-	WATER		-2.74022	-483.701
WATER		MEA+	HCO_3-	5.3541	965.24
MEA+	HCO_3-	WATER		-4.0705	-11.067
WATER		MEA+	MEACOO-	9.8877	10.813
MEA+	MEACOO-	WATER		-4.9511	0
WATER		MDEA+	HS-	-22.6956	8864.561
MDEA+	HS-	WATER		7.526381	-3145.96
WATER		MDEA+	HCO_3-	26.16413	-6647.96
MDEA+	HCO_3-	WATER		-14.3515	3814.242
WATER		H_3O+	HS-	8.045	0
H_3O+	HS-	WATER		-4.072	-3937.1
WATER		H_3O+	S--	8.045	0
H_3O+	S--	WATER		-4.072	0
WATER		H_3O+	HCO_3-	8.045	0

H₃O+	HCO₃-	WATER		-4.072	0
WATER		H₃O+	CO₃--	8.045	0
H₃O+	CO₃--	WATER		-4.072	0
WATER		H₃O+	OH-	8.045	0
H₃O+	OH-	WATER		-4.072	0
MDEA		MDEA+	HS-	15	0
MDEA+	HS-	MDEA		5.129168	0
MDEA		MDEA+	S--	15	0
MDEA+	S--	MDEA		-8	0
MDEA		MDEA+	HCO₃-	8.666588	0
MDEA+	HCO₃-	MDEA		-5.8048	0
MDEA+	HS-	MDEA+	HCO₃-	-0.73203	0
MDEA+	HCO₃-	MDEA+	HS-	1.199228	0

Table A.4: Henry's constants of solutes in water (lnH=A+B/T+ClnT+DT)

	H₂S	CO₂
A	346.6251	159.1997
B	-13236.8	-8477.71
C	-55.0551	-21.9574
D	0.059565	0.005781

A.2.   Parameters for UMR-PRU, eUMR-PRU models and Peng-Robinson EoS

The parameters used in this thesis for UMR-PRU and eUMR-PRU models and Peng-Robinson EoS are presented.

Table A.5: Critical properties, acentric factor and Mathias-Copeman parameters for pure components for PR, UMR-PRU and eUMR-PRU models (Ref_A refers to critical properties and acentric factor, Ref_B refers to Mathias-Copeman parameters).

	Ref_A	Ref_B	Tc (K)	Pc (bar)	w	c1	c2	c3
CO₂	[1]		304.19	73.815	0.22760	-	-	-
H₂S	[1]	this work	373.53	89.607	0.09420	0.509088	-0.00281	0.36215
CH₄	[1]		190.56	45.990	0.01150	-	-	-
H₂O	[1]	[2]	647.13	220.550	0.34486	0.92366	-0.37937	0.44243
MEA	[1]	[3]	638.00	68.700	0.79660	1.88178	-3.45167	5.84089
MDEA	[1]	[3]	677.79	38.760	1.24000	2.46940	-3.81470	2.87170

N_2	[1]		126.10	33.944	0.04030	-	-	-
C_2	[1]		305.32	48.720	0.09950	-	-	-
C_3	[1]		369.83	42.480	0.15230	-	-	-
n-C_4	[1]		425.12	37.960	0.20020	-	-	-
i-C_4	[1]		408.14	36.480	0.17700	-	-	-
n-C_5	[1]		469.70	33.700	0.25150	-	-	-
neo-C_5	[1]		433.78	31.992	0.19640	-	-	-
i-C_5	[1]		460.43	33.812	0.22750	-	-	-
n-C_6	[1]		507.60	30.250	0.30130	-	-	-
n-C_7	[1]		540.20	27.400	0.34950	-	-	-
i-C_8	[1]		543.96	25.676	0.30310	-	-	-
n-C_9	[1]		595.65	23.056	0.43770	-	-	-
n-C_{10}	[1]		617.70	21.100	0.49230	-	-	-
n-C_{12}	[1]		658.00	18.200	0.57640	-	-	-
n-C_{13}	[1]		675.00	16.800	0.61740	-	-	-
n-C_{15}	[1]		708.00	14.800	0.68630	-	-	-
n-C_{16}	[1]		723.00	14.000	0.71740	-	-	-
n-C_{20}	[1]		768.00	11.600	0.90690	-	-	-
cy-C_6	[1]		553.54	40.748	0.21180	-	-	-
m-cy-C_6	[1]		572.19	34.714	0.23500	-	-	-
e-cy-C_6	[1]		609.15	30.398	0.24550	-	-	-
p-cy-C_6	[1]		639.15	28.067	0.25950	-	-	-
benzene	[1]		562.16	48.980	0.21080	-	-	-
m-xylene	[1]		617.05	35.412	0.32600	-	-	-
toluene	[1]		591.79	41.086	0.26410	-	-	-
propyl-benzene	[1]		638.38	31.998	0.34620	-	-	-
mesitylene	[1]		637.37	31.269	0.39770	-	-	-
[emim][BF$_4$]	This work	This work	1050.00	45.800		2.08171	0.00000	0.00000
[bmim][BF$_4$]	This work	This work	1123.90	39.500		2.68792	-1.60576	0.04864
[hmim][BF$_4$]	This work	This work	1160.50	33.500		2.00556	0.00000	0.00000
[omim][BF$_4$]	This work	This work	1270.90	32.000		1.85051	0.00000	0.00000
[emim][PF$_6$]	This work	This work	1050.40	38.900		3.13609	-2.05341	-0.64425
[bmim][PF$_6$]	This work	This work	1120.10	35.600		3.20163	-2.68354	-0.97883
[hmim][PF$_6$]	This work	This work	1353.50	35.600		1.81275	-1.43593	1.21397
[omim][PF$_6$]	This work	This work	1425.70	34.600		1.80254	-1.28732	0.40091
[emim][Tf$_2$N]	This work	This work	1110.90	27.300		1.66641	0.96851	-1.81562
[bmim][Tf$_2$N]	This work	This work	1150.90	24.900		1.58948	0.83927	-1.79970
[hmim][Tf$_2$N]	This work	This work	1186.60	23.400		1.79269	-0.95482	0.63745
[omim][Tf$_2$N]	This work	This work	1298.30	23.200		0.72269	1.65483	-0.83745
MeOH	[1]	[4]	512.64	80.970	0.56399	1.22400	-0.27350	-0.39823

Table A.6: Coefficients for dielectric constants of eUMR-PRU taken from literature[3] (eq.5.60)

	H_2O	MEA	MDEA
$d^{(0)}$	-19.2905	-18.5545	-8.16976
$d^{(1)}$	29814.5	14836	8989.3
$d^{(2)}$	-0.01968	0	0
$d^{(3)}$	0.000132	0	0
$d^{(4)}$	3.11E-07	0	0

Table A.7: Van der Waals Volume (R) and Area parameters (Q) for UMR-PRU and eUMR-PRU models.

	R	Q
CO_2	1.296	1.261
H_2S	1.1665	1.163
CH_4	1.129	1.124
H_2O	0.92	1.4
CH_3OH	1.4311	1.432
N_2	0.934	0.985
C_2H_6	1.8022	1.696
CH_3	0.9011	0.848
CH_2	0.6744	0.54
CH	0.4469	0.228
C	0.2195	0
ACH	0.5313	0.4
AC	0.3652	0.12
$ACCH_3$	1.2663	0.968
$ACCH_2$	1.0396	0.66
ACCH	0.8121	0.348
MEA	2.5736	2.36
$MEAH^+$	9.80123	0.000545
MDEA	4.9441	4.268
$MDEAH^+$	0.028224	12.76446
H_3O^+	1.1467	1
HS^-	7.367332	2.95982
HCO_3^-	10.07559	0.078893
CO_3^{2-}	0.085867	0.896232
S^{2-}	0.7131	1.189
OH^-	1	3.331

MEACOO⁻	4.113988	6.489484
mimBF₄	10.296694	4.836818
mimPF₆	10.20147	4.774102
mimTf₂N	12.09975	10.62884
hmim[Tf₂N]	16.37285	14.17684

Table A.8: Binary interaction parameters of equation 5.54 of UMR-PRU and eUMR-PRU models.

n	l	Ref	A_{nl}	B_{nl}	C_{nl}	A_{ln}	B_{ln}	C_{ln}
CO_2	H_2S	This work	374.6273	-0.96144	0.000000	-16.3670	0.48040	0.000000
CO_2	CH_4	[5]	258.5588	-0.44390	0.000000	144.2076	-0.19590	0.000000
CO_2	H_2O	[6]	2543.1180	-7.04259	0.003950	-365.0710	1.51078	0.001723
CO_2	CH_2	[5]	322.0018	-0.82620	-0.000080	773.9580	-4.01205	0.005770
CO_2	MEA	This work	133.3261	-8.27537	0.000000	311.5086	-2.03484	0.000000
CO_2	MEAH⁺	This work	0.0000	0.00000	0.000000	86.5500	-0.09000	0.000000
CO_2	MDEA	This work	2750.4000	1.89000	0.000000	2558.8900	2.19000	0.000000
CO_2	MDEAH⁺	This work	-36.0425	-0.87349	0.000000	246.9670	-0.70237	0.000000
CO_2	HS⁻	This work	-1192.0282	1.89528	0.000000	-1140.4100	67.11000	0.000000
CO_2	HCO3⁻	This work	-888.2890	-3.52802	0.000000	-177.6630	28.36600	0.000000
CO_2	CO3⁻⁻	This work	788.8078	-7.78547	0.000000	275.0088	0.04644	0.000000
CO_2	S⁻⁻	This work	-115.0000	0.60000	0.000000	700.0000	-0.08000	0.000000
CO_2	MEACOO⁻	This work	-33.7564	-1.27910	0.000000	331.1626	0.31649	0.000000
CO_2	mimBF₄	This work	-57.995	-0.73683	0.001671	544.3908	-3.56749	0.003943
CO_2	mimPF₆	This work	-381.546	1.757284	-0.00343	-173.823	1.007152	-0.00327
CO_2	mimTf₂N	This work	926.4337	-5.77828	0.006198	-3764.25	21.91963	-0.02849
CO_2	hmim[Tf₂N]	This work	222.4032	-1.84434	0.000849	-656.462	3.945606	-0.00342
CH_2	mimBF₄	This work	473.1423	-1.85558	0.006685	-664.767	3.160253	-0.00323
CH_2	mimPF₆	This work	-953.681	7.959626	-0.01166	-7049.14	44.24452	-0.07136
CH_2	mimTf₂N	This work	-9135.01	55.94909	-0.07934	-13188.1	84.34806	-0.1379
H_2S	H_2O	This work	-4600.2100	27.77610	-0.039800	-643.6650	6.12891	-0.007830
H_2S	C_2H_6	This work	486.2504	-2.75169	0.005079	670.5803	-3.55890	0.006173
H_2S	CH_2	This work	-396.7838	3.37062	-0.004905	1128.5829	-5.62250	0.006564
H_2S	ACH	This work	1548.6189	-10.97690	0.020113	633.9217	-2.57642	0.000606
H_2S	ACCH₂	This work	773.3054	-5.24157	0.007750	-1514.7579	11.88046	-0.018859
H_2S	N_2	This work	97.6567	3.24444	-0.007935	3678.2760	-23.58042	0.041210
H_2S	CH_4	This work	439.2140	-0.54380	0.000000	79.1279	-0.05520	0.000000
H_2S	MEA	This work	-39.0042	-1.23385	0.000000	-411.2561	-0.37378	0.000000
H_2S	MDEA	This work	250.8740	-1.60940	0.000000	-761.1758	3.39473	0.000000
H_2S	MDEAH⁺	This work	121.1634	-3.93580	0.000000	-1473.3442	4.35842	0.000000
H_2S	HS⁻	This work	84.8831	0.05702	0.000000	2410.9800	27.80000	0.000000
H_2S	HCO₃⁻	This work	-1934.9400	-0.86640	0.000000	-850.0329	62.33759	0.000000

H_2S	CO_3^{--}	This work	0.0000	0.00000	0.000000	2089.8862	-12.92670	0.000000
H_2S	$MEACOO^-$	This work	3000.0000	0.00000	0.000000	704.5149	-0.12291	0.000000
CH_4	H_2O	[6]	5133.7260	-17.90650	0.018500	-2083.7459	13.17183	-0.013510
CH_4	MDEA	This work	5339.0610	-27.05140	0.034260	128.2163	4.46812	-0.008700
CH_4	$MDEAH^+$	This work	0.0000	0.00000	0.000000	1150.0000	0.00000	0.000000
CH_4	$hmim[Tf_2N]$	This work	-448.123	1.461475	-0.00225	802.0049	-2.3991	0.001862
H_2O	MEA	[3]	175.2500	-0.81000	0.000000	-555.4600	1.16000	0.000000
H_2O	$MEAH^+$	This work	48.3900	-0.62000	0.000000	-781.8600	2.16000	0.000000
H_2O	MDEA	[7]	-1678.2000	10.79400	-0.016900	705.6000	-6.22900	0.011100
H_2O	$MDEAH^+$	This work	4.5971	0.54081	0.000000	2688.4360	-0.10607	0.000000
H_2O	HS^-	This work	3208.0400	-1.16000	0.000000	-522.7300	-0.12000	0.000000
H_2O	$HCO3^-$	This work	1879.2200	-2.09000	0.000000	-2903.7300	0.45000	0.000000
H_2O	OH^-	This work	0.0000	0.00000	0.000000	-116.8100	-10.25000	0.000000
H_2O	$MEACOO^-$	This work	-231.8200	0.07000	0.000000	-243.0900	0.51000	0.000000
MEA	$MEAH^+$	This work	346.4600	-8.92000	0.000000	-309.4800	-25.06000	0.000000
MEA	HS^-	This work	7093.1706	-5.72116	0.000000	-3000.0000	10.00000	0.000000
$MEAH^+$	HS^-	This work	-4000.0000	0.00000	0.000000	3000.0000	0.00000	0.000000
$MEAH^+$	$HCO3^-$	This work	-681.6300	-0.13000	0.000000	0.0000	0.00000	0.000000
MDEA	$MDEAH^+$	This work	-47.7467	0.12562	0.000000	-2.5737	0.00805	0.000000
MDEA	HS^-	This work	-21.0415	0.06764	0.000000	78.9654	-0.18273	0.000000
$MDEAH^+$	HS^-	This work	1212.5453	-3.93666	0.000000	-1342.9850	-2.46497	0.000000
$MDEAH^+$	$HCO3^-$	This work	-36.1232	-1.26746	0.000000	-3727.4072	-0.13605	0.000000
HS^-	$MEACOO^-$	This work	-1550.8700	-3.90000	0.000000	0.0000	0.00000	0.000000
CH_3OH	$hmim[Tf_2N]$	This work	-207.248	0	0	292.4751	0	0
CH_3OH	CO_2	[4]	155.8218	-2.31929	0.00511	9356.755	-58.7481	0.096718
CH_3OH	N_2	[4]	303.3771	-0.60625	0.000391	-546.854	3.64175	0.0005
CH_3OH	CH_4	[4]	817.8704	-6.64625	0.012878	2297.682	-3.08046	-0.00607
N_2	$hmim[Tf_2N]$	This work	293.5814	0	0	678.6857	0	0
N_2	CH_4	[4]	112.1786	-0.8494	0	-43.7468	0.7909	0
N_2	CO_2	[4]	368.2498	-1.665	0	-89.5495	1.53	0

Table A.9: D_1, D_2 parameters for l_{ij} interaction parameter in UMR-PRU estimated in this work.

	D_1	D_2
CO_2-BF_4	-0.19273	-0.03039
CO_2-PF_6	-0.20238	-0.01929
CO_2-Tf_2N	0.006037	-0.03024

Table A.10: Parameters of Peng-Robinson EoS for the correlations of k_{ij} and l_{ij} presented in eq.8.3-8.4, estimated in this work.

	A_1	A_2	A_3
CO_2-BF_4	-1.70000409254743E-01	3.51293008297701E-04	-9.96890197803209E-07
CO_2-PF_6	-1.37050857667216E-01	-1.05489211995715E-04	7.01451995580844E-07
CO_2-Tf_2N	-6.17561209566698E-02	6.45924588108260E-04	-1.76878029719997E-06

Table A.10 (continued)

	B_1	B_2	B_3
CO_2-BF_4	8.41701514309301E-02	-4.07909960965795E-04	5.71927254912578E-07
CO_2-PF_6	-9.35406414982196E-03	4.06583779604777E-04	-1.04632720989145E-06
CO_2-Tf_2N	1.21974084801426E-01	-7.23101294813766E-04	1.08183520259690E-06

Table A.10 (continued)

	D_1	D_2
CO_2-BF_4	-4.43473677088369E-03	2.06954686963327E-03
CO_2-PF_6	-1.64126934707865E-04	3.00139749198775E-03
CO_2-Tf_2N	1.46316805218788E-02	9.35209706136135E-04

References

1.   Daubert, T. E.; Danner, R. P., *Data compilation tables of properties of pure compounds*. Design Institute for Physical Property Data, American Institute of Chemical …: 1985.

2.   Boukouvalas, C.; Spiliotis, N.; Coutsikos, P.; Tzouvaras, N.; Tassios, D., Prediction of vapor-liquid equilibrium with the LCVM model: a linear combination of the Vidal and Michelsen mixing rules coupled with the original UNIF. *Fluid Phase Equilibria* **1994,** *92*, 75-106.

3.   Vrachnos, A.; Kontogeorgis, G.; Voutsas, E., Thermodynamic Modeling of Acidic Gas Solubility in Aqueous Solutions of MEA, MDEA and MEA–MDEA Blends. *Industrial & Engineering Chemistry Research* **2006,** *45* (14), 5148-5154.

4.   Petropoulou, E., Development of a group–contribution equation of state for the thermodynamic modelling of associating mixtures. **2018**.

5.   Louli, V.; Pappa, G.; Boukouvalas, C.; Skouras, S.; Solbraa, E.; Christensen, K.; Voutsas, E., Measurement and prediction of dew point curves of natural gas mixtures. *Fluid Phase Equilibria* **2012,** *334*, 1–9.

6.   Petropoulou, E. G.; Voutsas, E. C., Thermodynamic Modeling and Simulation of Natural Gas Dehydration Using Triethylene Glycol with the UMR-PRU Model. *Industrial & Engineering Chemistry Research* **2018,** *57* (25), 8584-8604.

7.   Voutsas, E.; Vrachnos, A.; Magoulas, K., Measurement and thermodynamic modeling of the phase equilibrium of aqueous N-methyldiethanolamine solutions. *Fluid Phase Equilibria* **2004,** *224* (2), 193-197.

B. Appendix: Experimental databases

Table B.1: Experimental database for the system CO_2-H_2O-MEA

Reference	T range (K)	P_{CO2} range (bar)	P_{total} (bar)	MEA % w/w	CO_2 loading
1	313-393	0.001-100		6.1-30.2	0.065-1.935
2	313-423	0.000014-199.14	1.10-200	30	0.002-1.18
3	313	0.157-25.50		15.3	0.561-1.049
4	313-353	0.00093-2.28		15.3	0.267-0.676
5	373-443	0.12-16.26	1.25-22.16	30	0.303-0.52
6	313-333	0.00005-0.502		17.6-40.8	0.114-0.591
7	313-413	0.013-27.86		15.2	0.11-0.998
8	353-373	0.00007-0.0175		15.7	0.035-0.315
9	353	0.0357-1.218		15.7	0.363-0.58
10	313-413	0.00002-9.30		15.3	0.017-0.728
11	313	0.031-23.59		15.3	0.49-1.061
12	313.15-373.15	0.0115-66.162		15.2-30.2	0.139-1.19
13	373	4.55-38.63		26.8	0.541-0.725
14	393	0.07354-1.919		30	0.155-0.4182
15	313.2	0.0347-20.92		15.3	0.512-1.046
16	313-393	0.000016-10.60	0.563-10.602	15-60	0.017-0.625
17	313.15-393.15		20-100	30	0.55-1.07
18	313.15-393.15	0.000033-62.93	1.613-63.88	20-30	0.0298-1.18

Table B.2: Experimental data for the system CO_2-H_2O-MDEA."c" denotes the publications for which all or some data were excluded from the database.

Reference	T range (K)	P_{CO2} range (bar)	P_{total} (bar)	MDEA % w/w	CO_2 loading
19	298-393	0.0000161-66.30		23.3-48.9	0.00037-1.68
20	313-373	0.00004-2.62		35	0.002-0.79
21	298.15-393.15	0.0000251-198.54	1-200	30	0.00114-1.498
22	313		0.121-40.80	23.8	0.24-1.31
23	313-348		0.0547-45.595	25.7-46.8	0.008-1.303
18	313-393	0.00002-53.27	1.792-53.61	23-50	0.00119-1.34
24	313-323	0.0000007-0.010018		23-50	0.000249-0.12
25	313-413		0.735-50.367	18.8-32.1	0.1-1.36
26c	323-373	0.00775-2.683		5.2-75	0.015-0.84
27	313-393		1.765-75.65	32-48.8	0.12-1.24
14	328-358	0.6575-8.134		50	0.16-0.81
28	313		11.55-40.80	23.8	1.06-1.27
29	313	0.0117-37.70		23.9	0.124-1.203
30	373-473	1.03-49.30		21.9-52.8	0.013-1.30
13	373-393	1.62-38.32		52.8	0.091-0.82
31	313-393		20-100	30	0.51-1.35
32	313	0.0102-19.16		30	0.12-1.13

[24]	313-323	0.0000007-0.010018		23-50	0.00025-0.1177
[33]	313		8.374-48.83	18.8	1.05-1.41
[34c]	313-353	0.0006-0.9561		23.9	0.05-0.8
[4]	313	0.000056-0.936		23.3-50	0.006-0.842
[35]	313-373	0.00876-10.13		36.5-41.5	0.0091-0.911
[36]	298-373	0.0078-1.404		50	0.0087-0.4923
[37]	298-388	0.111-61.641	0.135-63.314	5.9-20	0.15-1.51
[38c]	313	0.0108-0.073		50.8	0.013-0.032

Table B.3: Experimental database for mixtures containing methane.

CH_4 with	References	T-range (K)	x_{CH4}-range	P_{tot}-range (bar)
MDEA	[39]	298.15-403.15	0.0006-0.0859	1-203
MDEA-H_2O	[40], [41]	298.15-423.15	3.7e-05-0.008546	0.95-200
CO_2-MDEA-H_2O	[28]	313.15-353.15	0.000971-0.004134	100-200

Table B.4: Experimental database for binary mixtures.

	T-range (K)	P-range (bar)	x_{H2S}-range	y_{H2S}-range	References
H_2S-H_2O	298.17-423.15	0.5-206.8	0.0005-0.111	0.7078-0.9969	[42-46]
H_2S-CO_2	283.15-360.9	20.265-82.737	0.033-0.991	0.031-0.965	[47-49]

Table B.5: Experimental database for H_2S-MEA-H_2O mixture.

References	T-range (K)	P_{H2S}-range (bar)	P_{total}-range (bar)	MEA % w/w	H_2S loading
		Correlation			
[50]	298.15-393.15	0.00152-23.17		15.3-30.5	0.108-1.61
[51]	313.15-413.15	0.000012-38.53		15.2	0.0052-1.633
		Prediction			
[52]	313.15-373.15	0.016341-42.47		15.3-30.5	0.123-1.55
[18a]	313.15-393.15	0.0000164-38.85	1.957-39.15	20	0.00363-1.58
[53]	298.15	0.0662-13.9187	0.0951-13.9476	15.3	0.717-1.454
[54b]	313.15-373.15	0.00963-4.353		15.3-30.1	0.135-1.016
[55b]	298.15-333.15	0.033-0.933		3.66-30.5	0.285-1.148
[8b]	373.15	0.00009-0.0167		15.3	0.016-0.092

[a] Only the total pressure data of this reference were excluded from the database.

[b] Data excluded from the database.

Table B.6: Experimental database for H_2S-MDEA-H_2O mixture.

References	T-range (K)	P_{H2S}-range (bar)	P_{total}-range (bar)	MDEA % w/w	H_2S loading
		Correlation			

References	T-range (K)	P_H2S-range (bar)	P_CO2-range (bar)	% w/w	loading
[56]	313.25	0.0004-0.0161		23.6	0.0151-0.1494
[25]	313.15-413.15		1.652-48.959	18.7-32.2	0.48-1.933
[19]	298.15-393.15	0.000013-58.9		11.94-50.42	0.00129-3.229
Prediction					
[57]	313.15-373.15		0.0621-10.4	46.8	0-1.116
[27]	313.15-393.15		1.479-27.83	48.8	0.153-1.428
[29]	313.15	0.0052-16		23.9	0.13-1.725
[58]	313.15-373.15	0.00002-3.13		35-50	0.0041-1.077
[18a]	313.15-393.15	0.00003-36.73	1.679-37.49	23.1-50	0.0024-1.74
[53]	298.15-388.65	0.1323-15.37	0.1654-15.5986	12-20	0.18-2.1703
[54b]	313.15-373.15	0.0149-4.457		30.5	0.082-0.902

[a] Only the total pressure data of this reference were excluded from the database.

[b] Data excluded from the database.

Table B.7: Experimental database for CO_2-H_2S-MEA-H_2O mixture.

References	T-range (K)	P_{H2S}-range (bar)	P_{CO2}-range (bar)	MEA % w/w	H_2S loading	CO_2 loading
Correlation						
[59]	313.15-373.15	0.006-41.36	0.0006-68.94	30.5	0-1.3	0-1
[60]	313.15-373.15	0.001-70	0.001-70	15.3	0-3.2	0-1.2
Prediction						
[8]	373.15	0.00024-0.0392	0.000027-0.0136	15.3	0.0181-0.136	0.0062-0.141

Table B.8: Experimental database for CO_2-H_2S-MDEA-H_2O mixture.

References	T-range (K)	P_{H2S}-range (bar)	P_{CO2}-range (bar)	MDEA % w/w	H_2S loading	CO_2 loading
Correlation						
[61]	313.15-373.15	0.000323-1.96	0.00005-5.29	35	0.00351-0.888	0.00017-0.788
Prediction						
[18]	313.15-373.15	0.00381-1.2	0.00144-7.72	50	0.01-0.302	0.0024-0.981
[24]	313.15-323.15	0-0.05268	0.000001-0.017	23-50	0-0.313	0.00003-0.1023

Table B.9: Experimental database used for fitting procedure of H$_2$S-gases and H$_2$S-HC mixtures.

Hydrogen Sulfide with	Ref	NP_p	NP_y	T-range (K)	P-range (bar)	x_{H2S} range	y_{H2S} range
Nitrogen	[62 63]	71	71	200.15-344.3	3.3-212.9	0.839-0.9996	0.0127-0.892
Methane	[64 65]	109	109	188.7-366.5	13.8-131	0.5599-0.9993	0.031-0.9883
Ethane	[66 67]	51	51	182-283.15	0.6-30.5	0.0259-0.9915	0.0297-0.9112
Propane	[67 68]	27	27	182-288.15	0.1-17	0.033-0.967	0.1-0.95
n-Butane	[67 69]	57	57	182-418	0.06-79	0.0099-0.993	0.0195-0.994
isobutane	[70]	34	34	277-378	2.1-62	0.0175-0.9772	0.127-0.9846
n-pentane	[71]	53	53	277-444	1.4-90	0.0062-0.966	0.0559-0.993
neopentane	[72]	28	28	323-413	6-73.1	0.01-0.998	0.034-0.999
isopentane	[72]	33	33	323-413	3.1-83	0.009-0.993	0.071-0.996
n-hexane	[73]	25	25	323-423	4.1-76	0.023-0.914	0.184-0.9874
n-heptane	[74]	49	49	311-478	1.5-96	0.0177-0.927	0.104-0.997
isooctane	[75]	19	0	323-473	2-16.6	0.0246-0.2598	
n-nonane	[76]	15	15	310-478	1.4-28	0.0419-0.2088	0.5449-0.9975
n-decane	[77 75]	68	30	278-523	1.3-124.1	0.0181-0.9324	0.9234-0.999
n-dodecane	[78]	33	0	313-434	5.2-57	0.07-0.902	
n-tridecane	[75]	25	0	373-523	2.02-11.23	0.0187-0.1822	
n-pentadecane	[73]	8	8	422.6	11.3-112.1	0.167-0.843	0.996-0.9987
n-hexadecane	[79 75]	53	0	323-473	2.1-74	0.0233-0.878	
n-eicosane	[80]	35	0	323-423	4.04-77	0.0669-0.908	
cyC6	[73]	24	24	323-422.6	4-94.95	0.0544-0.89	0.477-0.9895
mcyC6	[81]	29	29	310.9-477.6	2.5-94.5	0.029-0.97	0.411-0.999
ecyC6	[82]	28	28	310.9-477.6	1.7-125	0.016-0.9841	0.3444-0.9998
pcyC6	[82]	35	35	310.9-477.6	1.7-130.6	0.0418-0.9832	0.6356-0.9998
Benzene	[73, 83]	46	24	304.3-422.6	1.02-98	0.0339-0.936	0.437-0.9966
m-xylene	[84]	30	30	310.9-477.6	1.5-131.2	0.0206-0.9931	0.5592-0.9999
Toluene	[74]	27	27	310.9-477.6	2.03-115-8	0.031-0.954	0.352-0.999
Propyl-benzene	[85]	25	25	313.2-473.5	3.9-129.7	0.093-0.921	0.787-0.9999
Mesitylene	[84]	29	29	310.9-477.6	1.72-137.5	0.028-0.9953	0.6247-0.9999

Table B.10: Molecular weight of ionic liquids.

Ionic liquid	Reference	Molecular weight (g/mol)
[emim]PF$_6$	[86]	256.2
[bmim]PF$_6$	[86]	284.2
[hmim]PF$_6$	[86]	312.2
[omim]PF$_6$	[86]	340.3
[emim]Tf$_2$N	[86]	391.2
[bmim]Tf$_2$N	[86]	419.2

[hmim]Tf$_2$N	[86]		447.3
[omim]Tf$_2$N	[86]		475.4
[emim]BF$_4$	[86]		198.0
[bmim]BF$_4$	[86]		226.0
[hmim]BF$_4$	[86]		254.0
[omim]BF$_4$	[86]		282.1

Table B.11: Experimental database of liquid density of ionic liquids.

	References	NP	T-range (K)	ρ (kg/m3)
[emim]PF$_6$	[87]	2	353.15-373.15	1422-1405
[bmim]PF$_6$	[88-89 90-92]	64	278.15-413.2	1276-1385.4
[hmim]PF$_6$	[93-95]	47	277.88-393.15	1219.4-1308.85
[omim]PF$_6$	[92-93, 96-97]	53	273.1-393.15	1166-1256.1
[emim]Tf$_2$N	[98-99]	38	273.15-473.15	1345.2-1543.92
[bmim]Tf$_2$N	[100-101]	29	273.15-473.15	1272-1460.4
[hmim]Tf$_2$N	[99, 102]	38	258.15-473.15	1214.9-1407.6
[omim]Tf$_2$N	[99, 103-104]	34	273.15-473.15	1168.8-1340
[emim]BF$_4$	[105-108]	55	278.15-363.15	1235.5-1299.1
[bmim]BF$_4$	[109-111]	17	264.16-393.15	1136.1-1227.3
[hmim]BF$_4$	[95, 112-115]	78	268.65-373.15	1094.5-1166.6
[omim]BF$_4$	[93]	11	293.15-393.15	1040.9-1108.7

Table B.12: Experimental database of vapor pressure of ionic liquids.

		T-range (K)	Vapor pressure-range (bar)
[emim]PF$_6$	[116]	414.05-456.79	6.5E-11-2.24E-09
[bmim]PF$_6$	[116]	402.56-449.91	2.4E-11-1.83E-09
[hmim]PF$_6$	[116]	407.51-454.94	3.1E-11-2.29E-09
[omim]PF$_6$	[116]	410.29-455.54	2.2E-11-1.46E-09
[emim]Tf$_2$N	[117-118]	441.7-484.16	6.2E-08-1.09E-06
[bmim]Tf$_2$N	[117-118]	437.84-517.45	3.6E-08-5.15E-06
[hmim]Tf$_2$N	[117-118]	445.79-493.67	6.7E-08-1.72E-06
[omim]Tf$_2$N	[117-118]	455.46-498.19	7.8E-08-1.542E-06
[bmim]BF$_4$	[119]	396.3-465.5	7.2E-12-1.7E-09

Table B.13:Experimental database of CO$_2$ solubility in ionic liquids.

CO$_2$ with	References	NP	T-range (K)	P-range (bar)	xCO$_2$-range
[emim]PF$_6$	[120]	62	313.1-347.9	14.9-971	0.104-0.619
[bmim]PF$_6$	[109-110, 121-122]	298	283.1-393.15	0-735	0-0.65
[hmim]PF$_6$	[123-124]	108	298.15-358.52	2.96-946	0.058-0.727
[omim]PF$_6$	[125]	15	313.15-333.15	0.97-44.27	0.0001-0.452
[emim]Tf$_2$N	[126-129]	174	283.43-450.5	0.5-478.5	0.0137-0.75
[bmim]Tf$_2$N	[109, 130-132]	160	279.98-344.51	0-199.974	0-0.7562
[hmim]Tf$_2$N	[133-135]	125	282-413.2	0.09-99.11	0.001-0.721
[omim]Tf$_2$N	[136, 137]	123	298.25-353.15	1.123-175	0.0311-0.812
[emim]BF$_4$	[138-140]	36	298.2-333.2	5.05-59.86	0.0425-0.384
[bmim]BF$_4$	[109-111]	216	282.75-368.14	0.01-676.2	0.0002-0.6017
[hmim]BF$_4$	[123, 141]	111	293.18-368.14	3.12-866	0.071-0.703
[omim]BF$_4$	[125]	86	308.2-363.1	5.71-858	0.1005-0.7523

References

1.   Lee, J. I.; Otto, F. D.; Mather, A. E., Equilibrium between carbon dioxide and aqueous monoethanolamine solutions. *Journal of Applied Chemistry and Biotechnology* **1976,** *26* (1), 541-549.

2.   Jou, F.-Y.; Mather, A. E.; Otto, F. D., The solubility of CO2 in a 30 mass percent monoethanolamine solution. *The Canadian Journal of Chemical Engineering* **1995,** *73* (1), 140-147.

3.   Shen, K. P.; Li, M. H., Solubility of carbon dioxide in aqueous mixtures of monoethanolamine with methyldiethanolamine. *Journal of Chemical & Engineering Data* **1992,** *37* (1), 96-100.

4.   Austgen, D. M.; Rochelle, G. T.; Chen, C. C., Model of vapor-liquid equilibria for aqueous acid gas-alkanolamine systems. 2. Representation of hydrogen sulfide and carbon dioxide solubility in aqueous MDEA and carbon dioxide solubility in aqueous mixtures of MDEA with MEA or DEA. *Industrial & Engineering Chemistry Research* **1991,** *30* (3), 543-555.

5.   Xu, Q.; Rochelle, G., Total pressure and CO2 solubility at high temperature in aqueous amines. *Energy Procedia* **2011,** *4*, 117-124.

6.   Hilliard, M., A Predictive Thermodynamic Model for an Aqueous Blend of Potassium Carbonate, Piperazine, and Monoethanolamine for Carbon Dioxide Capture from Flue Gas. **2008**.

7.   Lawson, J. D.; Garst, A., Gas sweetening data: equilibrium solubility of hydrogen sulfide and carbon dioxide in aqueous monoethanolamine and aqueous diethanolamine solutions. *Journal of Chemical and Engineering Data* **1976,** *21* (1), 20-30.

8.   Isaacs, E. E.; Otto, F. D.; Mather, A. E., Solubility of mixtures of hydrogen sulfide and carbon dioxide in a monoethanolamine solution at low partial pressures. *Journal of Chemical and Engineering Data* **1980,** *25* (2), 118-120.

9.   Jane, I.-S.; Li, M.-H., Solubilities of mixtures of carbon dioxide and hydrogen sulfide in water+ diethanolamine+ 2-amino-2-methyl-1-propanol. *Journal of Chemical & Engineering Data* **1997,** *42* (1), 98-105.

10.   Jones, J.; Froning, H.; Claytor Jr, E., Solubility of Acidic Gases in Aqueous Monoethanolamine. *Journal of chemical and engineering data* **1959,** *4* (1), 85-92.

11.   Song, J.-H.; Yoon, J.-H.; Lee, H.; Lee, K.-H., Solubility of carbon dioxide in monoethanolamine+ ethylene glycol+ water and monoethanolamine+ poly (ethylene glycol)+ water. *Journal of Chemical & Engineering Data* **1996,** *41* (3), 497-499.

12.   Lee, J.; Otto, F. D.; Mather, A. E., The solubility of H2S and CO2 in aqueous monoethanolamine solutions. *The Canadian Journal of Chemical Engineering* **1974,** *52* (6), 803-805.

13.   Dawodu, O. F.; Meisen, A., Solubility of carbon dioxide in aqueous mixtures of alkanolamines. *Journal of Chemical and Engineering Data* **1994,** *39* (3), 548-552.

14.   Ma'mun, S.; Nilsen, R.; Svendsen, H. F.; Juliussen, O., Solubility of carbon dioxide in 30 mass% monoethanolamine and 50 mass% methyldiethanolamine solutions. *Journal of Chemical & Engineering Data* **2005,** *50* (2), 630-634.

15.   Park, S.-B.; Lee, H.; Lee, K.-H., Solubilities of carbon dioxide in aqueous potassium carbonate solutions mixed with physical solvents. *International journal of thermophysics* **1998,** *19* (5), 1421-1428.

16.   Aronu, U.; Gondal, S.; Hessen, E.; Haug-Warberg, T.; Hartono, A.; Hoff, K.; Svendsen, H., Solubility of CO2 in 15, 30, 45 and 60 mass% MEA from 40 to 120 °C and model representation using the extended UNIQUAC framework. *Chemical Engineering Science* **2011,** *66*, 6393–6406.

17.   Mathonat, C.; Majer, V.; Mather, A.; Grolier, J.-P., Use of flow calorimetry for determining enthalpies of absorption and the solubility of CO2 in aqueous monoethanolamine solutions. *Industrial & engineering chemistry research* **1998,** *37* (10), 4136-4141.

18.   Huang, S.; Ng, H., Solubility of H2S and CO2 in Alkanolamines: GPA Research Report RR-155. **1998**.

19.   Jou, F. Y.; Mather, A. E.; Otto, F. D., Solubility of hydrogen sulfide and carbon dioxide in aqueous methyldiethanolamine solutions. *Industrial & Engineering Chemistry Process Design and Development* **1982,** *21* (4), 539-544.

20.   Jou, F. Y.; Carroll, J. J.; Mather, A. E.; Otto, F. D., The solubility of carbon dioxide and hydrogen sulfide in a 35 wt% aqueous solution of methyldiethanolamine. *The Canadian Journal of Chemical Engineering* **1993,** *71* (2), 264-268.

21.   Jou, F.-Y.; Otto, F. D.; Mather, A. E., Vapor-liquid equilibrium of carbon dioxide in aqueous mixtures of monoethanolamine and methyldiethanolamine. *Industrial & engineering chemistry research* **1994,** *33* (8), 2002-2005.

22.   Silkenbäumer, D.; Rumpf, B.; Lichtenthaler, R. N., Solubility of Carbon Dioxide in Aqueous Solutions of 2-Amino-2-methyl-1-propanol and N-Methyldiethanolamine and

Their Mixtures in the Temperature Range from 313 to 353 K and Pressures up to 2.7 MPa. *Industrial & engineering chemistry research* **1998,** *37* (8), 3133-3141.

23.   Sidi-Boumedine, R.; Horstmann, S.; Fischer, K.; Provost, E.; Fürst, W.; Gmehling, J., Experimental determination of carbon dioxide solubility data in aqueous alkanolamine solutions. *Fluid phase equilibria* **2004,** *218* (1), 85-94.

24.   Rogers, W. J.; Bullin, J. A.; Davison, R. R., FTIR measurements of acid-gas–methyldiethanolamine systems. *AIChE journal* **1998,** *44* (11), 2423-2430.

25.   Kuranov, G.; Rumpf, B.; Smirnova, N. A.; Maurer, G., Solubility of single gases carbon dioxide and hydrogen sulfide in aqueous solutions of N-methyldiethanolamine in the temperature range 313– 413 K at pressures up to 5 MPa. *Industrial & engineering chemistry research* **1996,** *35* (6), 1959-1966.

26.   Rho, S.-W.; Yoo, K.-P.; Lee, J. S.; Nam, S. C.; Son, J. E.; Min, B.-M., Solubility of CO2 in Aqueous Methyldiethanolamine Solutions. *Journal of Chemical & Engineering Data* **1997,** *42* (6), 1161-1164.

27.   Kamps, Á. P.-S.; Balaban, A.; Jödecke, M.; Kuranov, G.; Smirnova, N. A.; Maurer, G., Solubility of single gases carbon dioxide and hydrogen sulfide in aqueous solutions of N-methyldiethanolamine at temperatures from 313 to 393 K and pressures up to 7.6 MPa: new experimental data and model extension. *Industrial & engineering chemistry research* **2001,** *40* (2), 696-706.

28.   Addicks, J.; Owren, G. A.; Fredheim, A. O.; Tangvik, K., Solubility of carbon dioxide and methane in aqueous methyldiethanolamine solutions. *Journal of Chemical & Engineering Data* **2002,** *47* (4), 855-860.

29.   Macgregor, R. J.; Mather, A. E., Equilibrium solubility of H2S and CO2 and their mixtures in a mixed solvent. *The Canadian Journal of Chemical Engineering* **1991,** *69* (6), 1357-1366.

30.   Chakma, A.; Meisen, A., Solubility of carbon dioxide in aqueous methyldiethanolamine and N,N-bis(hydroxyethyl)piperazine solutions. *Industrial & Engineering Chemistry Research* **1987,** *26* (12), 2461-2466.

31.   Mathonat, C.; Majer, V.; Mather, A.; Grolier, J.-P., Enthalpies of absorption and solubility of CO2 in aqueous solutions of methyldiethanolamine. *Fluid phase equilibria* **1997,** *140* (1-2), 171-182.

32.   Baek, J.-I.; Yoon, J.-H., Solubility of carbon dioxide in aqueous solutions of 2-amino-2-methyl-1, 3-propanediol. *Journal of Chemical & Engineering Data* **1998,** *43* (4), 635-637.

33.   Kamps, Á. P. S.; Rumpf, B.; Maurer, G.; Anoufrikov, Y.; Kuranov, G.; Smirnova, N. A., Solubility of CO2 in H2O+ N-methyldiethanolamine+(H2SO4 or Na2SO4). *AIChE Journal* **2002,** *48* (1), 168-177.

34.   Ali, B. S.; Aroua, M. K., Effect of Piperazine on CO 2 Loading in Aqueous Solutions of MDEA at Low Pressure. *International Journal of Thermophysics* **2004,** *25* (6), 1863-1870.

35.   Xu, G.-W.; Zhang, C.-F.; Qin, S.-J.; Gao, W.-H.; Liu, H.-B., Gas– liquid equilibrium in a CO2– MDEA– H2O system and the effect of piperazine on it. *Industrial & engineering chemistry research* **1998,** *37* (4), 1473-1477.

36.   Park, M. K.; Sandall, O. C., Solubility of carbon dioxide and nitrous oxide in 50 mass methyldiethanolamine. *Journal of Chemical & Engineering Data* **2001,** *46* (1), 166-168.

37.   Bhairi, A. M. Experimental equilibrium between acid gases and ethanolamine solutions. Oklahoma State University, 1984.

38.   Bishnoi,   S.;   Rochelle,   G.   T.,   Thermodynamics   of Piperazine/Methyldiethanolamine/Water/Carbon Dioxide. *Industrial & Engineering Chemistry Research* **2002,** *41* (3), 604-612.

39.   Jou, F.-Y.; Mather, A. E., Solubility of Methane in Methyldiethanolamine. *Journal of Chemical & Engineering Data* **2006,** *51* (4), 1429-1430.

40.   Jou, F.-Y.; Carroll, J. J.; Mather, A. E.; Otto, F. D., Solubility of Methane and Ethane in Aqueous Solutions of Methyldiethanolamine. *Journal of Chemical & Engineering Data* **1998,** *43* (5), 781-784.

41.   Schmidt, K. A. G.; Jou, F.-Y.; Mather, A. E., Solubility of Methane in an Aqueous Methyldiethanolamine Solution (Mass Fraction 50 %). *Journal of Chemical & Engineering Data* **2008,** *53* (8), 1725-1727.

42.   Clarke, E. C. W.; Glew, D. N., Aqueous Nonelectrolyte Solutions. Part VIII. Deuterium and Hydrogen Sulfides Solubilities in Deuterium Oxide and Water. *Canadian Journal of Chemistry* **1971,** *49* (5), 691-698.

43.   Burgess, M. P.; Germann, R. P., Physical properties of hydrogen sulfide-water mixtures. *AIChE Journal* **1969,** *15* (2), 272-275.

44.   Gillespie, P. C.; Wilson, G. M.; Gas Processors, A., *Vapor-liquid and liquid-liquid equilibria : water-methane, water-carbon dioxide, water-hydrogen sulfide, water-npentane, water-methane-npentane*. Gas Processors Association: Tulsa, Okla., 1982.

45.   Selleck, F. T.; Carmichael, L. T.; Sage, B. H., Phase Behavior in the Hydrogen Sulfide-Water System. *Industrial & Engineering Chemistry* **1952,** *44* (9), 2219-2226.

46.   Yu, Q. L., D.; Liu, R.; Zhou, H.; Chen, M.; Chen, G.; Chen, Y.; Hu, Y.; Xu, X.; Shen, L.; Han, S.-J., , VLE OF H2S-H2O System. *Chemical Engineering (China)* **1980,** *4*.

47.   Bierlein, J. A.; Kay, W. B., Phase-Equilibrium Properties of System Carbon Dioxide-Hydrogen Sulfide. *Industrial & Engineering Chemistry* **1953,** *45* (3), 618-624.

48.   Chapoy, A.; Coquelet, C.; Liu, H.; Valtz, A.; Tohidi, B., Vapour–liquid equilibrium data for the hydrogen sulphide (H2S)+carbon dioxide (CO2) system at temperatures from 258 to 313K. *Fluid Phase Equilibria* **2013,** *356*, 223-228.

49.   Sobocinski, D. P.; Kurata, F., Heterogeneous phase equilibria of the hydrogen sulfide–carbon dioxide system. *AIChE Journal* **1959,** *5* (4), 545-551.

50.   Lee, J. I.; Otto, F. D.; Mather, A. E., Equilibrium in hydrogen sulfide-monoethanolamine-water system. *Journal of Chemical & Engineering Data* **1976,** *21* (2), 207-208.

51.   Lawson, J. D.; Garst, A. W., Gas sweetening data: equilibrium solubility of hydrogen sulfide and carbon dioxide in aqueous monoethanolamine and aqueous diethanolamine solutions. *Journal of Chemical & Engineering Data* **1976,** *21* (1), 20-30.

52.   Lee, J. I.; Otto, F. D.; Mather, A. E., The solubility of H2S and CO2 in aqueous monoethanolamine solutions. *The Canadian Journal of Chemical Engineering* **1974,** *52* (6), 803-805.

53.   Maddox, R. N. B., A. H.; Diers, J. R.; Thomas, P. A. , Equilibrium Solubility of Carbon Dioxide or Hydrogen Sulfide in Aqueous Solutions of Monoethanolamine, Diglycolamine, Diethanolamine and Methyldiethanolamine. *Gas Processors, A.; Gas Research, I* **1987**.

54.   Li, M. H.; Shen, K. P., Solubility of hydrogen sulfide in aqueous mixtures of monoethanolamine with N-methyldiethanolamine. *Journal of Chemical & Engineering Data* **1993,** *38* (1), 105-108.

55.   Riegger, E.; Tartar, H. V.; Lingafelter, E. C., Equilibria between Hydrogen Sulfide and Aqueous Solutions of Monoethanolamine at 25°, 45° and 60°. *Journal of the American Chemical Society* **1944,** *66* (12), 2024-2027.

56.   Lemoine, B.; Li, Y.-G.; Cadours, R.; Bouallou, C.; Richon, D., Partial Vapor Pressure of CO2 and H2S Over Aqueous Methyldiethanolamine Solutions. *Fluid Phase Equilibria* **2000,** *172*, 261-277.

57.   Sidi-Boumedine, R.; Horstmann, S.; Fischer, K.; Provost, E.; Fürst, W.; Gmehling, J., Experimental determination of hydrogen sulfide solubility data in aqueous alkanolamine solutions. *Fluid Phase Equilibria* **2004,** *218*, 149-155.

58.   Jou, F.-Y.; Carroll, J. J.; Mather, A. E.; Otto, F. D., The solubility of carbon dioxide and hydrogen sulfide in a 35 wt% aqueous solution of methyldiethanolamine. *The Canadian Journal of Chemical Engineering* **1993,** *71* (2), 264-268.

59.   Lee, J. I.; Otto, F. D.; Mather, A. E., Solubility of mixtures of carbon dioxide and hydrogen sulfide in 5.0N monoethanolamine solution. *Journal of Chemical & Engineering Data* **1975,** *20* (2), 161-163.

60.   Lee, J. I.; Otto, F. D.; Mather, A. E., The measurement and prediction of the solubility of mixtures of carbon dioxide and hydrogen sulphide in a 2.5 N monoethanolamine solution. *The Canadian Journal of Chemical Engineering* **1976,** *54* (3), 214-219.

61.   Jou, F. Y.; Carroll, J. J.; Mather, A. E.; Otto, F. D., Solubility of mixtures of hydrogen sulfide and carbon dioxide in aqueous N-methyldiethanolamine solutions. *Journal of Chemical & Engineering Data* **1993,** *38* (1), 75-77.

62.   Kalra, H.; Krishnana, T. R.; Robinson, D. B., Equilibrium-phase properties of carbon dioxide-butane and nitrogen-hydrogen sulfide systems at subambient temperatures. *Journal of Chemical and Engineering Data* **1976,** *21* (2), 222-225.

63.   Besserer, G. J.; Robinson, D. B., Equilibrium-phase properties of nitrogen-hydrogen sulfide system. *Journal of Chemical and Engineering Data* **1975,** *20* (2), 157-161.

64.   Reamer, H.; Sage, B.; Lacey, W., Phase equilibria in hydrocarbon systems-volumetric and phase behavior of the methane-hydrogen sulfide system. *Industrial & Engineering Chemistry* **1951,** *43* (4), 976-981.

65.   Kohn, J. P.; Kurata, F., Heterogeneous phase equilibria of the methane—hydrogen sulfide system. *AIChE Journal* **1958,** *4* (2), 211-217.

66.   Kalra, H.; Robinson, D. B.; Krishnan, T. R., The equilibrium phase properties of the ethane-hydrogen sulfide system at subambient temperatures. *Journal of Chemical and Engineering Data* **1977,** *22* (1), 85-88.

67.   Lobo, L.; Ferreira, A.; Fonseca, I.; Senra, A., Vapour pressure and excess Gibbs free energy of binary mixtures of hydrogen sulphide with ethane, propane, and n-butane at

temperature of 182.33 K. *The Journal of Chemical Thermodynamics* **2006,** *38* (12), 1651-1654.

68.   Von Steckel, F., Dampf-Flussigkeits-Gleichgewichte einiger binarer, schwefelwasserstoffhaltiger systeme unter Druck. *Svensk Kemisk Tidskrift* **1945,** *9*, 209-216.

69.   Leu, A. D.; Robinson, D. B., Equilibrium phase properties of the n-butane-hydrogen sulfide and isobutane-hydrogen sulfide binary systems. *Journal of Chemical and Engineering Data* **1989,** *34* (3), 315-319.

70.   Knapp, H.; Döring, R.; Oellrich, L.; Plöcker, U.; Prausnitz, J., Chemistry Data Series, Vol. VI. *VLE for Mixtures of Low Boiling Substances, D. Behrens and R. Eckerman, eds., Frankfurt AM, DECHEMA, Germany* **1982**.

71.   Reamer, H.; Sage, B.; Lacey, W., Phase equilibria in hydrocarbon systems-volumetric and phase behavior of n-pentane–hydrogen sulfide system. *Industrial & Engineering Chemistry* **1953,** *45* (8), 1805-1809.

72.   Leu, A. D.; Robinson, D. B., High-pressure vapor-liquid equilibrium phase properties of the isopentane-hydrogen sulfide and neopentane-hydrogen sulfide binary systems. *Journal of Chemical and Engineering Data* **1992,** *37* (1), 14-17.

73.   Laugier, S.; Richon, D., Vapor-liquid equilibria for hydrogen sulfide+ hexane,+ cyclohexane,+ benzene,+ pentadecane, and+(hexane+ pentadecane). *Journal of Chemical and Engineering Data* **1995,** *40* (1), 153-159.

74.   Ng, H.-J.; Kalra, H.; Robinson, D. B.; Kubota, H., Equilibrium phase properties of the toluene-hydrogen sulfide and heptane-hydrogen sulfide binary systems. *Journal of Chemical and Engineering Data* **1980,** *25* (1), 51-55.

75.   Yokoyama, C.; Usui, A.; Takahashi, S., Solubility of hydrogen sulfide in isooctane, n-decane, n-tridecane, n-hexadecane and squalane at temperatures from 323 to 523 K and pressures up to 1.6 MPa. *Fluid phase equilibria* **1993,** *85*, 257-269.

76.   Eakin, B.; De Vaney, W., Vapor-liquid equilibria in hydrogen-hydrogen sulfide-C9 hydrocarbon systems. **1974**.

77.   Reamer, H.; Selleck, F.; Sage, B.; Lacey, W., PHASE EQUILIBRIA IN HYDROCARBON SYSTEMS-Volumetric and Phase Behavior of Decane–Hydrogen Sulfide System. *Industrial & Engineering Chemistry* **1953,** *45* (8), 1810-1812.

78.   Feng, G.-X.; Mather, A. E., Solubility of H2S in n-dodecane. *Fluid phase equilibria* **1993,** *87* (2), 341-346.

79.   Feng, G. X.; Mather, A. E., Solubility of H2S in n-hexadecane at elevated pressure. *The Canadian Journal of Chemical Engineering* **1993,** *71* (2), 327-328.

80.   Feng, G. X.; Mather, A. E., Solubility of hydrogen sulfide in n-eicosane at elevated pressure. *Journal of Chemical and Engineering Data* **1992,** *37* (4), 412-413.

81.   Ng, H.-J.; Robinson, D. B., The equilibrium phase properties of selected naphthenic binary systems: carbon dioxide-methylcyclohexane, hydrogen sulfide-methylcyclohexane. *Fluid Phase Equilibria* **1979,** *2* (4), 283-292.

82.   Huang, S. S.; Robinson, D. B., Equilibrium phase properties of the ethylcyclohexane-hydrogen sulfide and n-propylcyclohexane-hydrogen sulfide binary systems. *Journal of Chemical and Engineering Data* **1985,** *30* (2), 154-157.

83.   Fischer, K.; Chen, J.; Petri, M.; Gmehling, J., Solubility of H2S and CO2 in N-octyl-2-pyrrolidone and of H2S in methanol and benzene. *AIChE journal* **2002,** *48* (4), 887-893.

84.   Huang, S. S.-S.; Robinson, D. B., Vapor-liquid equilibrium in selected aromatic binary systems: m-xylene-hydrogen sulfide and mesitylene-hydrogen sulfide. *Fluid phase equilibria* **1984,** *17* (3), 373-382.

85.   Richon, D.; Laugier, S.; Renon, H., High-pressure vapor-liquid equilibrium data for binary mixtures containing molecular nitrogen, carbon dioxide, hydrogen sulfide and an aromatic hydrocarbon or propylcyclohexane in the range 313-473 K. *Journal of Chemical and Engineering Data* **1992,** *37* (2), 264-268.

86.   Valderrama, J.; Robles, P., Critical properties, normal boiling temperatures, and acentric factors of fifty ionic liquids. *Industrial & Engineering Chemistry Research* **2007,** *46* (4), 1338-1344.

87.   Taguchi, R.; Machida, H.; Sato, Y.; Smith Jr, R. L., High-Pressure Densities of 1-Alkyl-3-methylimidazolium Hexafluorophosphates and 1-Alkyl-3-methylimidazolium Tetrafluoroborates at Temperatures from (313 to 473) K and at Pressures up to 200 MPa. *Journal of Chemical & Engineering Data* **2009,** *54* (1), 22-27.

88.   Currás, M. R.; Mato, M. M.; Sanchez, P. B.; Garcia, J., Experimental densities of 2, 2, 2-trifluoroethanol with 1-butyl-3-methylimidazolium hexafluorophosphate at high pressures and modelling with PC-SAFT. *The Journal of Chemical Thermodynamics* **2017,** *113*, 29-40.

89.   Qiao, Y.; Yan, F.; Xia, S.; Yin, S.; Ma, P., Densities and viscosities of [Bmim][PF6] and binary systems [Bmim][PF6]+ ethanol,[Bmim][PF6]+ benzene at several temperatures and pressures: determined by the falling-ball method. *Journal of chemical & engineering data* **2011,** *56* (5), 2379-2385.

90.   Salgado, J.; Regueira, T.; Lugo, L.; Vijande, J.; Fernández, J.; García, J., Density and viscosity of three (2, 2, 2-trifluoroethanol+ 1-butyl-3-methylimidazolium) ionic liquid binary systems. *The Journal of Chemical Thermodynamics* **2014,** *70*, 101-110.

91.   Almeida, H. F.; Canongia Lopes, J. N.; Rebelo, L. P.; Coutinho, J. o. A.; Freire, M. G.; Marrucho, I. M., Densities and viscosities of mixtures of two ionic liquids containing a common cation. *Journal of Chemical & Engineering Data* **2016,** *61* (8), 2828-2843.

92.   Rocha, M. A.; Ribeiro, F. M.; Ferreira, A. I. L.; Coutinho, J. A.; Santos, L. M., Thermophysical properties of [CN– 1C1im][PF6] ionic liquids. *Journal of Molecular Liquids* **2013,** *188*, 196-202.

93.   Gardas, R. L.; Freire, M. G.; Carvalho, P. J.; Marrucho, I. M.; Fonseca, I. M.; Ferreira, A. G.; Coutinho, J. A., High-pressure densities and derived thermodynamic properties of imidazolium-based ionic liquids. *Journal of Chemical & Engineering Data* **2007,** *52* (1), 80-88.

94.   Klomfar, J.; Součková, M.; Pátek, J., Low Temperature Densities from (218 to 364) K and up to 50 MPa in Pressure and Surface Tension for Trihexyl (tetradecyl) phosphonium Bis (trifluoromethylsulfonyl) imide and Dicyanamide and 1-Hexyl-3-methylimidazolium Hexafluorophosphate. *Journal of Chemical & Engineering Data* **2014,** *59* (7), 2263-2274.

95.   Vakili-Nezhaad, G.; Vatani, M.; Asghari, M.; Ashour, I., Effect of temperature on the physical properties of 1-butyl-3-methylimidazolium based ionic liquids with thiocyanate and tetrafluoroborate anions, and 1-hexyl-3-methylimidazolium with

tetrafluoroborate and hexafluorophosphate anions. *The Journal of Chemical Thermodynamics* **2012,** *54*, 148-154.

96. Pereiro, A. B.; Legido, J. L.; Rodrı́guez, A., Physical properties of ionic liquids based on 1-alkyl-3-methylimidazolium cation and hexafluorophosphate as anion and temperature dependence. *The Journal of Chemical Thermodynamics* **2007,** *39* (8), 1168-1175.

97. Harris, K. R.; Kanakubo, M.; Woolf, L. A., Temperature and Pressure Dependence of the Viscosity of the Ionic Liquids 1-Methyl-3-octylimidazolium Hexafluorophosphate and 1-Methyl-3-octylimidazolium Tetrafluoroborate. *Journal of Chemical & Engineering Data* **2006,** *51* (3), 1161-1167.

98. Fröba, A. P.; Kremer, H.; Leipertz, A., Density, Refractive Index, Interfacial Tension, and Viscosity of Ionic Liquids [EMIM][EtSO4], [EMIM][NTf2], [EMIM][N(CN)2], and [OMA][NTf2] in Dependence on Temperature at Atmospheric Pressure. *The Journal of Physical Chemistry B* **2008,** *112* (39), 12420-12430.

99. Tariq, M.; Serro, A. P.; Mata, J. L.; Saramago, B.; Esperança, J. M.; Lopes, J. N. C.; Rebelo, L. P. N., High-temperature surface tension and density measurements of 1-alkyl-3-methylimidazolium bistriflamide ionic liquids. *Fluid phase equilibria* **2010,** *294* (1-2), 131-138.

100. Nieto de Castro, C. A.; Langa, E.; Morais, A. L.; Lopes, M. L. M.; Lourenço, M. J. V.; Santos, F. J. V.; Santos, M. S. C. S.; Lopes, J. N. C.; Veiga, H. I. M.; Macatrão, M.; Esperança, J. M. S. S.; Marques, C. S.; Rebelo, L. P. N.; Afonso, C. A. M., Studies on the density, heat capacity, surface tension and infinite dilution diffusion with the ionic liquids [C4mim][NTf2], [C4mim][dca], [C2mim][EtOSO3] and [Aliquat][dca]. *Fluid Phase Equilibria* **2010,** *294* (1), 157-179.

101. Hamidova, R.; Kul, I.; Safarov, J.; Shahverdiyev, A.; Hassel, E., Thermophysical properties of 1-butyl-3-methylimidazolium bis (trifluoromethylsulfonyl) imide at high temperatures and pressures. *Brazilian Journal of Chemical Engineering* **2015,** *32* (1), 303-316.

102. Widegren, J. A.; Magee, J. W., Density, viscosity, speed of sound, and electrolytic conductivity for the ionic liquid 1-hexyl-3-methylimidazolium bis (trifluoromethylsulfonyl) imide and its mixtures with water. *Journal of Chemical & Engineering Data* **2007,** *52* (6), 2331-2338.

103. Papović, S.; Bešter-Rogač, M.; Vraneš, M.; Gadžurić, S., The effect of the alkyl chain length on physicochemical features of (ionic liquids+ γ-butyrolactone) binary mixtures. *The Journal of Chemical Thermodynamics* **2016,** *99*, 1-10.

104. Montalbán, M.; Bolívar, C.; Diaz Banos, F. G.; Víllora, G., Effect of temperature, anion, and alkyl chain length on the density and refractive index of 1-alkyl-3-methylimidazolium-based ionic liquids. *Journal of Chemical & Engineering Data* **2015,** *60* (7), 1986-1996.

105. Neves, C. M.; Kurnia, K. A.; Coutinho, J. o. A.; Marrucho, I. M.; Lopes, J. N. C.; Freire, M. G.; Rebelo, L. P. N., Systematic study of the thermophysical properties of imidazolium-based ionic liquids with cyano-functionalized anions. *The Journal of Physical Chemistry B* **2013,** *117* (35), 10271-10283.

106.   Klomfar, J.; Součková, M.; Pátek, J., Buoyancy density measurements for 1-alkyl-3-methylimidazolium based ionic liquids with tetrafluoroborate anion. *Fluid phase equilibria* **2009,** *282* (1), 31-37.

107.   Jia-zhen, Y.; Jing-Bin, L.; Jing, T.; Mei, H., Study on the density and surface tension of ionic liquid EMIBF4 in terms of standard addition method. **2007.**

108.   Zarei, H.; Keley, V., Density and speed of sound of binary mixtures of ionic liquid 1-ethyl-3-methylimidazolium tetrafluoroborate, N, N-dimethylformamide, and N, N-dimethylacetamide at temperature range of 293.15–343.15 K: measurement and PC-SAFT modeling. *Journal of Chemical & Engineering Data* **2017,** *62* (3), 913-923.

109.   Anthony, J. L.; Anderson, J. L.; Maginn, E. J.; Brennecke, J. F., Anion effects on gas solubility in ionic liquids. *The Journal of Physical Chemistry B* **2005,** *109* (13), 6366-6374.

110.   Shiflett, M. B.; Yokozeki, A., Solubilities and diffusivities of carbon dioxide in ionic liquids:[bmim][PF6] and [bmim][BF4]. *Industrial & Engineering Chemistry Research* **2005,** *44* (12), 4453-4464.

111.   Kroon, M. C.; Shariati, A.; Costantini, M.; van Spronsen, J.; Witkamp, G.-J.; Sheldon, R. A.; Peters, C. J., High-pressure phase behavior of systems with ionic liquids: Part V. The binary system carbon dioxide+ 1-butyl-3-methylimidazolium tetrafluoroborate. *Journal of Chemical & Engineering Data* **2005,** *50* (1), 173-176.

112.   Sanmamed, Y.; González-Salgado, D.; Troncoso, J.; Romani, L.; Baylaucq, A.; Boned, C., Experimental methodology for precise determination of density of RTILs as a function of temperature and pressure using vibrating tube densimeters. *The Journal of Chemical Thermodynamics* **2010,** *42* (4), 553-563.

113.   Sanmamed, Y.; González-Salgado, D.; Troncoso, J.; Cerdeirina, C.; Romani, L., Viscosity-induced errors in the density determination of room temperature ionic liquids using vibrating tube densitometry. *Fluid phase equilibria* **2007,** *252* (1-2), 96-102.

114.   Klomfar, J.; Součková, M.; Pátek, J., Temperature dependence measurements of the density at 0.1 MPa for 1-alkyl-3-methylimidazolium-based ionic liquids with the trifluoromethanesulfonate and tetrafluoroborate anion. *Journal of Chemical & Engineering Data* **2010,** *55* (9), 4054-4057.

115.   Navia, P.; Troncoso, J.; Romaní, L., Excess magnitudes for ionic liquid binary mixtures with a common ion. *Journal of Chemical & Engineering Data* **2007,** *52* (4), 1369-1374.

116.   Zaitsau, D. H.; Yermalayeu, A. V.; Emel'yanenko, V. N.; Butler, S.; Schubert, T.; Verevkin, S. P., Thermodynamics of Imidazolium-Based Ionic Liquids Containing PF6 Anions. *The Journal of Physical Chemistry B* **2016,** *120* (32), 7949-7957.

117.   Zaitsau, D. H.; Kabo, G. J.; Strechan, A. A.; Paulechka, Y. U.; Tschersich, A.; Verevkin, S. P.; Heintz, A., Experimental Vapor Pressures of 1-Alkyl-3-methylimidazolium Bis(trifluoromethylsulfonyl)imides and a Correlation Scheme for Estimation of Vaporization Enthalpies of Ionic Liquids. *The Journal of Physical Chemistry A* **2006,** *110* (22), 7303-7306.

118.   Rocha, M. A. A.; Lima, C. F. R. A. C.; Gomes, L. R.; Schröder, B.; Coutinho, J. A. P.; Marrucho, I. M.; Esperança, J. M. S. S.; Rebelo, L. P. N.; Shimizu, K.; Lopes, J. N. C.; Santos, L. M. N. B. F., High-Accuracy Vapor Pressure Data of the Extended [CnC1im][Ntf2] Ionic

Liquid Series: Trend Changes and Structural Shifts. *The Journal of Physical Chemistry B* **2011,** *115* (37), 10919-10926.

119.   Krannich, M.; Heym, F.; Jess, A., Characterization of Six Hygroscopic Ionic Liquids with Regard to Their Suitability for Gas Dehydration: Density, Viscosity, Thermal and Oxidative Stability, Vapor Pressure, Diffusion Coefficient, and Activity Coefficient of Water. *Journal of Chemical & Engineering Data* **2016,** *61* (3), 1162-1176.

120.   Shariati, A.; Peters, C., High-pressure phase behavior of systems with ionic liquids: II. The binary system carbon dioxide+ 1-ethyl-3-methylimidazolium hexafluorophosphate. *The Journal of supercritical fluids* **2004,** *29* (1-2), 43-48.

121.   Kim, J. E.; Lim, J. S.; Kang, J. W., Measurement and correlation of solubility of carbon dioxide in 1-alkyl-3-methylimidazolium hexafluorophosphate ionic liquids. *Fluid phase equilibria* **2011,** *306* (2), 251-255.

122.   Perez-Salado Kamps, A.; Tuma, D.; Xia, J.; Maurer, G., Solubility of CO2 in the ionic liquid [bmim][PF6]. *Journal of Chemical & Engineering Data* **2003,** *48* (3), 746-749.

123.   Kim, Y.; Choi, W.; Jang, J.; Yoo, K.-P.; Lee, C., Solubility measurement and prediction of carbon dioxide in ionic liquids. *Fluid Phase Equilibria* **2005,** *228*, 439-445.

124.   Shariati, A.; Peters, C. J., High-pressure phase behavior of systems with ionic liquids: Part III. The binary system carbon dioxide+ 1-hexyl-3-methylimidazolium hexafluorophosphate. *The Journal of supercritical fluids* **2004,** *30* (2), 139-144.

125.   Blanchard, L. A.; Gu, Z.; Brennecke, J. F., High-pressure phase behavior of ionic liquid/CO2 systems. *The Journal of Physical Chemistry B* **2001,** *105* (12), 2437-2444.

126.   Moya, C.; Gonzalez-Miquel, M.; Rodriguez, F.; Soto, A.; Rodriguez, H.; Palomar, J., Non-ideal behavior of ionic liquid mixtures to enhance CO2 capture. *Fluid Phase Equilibria* **2017,** *450*, 175-183.

127.   Carvalho, P. J.; Álvarez, V. H.; Machado, J. J.; Pauly, J.; Daridon, J.-L.; Marrucho, I. M.; Aznar, M.; Coutinho, J. A., High pressure phase behavior of carbon dioxide in 1-alkyl-3-methylimidazolium bis (trifluoromethylsulfonyl) imide ionic liquids. *The Journal of Supercritical Fluids* **2009,** *48* (2), 99-107.

128.   Schilderman, A. M.; Raeissi, S.; Peters, C. J., Solubility of carbon dioxide in the ionic liquid 1-ethyl-3-methylimidazolium bis (trifluoromethylsulfonyl) imide. *Fluid Phase Equilibria* **2007,** *260* (1), 19-22.

129.   Jacquemin, J.; Husson, P.; Majer, V.; Gomes, M. F. C., Influence of the cation on the solubility of CO 2 and H 2 in ionic liquids based on the bis (trifluoromethylsulfonyl) imide anion. *Journal of solution chemistry* **2007,** *36* (8), 967-979.

130.   Karadas, F.; Köz, B.; Jacquemin, J.; Deniz, E.; Rooney, D.; Thompson, J.; Yavuz, C. T.; Khraisheh, M.; Aparicio, S.; Atihan, M., High pressure CO2 absorption studies on imidazolium-based ionic liquids: Experimental and simulation approaches. *Fluid Phase Equilibria* **2013,** *351*, 74-86.

131.   Lee, B.-C.; Outcalt, S. L., Solubilities of Gases in the Ionic Liquid 1-n-Butyl-3-methylimidazolium Bis(trifluoromethylsulfonyl)imide. *Journal of Chemical & Engineering Data* **2006,** *51* (3), 892-897.

132.   Oh, D.-J.; Lee, B.-C., High-pressure phase behavior of carbon dioxide in ionic liquid 1-butyl-3-methylimidazolium bis (trifluoromethylsulfonyl) imide. *Korean Journal of Chemical Engineering* **2006,** *23* (5), 800-805.

133.   Shiflett, M. B.; Yokozeki, A., Solubility of CO2 in room temperature ionic liquid [hmim][Tf2N]. *The Journal of Physical Chemistry B* **2007,** *111* (8), 2070-2074.

134.   Kumełan, J.; Kamps, A. P.-S.; Tuma, D.; Maurer, G., Solubility of CO2 in the ionic liquid [hmim][Tf2N]. *The Journal of Chemical Thermodynamics* **2006,** *38* (11), 1396-1401.

135.   Yim, J.-H.; Lim, J. S., CO2 solubility measurement in 1-hexyl-3-methylimidazolium ([HMIM]) cation based ionic liquids. *Fluid Phase Equilibria* **2013,** *352*, 67-74.

136.   Jalili, A. H.; Safavi, M.; Ghotbi, C.; Mehdizadeh, A.; Hosseini-Jenab, M.; Taghikhani, V., Solubility of CO2, H2S, and their mixture in the ionic liquid 1-octyl-3-methylimidazolium bis (trifluoromethyl) sulfonylimide. *The Journal of Physical Chemistry B* **2012,** *116* (9), 2758-2774.

137.   Shin, E.-K.; Lee, B.-C.; Lim, J. S., High-pressure solubilities of carbon dioxide in ionic liquids: 1-Alkyl-3-methylimidazolium bis(trifluoromethylsulfonyl)imide. *The Journal of Supercritical Fluids* **2008,** *45* (3), 282-292.

138.   Lei, Z.; Yuan, J.; Zhu, J., Solubility of CO2 in propanone, 1-ethyl-3-methylimidazolium tetrafluoroborate, and their mixtures. *Journal of Chemical & Engineering Data* **2010,** *55* (10), 4190-4194.

139.   Lei, Z.; Han, J.; Zhang, B.; Li, Q.; Zhu, J.; Chen, B., Solubility of CO2 in binary mixtures of room-temperature ionic liquids at high pressures. *Journal of Chemical & Engineering Data* **2012,** *57* (8), 2153-2159.

140.   Watanabe, M.; Kodama, D.; Makino, T.; Kanakubo, M., CO2 absorption properties of imidazolium based ionic liquids using a magnetic suspension balance. *Fluid Phase Equilibria* **2016,** *420*, 44-49.

141.   Costantini, M.; Toussaint, V. A.; Shariati, A.; Peters, C. J.; Kikic, I., High-pressure phase behavior of systems with ionic liquids: Part IV. Binary system carbon dioxide+ 1-hexyl-3-methylimidazolium tetrafluoroborate. *Journal of Chemical & Engineering Data* **2005,** *50* (1), 52-55.

C. Appendix: Partial Derivatives of Debye-Hückel activity coefficient term

First partial derivative with respect to temperature

Density of pure solvent

$$d_n = \frac{E}{H^{\left(1+\left(1-\frac{T}{C}\right)^G\right)}} \cdot M_n \cdot 1000 \qquad\qquad \text{eq. C.1}$$

$$\frac{\partial d_n}{\partial T} = 1000 \cdot E \cdot M_n \cdot lnH \cdot \frac{G}{C} \cdot \frac{(1-\frac{T}{C})^{(G-1)}}{H^{\left(1+\left(1-\frac{T}{C}\right)^G\right)}} \qquad\qquad \text{eq. C.2}$$

$$\frac{\partial d_n{}^*}{\partial T} = E \cdot lnH \cdot \frac{G}{C} \cdot \frac{(1-\frac{T}{C})^{(G-1)}}{H^{\left(1+\left(1-\frac{T}{C}\right)^G\right)}} \qquad\qquad \text{eq. C.3}$$

Derivative of density of solvent mixture

$$\frac{\partial d_s}{\partial T} = 1000 \cdot \left(\sum_{i=1}^{Nmolecules} x_i \cdot Mr_i\right) \cdot \frac{1}{\left(\sum_{i=1}^{Nsol}\frac{x_i{'}}{d_{ni}{}^*}\right)^2} \cdot \sum_{i=1}^{Nsol} \frac{x_i{'}}{(d_{ni}{}^*)^2} \cdot \frac{\partial d_{ni}}{\partial T} \qquad \text{eq. C.4}$$

Derivative of volume with respect to temperature

$$\frac{\partial V}{\partial T} = \frac{\partial\left(\sum_{i=1}^{Nsol}\frac{x_i{'}}{d_{ni}{}^*}\right)}{\partial T} = \sum_{i=1}^{Nsol} -\frac{x_i{'}}{(d_{ni}{}^*)^2} \cdot \frac{\partial d_{ni}{}^*}{\partial T} \qquad\qquad \text{eq. C.5}$$

Derivative of dielectric constant with respect to temperature

$$\frac{\partial D_n}{\partial T} = -\frac{d^{(1)}}{T^2} + d^{(2)} + 2 \cdot d^{(3)}T + 3 \cdot d^{(4)}T^2 \qquad\qquad \text{eq. C.6}$$

Derivative of the rest terms of Debye-Hueckel term

$$\frac{\partial\frac{V_2}{V}}{\partial T} = \frac{1}{\left[\left(\sum_{i=1}^{Nsol}\frac{x_i{'}}{d_{ni}{}^*}\right)\right]^2} \cdot \left[\frac{\partial\frac{1}{d_{n2}{}^*}}{\partial T} \cdot \left(\sum_{i=1}^{Nsol}\frac{x_i{'}}{d_{ni}{}^*}\right) + \frac{1}{d_{n2}{}^*} \cdot \frac{\partial\left(\sum_{i=1}^{Nsol}\frac{x_i{'}}{d_{ni}{}^*}\right)}{\partial T}\right] \qquad \text{eq. C.7}$$

$$\frac{\partial\left[\frac{(D_2-1)\cdot(2D_2+1)}{2\cdot D_2}-(D_1-1)\right]}{\partial T} = \frac{\frac{\partial D_2}{\partial T}}{2\cdot D_2{}^2} \cdot \left(2 \cdot D_2{}^2 + 1\right) - \frac{\partial D_1}{\partial T} \qquad\qquad \text{eq. C.8}$$

Derivative of dielectric constant for one amine

$$\frac{\partial D_i}{\partial T} = \frac{\partial D_1}{\partial T} + \frac{\partial \left[\frac{(D_2-1)\cdot(2D_2+1)}{2\cdot D_2} - (D_1-1) \right]}{\partial T} \cdot x_2{}' \cdot \frac{V_2}{V} + \left[\frac{(D_2-1)\cdot(2D_2+1)}{2D_2} - (D_1-1) \right] \cdot x_2{}' \cdot \frac{\partial \frac{V_2}{V}}{\partial T} \quad \text{eq. C.9}$$

Derivative of dielectric constant for mixture of amines

$$\frac{\partial D}{\partial T} = \sum_{i=1}^{amines} x_i{}^* \cdot \frac{\partial D_i}{\partial T} \qquad\qquad \text{eq. C.10}$$

Derivative of term B with respect to temperature

$$\frac{\partial B}{\partial T} = 6{,}359696 \cdot \left[\frac{1}{2\sqrt{d_s}} \cdot \frac{\partial d_s}{\partial T} \cdot (D \cdot T)^{-\frac{1}{2}} - d_s^{\frac{1}{2}} \cdot \frac{1}{2} (D \cdot T)^{-\frac{3}{2}} \cdot \left(\frac{\partial D}{\partial T} \cdot T + D \right) \right] \qquad \text{eq. C.11}$$

Definition of two more derivatives

$$\frac{\partial F}{\partial T} = \frac{\partial \left[1032{,}379865 \cdot M_n \cdot \frac{1}{d_n} \right]}{\partial T} =>$$

$$\frac{\partial F}{\partial T} = -1032{,}379865 \cdot M_n \cdot \frac{1}{d_n{}^2} \cdot \frac{\partial d_n}{\partial T} \qquad\qquad \text{eq. C.12}$$

$$\frac{\partial P}{\partial T} = \frac{\partial \left(1 + B\sqrt{I} - \frac{1}{1+B\sqrt{I}} - 2\ln(1+B\sqrt{I}) \right)}{\partial T} =>$$

$$\frac{\partial P}{\partial T} = \left(\frac{\partial B}{\partial T} \sqrt{I} \right) \cdot \left(1 + \frac{1}{\left(1+B\sqrt{I}\right)^2} - \frac{2}{1+B\sqrt{I}} \right) \qquad\qquad \text{eq. C.13}$$

Derivative o Debye-Hueckel term

$$\frac{\partial \ln \gamma_n{}^{DH}}{\partial T} = \frac{\partial [F \cdot P]}{\partial T} =>$$

$$\frac{\partial \ln \gamma_n{}^{DH}}{\partial T} = \frac{\partial F}{\partial T} \cdot P + F \cdot \frac{\partial P}{\partial T} \qquad\qquad \text{eq. C.14}$$

Second partial derivative with respect to temperature

Second partial derivative of solvent density

$$\frac{\partial^2 d_n}{\partial T^2} = 1000 E M_n \ln H \frac{G}{C} \cdot \left[\frac{\left(-\frac{1}{C}\right)\cdot(G-1)\cdot\left(1-\frac{T}{C}\right)^{G-2} + \left(\frac{G}{C}\right)\cdot \ln H \cdot \left(1-\frac{T}{C}\right)^{2(G-1)}}{H^{\left(1+\left(1-\frac{T}{C}\right)^{G}\right)}} \right] \qquad \text{eq. C.15}$$

$$\frac{\partial^2 d_n{}^*}{\partial T^2} = ElnH\,\frac{G}{C}\cdot\left[\frac{\left(-\frac{1}{C}\right)\cdot(G-1)\cdot\left(1-\frac{T}{C}\right)^{G-2}+\left(\frac{G}{C}\right)\cdot lnH\cdot\left(1-\frac{T}{C}\right)^{2(G-1)}}{H^{\left(1+\left(1-\frac{T}{C}\right)^{G}\right)}}\right]$$
eq. C.16

Second partial derivative of volume

$$\frac{\partial^2 V}{\partial T^2} = \sum_{i=1}^{Nsol}\left(-\frac{x_i}{(d_{ni}{}^*)^2}\cdot\frac{\partial^2 d_{ni}{}^*}{\partial T^2}+\frac{x_i}{(d_{ni}{}^*)^3}\cdot 2\left(\frac{\partial d_{ni}{}^*}{\partial T}\right)^2\right)$$
eq. C.17

Second partial derivative of mixture density

$$\frac{\partial\left[-1000\cdot\left(\sum_{\iota=1}^{Nmolecules}x_i\cdot Mr_i\right)\cdot\dfrac{1}{\left(\sum_{i=1}^{Nsol}\frac{x_i{}'}{d_{ni}{}^*}\right)^2}\right]}{\partial T}$$

$$=\frac{1000\cdot\left(\sum_{\iota=1}^{Nmolecules}x_i\cdot Mr_i\right)}{\left(\sum_{i=1}^{Nsol}\frac{x_i{}'}{d_{ni}{}^*}\right)^3}\cdot 2\,\frac{\partial V}{\partial T}$$
eq. C.18

$$\frac{\partial^2 d_s}{\partial T^2} = \frac{\partial\left[-1000\cdot\left(\sum_{\iota=1}^{Nmolecules}x_i\cdot Mr_i\right)\cdot\frac{1}{\left(\sum_{i=1}^{Nsol}\frac{x_i{}'}{d_{ni}{}^*}\right)^2}\right]}{\partial T}\cdot\frac{\partial V}{\partial T}-1000\cdot\left(\sum_{\iota=1}^{Nmolecules}x_i\cdot Mr_i\right)\cdot\frac{1}{\left(\sum_{i=1}^{Nsol}\frac{x_i{}'}{d_{ni}{}^*}\right)^2}\cdot$$

$$\frac{\partial^2 V}{\partial T^2}$$
eq. C.19

Second partial derivative of dielectric constant

$$\frac{\partial^2 D_n}{\partial T^2} = \frac{\partial\left[-\frac{d^{(1)}}{T^2}+d^{(2)}+2\cdot d^{(3)}T+3\cdot d^{(4)}T^2\right]}{\partial T}\;=>$$

$$\frac{\partial^2 D_n}{\partial T^2} = 2\cdot\frac{d^{(1)}}{T^3}+2\cdot d^{(3)}+6\cdot d^{(4)}T$$
eq. C.20

$$\frac{\partial^2\left[\frac{(D_2-1)\cdot(2D_2+1)}{2\cdot D_2}-(D_1-1)\right]}{\partial T^2}=\frac{D_2\frac{\partial^2 D_2}{\partial T^2}-2\left(\frac{\partial D_2}{\partial T}\right)^2}{2(D_2)^3}\cdot\left(2D_2{}^2+1\right)+\frac{\frac{\partial D_2}{\partial T}}{2D_2{}^2}\cdot 4D_2\frac{\partial D_2}{\partial T}-\frac{\partial^2 D_1}{\partial T^2}$$
eq. C.21

$$x_2{}'\frac{\partial^2\frac{V_2}{V}}{\partial T^2}=-x_2{}'\cdot\left(-\frac{2}{\left[d_{n2}{}^*\cdot\left(\sum_{i=1}^{Nsol}\frac{x_i{}'}{d_{ni}{}^*}\right)\right]^3}\right)\cdot\left(\frac{\partial d_{n2}{}^*}{\partial T}\cdot\sum_{i=1}^{Nsol}\frac{x_i{}'}{d_{ni}{}^*}+d_{n2}{}^*\cdot\frac{\partial\left(\sum_{i=1}^{Nsol}\frac{x_i{}'}{d_{ni}{}^*}\right)}{\partial T}\right)^2-x_2{}'\cdot$$

$$\frac{1}{\left[d_{n2}{}^*\cdot\left(\sum_{i=1}^{Nsol}\frac{x_i{}'}{d_{ni}{}^*}\right)\right]^2}\cdot\left(\frac{\partial^2 d_{n2}{}^*}{\partial T^2}\cdot\sum_{i=1}^{Nsol}\frac{x_i{}'}{d_{ni}{}^*}+2\frac{\partial d_{n2}{}^*}{\partial T}\frac{\partial\left(\sum_{i=1}^{Nsol}\frac{x_i{}'}{d_{ni}{}^*}\right)}{\partial T}+d_{n2}{}^*\cdot\frac{\partial^2\left(\sum_{i=1}^{Nsol}\frac{x_i{}'}{d_{ni}{}^*}\right)}{\partial T^2}\right)$$
eq. C.22

For one amine:

$$\frac{\partial^2 D_i}{\partial T^2} = \frac{\partial^2 D_1}{\partial T^2} + \left(\frac{\partial^2 \left[\frac{(D_2-1)\cdot(2D_2+1)}{2\cdot D_2} - (D_1-1)\right]}{\partial T^2}\right)\left(x_2'\frac{V_2}{V}\right)$$

$$+ 2\left(\frac{\partial \left[\frac{(D_2-1)\cdot(2D_2+1)}{2\cdot D_2} - (D_1-1)\right]}{\partial T}\right)\left(x_2'\frac{\partial\frac{V_2}{V}}{\partial T}\right)$$

$$+ \left(\frac{(D_2-1)\cdot(2D_2+1)}{2\cdot D_2} - (D_1-1)\right)(x_2'\frac{\partial^2\frac{V_2}{V}}{\partial T^2})$$

eq. C.23

For amine mixture:

$$\frac{\partial^2 D}{\partial T^2} = \sum_{i=1}^{N=amines} x_i^* \cdot \frac{\partial^2 D_i}{\partial T^2}$$

eq. C.24

Second derivative of B

$$\frac{\partial[0{,}5(d_s)^{-\frac{1}{2}}\cdot\frac{\partial d_s}{\partial T}\cdot(DT)^{-\frac{1}{2}}]}{\partial T} = (-0{,}25(d_s)^{-\frac{3}{2}}\cdot\frac{\partial d_s}{\partial T}^2\cdot(DT)^{-\frac{1}{2}}) + (0{,}5(d_s)^{-\frac{1}{2}}\cdot\frac{\partial^2 d_s}{\partial T^2}\cdot(DT)^{-\frac{1}{2}}) - $$
$$(0{,}5(d_s)^{-\frac{1}{2}}\cdot\frac{\partial d_s}{\partial T}\cdot 0{,}5(DT)^{-\frac{3}{2}}\cdot\left(\frac{\partial D}{\partial T}T + D\right))$$

eq. C.25

$$\frac{\partial[d_s^{1/2}\cdot 0{,}5(DT)^{-\frac{3}{2}}\cdot(\frac{\partial D}{\partial T}T+D)]}{\partial T} = \left(0{,}25d_s^{-\frac{1}{2}}\cdot\frac{\partial d_s}{\partial T}\cdot(DT)^{-\frac{3}{2}}\cdot\left(\frac{\partial D}{\partial T}T+D\right)\right) - (d_s^{\frac{1}{2}}\cdot 0{,}75(DT)^{-\frac{5}{2}}\cdot$$
$$\left(\frac{\partial D}{\partial T}T+D\right)^2) + (d_s^{\frac{1}{2}}\cdot 0{,}5(DT)^{-\frac{3}{2}}\cdot(\frac{\partial^2 D}{\partial T^2}T+2\frac{\partial D}{\partial T}))$$

eq. C.26

$$\frac{\partial^2 B}{\partial T^2} = \frac{\partial(\frac{\partial B}{\partial T})}{\partial T} = 6{,}359696\frac{\partial[0{,}5(d_s)^{-\frac{1}{2}}\cdot\frac{\partial d_s}{\partial T}\cdot(DT)^{-\frac{1}{2}}]}{\partial T}$$

$$- 6{,}359696\frac{\partial[d_s^{1/2}\cdot 0{,}5(DT)^{-\frac{3}{2}}\cdot(\frac{\partial D}{\partial T}T+D)]}{\partial T}$$

eq. C.27

$$\frac{\partial^2 F}{\partial T^2} = 1032{,}379865 M_n\frac{1}{d_n^2}\cdot(-\frac{\partial^2 d_n}{\partial T^2} + \frac{2}{d_n}(\frac{\partial d_n}{\partial T})^2)$$

eq. C.28

$$\frac{\partial^2 P}{\partial T^2} = \left(\frac{\partial^2 B}{\partial T^2}\sqrt{I}\right)\cdot\left(1 + \frac{1}{(1+B\sqrt{I})^2} - \frac{2}{1+B\sqrt{I}}\right) + \frac{2\left(\frac{\partial B}{\partial T}\right)^2 I}{(1+B\sqrt{I})^2}\cdot\left(\frac{-1}{1+B\sqrt{I}} + 1\right)$$

eq. C.29

$$\frac{\partial^2 \ln\gamma_n^{DH}}{\partial T^2} = \frac{\partial^2 F}{\partial T^2}P + 2\frac{\partial F}{\partial T}\frac{\partial P}{\partial T} + F\frac{\partial^2 P}{\partial T^2}$$

eq. C.30

First partial derivative with respect to moles of molecular species

First derivative of molecular weight

$$\frac{\partial(\sum_{k=1}^{k=molecules} x_k'Mr_k)}{\partial n_i} = \frac{N_{o\lambda\iota\kappa\acute{o}}-\sum_{\iota=1}^{ions} n_{ions}-n_i}{(N_{o\lambda\iota\kappa\acute{o}}-\sum_{\iota=1}^{ions} n_{ions})^2} \cdot Mr_i + \sum_{j=1}^{molecules-1} \frac{-n_j \cdot Mr_j}{(N_{o\lambda\iota\kappa\acute{o}}-\sum_{\iota=1}^{ions} n_{ions})^2} \qquad eq.\ C.31$$

First derivative of volume

$$\frac{\partial(\sum_{k=1}^{k=solvents} \frac{x_k'}{dn_k^*})}{\partial n_i} = \frac{N_{o\lambda\iota\kappa\acute{o}}-\sum_{\iota=1}^{ions} n_{ions}-n_i}{(N_{o\lambda\iota\kappa\acute{o}}-\sum_{\iota=1}^{ions} n_{ions})^2} \cdot \left(\frac{1}{dn_i^*}\right) + \sum_{j=1}^{solvents-1} \frac{-n_j/dn_j^*}{(N_{o\lambda\iota\kappa\acute{o}}-\sum_{\iota=1}^{ions} n_{ions})^2} \qquad eq.\ C.32$$

First derivative of mixture density

$$\frac{\partial d_s}{\partial n_i} = \frac{\partial[1000 \cdot (\sum_{k=1}^{molecules} x_k \cdot Mr_k) \cdot \frac{1}{(\sum_{k=1}^{Nsol} \frac{x_k'}{d_{nk}^*})}]}{\partial n_i} = \left(-\frac{1000}{(\sum_{k=1}^{Nsol} \frac{x_k'}{d_{nk}^*})^2} \cdot \frac{\partial\left(\sum_{k=1}^{k=solvents} \frac{x_k'}{d_{nk}^*}\right)}{\partial n_i} \cdot \right.$$

$$\left. \left(\sum_{k=1}^{k=molecules} x_k'Mr_k\right)\right) + \left(\frac{1000}{(\sum_{k=1}^{Nsol} \frac{x_k'}{d_{nk}^*})} \cdot \frac{\partial\left(\sum_{k=1}^{k=molecules} x_k'Mr_k\right)}{\partial n_i}\right) \qquad eq.\ C.33$$

First derivative of ionic strength

$$\frac{\partial I}{\partial n_i} =$$

$$= 0,5 \cdot \sum_{k=1}^{Nions} \left(\left(\frac{-n_{ion}}{\left(N_{o\lambda\iota\kappa\acute{o}}-\sum_{\iota=1}^{ions} n_{ions}\right)^2} \cdot \frac{1}{\sum_{k=1}^{k=molecules} x_k'Mr_k}\right) - \left(\frac{n_{ion}}{N_{o\lambda\iota\kappa\acute{o}}-\sum_{\iota=1}^{ions} n_{ions}} \cdot \right.\right.$$

$$\left.\left. \frac{1}{(\sum_{k=1}^{k=molecules} x_k'Mr_k)^2} \cdot \frac{\partial(\sum_{k=1}^{k=molecules} x_k'Mr_k)}{\partial n_i}\right) \cdot z_{ion}\right) \qquad eq.\ C.34$$

First derivative of dielectric constant

- i≠amine

$$\frac{\partial\left(\frac{x_2{}'}{V}\right)}{\partial n_i} = \left(-\frac{n_{amine}}{(N_{o\lambda\iota\kappa\acute{o}}-\sum_{\iota=1}^{ions}n_{ions})^2} \cdot \frac{1}{\sum_{k=1}^{k=solvents}\frac{x_k{}'}{dn_k{}^*}}\right) - \left(\frac{n_{amine}}{N_{o\lambda\iota\kappa\acute{o}}-\sum_{\iota=1}^{ions}n_{ions}} \cdot \frac{1}{(\sum_{k=1}^{k=solvents}\frac{x_k{}'}{dn_k{}^*})^2} \cdot \right.$$

$$\left.\frac{\partial\left(\sum_{k=1}^{k=solvents}\frac{x_k{}'}{dn_k{}^*}\right)}{\partial n_i}\right) \qquad\qquad \text{eq. C.35}$$

- i=amine

$$\frac{\partial\left(\frac{x_2{}'}{V}\right)}{\partial n_i} = \left(\frac{(N_{o\lambda\iota\kappa\acute{o}}-\sum_{\iota=1}^{ions}n_{ions})-n_{amine}}{(N_{o\lambda\iota\kappa\acute{o}}-\sum_{\iota=1}^{ions}n_{ions})^2} \cdot \frac{1}{\sum_{k=1}^{k=solvents}\frac{x_k{}'}{dn_k{}^*}}\right) - \left(\frac{n_{amine}}{N_{o\lambda\iota\kappa\acute{o}}-\sum_{\iota=1}^{ions}n_{ions}} \cdot \frac{1}{(\sum_{k=1}^{k=solvents}\frac{x_k{}'}{dn_k{}^*})^2} \cdot \right.$$

$$\left.\frac{\partial\left(\sum_{k=1}^{k=solvents}\frac{x_k{}'}{dn_k{}^*}\right)}{\partial n_i}\right) \qquad\qquad \text{eq. C.36}$$

First derivative of dielectric constant for one amine

$$\frac{\partial D_k}{\partial n_i} = \left[\frac{(D_2-1)\cdot(2D_2+1)}{2D_2} - (D_1-1)\right] \cdot V_2 \cdot \frac{\partial\left(\frac{x_2{}'}{V}\right)}{\partial n_i} \qquad\qquad \text{eq. C.37}$$

First derivative of dielectric constant for amine mixtures

$$\frac{\partial D}{\partial n_i} = \sum_{k=1}^{amines} x_k{}^* \cdot \frac{\partial D_k}{\partial n_i} \qquad\qquad \text{eq. C.38}$$

First derivative of B

$$\frac{\partial B}{\partial n_i} = \frac{6,359696}{\sqrt{T}} \cdot \frac{\sqrt{D}}{2\sqrt{d_s}} \cdot \frac{\left(\frac{\partial d_s}{\partial n_i}\right)D - d_s\cdot\left(\frac{\partial D}{\partial n_i}\right)}{D^2} \qquad\qquad \text{eq. C.39}$$

If Debye-Hueckel term is not calculated for acid gas

$$F = 1032,379865 \cdot M_n \cdot \frac{1}{d_n} \qquad\qquad \text{eq. C.40}$$

If Debye-Hueckel term is calculated for acid gas

$$F = \frac{4M_n}{(1,5)^3} \qquad\qquad \text{eq. C.41}$$

For each molecule

$$\frac{\partial P}{\partial n_i} = \left(\frac{\partial B}{\partial n_i}\sqrt{I} + \frac{B\frac{\partial I}{\partial n_i}}{2\sqrt{I}}\right) \cdot \left(1 + \frac{1}{\left(1+B\sqrt{I}\right)^2} - \frac{2}{1+B\sqrt{I}}\right)$$
eq. C.42

$$\frac{\partial \ln\gamma_n^{DH}}{\partial n_i} = F \cdot \frac{\partial P}{\partial n_i}$$
eq. C.43

First partial derivative with respect to moles of ionic species

First derivative of ionic strength

$$\frac{\partial I}{\partial n_i} = 0.5 \cdot \left(\frac{\left(N_{o\lambda\iota\kappa\acute{o}} - \sum_{k=1}^{ions} n_{kions} + n_i\right)}{\left(N_{o\lambda\iota\kappa\acute{o}} - \sum_{k=1}^{ions} n_{kions}\right)^2} \cdot \frac{1}{\sum_{k=1}^{k=molecules} x_k' Mr_k} - \frac{n_\iota}{N_{o\lambda\iota\kappa\acute{o}} - \sum_{k=1}^{ions} n_{kions}} \cdot \frac{1}{\left(\sum_{k=1}^{k=molecules} x_k' Mr_k\right)^2} \cdot\right.$$
$$\sum_{k=1}^{Nmolecules} \frac{n_k Mr_k}{\left(N_{o\lambda\iota\kappa\acute{o}} - \sum_{k=1}^{ions} n_{kions}\right)^2}\Bigg) \cdot z_i{}^2 + 0.5 \cdot \sum_{j=2}^{Nions}\left(\left(\frac{n_j}{\left(N_{o\lambda\iota\kappa\acute{o}} - \sum_{k=1}^{ions} n_{kions}\right)^2} \cdot \frac{1}{\sum_{k=1}^{k=molecules} x_k' Mr_k} - \right.\right.$$
$$\frac{n_j}{N_{o\lambda\iota\kappa\acute{o}} - \sum_{k=1}^{ions} n_{kions}} \cdot \frac{1}{\left(\sum_{k=1}^{k=molecules} x_k' Mr_k\right)^2} \cdot \sum_{k=1}^{Nmolecules} \frac{n_k Mr_k}{\left(N_{o\lambda\iota\kappa\acute{o}} - \sum_{k=1}^{ions} n_{kions}\right)^2}\Bigg) \cdot z_j{}^2\Bigg)$$
eq. C.44

If Debye-Hueckel term is not referred to acid gas

$$F = 1032.379865 \cdot M_n \cdot \frac{1}{d_n}$$
eq. C.45

If Debye-Hueckel term is referred to acid gas

$$F = \frac{4M_n}{(1.5)^3}$$
eq. C.46

$$\frac{\partial P}{\partial n_i} = \left(\frac{B\frac{\partial I}{\partial n_i}}{2\sqrt{I}}\right) \cdot \left(1 + \frac{1}{\left(1+B\sqrt{I}\right)^2} - \frac{2}{1+B\sqrt{I}}\right)$$
eq. C.47

$$\frac{\partial \ln\gamma_n^{DH}}{\partial n_i} = F \cdot \frac{\partial P}{\partial n_i}$$
eq. C.48

D. Appendix: Simulation results

D.1. CO_2 absorption in methanol using new Mathias –Copeman parameters (UMR)

The results of the simulation of CO_2 absorption in methanol using new Mathias –Copeman parameters (UMR) are compared to the previous Mathias- Copeman parameters (UMR-old).

Table D.1: Results of the absorption column

	Acid gas	1		Solvent make-up		2		Purified gas		Rich solvent	
Model		UMR	UMR-old	UMR	UMR-old	UMR	UMR-old	UMR	UMR-old	UMR	UMR-old
T ºC	40	15.49	15.05	-50	-50	-50	-50	-46.32	-45.65	-0.02	3.96
P (bar)	30	60	60	60	60	60	60	60	60	60	60
Mass flow (kg/h)	99786	392011	406679	759	769	768956	768960	70801	70848	1090166	1104791
				Composition (mass fraction)							
Nitrogen	2.84E-02	7.77E-03	7.48E-03	0.00E+00	0.00E+00	7.46E-21	7.66E-21	4.00E-02	3.99E-02	2.00E-04	1.92E-04
CO_2	2.90E-01	7.54E-01	7.67E-01	0.00E+00	0.00E+00	6.34E-10	6.22E-10	6.09E-04	1.04E-03	2.71E-01	2.82E-01
Methane	6.82E-01	2.37E-01	2.24E-01	0.00E+00	0.00E+00	1.28E-15	1.22E-15	9.59E-01	9.59E-01	2.28E-02	2.08E-02
Methanol	0.00E+00	1.85E-03	1.76E-03	1.00E+00	1.00E+00	1.00E+00	1.00E+00	1.52E-04	1.46E-04	7.06E-01	6.97E-01

Table D.2: Results of the flash drum

	9		5		6	
Model	UMR	UMR-old	UMR	UMR-old	UMR	UMR-old
T ºC	-36.02062122	-35.38	-36.02	-35.38	-36.02	-35.38
P (bar)	1.01325	1.01325	1.01325	1.01325	1.01325	1.01325
Mass flow (kg/h)	1090166.46	1104790.68	292224.83	306892.83	797941.63	797897.85
			Composition (mass fraction)			
Nitrogen	2.00E-04	1.92E-04	7.47E-04	6.91E-04	2.42E-07	2.25E-07
CO_2	2.71E-01	2.82E-01	9.12E-01	9.22E-01	3.62E-02	3.61E-02
Methane	2.28E-02	2.08E-02	8.47E-02	7.46E-02	1.80E-04	1.58E-04
Methanol	7.06E-01	6.97E-01	2.49E-03	2.34E-03	9.64E-01	9.64E-01

Table D.3: Results of distillation column

	10		CO$_2$ stream		8	
Model	UMR	UMR-old	UMR	UMR-old	UMR	UMR-old
T °C	-36.04	-35.40	-3.83	-2.31	63.12	64.19
P (bar)	1	1	1	1	1	1
Mass flow (kg/h)	797941.63	797897.85	29744.70	29707.30	768196.93	768190.55
			Composition (mass fraction)			
Nitrogen	2.42E-07	2.25E-07	6.49E-06	6.04E-06	7.47E-21	7.55E-21
CO$_2$	3.62E-02	3.61E-02	9.70E-01	9.70E-01	6.35E-10	6.20E-10
Methane	1.80E-04	1.58E-04	4.82E-03	4.25E-03	1.29E-15	1.20E-15
Methanol	9.64E-01	9.64E-01	2.52E-02	2.56E-02	1.00E+00	1.00E+00

Table D.4: Energy requirements of the process

Equipment	Energy/mass of recovered CO$_2$ (kJ/kg)	
	UMR	UMR-old
Cooler_1	6.73E+02	6.73E+02
Cooler_2	2.72E+03	2.85E+03
Cooler_3	7.78E+03	7.56E+03
Compressor_1	4.26E+02	4.26E+02
Compressor_2	2.53E+03	2.62E+03
Condenser	5.22E+02	5.26E+02
Reboiler	7.78E+03	7.60E+03
Pump	3.27E+02	3.27E+02

D.2. CO$_2$ absorption in refrigerated methanol using a reboiler absorber

Table D.5: Results of the absorption column

	Acid gas	1		Solvent make-up		2		Purified gas		Rich solvent	
Model		UMR	PR	UMR	PR	UMR	PR	UMR	PR	UMR	PR
T °C	40	15.49	16.27	-50	-50.00	-50.00	-50.00	-46.32	-50.40	-0.02	-11.81
P (bar)	30	60	60	60	60	60	60	60	60	60	60
Mass flow (kg/h)	99786	392018	451681	81	550	768960	768957	70801	70783	1090174	1150454
Composition (mass fraction)											
Nitrogen	2.84E-02	7.77E-03	7.37E-03	0.00E+00	0.00E+00	1.53E-25	1.70E-23	4.00E-02	4.00E-02	2.00E-04	4.33E-04
CO$_2$	2.90E-01	7.54E-01	7.64E-01	0.00E+00	0.00E+00	6.90E-12	6.82E-07	6.10E-04	1.73E-04	2.71E-01	3.00E-01
Methane	6.82E-01	2.37E-01	2.28E-01	0.00E+00	0.00E+00	6.66E-19	4.67E-16	9.59E-01	9.60E-01	2.28E-02	3.05E-02
Methanol	0.00E+00	1.85E-03	7.67E-04	1.00E+00	1.00E+00	1	1.00E+00	1.52E-04	1.88E-04	7.06E-01	6.69E-01

Table D.6: Results of the flash drum

	9		5		6	
Model	UMR	PR	UMR	PR	UMR	PR
T °C	-36.02	-40.34	-36.02	-40.34	-36.02	-40.34
P	1.01325	1.01325	1.01325	1.01325	1.01325	1.01325
Mass flow (kg/h)	1090174	1150453.55	292232.1	351895.46	797942	798558.09
Composition (mass fraction)						
Nitrogen	2.00E-04	4.33E-04	7.47E-04	1.41E-03	2.42E-07	7.25E-07
CO$_2$	2.71E-01	3.00E-01	9.12E-01	8.98E-01	3.62E-02	3.62E-02
Methane	2.28E-02	3.05E-02	8.47E-02	9.92E-02	1.80E-04	1.66E-04
Methanol	7.06E-01	6.69E-01	2.49E-03	9.84E-04	9.64E-01	9.64E-01

Table D.7: Results of the reboiled absorber

	10		CO$_2$ stream		8	
Model	UMR	PR	UMR	PR	UMR	PR
T °C	-36.0374	-40.34	-34.95788	-3.94	63.11158	66.05
P (bar)	1	1	1	1	1	1
Mass flow (kg/h)	797942	798558.09	29065.96	29552.47	768876	769005.62
Composition (mass fraction)						
Nitrogen	2.42E-07	7.25E-07	6.65E-06	1.96E-05	1.70E-23	4.86E-24
CO$_2$	3.62E-02	3.62E-02	9.93E-01	9.77E-01	6.82E-07	6.11E-12
Methane	1.80E-04	1.66E-04	4.93E-03	4.49E-03	4.67E-16	5.40E-19
Methanol	9.64E-01	9.64E-01	2.42E-03	1.81E-02	1.00E+00	1.00E+00

Table D.8: Energy requirements of the process

Equipment	Energy/mass of recovered CO$_2$ (kJ/kg)	
	UMR	PR
Cooler_1	6.73E+02	6.73E+02
Cooler_2	2.72E+03	5.58E+03
Cooler_3	7.78E+03	1.08E+04

Compressor_1	4.26E+02	4.26E+02
Compressor_2	2.53E+03	5.44E+03
Reboiler	7.20E+03	1.02E+04
Pump	3.27E+02	3.60E+02

E. Appendix: Publications

E.1.   Scientific Journals

- A. Plakia, G. Pappa, E. Voutsas, "Modeling of CO_2 solubility in aqueous alkanolamine solutions with an extended UMR-PRU model", Fluid Phase Equil., 478 (2018), pp. 134-144.
- A. Plakia, E. Voutsas, "Modeling of H_2S, CO_2+H_2S and CH_4+CO_2 Solubilities in Aqueous Monoethanolamine and Methyldiethanolamine Solutions", Ind. Eng. Chem. Res., 59 (2020), pp. 11317–11328.

- V. Koulocheris, A. Plakia, V. Louli, E. Panteli, E. Voutsas, "Calculating the chemical and phase equilibria of mercury in natural gas". Chemical Engineering Science, 2021 (submitted).
- A. Plakia, E. Voutsas, "Description of pure imidazolium-based ionic liquids, binary CO_2-ionic liquid mixtures and simulation of CO_2 absorption process in an ionic liquid using UMR-PRU model", Fluid Phase Equil., 2021 (under preparation).

E.2.   Conferences

- N. Novak, E. Petropoulou, A. Plakia, C. Pittas, V. Louli, G. Pappa, C. Boukouvalas, E. Skouras, E. Solbraa, E. Voutsas, "Prediction of Dew Point and Liquid Dropout of Natural Gas and Gas Condensates", 29th European Symposium on Applied Thermodynamics, Bucharest, Romania, 18-21 May 2017
- N. Novak, E. Petropoulou, C. Pittas, A. Plakia, V. Louli, G. Pappa, C. Boukouvalas, E. Voutsas, "Thermodynamic Modeling and Simulation of Natural Gas Processes", 11th Chemical Engineering Greek Conference, Thessaloniki, 25- 27 May 2017
- A. Plakia, E.Voutsas,"Modeling and simulation of CO_2 and H_2S solubility in aqueous alkanolamine solutions", 12th Chemical Engineering Greek Conference Athens, Greece, 29-31 May 2019
- V. Koulocheris, N. Novak, A. Plakia, E. Petropoulou, Ch. Boukouvalas, V. Louli, G. Pappa, E. Voutsas, "UMR-PRU thermodynamic model: application to natural gas processing", CAPE-OPEN 2019 Annual Meeting, Amsterdam, Netherlands, 22-23 October 2019